

ENGINEERING SOLUTIONS TO ADDRESS SEVERAL CURRENT LIVESTOCK AND
POULTRY HOUSING CHALLENGES

BY

YIJIE XIONG

DISSERTATION

Submitted in partial fulfillment of the requirements
for the degree of Doctor of Philosophy in Agricultural and Biological Engineering
in the Graduate College of the
University of Illinois at Urbana-Champaign, 2019

Urbana, Illinois

Doctoral Committee:

Professor Richard S. Gates, Chair
Professor Xinlei Wang
Professor Kenneth W. Koelkebeck
Clinical Assistant Professor Neslihan Akdeniz Onuki

ABSTRACT

Robust and sustainable controlled environment agriculture is critical to achieve optimal animal production efficiency with the least impacts to animal welfare and our environment.

Achieving optimal agricultural environment is a consistent challenge for current livestock and poultry industries. Example challenges include: 1) high pre-weaning mortality of neonatal piglets in typical farrowing swine facilities, 2) maintaining egg production and sufficient well-being for laying hens under heat stress events, and 3) compromised air quality issues in most poultry housing systems. My research seeks to provide engineering solutions to address these three challenges currently faced by the animal production industry. This dissertation details research findings for projects specifically addressing these three challenges.

In the U.S., pre-weaning mortality ranges from about 9 - 15% of live-born piglets. Hypothermia and low vitality are believed to be among the leading causes of pre-weaning piglet mortality. To identify neonatal piglets that are prone to hypothermia, **a mathematical model was developed to predict neonatal piglet rectal temperature using surface temperatures.** Time series rectal temperatures (RT), thermal images, and corresponding farrowing room conditions were recorded for a group of 99 neonatal piglets. Results showed that RT of the piglets dropped immediately after birth, with a mean drop of 4.4°C recorded in the first 15 min. Piglets experienced the lowest RT at 30 min after birth, reaching a mean low temperature of 33.6°C, approximately 5°C below birth temperature. Linear regression models were developed

and assessed, with the refined linear regression model providing a more reliable prediction of piglet RT. The refined regression model presented can be used to provide a direct prediction of RT from simple measurement of the piglet ear surface temperature, with an uncertainty of about 1°C, and thus can be used as a convenient prediction tool for rapid estimation of piglet RT under typical farrowing conditions.

Alternative cooling methods, especially a cooled perch system, present an intriguing opportunity for heat removal from birds under heat stress. **A perch system was designed and used to examine the effects of water-cooled perches as a cooling alternative on hen performance, production, health and welfare on caged White Leghorn hens exposed to heat stress.** The cooled perch system consisted of two replicates of three-tier cage units with galvanized perch pipes forming a complete loop in each tier in which cooled water circulated. Flow for each loop was provided by loop pumps that drew chilled water from an open thermal storage and returned it to the same manifold. Each thermal storage was cooled by continuously circulating water through a water chiller. Each loop pump was thermostatically controlled based on cage air temperature. The performance of the cooled perch system was assessed for a stable system operation period by analyzing the water flowrate, characterizing the loop water temperature rise profile, and using this information to establish estimates of the system total heat gain. It was noted that the circulation pump performance decreased over time, and there was a discrepancy between the pumps' actual output and that provided by the manufacturer. Different

loops and CP replicates did not have equal performance regarding loop water temperature rise and loop net heat gains. There was a strong correlation between room temperature and perch heat gain, indicating natural convection from ambient air to perch surface was the major contributor to heat gain over other heat transfer mechanisms including hen conduction. Design criteria useful for future applications of cooled perch were provided. An average daily heat gain of about 128 W/m perch length or 43.2 W/hen housed was estimated, based on 12-h day/12-h night air temperature of 35/28°C and an average loop inlet water temperature of 20°C. A peak-day system heat load of 64.4 kWh was estimated and required a thermal storage capacity of 2.5 kWh. Information regarding hens' perching behavior, footpad area estimation, and thermal conductance or resistance of the footpad were provided.

The U.S. egg industry faces growing pressure from consumers and retailers to transition egg production from conventional caged systems to alternative housings such as “cage-free” aviaries and enrichable caged systems, despite research that has established that alternative housing has more challenges to maintain desired indoor air quality parameters. Given the current limited knowledge regarding the interior environment in such housings, **it is important to evaluate the thermal environment and air quality in order to provide additional scientific information for alternative hen houses.** Indoor air temperature, RH, CO₂ and NH₃ concentrations were continuously monitored using the six intelligent Portable Monitoring Unit (iPMUs) for three different laying hen houses, including two aviaries and an enrichable cage

house from February to July 2019. The thermal environment and the gas concentrations during the study were not uniformly distributed spatially in the houses. There was a variation in temperature distribution between the top and the bottom levels for all three houses. Hens in all three houses experienced THI conditions from normal to emergency (hot and cold) categories. The average CO₂ and NH₃ concentrations for the three hen houses ranged from approximately 400 to 5800 ppm and 0 to 94 ppm, respectively. During monitoring, 75% of the measurements in the three houses were lower than 5,000 ppm for CO₂ and below 60 ppm for NH₃ concentrations. Both winter minimum ventilation and summer tunnel ventilation were not sufficient during some monitoring periods, and further improvement to the ventilation management strategies would be helpful. Management practices to monitor the interior thermal environment, investigate the air inlets performance (number of inlets and air velocity), adjust operational static pressure (which drives the air inlets), or which fans to operate during coldest conditions, should be considered by the producer.

ACKNOWLEDGEMENTS

The author would like to express her most sincere gratitude to Dr. Rich S. Gates, Professor of Agricultural Engineering in the Agricultural and Biological Engineering Department. His experience, his influence, his wisdom and support have helped me more than words can ever voice, yet, it is merely the smallest part of his contribution. He always heartily looked after students, helping us to achieve to our best potential. His kind, selflessness, generosity, altruism and encouragement will always shine a positive ray in my life.

To the members of my committee: Dr. Kenneth W. Koelkebeck, for putting up with me when I became grumpy and impatient, and for always encouraging me positively; Dr. Xinlei Wang, who criticized my work and made sure I had comprehensive engineering analyses, and offered me mooncakes when I had to celebrate the mid-autumn festival alone; and Dr. Neslihan Akdeniz, who agreed to be on my committee and has provided many helpful suggestions and comments. To the staff members, Tim Lecher and Steve Ford, for providing help that was necessary for me to complete my projects.

The author thanks Dr. Bryan T. Lohmar, Director of the U.S. Grains Council – China Office, for offering me a part-time job and connections to industry and companies. His trust and support were significant to me and should be thanked more than I can express.

My gratitude also extends to my friends: Patricia for going to different restaurants with me and always taking care of Fiona when I cannot; to Di, for being my closest friend and for

successfully defeating her tumor so that I still have my closest friend; to Jiaying, for being such an efficient collaborator – without you we can never pull the thermal perch project out; to Ana Beatriz, Juliana, Mariane, and many, many others that I cannot fit all your names here, for supporting me and carrying me through this project.

To the undergraduate students that participated in my research projects – Thais Maurin, Lucas Vicente, Badu de Oliveira, and Nico Vassilakis, thank you all very much for stepping ahead and overcoming the most tedious components of a research project. I might already have the foundation of this project, but your work poured concrete to it and made it possible.

To Mimi and Fiona,

For giving me your fluffy hugs and soothing purrs,

for staying with me no matter what I do,

and for keeping me away from insanity...

To Mom,

For caring me with unfailing love,

for providing me the best things within your reach,

and for always supporting me with every step I take...

And to Dad,

For accepting me like I am of your own and trusting me

completely, for getting my back when I needed shelter,

and for always loving me unconditionally...

TABLE OF CONTENTS

CHAPTER 1	INTRODUCTION	- 1 -
CHAPTER 2	PREDICTION MODEL OF NEONATAL PIGLET BODY TEMPERATURE FROM SURFACE TEMPERATURE	- 5 -
2.1	INTRODUCTION	- 5 -
2.2	MATERIALS AND METHODS	- 10 -
2.2.1	PIGLET RECTAL TEMPERATURE MEASUREMENT AND PROCESSING	- 11 -
2.2.2	PIGLET SURFACE TEMPERATURE MEASUREMENT	- 12 -
2.2.3	STATISTICAL ANALYSIS	- 14 -
2.2.4	MODEL DEVELOPMENT AND ASSESSMENT	- 14 -
2.3	RESULTS AND DISCUSSION	- 15 -
2.3.1	CHANGE IN PIGLET BODY TEMPERATURE AFTER BIRTH	- 15 -
2.3.2	PIGLET BODY TEMPERATURE MODEL FROM SURFACE TEMPERATURE MEASUREMENT	- 19 -
2.3.3	PREDICTION MODEL DEVELOPMENT AND ASSESSMENT	- 22 -
2.4	SUMMARY AND CONCLUSIONS	- 30 -
2.5	ACKNOWLEDGMENT	- 31 -
CHAPTER 3	DESIGN AND PERFORMANCE ASSESSMENT OF A COOLED PERCH SYSTEM TO REDUCE HEAT STRESS IN LAYING HENS	- 32 -
3.1	INTRODUCTION	- 32 -
3.2	MATERIALS AND METHODS	- 38 -
3.2.1	COOLED PERCH SYSTEM DESIGN AND INSTRUMENTATION	- 38 -
3.2.2	EXPERIMENTAL DESIGN AND CHICKEN ARRANGEMENT	- 45 -
3.2.3	WATER FLOWRATE EVALUATION	- 47 -
3.2.4	ESTIMATION OF SYSTEM NET HEAT GAIN	- 54 -
3.2.5	HEAT TRANSFER COMPONENTS ANALYSIS OF THE COOLED PERCH SYSTEM	- 57 -
3.2.6	EVALUATION OF THE SYSTEM PERFORMANCE	- 67 -
3.2.7	IMPLICATIONS TO LAYING HENS	- 70 -
3.3	RESULTS AND DISCUSSION	- 75 -
3.3.1	SENSOR CALIBRATION AND DATA ACQUISITION PERFORMANCE	- 75 -
3.3.2	RESULTS OF THE WATER FLOWRATE EVALUATION	- 77 -
3.3.3	RESULTS OF LOOP TEMPERATURE RISE AND SYSTEM NET HEAT GAIN	- 80 -
3.3.4	RESULTS OF HEAT TRANSFER COMPONENT ANALYSIS	- 84 -
3.3.5	EVALUATION OF SYSTEM PERFORMANCE	- 88 -
3.3.6	IMPLICATIONS TO LAYING HENS	- 95 -
3.4	PERFORMANCE CHALLENGES AND RECOMMENDATION	- 101 -
3.5	SUMMARY AND CONCLUSIONS	- 103 -

3.6 ACKNOWLEDGEMENTS	- 105 -
CHAPTER 4 IMPROVEMENT TO THE INTELLIGENT PORTABLE MONITORING UNIT (IPMU) FOR AIR QUALITY MONITORING IN ALTERNATIVE POULTRY HOUSING SYSTEMS	- 106 -
4.1 INTRODUCTION	- 106 -
4.1.1 VENTILATION AND AIR QUALITY IN POULTRY HOUSES	- 106 -
4.1.2 MEASURING AIR QUALITY IN POULTRY HOUSES	- 112 -
4.1.3 OVERVIEW OF THE INTELLIGENT PORTABLE MONITORING UNIT (IPMU)	- 120 -
4.1.4 OBJECTIVES	- 123 -
4.2 MATERIALS AND METHODS	- 125 -
4.2.1 ENGINEERING IMPROVEMENT TO THE IPMU	- 125 -
4.2.2 AIR QUALITY AND THERMAL COMFORT ASSESSMENT IN COMMERCIAL LAYER FARM	- 129 -
4.3 RESULTS AND DISCUSSION	- 139 -
4.3.1 NH ₃ SENSOR CALIBRATION EQUATION	- 139 -
4.3.2 AIR QUALITY AND THERMAL COMFORT IN COMMERCIAL LAYER FARM	- 141 -
4.4 SUMMARY AND CONCLUSIONS	- 162 -
4.5 ACKNOWLEDGEMENTS	- 164 -
CHAPTER 5 SUMMARY	- 165 -
REFERENCES	- 168 -
APPENDIX A SELECTING CALIBRATION EQUATION FOR NH₃ SENSORS – RESULTS FOR METHODS NOT SELECTED	- 180 -
APPENDIX B UPDATED CORE ARDUINO CODE	- 182 -
B.1 SETTING THE SAMPLING PARAMETERS	- 182 -
B.2 CHANGING DATALOGGING RATES	- 183 -
B.3 MATCHING DATE AND TIME WITH A COMPUTER	- 184 -
B.4 PRINTING NH ₃ CONCENTRATIONS IN REAL TIME	- 184 -
APPENDIX C MATLAB CODE FOR DATA PROCESSING	- 186 -
C.1 THE GRAPHICAL USER INTERFACE (GUI)	- 186 -
C.2 EXPLANATION OF KEY COMPONENTS OF THE CODE	- 187 -
C.3 COMPLETE SET OF CODE FOR DATA PROCESSING	- 189 -

CHAPTER 1 INTRODUCTION

Animal production is one of the most important sectors in agriculture. Robust and sustainable livestock and poultry housing environment is critical to achieve optimal animal production efficiency with the least impacts to animal welfare and our environment, although different housing systems present trade-offs between competing factors including production efficiency, housing environment, animal health, welfare, and mortality. Achieving optimal housing is a consistent challenge for current livestock and poultry industries. Sustainable animal production systems will incorporate as many of the positive attributes as possible and reduce as many of the negative aspects as possible. Three challenges studied were: 1) high pre-weaning mortality of neonatal piglets in typical farrowing swine facilities, 2) maintaining egg production and sufficient well-being for laying hens under heat stress events, and 3) compromised air quality and thermal environment in most poultry housing systems.

This dissertation documents research findings for projects focused on these three challenges, seeking to provide and evaluate potential engineering solutions to address these challenges currently faced by the animal production industry. Each chapter in this dissertation specifically discussed a study that was conducted to address one of the three challenges.

Chapter 2 Prediction Model of Neonatal Piglet Body Temperature from Surface Temperature. This chapter focused on the development of mathematical models to predict

neonatal piglet rectal temperature using surface temperature and environmental measurements to identify newborn piglets that are prone to hypothermia. The **objective** of this chapter was to develop and evaluate linear regression models to predict piglets' body temperature (estimated from rectal temperature) from body surface temperature measured behind the ears of the piglets. The feasibility of the prediction model developed for use in a rapid estimation of piglet body temperature was evaluated, including the model's predictive uncertainty.

Chapter 3 Design and performance assessment of a water-cooled perch system to reduce heat stress in laying hens. This chapter describes a multi-year study using a perch system to examine the effects of water-chilled perches as a cooling alternative on hen performance, plumage condition, foot health, physiological parameters on caged White Leghorn hens exposed to acute and cyclic heat stress events. With the substantial positive benefits provided by the experimental cooled perch system, the importance of documenting the engineering design and evaluating the system performance was realized in the merit of future investigation and perhaps larger scale application in the industry. The **objectives** of this chapter are: 1) to document the design and instrumentation of the cooled perch system; 2) to evaluate perch performance based on water mass flowrate, loop temperature rise, and system net heat gain; 3) to quantify the heat transfer components including convective and radiative heat gains using the cooled perch performance data; 4) to provide design information for larger scale application; and 5) to update the estimated value of laying hens' footpad area. In the results and discussion section, the

engineering performance of the cooled perch system, design criteria useful for future design and application, and the cooled perch's implications to laying hens are provided. Heat transfer impacts to the performance of the cooled perch system are discussed.

Chapter 4 Improvement to the intelligent portable monitoring unit (iPMU) for air quality assessment in commercial alternative poultry housing systems. The U.S. egg industry has faced a growing pressure from consumers and retailers to transition egg production from conventional caged systems to alternative housing systems such as “cage-free” aviaries and enrichable caged systems. It was established in some studies that alternative housing had more challenges to maintain desired indoor air quality parameters when compared to traditional housing types such as conventional cages or enriched colonies. Given the currently limited knowledge regarding maintaining desirable ranges of thermal comfort and gaseous concentrations in such housing types, it is important to evaluate the interior thermal environment and air quality parameters in order to provide more scientific information for alternative laying hen houses. Therefore, the specific **objectives** of this chapter were: 1) to improve the six iPMUs with a robust NH₃ calibration procedure, develop appropriate calibration equations, improve coding programs to assure ample sampling duration, and develop user friendly post data processing and analysis procedures; and 2) to use the iPMUs for air quality monitoring in different commercial laying hen systems, and provide simultaneous measurements of interior environmental parameters, including house temperature, ammonia (NH₃), and carbon

dioxide (CO₂) concentrations during cold and warm weather conditions. Six upgraded iPMUs were used to conduct continuous evaluations of the interior thermal environment and air quality parameters in three alternative commercial laying hen houses (enrichable caged barn and aviaries). Information regarding ventilation and farm management implications are provided, along with management strategies suggestions to producers are discussed.

The problem statement, materials and methodologies, and results for each study are provided in the following chapters. Chapter 5 provides an insightful summary to the three research projects included in this dissertation.

CHAPTER 2 PREDICTION MODEL OF NEONATAL PIGLET BODY TEMPERATURE FROM SURFACE TEMPERATURE¹

2.1 INTRODUCTION

Pre-weaning mortality is not only an economic concern but is also a well-being issue in commercial pig production. The pre-weaning stage is one of the most important periods of a pigs' life and can greatly affect their subsequent development and growth performance. Many efforts such as genetic selection and improved management practices have resulted in a larger number of piglets born per litter. However, pre-weaning mortality has remained a challenge over the past 30 years (Baxter and Edwards, 2018; Lay et al., 2002; NAHMS, 1995). In the United Kingdom and European countries during the 90's, pre-weaning mortality of piglets born alive ranged from 8.7 to 15.4 % for indoor housing systems, and anywhere between 12 to 25 % for outdoor housing (Alonso-Spilsbury et al., 2007). In the U.S., pre-weaning mortality ranges from about 9 - 15% of live-born (Ellis et al., 2017; Lay et al., 2002; Smith et al., 2018; USDA, 2015). Several review papers have illustrated a positive linear relationship between the production cost and pre-weaning mortality. Thus, piglet mortality can be a substantial economic impact for the pork industry (Baxter and Edwards, 2018; Lay et al., 2002).

¹ Xiong, Y., R.S. Gates, N.C. Cooper and M. Ellis. 2018. Neo-natal piglet core body temperature model from surface temperature and environment measurements. Paper ILES18-128, 25-27 September. *10th Intl. Livestock Env. Symp*, Omaha, NE, USA. <https://doi.org/10.13031/iles.18-128>

Many causal factors, such as crushing, starvation, disease, and congenital abnormalities are possible underlying reasons or pre-disposing factors for pre-weaning piglet mortality, and the literature suggests that early mortality might be due to complex interactions that result from hypothermia, hypoxia, low viability, low colostrum intake, as well as other reasons (Baxter and Edwards, 2018; Curtis, 1970; Dyck and Swierstra, 1987; Edwards and Baxter, 2015; English and Morrison, 1984; Lay et al., 2002; Marchant et al., 2000). Numerous articles have introduced the role of the “hypothermia – starvation – crushing” mortality complex, suggesting that the causes leading up to pre-weaning mortality are not necessarily independent, but rather may be interlinked with one another; although the complex typically starts with hypoxia and low vitality (Baxter and Edwards, 2018; Curtis, 1970; Edwards and Baxter, 2015; English and Morrison, 1984; English, 1993; Kelley, 1985; Lay et al., 2002). Suboptimal birthweight has also been considered as a primary underlying factor that attributes to early mortality (Baxter and Edwards, 2018; Douglas et al., 2014; Gardner et al., 1989; Lay et al., 2002).

Early literature identified the first two to three days as the most critical to neonatal piglets and the most vulnerable of a pig’s entire life, as thermoregulation functions are not fully developed (Alonso-Spilsbury et al., 2007; Baxter and Edwards, 2018; Curtis and Rogler, 1970; English and Morrison, 1984; Le Dividich and Noblet, 1981; Marchant et al., 2000). Many studies have found that most piglets’ deaths occur during these first days, accounting for a majority of the total mortality over the entire pre-weaning period (Cieslak et al., 1983; Lay et al., 2002; Rudd

and Marchant, 1995). The first 24 h of life is the first major chance for pathogens to enter piglets' body, especially for any piglets experiencing delayed initial colostrum intake (Baxter and Edwards, 2018). Besides disease threats, piglets also are challenged to initialize their inherent thermoregulation during the first 24 h. Unlike other farm animals such as cattle and goats, pigs are one of the most cold-sensitive mammals due to their lack of adipose tissue and brown fat (Curtis and Rogler, 1970; Herpin et al., 2002). Neonatal piglets have almost no fat deposits when first born, with fat accounting for only approximately 1% of birth weight (Curtis and Rogler 1970). After the first day of age, piglets start to develop fat, and its deposition rapidly increases to 2-3% of birth weight at two days, and around 10% by their first week of age when their thermoregulatory functions and metabolism are fully developed (Curtis and Rogler, 1970).

Sow crushing is well-documented as the most common event for postnatal piglet death, accounting for roughly 50% of the total pre-weaning mortality (NAHMS, 1995; Lay et al., 2002). Studies have identified both direct and/or indirect association of hypothermia with pre-weaning piglet mortality (Curtis, 1970; Herpin et al., 2002; Baxter and Edwards, 2018). At birth, residual amniotic fluid covers a piglet, and its evaporation requires a supply of energy which can come from radiant and convective heat transfer with the surrounding microenvironment and heat conduction from the body core. To utilize surface temperature as a surrogate for homeostasis, an understanding of the relationship between net radiation, evaporative heat loss, convective heat loss or gain, and piglet heat production is necessary. The equilibrium surface temperature

depends not only on these factors but also on the air velocity around the piglet, which affects both convective and evaporative fluxes (Monteith, 1981; Porter and Gates, 1969). Early focus to improve the hypothermia issue for neonatal piglets included the use of radiant heaters, heated mats, a heated creep area next to the sow, and improved farrowing crate design (Baxter and Edwards, 2018; Morrison et al., 1983; Pedersen et al., 2016). Studies have shown that adding an under-floor heating system has greatly reduced neonatal piglets' mortality during the first 24 h post-farrowing, and the use of drying agents has also been proven to be effective to reduce post-farrowing mortality (Baxter and Edwards, 2018; Malmkvist et al., 2006; Westin et al., 2015). Radiant lamps or heat pads and higher temperature room conditions can provide the needed net thermal energy to the piglet, increasing surface temperature and reducing the rate of body heat loss; however, higher temperatures are uncomfortable for the sow, and radiant lamps or heat pads are not universally available to piglets post-birth. Invariably, some piglets will not use or be attracted to heat lamps (especially if on only one side of a pen) and thus may lose relatively more heat with a concurrent further reduction in core body temperature. Accordingly, the energy stored in a piglet's body at least partially drives amniotic fluid evaporation and can reduce core body temperature (CBT) to different degrees depending on ambient thermal conditions, which can be especially problematic in cooler and drier microclimates, such as wintertime.

Besides endeavors to provide radiant heat sources in farrowing facilities, understanding the underlying mechanisms creating hypothermic piglets remains a primary goal to reduce pre-

weaning mortality. Measurements of piglet body temperature have been a practical means to help identify piglets that may be prone to hypothermia. Various temperature-measuring methods have been used in previous studies to represent pigs' CBT, including measurements of rectal temperature (Carroll et al., 2001; Curtis and Rogler, 1970; Pattison et al., 1990), abdominal temperature (Brown-Brandl et al., 2003), tissue, esophageal, and tympanic membrane temperature (Dickson et al., 1979). However, implementing such temperature measurements in swine facilities is inconvenient, time inefficient, and involves additional expense. Alternatively, thermal imaging with infrared technologies has been used as an indirect tool to estimate the thermal condition of animals.

Thermography images from infrared cameras are widely used in agricultural, livestock and crop research, having merit for measuring surface temperature (Caldara et al., 2014), estimating body temperature (Hoffmann et al., 2013) and control of evaporative spray systems (Mutaf et al., 2008; Yanagi et al., 2002; Zolnier et al., 2001; Zolnier et al., 2003). They are a convenient alternative to more invasive wireless systems in animals (Brown-Brandl et al., 2003; Green et al., 2005). However, there is little information on the accuracy of using thermal imaging techniques to estimate neonatal piglets' core body temperature and the roles of other environmental parameters on the piglets' thermoregulatory mechanisms.

The objective of this chapter was to develop and evaluate mathematical models to predict piglets' core body temperature (estimated from rectal temperature) from body surface

temperature measured behind the ears of the piglets and elapsed time post-birth. Each model was developed by linear or non-linear regression. The feasibility of these prediction models for use in a rapid estimation of piglet body temperature was evaluated, including the model's predictive uncertainty.

2.2 MATERIALS AND METHODS

The study for this chapter was conducted at the farrowing facility of Swine Research Center (SRC) at the University of Illinois at Urbana-Champaign (Cooper et al., 2018; Xiong et al., 2018). All animal care procedures were approved by the University of Illinois Institutional Animal Care and Use Committee (IACUC Protocol No. 16163).

The indoor environment of the SRC farrowing facility was managed under typical farrowing house conditions. The farrowing facility had 20 pens; each pen had a farrowing crate and surrounding piglet area with a heat lamp on one side and provided 3.5 m² floor space. Room temperature was maintained at approximately 23°C. Pen temperature and relative humidity (**RH**), were recorded every 5 min during the experiment via attaching magnetic temperature and RH dataloggers (HOBO UX100-011, Onset Computer Corp., Bourne MA, USA) to the crate, which closely represent the thermal environment experienced by the sow. Wet bulb temperature was calculated from the temperature and RH recordings, from which was obtained the wet bulb depression (**WBD**, dry bulb temperature minus wet bulb temperature) for characterizing the thermal environment experienced by the sows and their piglets during this study.

2.2.1 Piglet rectal temperature measurement and processing

On each experiment day, piglets farrowed from one or two litters were measured. Piglets were weighed immediately after birth. In this study, rectal temperature (RT) was used to represent piglets' body temperature and was measured immediately after birth (0 min), and at 15 min, 30 min, 45 min, 60 min, 90 min, 120 min, 180 min, 240 min, and 1,440 min (24H) thereafter. A thermal camera (FLIR T450sc, FOL 18mm, FLIR Systems, Inc., Wilsonville OR, USA) was used to take thermal infrared (IR) images of the entire back, head, and ears of the piglet. The IR images were taken immediately after RT. Piglets were then put back into the same farrowing crate after each measurement at the sow's underline. In the study, no interventional drying methods (such as towel drying or wiping off piglet amniotic fluids) were used before the RT and IR measurements. Results for 99 newly born male and female piglets from nine litters that consist of a complete profile of both RT and IR image measurements are discussed in this paper.

Modified Type K thermocouples (OMEGA Engineering, Inc., Norwalk CT, USA) were used to measure the piglet rectal temperature. Prior to each daily use, the thermocouple sensors were checked and calibrated against a National Institute of Standards and Technology (NIST) certified temperature calibrator (CL 134-1, OMEGA Engineering, Inc., Norwalk CT, USA), within a calibration range from 30 to 40°C with a 2°C interval, and readings were adjusted with

the calibration equation. The tip of the thermocouple was covered with heat shrink and liquid tape to avoid creating any discomfort for piglets during measurements.

The measured piglet RTs were plotted against the elapsed time post birth, with a colored hollow circle representing the RT for a piglet. Due to uncontrollable reasons (such as crushing by the sow, found dead, or necessity to be euthanized during the first 24 h after birth), a very limited number of piglets (N=7) were missing the RT measurements for time 4H and/or 24H. A box-whisker plot was created for each measurement time, at 0H, 15 min, 30 min, 45 min, 1H, 90 min, 2H, 3H, 4H, and 24H. The box-whisker plot illustrated the interquartile range (IQR, 25 – 75% of readings) of the RTs for that measurement time, within which the median, mean, and ± 1.5 IQR were also shown. The piglets' mean RT at each measurement time were connected by a red dotted line to depict further the general trend of the RT change with post birth elapsed time for all neonatal piglets measured.

2.2.2 Piglet surface temperature measurement

For each thermal image, the back-of-ear temperature information was extracted using FLIR Camera software (FLIR Tools®, FLIR® Systems, Inc., Wilsonville, OR USA). Figure 2-1 shows a thermal image example of a piglet's back, head, and ears, with black-to-purple colors representing cooler piglet surface temperature, and orange-to-yellow colors representing warmer piglet surface temperatures. The Thermal Multi-Spectral Dynamic Imaging (MSX) feature and the selection tool provided in the FLIR Tools was used to choose surfaces of interest for analysis.

The images were analyzed with the default settings of the camera (an emissivity of 0.98, a reflecting temperature of 20°C, and an IR resolution of 320 x 240 pixels). An ellipse that covered the warmest surface temperature on the back of each ear image was identified (E11 or E12 in Figure 1), from which the minimum, average, and maximum surface temperatures were provided by the software. A straight line (Li1 or Li2 in Figure 2-1) was then drawn from the ellipse to the tip of the same piglet ear to explore the degree of potential temperature drop, and surface temperatures for the same criteria (minimum, average, and maximum) were provided. These measurements were repeated for each ear of the piglet.

From each IR temperatures extracted (maximum, minimum, and average of E11, E12, Li1, and Li2), the maximum temperature of the location, named maximum ear temperature, was selected to represent the piglet's IR temperature. Temperature difference derived from subtracting the maximum ear temperature from the piglet's corresponding RT was computed to explore the feasibility of using the maximum ear temperature to predict a piglet's body temperature in practice. A box-whisker plot for each measurement time (0H, 15 min, 30 min, 45 min, 1H, 90 min, 2H, 3H, 4H, and 24H) was created to show the distribution of the temperature difference between the piglets' RT and the maximum ear temperature.

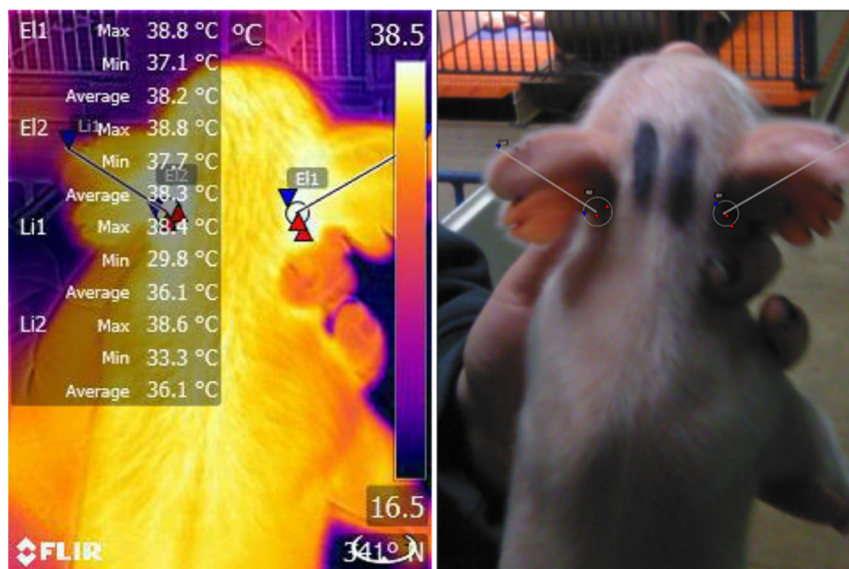


Figure 2-1. Example thermal image of a piglet’s back, head, and ears, with black-to-purple colors representing colder piglet surface temperature, and orange-to-yellow colors representing warmer piglet surface temperatures. The minimum, average, and maximum surface temperature for the warmest area of a piglet’s ear and a straight line from that area to the tip of the ear were analyzed.

2.2.3 Statistical analysis

The piglets’ RTs and their corresponding maximum ear surface temperatures at each measurement time were analyzed with the analysis package in OriginPro (OriginLab®, Northampton, MA, USA) using paired t-tests to determine if the means of the two temperature parameters analyzed are different from each other ($P < 0.05$).

2.2.4 Model development and assessment

The dry bulb air temperatures and the relative humidity measurements of the farrowing facilities were processed to obtain descriptive information of environmental factors, including the mean, standard deviation (std), the minimum and the maximum values of indoor air temperatures, relative humidity (RH), wet bulb temperature, and wet bulb temperature

depression (WBD), tabulated for each measurement time. Piglets' RT temperatures and their corresponding ear surface temperatures were used to develop mathematical models to predict pre-weaning piglets' body temperatures. A linear regression model was developed for the RT and the maximum ear temperature. Table 2-1 shows the dependent variable, the independent variable(s), and the generic equation for each model developed and tested. A fitted plot was generated for each model and the fitting curve, the 95% confidence band, and 95% prediction band were plotted. For every fitted parameter, the estimated value and its standard error, the coefficient of determination (R^2), and the adjusted coefficient of determination (adj. R^2) were provided.

Table 2-1. Model fitting parameters and generic expression.

Model Description	Dependent Variable	Independent Variable (x)	Generic Expression
Linear	RT	max ear temp	$y = a + bx$

2.3 RESULTS AND DISCUSSION

2.3.1 Change in piglet body temperature after birth

A descriptive summary of the body temperature measurements for the 99 neonatal piglets at the 10 measurement intervals is provided in Table 2-2. The mean, std of the piglets' RT, and the mean RT drop since birth at each measurement time are also provided. The RT change over time for these neonatal piglets after birth is shown in Figure 2-2(a). In Figure 2-2(a), the RT at a measurement time for each piglet is represented by a colored hollow circle, and box-whisker plots are shown for each measurement time. The mean, median, and ± 1.5 IQR (inter quartile

range) at each time are also shown. Means are connected by a red dotted line to depict the general trend of change in RT for all piglets included in this analysis.

Table 2-2. Mean piglet body temperature as measured from rectal temperature at each measurement time. The standard deviation (std) of the mean RT and the mean RT drop from birth are also provided.

Piglet rectal temperature (RT) at each measurement time (°C)										
	0H	15 min	30 min	45 min	1H	90 min	2H	3H	4H	24H
Mean	38.7	34.3	33.6	33.9	34.4	35.6	35.9	36.8	37.4	38.7
Standard deviation	0.88	1.83	2.19	2.71	2.76	3.11	2.73	2.44	1.69	0.81
Mean RT drop since birth*	-	4.4	5.1	4.8	4.3	3.1	2.8	1.9	1.3	0.0

Piglets' mean birth weight: 1.47 ± 0.39 kg
Piglets' sex: 52.5% barrow, 47.5% gilt

* the mean RT drop since birth is the temperature difference between the RT measured at time x and the initial birth RT measured at time 0H. The positive numbers indicate reductions in piglets' RT.

As illustrated in Table 2-2 and Figure 2-2(a), the RT of the piglets dropped immediately and significantly after birth. Starting from a uniform and warm 38.7°C birth RT, a mean temperature drop of 4.4°C occurred in the first 15 min. Most piglets experienced their lowest RT at 30 mins after birth, reaching a mean low temperature of 33.6°C (a 5.1°C average drop since birth). Between 30 to 45 mins after birth, the piglets continued to experience low RT with a slight mean increase of about 0.3°C. Not until one hour after birth did the piglets establish a steady increase in RT (<1°C per hour), and slowly returned to a mean of 37.4°C at 4H after birth, still about 1.3°C lower than their birth RT. Piglets eventually recovered back to their initial RT after 24 h.

Baxter and Edwards (2018) and Pattison et al. (1990) also found a 4 – 5°C reduction in RT during the first 30 min, but only for piglets that failed to suckle. By contrast, a reduced RT was apparent for the majority of neonatal piglets in this study, regardless of their ability to suckle

or not, although the magnitude of RT reduction during the first 30 mins is in agreement with findings revealed in this study.

Curiously, as can be seen from Figure 2-2(a), the ± 1.5 IQR of piglets' RT was larger in the first hours after birth, from 15 min to about 2H post-birth, indicating substantial variation among individuals. Thereafter, the ± 1.5 IQR shrank over time and fell into a very small range at 24H. This agrees the findings reported by Baxter and Edwards (2018), who found that the majority of pre-weaning mortality occurs during the first few hours post birth. Between 15 min to 2H after birth, the number of piglets that fell out of the ± 1.5 IQR (99.3% of the total sample population) increased with time, indicating that additional piglets likely had a hard time to regulate their metabolism and maintain their ideal RT range. Notably, some piglets RT were as low as 24°C for as long as 30 min, which was about an average 14°C drop from their birth RT. At 3H after birth, 13 piglets were still colder than the lower 1.5 IQR. Busija and Leffler (1987) concluded that a 4 – 5°C drop in CBT could result in 40 – 50% inhibition in blood flow and cerebral metabolic rate, which raises a great concern of neonatal piglet's survival (Baxter and Edwards, 2018). At 24H after birth, the number of piglets which fell out of the ± 1.5 IQR decreased, but two piglets continued having trouble getting back to equilibrium body thermal condition. It is of interest to track the status of the piglets that fell out of the ± 1.5 IQR distribution range and look for trends (for example, do piglets with lower RT at birth always

struggle in the lower quartile range and take longer than others to return to normal RT; or, how quickly a piglet finds milk and a heat lamp within the pen).

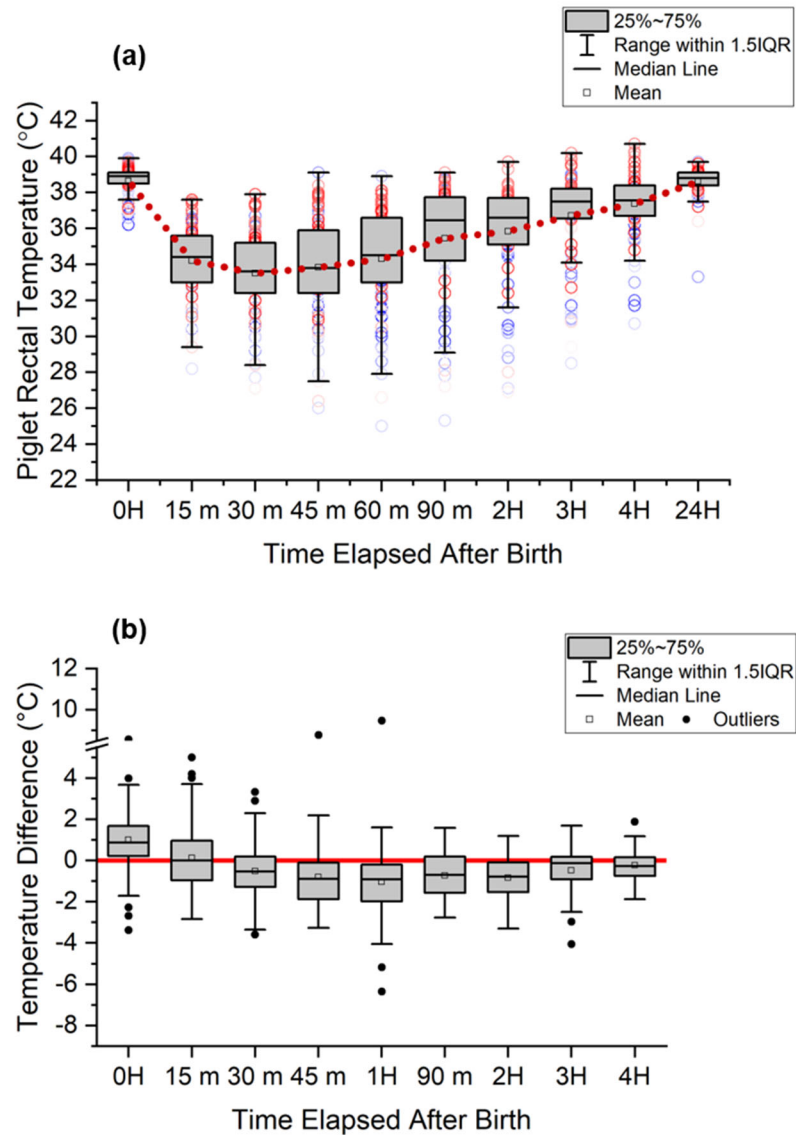


Figure 2-2. Change of the (a) rectal temperatures and (b) temperature differences (piglets' rectal temperature minus corresponding maximum back of ear surface temperature) with time for 99 neonatal piglets after birth. The rectal temperature of a piglet is represented by a colored hollow circle. Box-whisker plots are created for each measurement time (0H, 15 min, 30 min, 45 min, 1H, 90 min, 2H, 3H, 4H, and 24H) to illustrate the temperature distribution. Mean, median, ± 1.5 IQR are also shown. Means are connected by red dotted line in (a), and a reference line at 0°C difference is provided in (b).

While all piglets exhibited a drop in RT after birth, those born with a lower rectal temperature are of particular concern. Identifying such individuals via surface temperature readings would be of value and might be used to improve farrowing management with actions such as providing extra care to piglets. Douglas et al. (2014) demonstrated the importance of optimum birth weight to achieve optimum piglet survival and subsequent growth. For piglets with a birth weight under 1.8 kg, there was a higher chance that they would face greater challenges to achieve optimum weaning weights.

2.3.2 Piglet body temperature model from surface temperature measurement

Thermal information extracted from a total of 609 thermal images from 99 neonatal piglets were used for the modeling effort. The distribution of temperature differences (piglets' rectal temperature minus the corresponding maximum back of ear surface temperature) with time is shown in Figure 2-2(b). Box-whisker plots were created for the temperature difference at each measurement time (0H, 15 min, 30 min, 45 min, 1H, 90 min, 2H, 3H, 4H, and 24H). Mean, median, ± 1.5 IQR, and outliers identified are also shown. A reference line at 0°C is made available on the plot. Table 2-3 presents a summary of the number of observations, the mean, standard deviation (std), standard error of the mean (SEM), and the p-value for the paired t-test (mean temperature difference equals zero) are included.

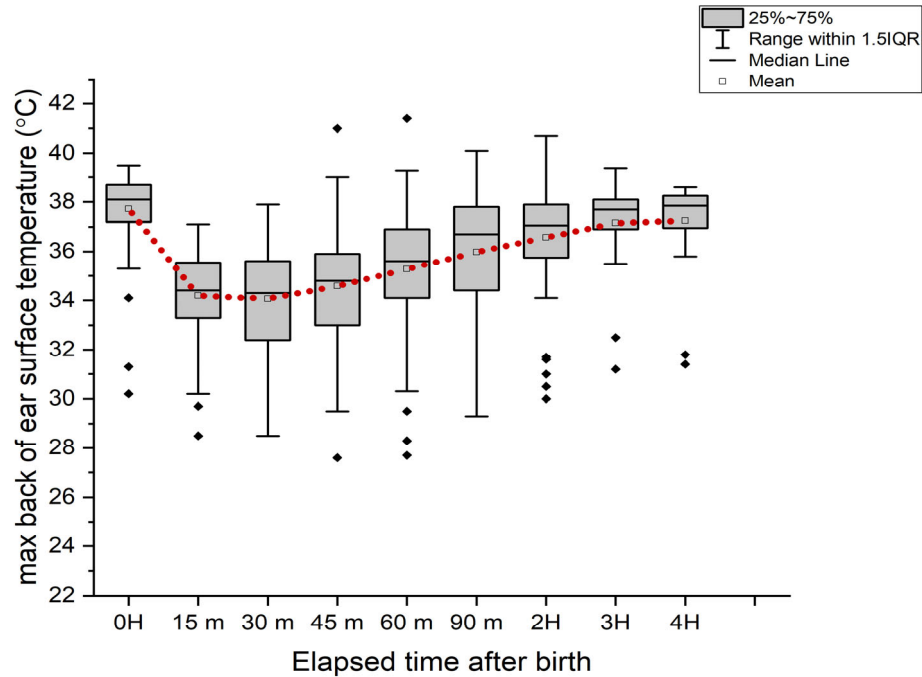


Figure 2-3. Change of piglets' maximum ear temperature with time for 99 neonatal piglets after birth. Box-whisker plots are created for each measurement time (0H, 15 min, 30 min, 45 min, 1H, 90 min, 2H, 3H, 4H, and 24H) to illustrate the temperature distribution. Mean, median, ± 1.5 IQR and outliers are also shown. Means are connected by red dotted line.

Table 2-3. Summary results of a paired t-test of piglets' rectal temperature and the corresponding maximum ear temperature at each measurement time from 0 h to 4 h after birth.

	Temperature difference* at each measurement time									
	0H	15 min	30 min	45 min	1H	90 min	2H	3H	4H	
N	91	88	89	83	81	58	52	23	28	
Mean (°C)	1.01	0.12	- 0.51	- 0.76	- 1.02	- 0.06	- 0.83	- 0.48	- 0.23	
Standard deviation (°C)	1.67	1.67	1.40	1.67	1.90	5.19	1.13	1.24	0.85	
SEM (°C)	0.17	0.18	0.15	0.18	0.21	0.68	0.16	0.26	0.16	
P-value	< 0.001	0.4905	< 0.001	< 0.001	< 0.001	0.9319	< 0.001	0.0774	0.1679	

* The temperature difference is calculated using the piglets' rectal temperature minus the corresponding maximum ear temperature at each measurement time.

At birth (0H), on average, the piglets' rectal temperatures appeared to be greater (1.0°C) than their maximum ear surface temperatures, probably from evaporation at the ear surface. After 15 min, this temperature difference became minimal (0.12°C), with no significant difference evident from the paired t-test performed (P = 0.4905). Starting about 30 min after

birth, RT was always cooler than the maximum ear temperatures extracted from the thermal images, and this trend was consistent throughout 4H after their birth. While not measured, this suggests sufficient vasodilation for blood flow to the ear was able to elevate temperature above the RT. At 1H after birth, the difference between the RT and maximum ear temperature was -1.0°C , which was the greatest difference observed throughout the first 24H postnatal stage. Curiously, at 90 min the difference was not significantly different ($P = 0.9319$) but there was a substantial larger std than at other measurement times (5.19 vs $0.85 - 1.90^{\circ}\text{C}$). Subsequently (90 min to 2H after birth), an approximate 0.8°C drop was seen, resulting in a -0.83°C difference between the RT and the maximum ear temperature; this temperature difference decreased in the next two hours (3H and 4H) of measurements. The means of RT and maximum ear temperature did not differ significantly at 3H or 4H time measurement ($p = 0.0774$ and $p = 0.1679$, specifically), although this may be due to the small number of observation pairs analyzed.

This observation of temperature difference between the piglets' RT and maximum ear temperature does not directly provide information as to which piglets were having trouble maintaining their RT in the desired range. As indicated by Figure 2(a), a minimum 2H was required by most piglets to establish a RT recovery that was above 36°C on average, which was approximately 3°C lower than their birth RT. During this stage, the temperature difference trend also explained the phenomena as the piglets were having unpredictable changes in the difference between their RT and their maximum ear temperatures. After the first 2H, the piglets were able

to manage their body temperature, evident by improvements can be seen in both the change of RT (Figure 2-2) and the temperature difference trend, with steady increased RT, a reduced temperature difference between the RT and maximum ear temperature, and a smaller standard deviation.

The maximum ear surface temperature alone was not an accurate model to predict the piglets' RT, because of the variability noted across individuals. However, it may provide a rough estimate given that the largest difference was approximately 1°C. However, caution should be taken if this is applied in practice because even though the temperature difference between the two parameters is smaller than 1°C for all the measurement times, the wide distributions were still evident in Figure 2-2(b). More parameters, such as the room temperature, RH, web bulb temperature, and evaporative potential may provide a more accurate model to predict the piglets' core body temperature.

2.3.3 Prediction model development and assessment

A summary of descriptive statistics of the environmental data for each piglet measurement time including the mean (\pm std) of the dry bulb air temperature, relative humidity (RH), wet bulb temperature, and the wet bulb temperature depression (WBD) is provided in Table 2-4.

Table 2-4. Descriptive statistics, including the mean (\pm standard deviation, std), the minimum (Min), and the maximum (Max) value of environmental measurements in the farrowing room, including the dry bulb air temperatures, relative humidity, wet bulb temperatures, and the wet bulb depression for each measurement time between 0 h and 4 h after piglets' birth.

Farrowing room environmental information at each measurement time									
	0H	15 min	30 min	45 min	1H	90 min	2H	3H	4H
Dry bulb air temperature (°C)									
Mean	23.4	23.5	23.5	23.5	23.5	23.6	23.6	23.7	23.8
std	0.97	0.93	0.78	0.78	0.82	0.93	0.97	1.05	1.17
Min	19.7	19.8	21.8	21.8	21.8	21.9	21.8	21.8	21.7
Max	25.1	25.2	25.0	25.0	25.1	25.1	25.2	25.8	26.0
Relative humidity (RH, %)									
Mean	47.1	47.0	46.6	46.6	46.5	45.4	44.6	43.6	41.1
std	10.3	10.7	10.3	10.1	9.35	9.11	8.88	7.79	7.12
Min	29.8	28.1	29.8	31.0	31.6	31.0	31.0	30.6	28.4
Max	66.3	69.3	69.3	69.3	63.8	66.6	66.2	61.8	52.1
Wet bulb temperature (°C)									
Mean	16.1	16.2	16.1	16.1	16.1	16.0	15.9	15.8	15.5
std	2.03	2.08	1.96	1.91	1.81	1.77	1.80	1.78	1.84
Min	10.9	10.5	13.0	13.0	13.3	13.2	13.2	12.4	11.9
Max	20.3	20.8	20.8	20.8	19.7	19.4	20.3	19.6	18.4
Wet bulb temperature depression (°C)									
Mean	7.3	7.3	7.38	7.4	7.4	7.6	7.7	7.9	8.3
std	1.59	1.64	1.60	1.58	1.47	1.46	1.42	1.19	1.04
Min	4.4	4.1	4.1	4.1	4.9	4.4	4.5	5.2	6.4
Max	10.0	10.0	10.0	10.0	9.9	10.4	10.4	9.8	10.0

Table 2-4 demonstrates that the environmental conditions of the farrowing facility were maintained relatively stable during the time of this study. Pigs of different breed, production stage, and age require different thermal neutral conditions, for example, the desired room temperature required by sows in the gestation room (18 – 21°C) and by piglets in farrowing room (32 – 35°C) is substantially different (Zhang and Xin, 2000). Although it is the farm managers' decision to manage the environmental conditions within each type of swine facility, it is commonly suggested that a relatively low temperature range of 18 – 22°C should be maintained in farrowing facilities to provide comfort conditions for the sows, and supplement the

piglets with supplemental heating methods such as heat lamps and mats (Lay et al., 2002; Xin et al., 1997; Zhang and Xin, 2000; Zhou and Xin, 1999). For this study, the overall average temperatures for all the measurement time intervals were smaller than 23.8°C with an average RH of below 50%. Our records showed that the air temperatures were slightly greater than the recommended range, however, since the temperature and RH dataloggers were attached onto the farrowing crate for more representative measurements for the sows, it was possible that the heat lamps in the farrowing crate had some influence. In addition, because the environmental conditions in the farrowing facility were maintained relatively constant year-round, it brought challenges and limitations regarding development of prediction models and their application.

The data and linear model regression assessed is shown in Figure 2-4. For Figure 2-4, the 95% confidence intervals and the 95% prediction intervals of the dependent variables are shown on the plot. A statistical summary for the prediction model, including adjusted R-square, standard error calculated for the model (represented by the root-MSE), and the fitted equation with estimated coefficient values are provided in Table 2-5.

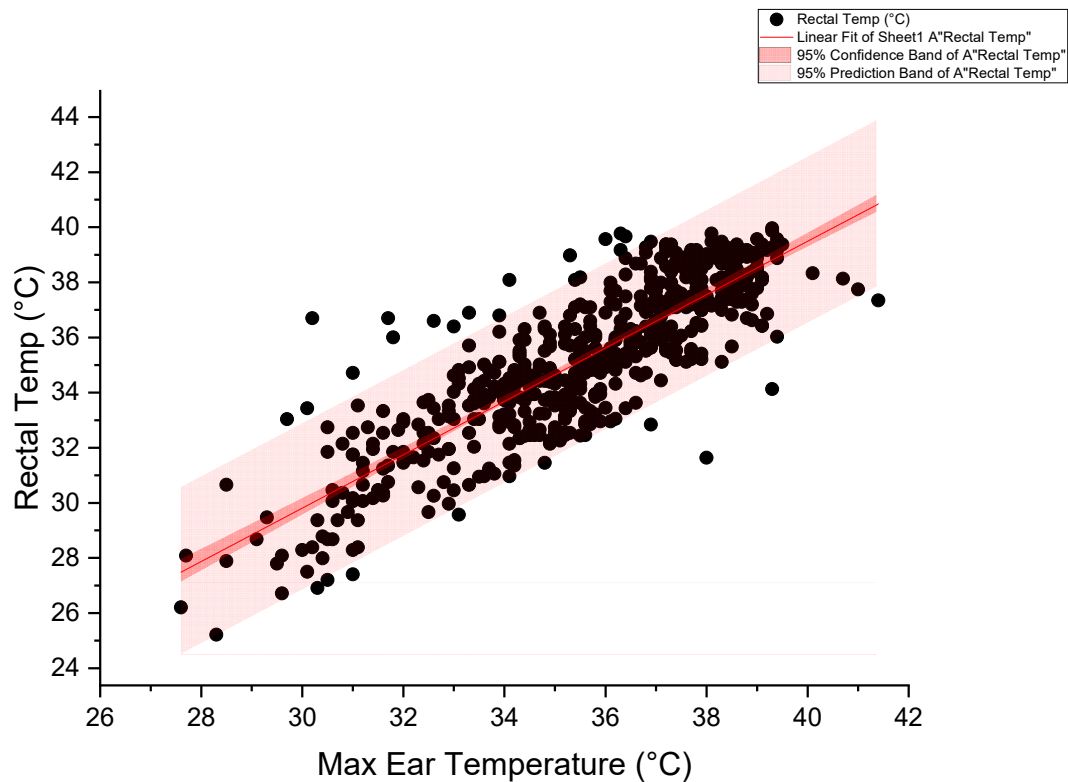


Figure 2-4. Linear regression model fitted between maximum ear temperature (x-axis) and rectal temperature (y-axis). Each dot represents a rectal temperature and corresponding maximum ear temperature combination for a piglet. The 95% confidence band and the 95% prediction band of the piglet rectal temperature from maximum ear temperature are shown on the fitted plot.

Table 2-5. Statistical summary of the three models fitted for predicting the body temperatures for piglets housed in farrowing facilities with typical environmental conditions. The adjusted R-square, standard error of the model as represented by the root-MSE, dependent variable, independent variables in the model, and fitted equation with estimated coefficient values are provided.

Model Description	Figure	adj. R-square	Root-MSE (°C)	Dependent variable	Independent variable(s)	Fitted equation with estimated coefficient values*
Original linear	2-4	0.71678	1.53	RT (y)	ear temp (x)	$y = 0.7625 + 0.9682x$
Refined linear	2-5	0.80981	1.24	RT (y)	ear temp (x)	$y^{**} = 1.0204x$

* All coefficients included in the equations are significantly different than 1, and all intercepts listed are significantly different from zero.

** The estimate intercept value is -1.53854 ($p = 0.12135$), not statistically different from zero, thus was eliminated from the fitted equation.

From Figure 2-4, a linear relation is evident between maximum ear temperature and corresponding RT, but with considerable variability induced by individual piglets. The adjusted R-square is 0.72, with a 1.5°C standard error of the predicted linear model as represented by the root-MSE. The relatively poor fit may be because the RT and maximum ear temperature at all piglet measurement times (0 – 24 h after birth) were included when fitting the model, which introduced the uncontrollable variability due to the notable significant drop of piglets' rectal temperatures in the first 45 min of their life. The prediction interval band showed that the majority of the data points were within the 95% prediction range, except for a few measurements showed high ear surface temperature but relatively low rectal temperature, or high rectal temperatures but low ear surface temperatures. This may result from the manual rectal temperature measurement process and the birth fluid often found covering the piglets' body surface.

Piglets covered with birth fluid was especially evident during the first 30 – 45 min during these piglets' life, where a spike in the generated surface is noted for values of WBD greater than 8°C. The required time for each piglet to reach a reasonably dry skin was not quantified in this study but based on our observations this process usually lasted between 30 – 45 min for most piglets, and the majority of the piglets' skin were notably drier after the first 45 min, compared to when they were first born. Wet skin surfaces and/or higher WBD, indicating higher evaporation potential, may be responsible for further reducing both ear surface temperature and rectal

temperature of a piglet, and thus made it more challenging for any model to accurately predict the piglet RT from the surface temperature and environmental factors.

The linear regression model was developed within a narrow and very limited range of input parameters due to the relatively constant environmental conditions maintained in a typical farrowing facility (18 – 21°C target temperature all year-round) and the small ranges of body or surface temperatures of pre-weaning piglets, which ranged from 34.3 to 38.7°C for rectal temperatures, and approximately 33 to 40°C for maximum ear temperatures, respectively, based on the results obtained from this study. In addition, every step and/or component involved in the process could introduce variation of the data recorded, including rectal temperature sensor and datalogger response time, the response time of the thermal camera, the time spent on taking extra thermal images due to some piglets' vigorous movements, and the time needed for the data acquisition team during data collection and transition to another crate if two litters were born during the same times. All these factors can become a source of uncertainty and impacted the accuracy and reliability of the non-linear models that have environmental measurements or time functions being independent variables.

To reduce uncertainty brought by environmental measurements and the time function and to explore in a model that would apply to a larger group of piglets (i.e. not limited to neonatal piglets), a refined linear regression was performed to obtain a more precise model practical for producers. For this improved model, data for older and drier piglets were selected by excluding

data from 0 H to 30 min after birth, for which we assumed the skin of most piglets remained wet. The data for the remaining RT measurements were linearly regressed against the corresponding maximum ear surface temperature. Outliers with a temperature difference greater than 6.5°C (N = 3) which likely resulted from measurements error or the majority of piglet's ears being covered by amniotic fluid, were also excluded from the regression analysis. The resultant regression was:

$$\text{Rectal temperature} = 1.0204 (\text{maximum ear temp}) - 1.5385 \quad (2-1)$$

Results and the summary statistical information of the refined linear model (Equation 2-1) are shown in Figure 2-5 and Table 2-4. The refined linear model demonstrated an improved adj. R-square value of 0.81 and a 0.3°C reduction in the standard error of the model (= 1.24°C), with narrower 95% prediction intervals shown on Figure 2-5 but capable of covering 98% of the measurement pairs included in the model. The results suggested that the improved model can provide a reasonably accurate estimate of a pre-weaning piglet's rectal temperatures simply from measuring their maximum back-of-ear surface temperatures.

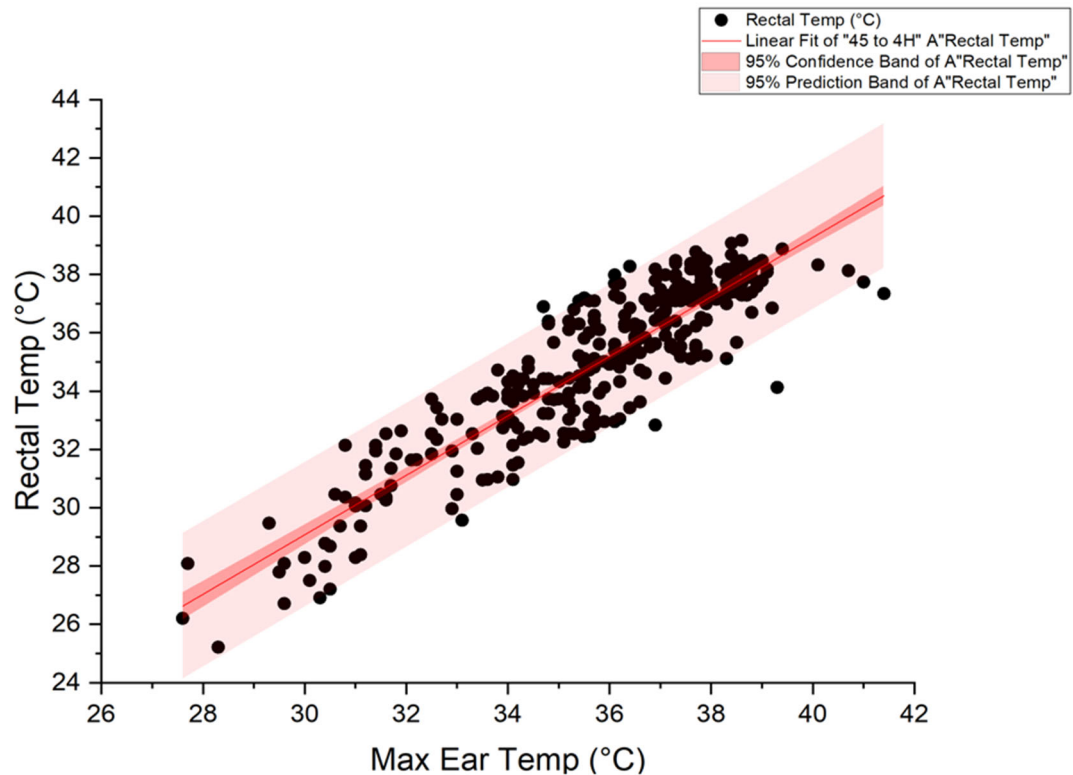


Figure 2-5. Refined linear regression model fitted between maximum ear temperature (x-axis) and piglets' rectal temperature (y-axis). Each dot represents the rectal temperature and corresponding maximum ear temperature for a piglet. The 95% confidence band and 95% prediction band of the piglet rectal temperature from maximum ear temperature are shown on the fitted plot.

Utilizing the refined linear model is straightforward, requiring only that a maximum ear surface temperature is collected. From a practical application perspective, a close estimate of a pre-weaning piglet's rectal temperature can be obtained by multiplying their maximum back-of-ear temperature taken when dry by 1.0204 (Equation 2-1). The predicted rectal temperature has an uncertainty of about 1.2°C.

However, this analysis was done with 99 piglets from 9 litters, which would be considered a very small sample size in current large swine operations that fit into large CAFO (confined animal feeding operations) categories. Except for the improved linear model that

excluded measurements taken when piglets' skin remained wet. More research to develop more accurate body temperature and surface temperature measurements, and automatic data collection is needed. From a precision livestock farming perspective, instead of clumping information from a group of piglets and developing a single model, it may be beneficial and perhaps more appropriate to develop a predictive model for each piglet, which allows better prediction for a specific piglet from select initial measurements, and monitor the individual's body temperature precisely during the entire pre-weaning stage.

2.4 SUMMARY AND CONCLUSIONS

The rectal temperatures of the piglets dropped immediately after birth. A mean drop of 4.4°C was recorded for all piglets in the first 15 min. The piglets experienced the lowest rectal temperature at 30 min after birth, reaching a mean low temperature of 33.6°C, an approximate 5°C drop since birth. After the first hour post-birth, the piglets started to establish a steady increase in their RT and eventually recovered back to their initial RT at birth after 24 h.

A paired student's t-test was performed for the temperature difference between piglets' RT and the corresponding maximum ear temperature. The biggest mean difference was 1°C at 0H and -1°C at 1H after birth. However, a wide distribution of the temperature difference was evident (0.85 to 5.19°C standard deviation observed across all time of measurements).

Results indicate that the first 2H can be the most critical time for neonatal piglets. Options for potential drying methods and abatement means may be beneficial for all piglets to

more quickly establish robust metabolism, especially during periods of larger WBD. The maximum ear surface temperature alone is not an accurate model to predict the piglets' body temperature overall times after birth.

Linear regression models were developed and assessed. The refined linear regression model provided a more reliable prediction of piglet RT. Use of the refined regression model can provide a direct prediction of the RT once the piglet ear surface temperature is given, with an uncertainty of about 1°C, thus can be used as a convenient prediction tool of rapid estimation of piglet RT under typical farrowing conditions.

2.5 ACKNOWLEDGMENT

Funding of this research project was supported by The Maschhoffs, LLC. The author would like to thank faculty and students in department of Animal Sciences, staff members in the Swine Research Center, University of Illinois at Urbana-Champaign, and undergraduate student Thais Maurin of the University of Sao Paulo—Pirassununga, Brazil for her effort in assisting in data collection and thermal image analyses.

CHAPTER 3 DESIGN AND PERFORMANCE ASSESSMENT OF A COOLED PERCH SYSTEM TO REDUCE HEAT STRESS IN LAYING HENS^{2 3}

3.1 INTRODUCTION

High ambient temperature, especially if it creates acute heat stress, is one of the most detrimental environmental stressors for the global poultry industry. Heat stress seriously compromises the welfare of laying hens in commercial egg production, negatively affects their performance and egg production and can cause death, leading to substantial economic losses (Ebeid et al., 2012; Felver-Gant et al., 2012; Lara and Rostagno, 2013; Mack et al., 2013; Mignon-Grasteau et al., 2015; Zulkifli et al., 2009). According to St-Pierre et al. (2003), hen mortalities climbed to 10% in the Midwest region due to heat events during the summers of 2011 and 2012. To alleviate the deleterious effects of heat stress, the industry regularly alters feed ration composition during chronic heat stress periods, and alternative feed additives have been investigated (Koelkebeck et al., 2014).

² Xiong, Y., W. Zheng, R.S. Gates, K.S.O. Rocha, J. Hu, M.M. Makagon, P.Y. Hester and H.W. Cheng. 2016. Cooled perch system performance for heat stress trials on laying hens: Year 2. Paper No. 16-2460523, *Annual International Meeting of the ASABE*, Orlando FL. 17-20 July. St. Joseph, MI: ASABE.

³ Xiong, Y., R.S. Gates, J. Hu, K.S.O. Rocha, M.M. Makagon, P.Y. Hester and H.W. Cheng. 2015. Performance Assessment of Cooled Perch System for Heat Stress Trials in Egg Laying Production: Year 1. Paper No. 152183776. *Annual International Meeting of the ASABE*, New Orleans, LA. 26-29 July. St. Joseph, MI: ASABE. <https://doi.org/10.13031/aim.20152183776>

Alternative cooling methods exist in other livestock housing systems that have not been widely employed in commercial egg facilities. Examples include zone cooling and drip cooling for pigs, and sprinkler and fan cooling for dairy or pigs in higher humidity locales. Physical cooling of the poultry, their environment, or both, are also options. A simulation assessment suggested that implementation of “heat abatement” technology would reduce annual economic losses of the U.S. layer industry from \$98.1 to \$61.4 million by using an economically optimal abatement method (St-Pierre et al., 2003). To date, cooling methods adopted in the poultry industry include increased convection with fresh high-velocity fresh air from tunnel ventilation or other means (Bottcher et al., 1995), and evaporative cooling systems that use cooling pads and/or fogging nozzles (Bell et al., 2002; Bottcher et al., 1991; Gates and Timmons, 1988; Gates et al., 1991a; Gates et al., 1991b; Timmons and Gates, 1988). Direct wetting of broilers and layers is rarely used due to challenges of implementation, although investigations have shown some promise (Chepete and Xin, 2000; Ikeguchi and Xin, 2001; Mutaf et al., 2008; Yanagi et al., 2002). Other methods have been topics of research, including surface wetting from high pressure fogging systems and partial surface wetting for broilers and layers (Liang et al., 2014; Mutaf et al., 2008; Mutaf et al., 2009; Wolfenson et al., 2001; Yanagi et al., 2002), drinking water temperature adjustment (Xin et al., 2002) and cooled perches for broilers and broiler breeders (Muiruri, 1989; Muiruri and Harrison, 1991; Reilly et al., 1991; Zhao et al., 2012; Zhao et al., 2013a).

Cooled perches present an intriguing opportunity for heat removal from birds under heat stress, and have been investigated for broilers (Muiruri, 1989; Muiruri and Harrison, 1991; Reilly et al., 1991; Zhao et al., 2013). The provision of a cooled perch, in which chilled water is circulated through a conventional galvanized perch pipe passing through the laying hen space offers the potential for improved welfare and performance during both acute and chronic heat stress events. The cooled perch is amenable to both natural and mechanically ventilated systems, provides a positive welfare aspect by providing birds with a means to express their natural perching behavior, and benefits to their skeletal health (Hester et al., 2013; Hester et al., 2014; Lay et al., 2011; Tactacan et al., 2009). In particular, alternatives to conventional cages such as enriched colonies and vertical aviaries that provide laying hens with more space and varying environmental features such as nest boxes, scratch pads and perches may be readily modified to incorporate a cooled perch into the design. Cooled perches can provide birds with an alternative means of heat loss via conduction from feet to perch, and since bird legs are highly vascularized, this additional heat loss has the potential to offset problems related to compromised ventilation. Previous studies estimated that up to 25% of bird metabolic heat produced can be lost through chicken's legs and feet because of an efficient vascular arrangement (Hillman et al., 1982; Hillman and Scott, 1989). Studies showed that broiler breeders (parents of the broiler meat-type chicken) housed on litter floors and given access to cooled perches during 3 wk of 35°C ambient temperature showed improved egg production, hatchability, and feed consumption as compared to broiler breeders given non-cooled or air-equilibrated perches (Muiruri, 1989; Muiruri and

Harrison, 1991). Zhao et al. (2013) reported broiler chickens showed increased weight gain and feed efficiency in high ambient temperatures if provided with cooled perches. However, cooled perches for laying hens have not been widely studied due to challenges with the design and implementation of the system including capital cost and the lack of research data on bird production performance and behavior changes.

This chapter describes a multi-year study using a perch system to examine the effects of water-chilled perches as a cooling alternative on hen performance, plumage condition, foot health, physiological parameters on caged White Leghorn hens exposed to acute and cyclic heat stress events (Cheng et al., 2013; Hester et al., 2013). The results of hens housed in cooled perch treatment (CP) were compared to that of air perch (perches open to room air, AP) and no perch (control). Information regarding the hen strain, age, experimental design, data collection protocols, and cooled perch effects on hen performance and foot health are described in (Hu et al., 2016); Hu et al. (2019a); cooled perch effects on physiological parameters and foot health for hens exposed to cyclic heat stress are described in (Hu et al., 2019b); and effects on induced molting of White Leghorn hens previously exposed to heat stress are described in (Hu et al., 2019c). Results of these studies indicated that cooled perches showed promising benefits to White Leghorns with regards to performance, plumage condition, foot health, physiological parameters, and post-molt egg production. During cyclic heat episodes, CP hens had higher egg production ($p < 0.0001$) and feed consumption ($p < 0.04$) than that of AP or control hens. CP

hens had higher body weight at 35 and 72 wk of age ($p_{\text{treatment} \times \text{age}} < 0.05$) and a reduced cumulative mortality ($p = 0.02$) than control hens but not AP hens. Heavier egg weights ($p < 0.0001$), higher breaking force ($p < 0.0001$), greater eggshell percentage ($p_{\text{treatment} \times \text{age}} < 0.05$) and eggshell thickness ($p_{\text{treatment} \times \text{age}} < 0.05$) were observed from CP hens than those from AP or control hens. No difference was found for nail length, feet hyperkeratosis and overall feather score (Hu et al., 2019a). During hens age 21 – 35 wk, CP hens demonstrated lower rectal temperature ($p = 0.02$), and lower heat shock protein (HSP) 70 ($p = 0.04$) than the control hens but not the AP hens. During hens aged 73 – 80 wk, CP hens had lower rectal temperature ($p = 0.02$) and lower circulating heterophil to lymphocyte (H/L) ratio. The levels of plasma levels of triiodothyronine (T3) and T3/T4 (thyroxine) ratio from CP hens were higher ($p = 0.002$ and $p = 0.0006$, respectively) than the control hens, but not AP hens. The CP hens had greater packed cell volume than AP hens ($p = 0.02$) but not control hens. No difference was found for Cytokines or IgY levels (Hu et al., 2019b). Makagon et al. (2015) summarized that for the acute heat episode, CP hens utilized the perch at a higher frequency ($p < 0.001$) at all observation times than the AP hens. An induced molt study was conducted with the same group of hens after the cyclic heat episode to examine the efficacy of the induced molt on hen production and physiological responses (Hu et al., 2019c). Results showed that at the end of molt, CP hens had higher feed consumption and greater body weight loss, lower heterophil/lymphocyte ratios ($p < 0.05$). CP hens also had better breast feather scores than AP hens but worst vent plumage ($p < 0.05$).

Bird's feet play an important role in whole-body thermoregulation (Martineau and Larochelle, 1988). The feet and shanks of chickens are effective conductors of heat because they are un-feathered, have little muscle tissue for heat production, and are richly vascularized. In hot weather, the venous return in the limb is through superficial veins, so that the blood is cooled on its return to the heart. The arterial blood entering the limb is not cooled until it reaches the skin's surface (Bell and Rome, 1984; Hillman et al., 1982; Midtgård, 1981; Shinder et al., 2007; Steen and Steen, 1965). Blood flow rate through chicken's feet is highly variable and dependent on environmental temperature. Blood flow rates increase in chicken's feet with surrounding air temperature rises (Hillman et al., 1982). Chickens can lose more than 25% of their metabolic heat through their feet at thermoneutral temperatures (Hillman and Scott, 1989). If a thermally cooled perch can be economically developed as a part of existing and developing enriched colony cage systems, it may prove beneficial for egg production in hot climates. However, existing research for the chicken feet area were mostly conducted in late 80s or 90s (Hillman et al., 1982; Muiruri, 1989; Albright, 1990), and are most likely outdated given the evolution of poultry genetics, production, and the technology. ASAE standards (ASAE D321.2) reported weight and height reference values for commercial broilers, however their footpad area was not listed. The development and use of a mathematical model could be an important tool to improve system design evaluation and contribute to our understanding of well-being conditions of poultry. Thus, the challenge remains for robust system design to provide adequate cooling benefits to laying hens including practical issues of management and maintenance.

With the substantial positive benefits provided by the experimental cooled perch system, it is important to document the engineering design and to evaluate the system performance in the merit of future investigation and perhaps larger scale application in the industry. The objectives of this chapter are:

- 1) to document the design and instrumentation of the cooled perch system;
- 2) to evaluate perch performance based on water mass flowrate, loop temperature rise, and system net heat gain;
- 3) to quantify the heat transfer components including convective and radiative heat gains using the cooled perch performance data;
- 4) to provide design information for larger scale application; and
- 5) to update the estimated value of laying hens' footpad area.

3.2 MATERIALS AND METHODS

3.2.1 Cooled perch system design and instrumentation

3.2.1.1 Cooled perch system design

A prototype cooled perch system equipped with thermostatic control and environmental monitoring instruments was developed to assess the cooled perch effects on heat dissipation of laying hens during heat stress. Key parameters of the design included the ability to maintain a perch temperature that provides potential for conductive cooling of bird feet, and a reliable means of controlling the system and monitoring its performance.

The caging system consists of a single bank of 3 cage decks, with two cages per deck. Each cage measured 76 cm W x 52 cm D x 48 cm H (Figure 3-1). Holes were cut into each end wall and the center partition wall of each deck to allow for passage of two pieces of galvanized perch pipe (measured 33.8 mm OD and 28.5 mm ID), functioned as one supply pipe and one return pipe that forms a complete perch loop with two 90° elbows for each deck. The perch loop on each deck was measured to be approximately 6.1 m (Xiong et al., 2015).

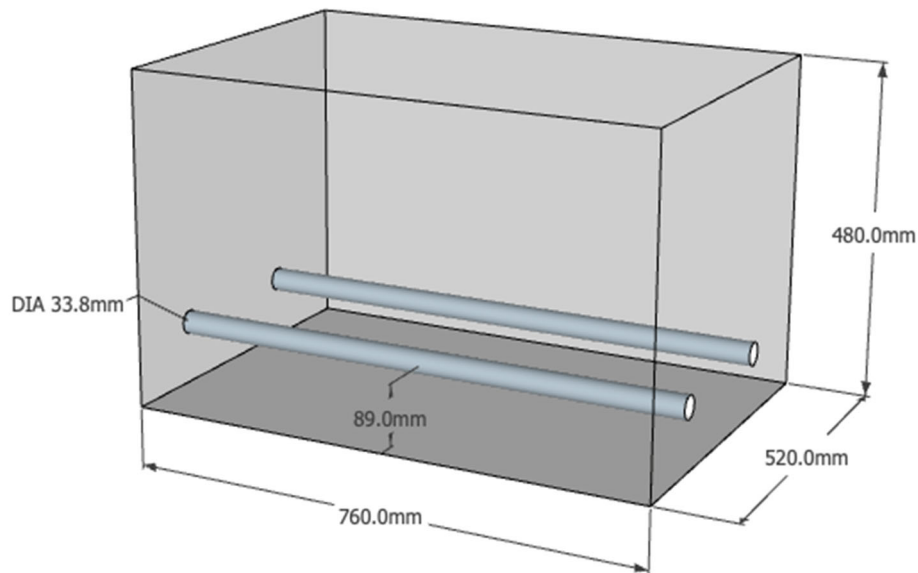


Figure 3-1. Cage dimensions and perch placement. The designs of cages and perches are identical to the study of Hester et al. (2013). Perch height for both perches is 8.9 cm (3.5 in) from the cage floor so that eggs can roll to the collection area and provide enough heights for the birds. In the experiment, two cages formed a single deck.

Chilled water was pumped to the caging unit on demand from a common vertical manifold constructed of a 13 cm ID PVC pipe, 1.70 m tall. Chilled water returned to the common manifold via a return line, which was 1.2 m above the supply outlet of the manifold. There was a

pump (model 006-B4-15 Cartridge Circulator, nominal flow 30 L/min at 1 m, 43 L/min at 0 m, Taco Inc., Cranston, RI, USA) for each deck that was activated when cage air temperature exceeded a set point temperature. The chilled water manifold volume was cooled by an independent loop consisting of a fourth pump and continuously circulating water between the manifold and a water chiller (model ER-101y, rated cooling capacity 0.6 L/min at 22°C temperature drop, ELKAY Manufacturing Co., Oak Brook, IL, USA). This water chiller had an independent thermostat set at approximately 10°C during operation. All exposed sections of pipe outside the cages and manifold were heavily insulated to conserve energy and to minimize potential for condensation.

3.2.1.2 Physical properties of perch material

The cooled perch was made of commercial galvanized steel pipe, which had an inside diameter (d_i) of 0.0285 m, an outside diameter (d_o) of 0.0338 m. The thermal conductivity of the galvanized steel k_s is 52 Wm⁻¹K⁻¹ (Bergman et al., 2011); and the solar emissivity of galvanized steel (old) is 0.88 (EngineeringToolBox, 2001).

We assume the inner surface of the galvanized steel pipe is smooth ($\frac{\epsilon}{D_o} = 0.000005$), where ϵ is the roughness of the pipe surface (mm), and D_o is the outside diameter of the perch pipe (mm). The pressure drop that occurs inside the perch pipe in conjunction with the friction factor was estimated using the smooth pipe curve from the Moody diagram (ASHRAE, 2017a).

The friction loss caused by the 90° elbows present in the perch loop on each deck was quantified in terms of equivalent length of perch pipe. For schedule 40 PVC pipe with nominal size of 2.5 cm (1 in. PVC), the equivalent length for the standard fittings used on each deck was 0.8 m (AetnaPlastics, 2015). Thus, the total equivalent length for the perch loop on each deck was 7.7 m, resulting in a total of 23.1 m equivalent length for the perch loop per bank.

3.2.1.3 Environmental measurements and instrumentation

Instrumentation overview

A wireless monitoring system was used to assess the thermal environment inside the cages. The system consisted of instruments for measuring air temperature and relative humidity (RH) near the ceiling at the partition between the two cages on each tier, water temperatures of the supply and return perches containing chilled water, and air temperature of the perches containing air with no circulating water (AP). In addition to measuring the cage environment, room conditions (air temperature and RH) were recorded by a wireless data logger at the same sampling rate. For each tier of the CP cages, an air temperature sensor was installed for the controller to activate water circulation. A summary of the instrumentation used in this study is presented in Table 3-1. The placements of each sensor within the cage are demonstrated in Figures 3-2 to 3-4. The data acquisition center was located outside of the room, connected by a wireless receiver.

Table 3-1. Instrumentation summary. Environmental responses were measured with a set of measurements to represent the cage environment by collecting air temperature and RH of the cages, and water/perch temperature experienced by the birds.

Measurement	Location	Model, Manufacturer	Operating Frequency
Air temperature/RH	CP / AP	ZW-007, Onset Computer	1 minute
Air temperature/RH	CTRL / Room condition	ZW-003, Onset Computer	1 minute
Perch temperature	CP / AP	TH-44031-1/8NPT-80, OMEGA	1 minute
Air temperature	Controller	ON-405-Stripped, OMEGA	1 minute
Relay unit	Relay	URM-400, OMEGA	1 minute
Controller	Controller	CN1514-TH, OMEGA	1 minute
Receiver	Outside	ZW- RCVR, Onset Computer	2 minutes

Cage air temperature and RH measurements

For data recording and collection, wireless data loggers with either a built-in data node and 2 analog channels (ZW-007) or one built-in data node (ZW-003, Onset Computer Corporation, Bourne, MA, USA) were selected to record the air temperature and RH. The ZW-007 temperature/RH probe operates from -40 to 70°C and 0 to 100% RH with a typical accuracy of $\pm 0.21^\circ\text{C}$ and ± 2.5 to 3.5%. The ZW-003 temperature/RH node operates from -20 to 50°C and 5 to 95% RH with a typical accuracy of $\pm 0.21^\circ\text{C}$ and ± 2.5 to 3.5%. Both ZW-007 and ZW-003 data nodes were configured to record data every 1 minute and deliver data to the receiver every 2 minutes.

Water temperature measurements

Nine pipe-plug thermistor probes (TH-44031-1/4NPT-80, 10 k Ω , Omega Engineering, Stamford, CT, USA) were used to measure the perch water or air temperatures. The thermistor probes operate from -80 to 75°C with $\pm 0.1\%$ accuracy (presumably full-scale, or about 0.8°C) and 0.1°C interchangeability. Before sensor installation, each thermistor pipe-plug probe was

soldered with a 2.5mm stereo plug for compatible connection with ZW-007 datalogger. A voltage divider was created by soldering a 10 k Ω resistor between the thermistor positive lead and the center tap of the stereo plug for direct temperature signal recording. Sensors were threaded into tees mounted on supply and return lines of the cooled perch. The perch water/air temperatures were recorded by ZW-007 loggers and the wireless data acquisition system.

Cooled perch control system

The thermostatic actuation of the chilled water pump for each CP line was accomplished using a multi-zone controller (model CN1514-TH, Omega Engineering, Stamford, CT, USA). Chilled water line pumps were turned on when air temperature at the center partition between the two cages (one per tier) exceeded a set point temperature programmed into the controller. Air temperature was measured using a thermistor with a protective assembly (ON-405, 2252 Ω , Omega Engineering, Stamford, CT, USA) rated at $\pm 0.5^{\circ}\text{C}$. Water circulating pumps were activated via a relay module (model Relay-URM-400, 4 electromechanical relays rated at 15A SPDT, Omega Engineering, Stamford, CT, USA) connected via serial interface to the controller.

3.2.1.4 Data quality assurance

All sensors deployed in this study were checked for accuracy and, if needed, calibrated prior to environmental monitoring. The wireless data nodes (ZW-007 and ZW-003) for cage air temperature and RH measurements were spot checked over the range 20 to 45 $^{\circ}\text{C}$, using an

environmental controlled chamber with a National Institute of Standards and Technology (NIST) certified temperature/RH device (model HP23, accuracy at 23°C: $\pm 0.8\%$ RH, $\pm 0.1^\circ\text{C}$ temperature; Rotronic Instrument Corp., Hauppauge, NY, USA). The air temperature sensors for activating chiller pumps were checked at room temperature against the NIST certified Rotronic HP-23. Any problematic temperature/humidity sensors owing to damage/malfunction were replaced promptly.

Sensor calibration and data acquisition performance

All sensors for cage air temperature and RH measurements conformed to manufacturer specifications. However, the pipe-plug thermistors used to measure perch temperature (whether air or water) were self-customized with a 10 k Ω resistor that worked as a voltage divider to compensate the ZW series dataloggers with a desired signal output, and thus all required independent calibration. They were calibrated over the range 10 to 30°C against an NIST certified block temperature calibrator (model CL-134, Omega Engineering, Stamford, CT, USA). Individual calibration curves were developed, documented, and applied for each specific pipe-plug thermistor probe. The slope, intercept, and coefficient of determination (R^2) were included in the calibration equation. The accuracy of the pipe-plug sensors was based on the standard error (SE) of the predicted temperature of the sensors.

3.2.2 Experimental design and chicken arrangement

The experiment was conducted in the Layer Research Unit at Purdue University Poultry Research Farm, in West Lafayette, Indiana, USA. All animal care procedures were approved by the Purdue University Animal Care and Use Committee (PACUC Protocol No. 1302000813).

The cooled perch system was used in two phases of studies from summer 2013 to summer 2016. A pilot study was conducted with a single caging system, from 16 to 32 wk of bird age, from June to September of 2013 for system validation during short term acute heat stress episode (Hu et al., 2016). A total of 162 Hy-Line W36 White Leghorns, initially at 16 wk of age were randomly assigned to one of three treatments: 1) conventional cages with circular perches that were cooled with water, with circulation pump activated when cage air temperature exceeded 25°C (**Cooled perch** or **CP**, Figure 3-2), 2) conventional cages fitted with uncooled perches, open to ambient air (**Air perches** or **AP**, Figure 3-3), and 3) conventional cages with no perches (**Control** or **CTRL**, Figure 3-4). When birds were 27.6 wk of age, an acute heat stress event was initiated for 4 h daily, during which the ambient room temperature was increased to the range of 32.0 to 34.6°C through use of a conventional room furnace located inside the experiment facility. Six ZW-007 and three ZW-003 data nodes were placed near the ceiling of each tier of CP and AP cages, at the partition between the two cages, to measure the air temperature and RH. On each of the three tiers of the CP cages, pipe-plug thermistor probes were threaded into the supply and return loops in bottom up direction to measure the corresponding

water temperature and to reduce the potential of air bubble interference. In the AP cages, one probe was threaded into the perch to measure the air temperature of the open-ended perch on each tier. Three ON-405 air temperature thermistors were placed at the same level as the ZW-007 data nodes on each tier to monitor air temperature in the cage and activate the chiller when the temperature exceeded the heat stress temperature set point. In addition to the cage environmental monitoring, a ZW-003 data node was also installed at a high, central area of the room to collect room level air temperature and RH. Each cage housed nine laying hens (439 cm² per hen), resulting in a total of 54 hens per treatment (Hu et al., 2016). There was enough loop to allow all hens to perch at the same time (perching allowance 16.9 cm per hen).

A second phase study was conducted in the following year, from June 2014 to June 2016 to evaluate the effects of cooled perches on laying hen performance and health during cyclic heat stress episodes. The second phase system was fabricated by doubling hen capacity of the original treatment design, resulting in two replicates of the system that included two sets each of the CP (**CP-1 and CP-2**), AP (**AP-1 and AP-2**) and CTRL (**CTRL-1 and CTRL-2**) units, and 12 cages per treatment. A total of 326 Hy-Line W36 White Leghorns at 16 wk of age were randomly assigned to CP, AP, or CTRL treatments, and were subjected to a daily cyclic heat of 35°C from 0600 to 1800 h. The ambient temperature was lowered to 28°C from 1800 to 0600 h. The daily cyclic heat was applied using a conventional room furnace from 21 to 35 wk of bird age (2014 summer) and from 73 to 80 wk of bird age (2015 summer). From 36 to 39 wk of bird age, the

ambient room temperature was stepped down from 35°C and 28°C by 2°C per wk until the ambient temperature reached a range between 20 and 25°C. At all other ages, hens were kept between 20 to 25°C daily temperatures.

The experiment room temperature was controlled by a fan ventilation system without evaporative cooling. The Layer Research Unit was ventilated with a simple staged ventilation system and had a continuously operating poly-tube distribution system and we assume the room air was well mixed.

3.2.3 Water flowrate evaluation

Mass flowrate of the chilled water was used to assess the performance of cooled perch system and was evaluated using two methods: 1) measured directly, and 2) estimated from empirical equations and the pump curve provided from the manufacturer. The water flowrates obtained from the two methods were compared to determine the system performance uncertainty between system design and field measurement.

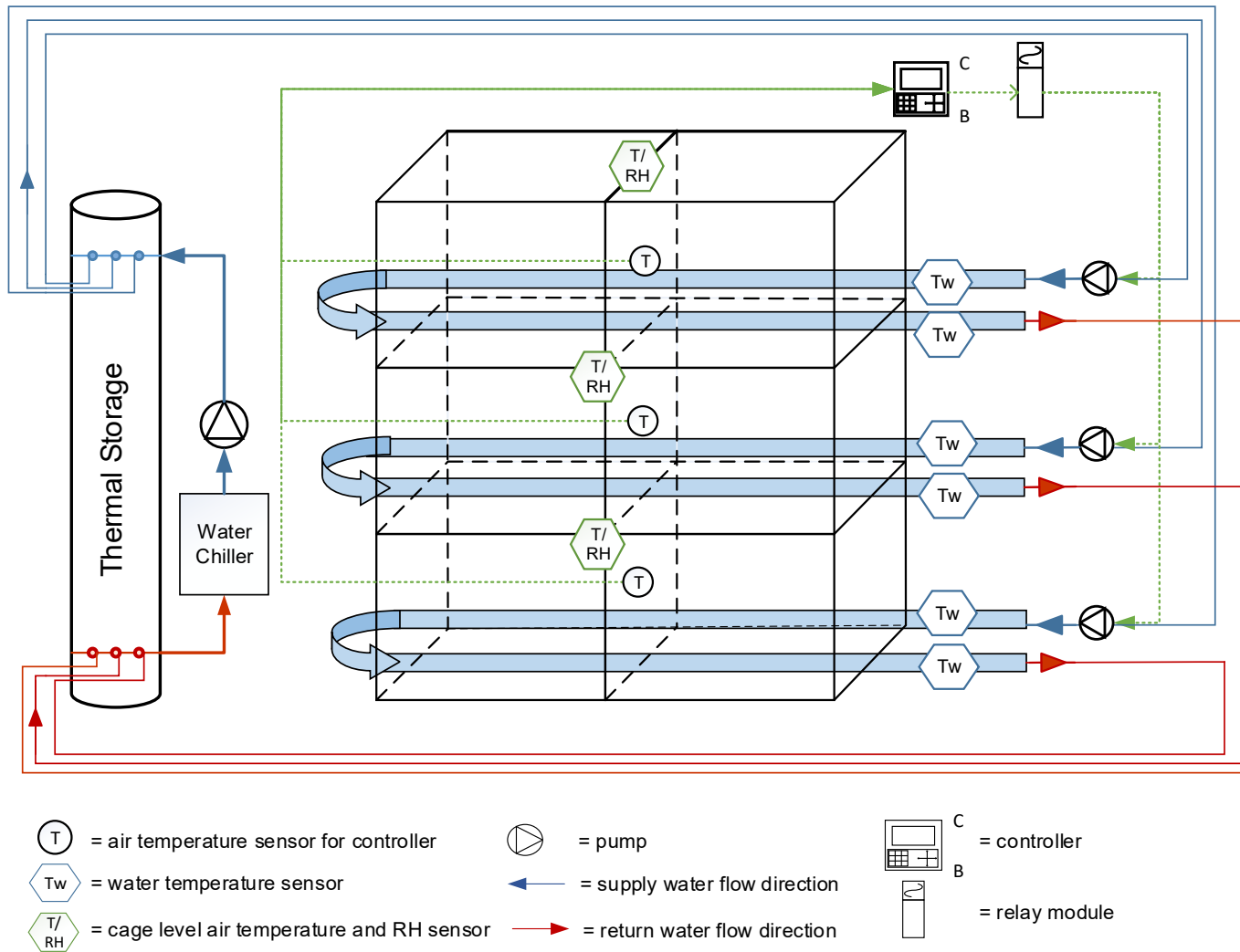
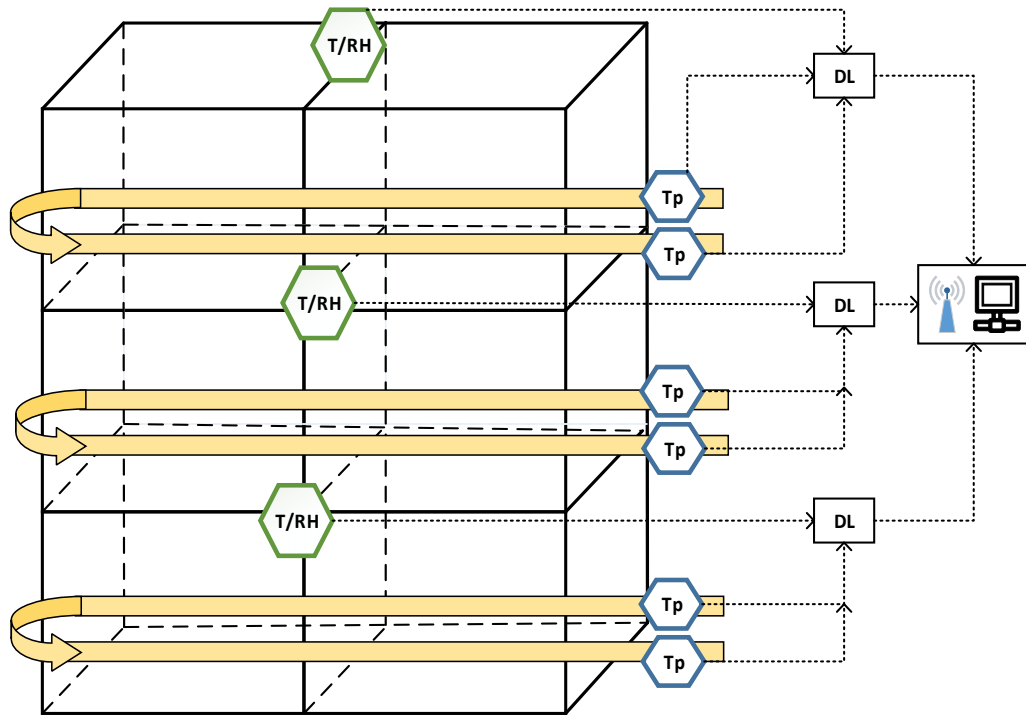


Figure 3-2. Schematic representations of the cooled perch system design and instrumentation. Two systems were fabricated and used. Each system consisted of three loops (top, middle, bottom) individually operated by pumps which drew cooled water from a thermal storage manifold and return to the same manifold. Each pump saw effectively the same head loss. The thermal storage was cooled by an independent loop consisting of a fourth pump that continuously circulated water between the manifold and a water chiller. Each loop pump was individually thermostatically controlled based on air temperature within the cage. Instrumentation included inlet and return line water temperatures, cage air temperatures and RH.



T/RH = ZW-007 built-in sensor to read cage air temperature and RH

Tp = thermistor to read perch air temperatures

DL = HOBO wireless datalogger – temp/RH with 2 extra ports for air perch temperatures


 = wireless data acquisition center

Figure 3-3. Treatment assignments for air perch cages (AP) showing locations for recording environmental responses. Air temperature and RH in each tier (top, middle, and bottom) were recorded near the cage ceiling. Air temperatures of the perches for each tier were recorded.

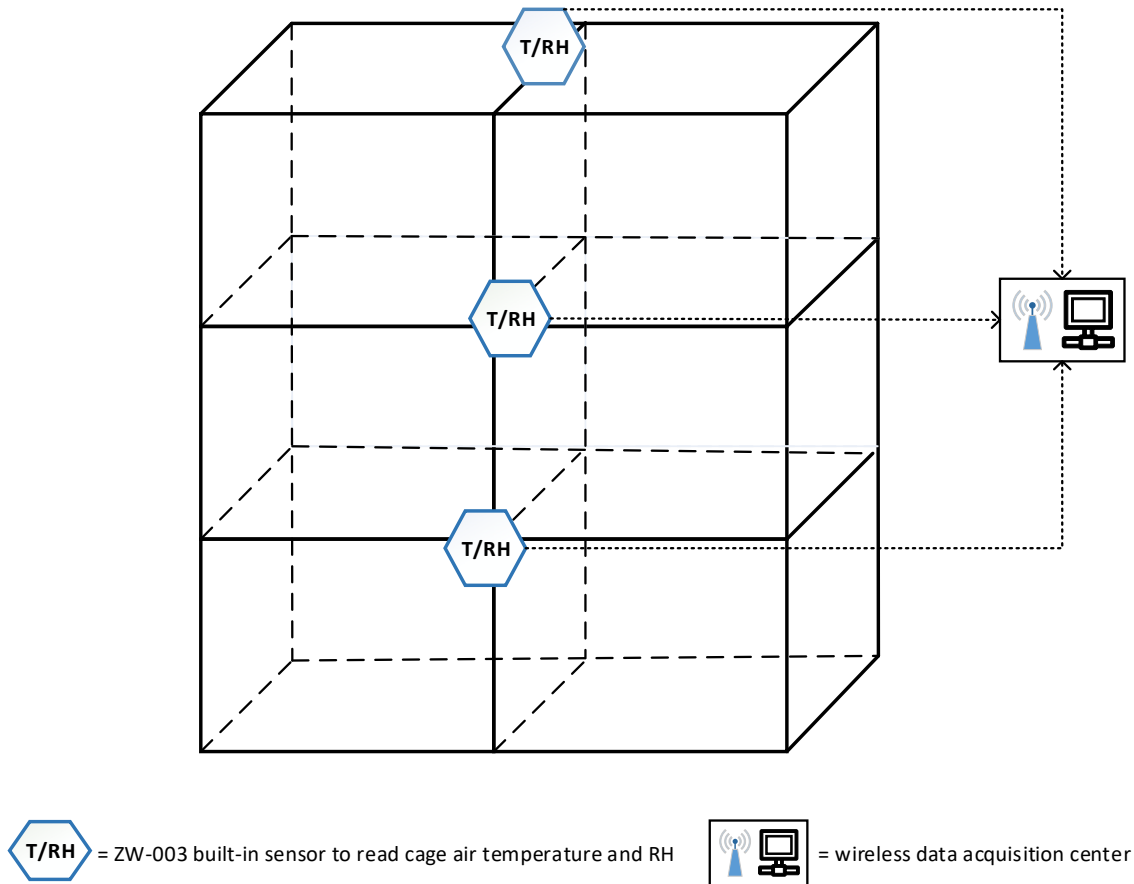


Figure 3-4. Treatment assignments for control cages (CTRL) showing locations for recording environmental responses. Air temperature and RH within each tier (top, middle, and bottom) were recorded near the cage ceiling.

3.2.3.1 Water flowrate measured directly

The water flowrate data was collected over a total of seven days over two years during the chronic heat stress experiment (three days in 2015 and four days in 2016, respectively), with multiple repeated measurements ($N \geq 3$) taken each day. A tee-valve was installed at the end of each loop where the return water temperature was monitored to create a pathway to capture water without interfering with the experiment. The water stream flowing through each loop for each treatment replicate was collected over a period of time (approximately 30 sec, recorded by a

stopwatch). The mass flowrate of the cooled water for each loop was calculated by dividing the collective weight of water captured from the end of each loop by the corresponding elapsed time recorded by stopwatch.

The average water flowrate on each day was used to represent the daily average of the flowrate. Average water flowrate measured in 2015 and 2016 was taken respectively to represent the yearly mean water flowrate for each loop and was plotted for CP-1 and CP-2. The mean water flowrates measured for each cooled perch loop over two years during the chronic heat stress experiment was plotted. The standard deviation of the daily mean for each perch loop was indicated. Descriptive statistical information including the yearly mean and the standard deviation of the mean (SD) of water flowrate measured for each cooled perch loop in year 2015 and 2016 was tabulated.

3.2.3.2 Water flowrate estimated from empirical equations

A set of empirical equations was used to obtain an estimated value of the water flowrate, and the result was used to evaluate the robustness of the mass flowrate that was measured directly. The process of obtaining the estimated mass flowrate using the empirical equations is illustrated in the following equations below. The mean flow velocity (u_{av}) of the chilled water was computed using Equation 3-1 (Bergman et al., 2011):

$$u_{av} = \frac{\dot{V}}{(\pi/4)d_i^2} \quad (3-1)$$

where \dot{V} is the volumetric flowrate read from the pump curve at the estimated total system pressure; d_i is the inside diameter (= 28.5 mm) of the perch pipe.

After obtaining the mean flow velocity of the cooled water, the Reynolds number (Re) was then computed by Equation 3-2 (Bergman et al., 2011) and was used to determine the nature of the chilled water circulating inside the perch loop:

$$Re = \frac{\rho_w u_{av} L_c}{\mu_w} = \frac{\rho_w u_{av} d_i}{\mu_w} \quad (3-2)$$

where ρ_w is the density of the chilled water at 20°C (the overall average of water inlet and outlet temperatures across all six loops) was used. At 20°C, $\rho_w = 998 \text{ kgm}^{-3}$ (ASHRAE, 2017b). u_{av} is the mean flow velocity of the chilled water computed from Equation 3-1; L_c is the characteristic dimension for the flow geometry (= $d_i = 28.5 \text{ mm}$ in this case); and μ_w is the dynamic viscosity of the cooled water, which is $1.003 \times 10^{-3} \text{ kgm}^{-1}\text{s}^{-1}$ at 20°C.

The mean pressure drop ($p_1 - p_2$) of the chilled water pumped to the system was estimated by Equation 3-3 (ASHRAE, 2017a):

$$p_1 - p_2 = f \left(\frac{\rho u_{av}^2}{2g_c} \right) \left(\frac{L_{eq}}{D} \right) \quad (3-3)$$

where L_{eq} is the equivalent length of the perch loop with all fittings considered; f is the Darcy-Weisbach friction factor; and the velocity head, $\rho u_{av}^2 / 2g_c$. For this analysis, we assumed the inner surface of the galvanized perch pipe is smooth ($\frac{\epsilon}{D} = 0.000005$), where ϵ = roughness of the perch pipe inner surface (mm). The pressure drop that occurs inside the loop in conjunction with the friction factor can be estimated by the smooth pipe curve from the Moody diagram

(ASHRAE, 2017a). The friction loss caused by any fittings present in the loop needs to be considered for the equivalent length of the loop. For schedule 40 PVC pipe with nominal size of 2.5 cm (1 in. PVC), the equivalent length is 0.5 m for elbow (“*street el*”) fittings (AetnaPlastics, 2015).

The mass flowrate of the cooled water can be calculated using the volumetric flowrate V_w . The newly obtained pressure drop was then used in the pump curve (Figure 3-5) to determine a closer estimate of the volumetric water flowrate (\dot{V}). An iterative process was performed by repeating Equations (3-1) to (3-3), until the pressure drop and the volumetric water flowrate both converged to unchanged values. The thermodynamic properties of the chilled water obtained from empirical equations, including the total number of iterations performed, the Reynolds number (Re), the friction factor (f), the pressure drop, the estimated flowrate (in L/s and kg/s) for each iteration were provided and were compared to the measured water flowrate for design uncertainty.

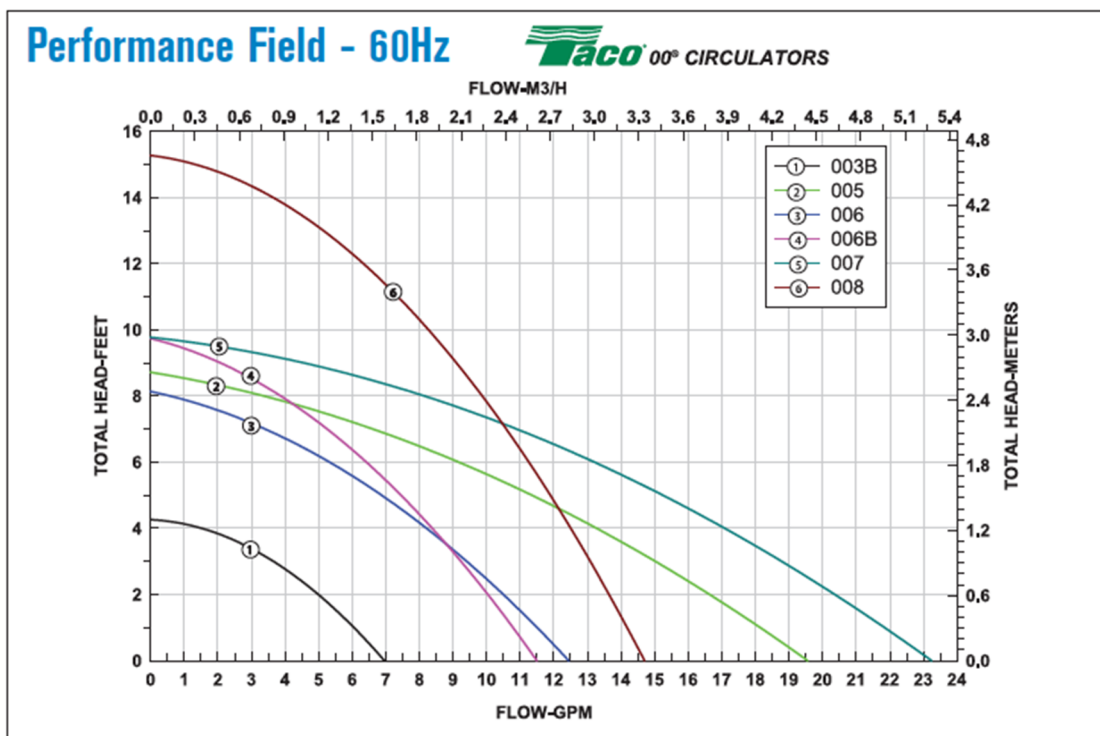


Figure 3-5. Performance field chart of the circulator pump deployed in the cooled perch system (curve 4, model 006-B4-15 Cartridge Circulator, Taco Inc., Cranston, RI, USA). Made available by the manufacturer and obtained from <https://www.taco-hvac.com/uploads/FileLibrary/100-1.7.pdf>.

3.2.4 Estimation of system net heat gain

3.2.4.1 Loop water temperature rise

The water temperature rise for each loop is useful for evaluating the water chiller performance and estimating the average heat gain of the CP system. The daily water temperature rise between the perch outlet and the perch inlet for each loop was plotted against time of day for every 24 h (midnight to midnight) during the chronic heat stress episodes (21 – 35 and 73 – 80 wk. of bird age) for visualization of the water pump and chiller performance. Two representative heat stress periods were selected to assess the characteristics of the loop temperature rise. These two consecutive periods contain a) water temperature rise profile for June 25th to June 30th, 2014,

during which the two CP replicates were performing as expected (i.e. no sudden changes or stagnant temperature performance in loop temperature rise, no sudden temperature overshoot in either perch inlet or outlet during pump startup, etc.) ; and b) the following week, from July 1st to July 7th, 2014, during which pump malfunctioning was observed. The loop water temperature rise for both CP replicates was calculated from data recorded every minute and was plotted against time during each of the two representative periods. The air temperature of the experiment room was included to indicate the heat stress regime.

Descriptive statistics, including the mean loop temperature rise and the standard deviation for the top, middle, and bottom tier in CP-1 and CP-2 are provided. The loop temperature rise analysis was assessed over a period of stable system performance, defined as no sudden changes in loop temperature rise in any tier for either CP replicate, which would provide useful information for analyzing system performance as well as designing for a bigger scale utilization.

3.2.4.2 System net heat gain

Obtaining system net heat gain is useful for sizing similar systems that are proposed for different scale applications for industrial use. The descriptive statistics of the measured water flowrate, temperature rise during stable system performance, and the corresponding water characteristics were used to estimate the total heat gain of the CP systems. The system net heat gain (W) is estimated using the following equation:

$$Q_{gain} = \dot{m}C_p\Delta t \quad (3-4)$$

where \dot{m} is the average water flowrate of each loop measured in 2015, in kg/s; C_p is the specific heat of water at specific temperature, in J/kg°C. For this estimation, the specific heat of water at 20°C (the overall approximate average of water inlet and outlet temperatures across all six loops) was used. At 20°C, $C_p = 4,180$ J/kg°C (ASHRAE, 2017b); and Δt is the loop temperature rise calculated at every minute during stable system operation, in °C.

For the representative stable system operation during June 25th to June 30th, 2014, the system heat gain for each loop in CP-1 and CP-2 was estimated using water flowrate measured in 2015 and the specific loop temperature rise. The estimated heat gain of each loop was averaged every hour and was plotted against time. Mean water inlet temperatures of the three loops in CP-1 and CP-2 were averaged hourly and were plotted against time to demonstrate the chiller performance. Descriptive statistics, including the overall average net heat gain and the standard deviation over the entire plotted time are provided for each loop within replication, and each replication, respectively.

3.2.4.3 Statistical analysis

The following statistical analyses were performed using SAS (version 9.4, SAS Institute Inc., Cary, NC, USA) for relatively stable system operation period from June 25 to 30, 2014. The hourly net heat gain data from three tiers in each replicate CP system were averaged to represent replicate-level net heat gain. The hourly net heat gain at individual loop-level and replicate-level for both CP replicates were tested for correlation effects with experimental facility's room

temperature. The analysis was done by PROC CORR in SAS. PROC UNIVARIATE was used to verify normality of the dependent variable and accepted at $P > 0.01$. The Spearman method and the Spearman correlation coefficient (r_s) were used to determine correlation effect ($P < 0.05$). A student's t-test was performed by PROC TTEST in SAS for the hourly net heat gain and inlet temperatures of the three loops within each replication to further explore if difference in system heat gain or inlet temperatures presents in different loops within the same replication ($P < 0.05$).

3.2.5 Heat transfer components analysis of the cooled perch system

It is of interest to perform a component analysis of the heat transfer in the cooled perch system for better understanding and identifying of the major contributors to the net system heat gain. A conceptual diagram illustrating a section of the cooled perch is provided in Figure 3-6 to demonstrate the heat transfer mechanisms occurred at the cooled perch system and the surrounding environment.

From Figure 3-6, during a heat stress event, multiple heat transfer mechanisms occur, including: **1)** heat convection of the internal chilled water circulating inside the perch loop, which depends on the internal water temperature T_i and the convective coefficient h_i ; **2)** natural convection (also known as free convection) from ambient air to the pipe outside surface, which depends on the temperature difference between air temperature T_∞ and the pipe exterior surface temperature T_{OS} , and the natural convective coefficient h_o ; **3)** forced convection also occurs as a result from the air flow from the ventilation distribution tube, and is expressed as a function of

the temperature difference between the air temperature T_∞ and the pipe exterior surface temperature T_{OS} , and the forced convective coefficient h_f ; and 4) radiation from the surrounding surfaces to the pipe outer surface, driven by the temperature difference of the surrounding surfaces $T_s (\cong T_\infty)$ and the radiative coefficient h_r . At steady state, we assume the temperature of the surrounding surfaces around the system within the experiment room is approximately equal to the room ambient temperature ($T_s \cong T_\infty$). Lastly, is the heat conduction to the perch from hens' footpads, which depends on the effective contact area and the temperature difference between hens' footpads and the perch outer surface.

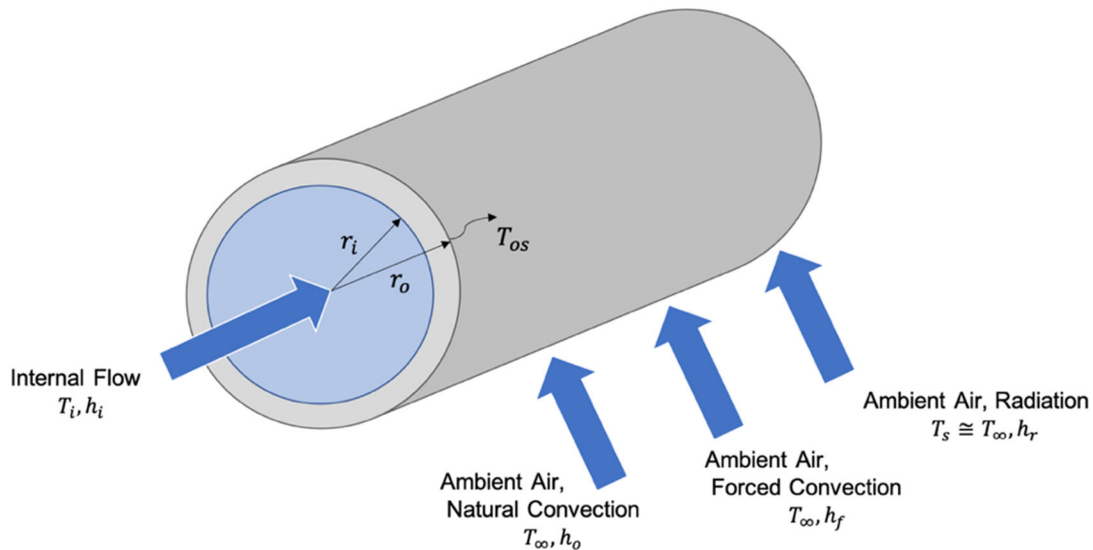


Figure 3-6. Conceptual diagram of a section of the cooled perch pipe and the heat transfer mechanisms of the system. Key parameters include: convection of the internal cooled water, estimated from the internal water temperature T_i and the convective coefficient h_i ; the natural convection and forced convection from ambient air to the pipe outside surface, depends on the temperature difference between the air (T_∞) and the pipe exterior surface (T_{OS}), natural convective coefficient h_o or forced convective coefficient h_f ; and radiation from the surrounding surface to the pipe outer surface, depends on the difference between the surrounding surface temperature $T_s (\cong T_\infty)$ and the radiative coefficient h_r .

The following estimation of heat transfer components was performed using a set of empirical equations and an iteration method⁴ (ASHRAE, 2017c), following with numeric examples using the daily averages of the environmental measurements during stable system operation period (June 25 – July 1, 2014; corresponding to Figures 3-8a and 3-9).

3.2.5.1 Estimating the convection of internal flow

Bergman et al. (2011) provides a textbook explanation of convection, which is the heat transfer of internal energy into or out of an object (e.g. cooled perches) by the physical movement of a surrounding fluid (e.g. cooled water, or heated air) that transfers the internal energy along with its mass (e.g. cooled water circulation). Procedures and empirical equations for estimating the convection of the cooled water circulating inside the perch loop are listed in the following steps:

Step (1): The theoretical water temperature at the center of the interior perch loop is calculated as:

$$t_i = \frac{(t_{w,in} + t_{w,o})}{2} \quad (3-5)$$

where the corresponding thermodynamic properties of water, including the density (ρ_w), specific heat ($C_{p,w}$), thermal conductivity (k_w), the dynamic viscosity (μ_w), and the Prandtl Number (Pr_w) at temperature t_i are needed and can be found in textbooks (Bergman et al., 2011).

⁴ Empirical equations and the iteration method used in this analysis is provided in Chapter 4: Heat transfer in ASHRAE Handbook – Fundamentals. SI ed. pp 4.17 – 4.22.

The mean flow velocity (u_{av}) can be computed using Equation 3-6 and the inside diameter of the perch pipe d_i (Karlekar and Desmond, 1977):

$$u_{av} = \frac{\dot{m}}{\rho(\pi/4)d_i^2} \quad (3-6)$$

Step (2): *Reynolds number* (Re) is required for determining the nature of the chilled water circulating inside the perch loop and can be computed using Equation 3-2 previously listed in Section 3.2.3.2.

For flow inside circular tubes, the flow characteristics corresponding to the *Reynolds number* are described as follows: laminar flow presents when a *Reynolds number* smaller than 2300 was found; when the *Reynolds number* is between 2300 and 4000, the flow is recognized as transitional flow; when a *Reynolds number* larger than 4000 was found, the flow transitions from laminar flow to turbulent flow (ASHRAE, 2017a, 2017c; Bergman et al., 2011). Compared to laminar or turbulent flow, the characteristics of transitional flow are difficult to determine, as the nature of the flow is in transition and is much more complicated than laminar or turbulent flow alone (ASHRAE, 2017a, 2017c; Bergman et al., 2011; Grigull et al., 1982; Metais and Eckert, 1964). Therefore, as a practical measure, it is generally suggested that for transitional flows, the characteristics of either fully developed laminar flow or fully developed turbulent flow are used to provide an approximate estimate of the flow properties.

Step (3): From the previous step, the cooled perch water characteristics fit in fully developed flows. For fully developed laminar flows ($Re < 2300$) in round pipe or duct with

assumption of uniform surface temperature, the Nusselt number (Nu) of 3.66 is independent of Re , Pr , and negligible axial conduction (Bergman et al., 2011) and is used to estimate the convective heat transfer coefficient (h_i) for the internal flow (ASHRAE, 2017a, 2017c; Bergman et al., 2011).

$$h_i = \frac{Nu k}{L_c}, \quad (\text{W m}^{-2}\text{K}^{-1}) \quad (3-7)$$

where k is the thermal conductivity of the cooled water corresponding to temperature t_i ; and L_c is the characteristic dimension for the flow geometry (=28.5 mm).

3.2.5.2 Estimating the natural convection and radiation from ambient to perch

Natural convection, or free convection, refers to fluid motion due to buoyancy forces. Monteith and Unsworth (2013) described that in free convection, heat transfer depends on the circulation of fluid (e.g. air) over and around an object (e.g. cooled perches), maintained by gradients of temperature (e.g. temperature difference between air and perch exterior surface temperature) which create gradients of air density.

Step (4): To obtain the heat transfer of the internal fluid or the convective and radiative heat transfer between the surrounding environment to the outer surface of the pipe, the outside surface temperature of the pipe is needed. A thermal circuit analog diagram is provided in Figure 3-11. Under assumption of steady state and uniform heat flux, the heat transfer between the pipe outside surface to the internal flow equals the summation of convective and radiative heat transfer from ambient environment to the pipe exterior surface. In this model, the inner water

temperature is assumed constant at either the average of inlet and outlet temperature, or the log mean temperature difference (LMTD). In this work, we use the average temperature. Thus, a theoretical balance equation can be developed and solved using an iterative method (ASHRAE, 2017c):

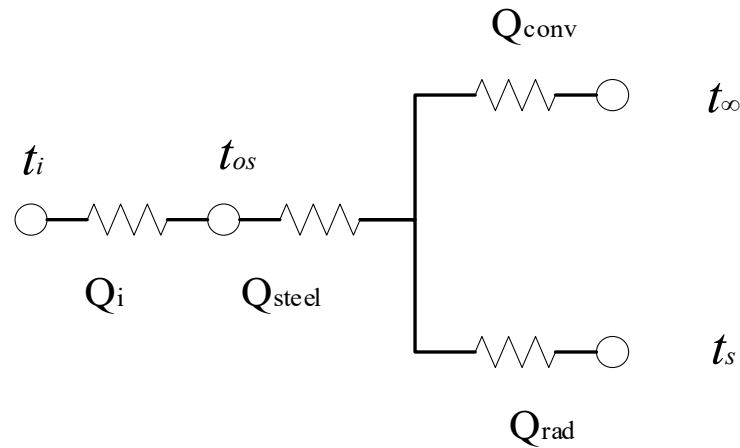


Figure 3-7. Thermal circuit analog diagram illustrating heat transfer mechanisms occur at the cooled perch system. Q_i , Q_{steel} , Q_{conv} , and Q_{rad} are convection of the internal flow, conduction through the steel perch pipe, convection from ambient air to perch surface, and radiation from surroundings to the perch.

$$\frac{t_{os} - t_i}{\frac{1}{h_i d_i} + \frac{1}{2k_s \ln \frac{d_o}{d_i}}} = \frac{t_{\infty} - t_{os}}{\frac{1}{h_{ot} d_o}} \quad (3-8)$$

where t_{os} , t_i , and t_{∞} are the temperature of the pipe exterior surface, the theoretically calculated water temperature at the center of the pipe inside, and the ambient room temperature, respectively; d_i and d_o are the inside and outside diameters of the perch pipe in m ; k_s is the thermal conductivity of old galvanized steel ($= 52 \text{ Wm}^{-1}\text{K}^{-1}$); h_i is the convective heat coefficient of the chilled water in $\text{Wm}^{-2}\text{K}^{-1}$; and h_{ot} is the summation of the natural- and forced- convection heat transfer coefficient and the radiation heat transfer coefficient in $\text{Wm}^{-2}\text{K}^{-1}$.

Step (5): To estimate the total heat transfer coefficient of the convective and radiative heat transfer from the ambient to the perch loops, iteration commenced with a beginning assumption that t_{os} equals the pipe outlet water temperature $t_{w,o}$. Air properties at the film temperature $t_f = \frac{1}{2}(t_{os} + t_{\infty})$ are needed and can be found in Bergman et al. (2011), including the density of air (ρ_a); the specific heat of air ($C_{p,a}$); the thermal conductivity of air (k_a); the dynamic viscosity of air (μ_a); the *Prandtl Number* (Pr_a). The volume expansion factor (β) of air is obtained at ambient temperature t_{∞} .

The *Rayleigh number* (Ra) can be calculated using the air properties obtained at the film temperature t_f (ASHRAE, 2017b):

$$Ra = GrPr = \frac{g\beta\rho_a^2|\Delta t|L_c^3}{\mu^2} Pr \quad (3-9)$$

where Gr is the *Grashof number* for air at the film temperature t_f ; Δt is the temperature difference between the ambient environment and the perch exterior surface.

Step (6): The *Nusselt number* is then obtained with the following correlation equation (ASHRAE, 2017c; Bergman et al., 2011):

$$Nu = \left\{ 0.6 + \frac{0.387Ra^{1/6}}{[1 + (0.559/Pr)^{9/16}]^{8/27}} \right\}^2 \quad (3-10)$$

Step (7): The natural convective heat transfer coefficient of ambient air to the perch loop exterior surface h_o is calculated using the equation below (ASHRAE, 2017c; Bergman et al., 2011):

$$h_o = \frac{Nuk_a}{d_o}, \quad (\text{W m}^{-2}\text{K}^{-1}) \quad (3-11)$$

Step (8): The radiative heat transfer coefficient h_r is calculated using the assumed per pipe exterior surface temperature and the ambient air temperature (ASHRAE, 2017c; Bergman et al., 2011):

$$h_r = \sigma \varepsilon (T_{os}^2 + T_{\infty}^2)(T_{os} + T_{\infty}) \quad (3-12)$$

where $\sigma = 5.678 \times 10^{-8}$ is the Boltzmann constant and ε is the emissivity of old galvanized steel (= 0.88), and T_{os} and T_{∞} are the pipe outer surface temperature and the ambient room temperature in K.

Step (9): The summation of the natural convective and radiative heat transfer coefficient is calculated as $h_{ot} = h_o + h_r$, using the estimated values of the natural convection and the radiation heat transfer coefficients derived from Steps (7) and (8).

Step (10): The calculated h_{ot} is put back to the heat transfer Equation 3-8 in Step (4), to get a second estimate of t_{os} . The film temperature $t_f = \frac{1}{2}(t_{os} + t_{\infty})$ is recalculated using the newly estimated t_{os} , and the air properties at the corresponding newly estimated film temperature are then obtained.

Step (11): The iteration then proceeded with the new estimate of t_{os} and air properties, and Steps (4) to (10) were repeated until the iterated t_{os} and h_{ot} were converged to unchanged values.

Once the final iteration was completed with converged values of t_{os} and h_{ot} , the convection heat transfer of the internal flow (Q_i), the natural convective heat transfer between ambient air and the perch exterior surfaces (Q_o), and the heat radiation between the surrounding surfaces and the perch exterior surfaces (Q_r) can be computed using the following equations:

$$Q_i = h_i A_i (t_{os} - t_i) = h_i \pi d_i L (t_{os} - t_i) \quad (3-13)$$

$$Q_o = h_o A_o (t_{\infty} - t_{os}) = h_o \pi d_o L (t_{\infty} - t_{os}) \quad (3-14)$$

$$Q_r = h_r A_o (t_{\infty} - t_{os}) = h_r \pi d_o L (t_{\infty} - t_{os}) \quad (3-15)$$

where L is the total length of the perch loop on each deck (= 6.1 m).

3.2.5.3 Estimating the forced convection from air to perch

The Layer Research Unit was ventilated with a simple staged ventilation system and had a continuously operating poly-tube distribution system which was assumed to provide a mean air velocity near the perches of approximately 1m/s. Thus, it is possible that a weak effect of forced convection from ambient air to the perch pipe may also exist.

The *Reynolds number* (Re) of the ambient air from forced convection (Re_{fc}) can be calculated using Equation 3-16 (ASHRAE, 2017c), with the assumed airflow velocity projected to the cooled perch system (V_{∞}) and the kinematic viscosity (ν_f) of air obtained at film temperature $t_f = \frac{1}{2}(t_{os} + t_{\infty})$.

$$Re_{fc} = \frac{V_{\infty} L_c}{\nu_f} \quad (3-16)$$

The coefficient of the forced convection heat transfer is then calculated using correlation equation for flows along horizontal cylinder and a *Reynolds number* ranges between 35 and

5000, and the forced convection heat transfer between the ambient air and the perch pipe (Q_f) can be calculated accordingly (ASHRAE, 2017c).

$$h_f = \frac{2.755V_\infty^{0.471}}{d_o^{0.529}}, \quad (\text{W m}^{-2}\text{K}^{-1}) \quad (3-17)$$

$$Q_f = h_f A_o (t_\infty - t_{os}) = h_f \pi d_o L (t_\infty - t_{os}) \quad (3-18)$$

Natural convection can affect the heat transfer coefficient in the presence of weak forced convection. As the forced-convection effect increases, “mixed convection” (superimposed forced-on-free convection) gives way to pure forced convection. Grigull et al. (1982), Metais and Eckert (1964) described that the heat transfer coefficient in the mixed-convection region is often larger than that calculated based on the natural-or-forced convection calculation alone (ASHRAE, 2017c).

Bergman et al. (2011) further explained a situation in which both natural and forced convection are comparable, a general rule to consider is to compare the magnitude of the free convection and forced convection using the expression G_r/R_e^2 , where G_{rL} is the *Grashof number*, also as the square of the *Reynolds number* R_e . If $G_r/R_e^2 \ll 1$, the free convection effect is negligible, and the forced convection effect is negligible if $G_r/R_e^2 \gg 1$ is found. If $G_r/R_e^2 \approx 1$, a combined free and forced-convection effect needs to be considered.

3.2.5.4 Heat transfer component analysis using measured environmental conditions

A set of hourly averages of the environmental measures during stable system operations of a representative heat stress period (June 25th – July 1st, 2014, as described in Section 3.2.4.1)

was used to demonstrate a component heat transfer analysis for CP-1 and CP-2, respectively. The combination was selected for the day June 27th, 2014 at noon time as it had the highest room temperature recorded (35.5°C), which was considered representative of a heat transfer component analysis for the heat stress episode. The hourly averages of the environmental measurements include ambient air temperature during heat stress (t_{∞}), average inlet water temperature for CP-1 and CP-2 ($t_{w,in}$), average outlet water temperature ($t_{w,o}$), and the average water flowrate (\dot{m}) directly measured in 2015 for CP-1 and CP-2, respectively. The replicate-specific values for CP-1 and CP-2 were similar and their average was used for this analysis.

The heat transfer component analysis was conducted following the steps listed in Section 3.2.5.3. Corresponding thermophysical properties of saturated water and air necessary for the analysis were obtained from Bergman et al. (2011) and ASHRAE (2017b). The iterative method for estimating the exterior perch loop surface temperature and the summation of the convective and radiative heat transfer coefficient was performed when needed. The combination of environmental measurement values used, and the results of the heat transfer component analysis were tabulated and discussed.

3.2.6 Evaluation of the system performance

3.2.6.1 System heat gain, chiller capacity, and pump performance

The system heat gain estimated from the water flowrate and loop water temperature rise measurements versus estimated from the empirical heat transfer equations with environmental

conditions were compared. The results of the discrepancy between the two estimation methods were discussed. Other system performance parameters such as the capacity of the chiller model used in this experiment and the pump performance were evaluated based on the water flowrate measurement and the loop water temperature rise profile between each CP replicate, and within the same CP replicate for different perch loops. To further evaluate the system performance, individual loop inlet water temperatures for CP-1 top through CP-2 bottom during a 24 h interval for two representative days of stable operation (June 28th and July 4th, 2014) are plotted for CP-1 and CP-2, respectively.

3.2.6.2 Design criteria for future application

Cooled perch design criteria can be extrapolated from this study. Using the results obtained from system net heat gain analysis (Section 3.2.4.2 in Materials and Methods, and Section 3.3.3 in Results and Discussion), useful design information were provided, including the total average daily net heat gain on a single replicate basis (considering a 3-tier stacked-cage system), the net heat gain per perch length (estimated using a total usable perch pipe length of 6.1 m used in this experiment), and the net heat gain on a per-hen basis (estimated using a maximum possible value of 9 hens per conventional cage, or 18 hens per perch loop). The overall average value for each design criteria was also included.

These details for each replicate cooled perch in this study can further provide a basis for selecting chiller and thermal energy storage (TES) capacity using either the full-storage or

partial-storage sizing method for a peak-day (ASHRAE, 2016). A properly sized chilled-water TES should include both the volume of the TES tank itself and the chiller sized for charging the system. A peak day 24 h cooling profile is the day with the largest total energy (kWh) needed by the TES system, which is often the day with the highest instantaneous peak cooling load (ASHRAE, 2016). Defined in ASHRAE (2016), a storage sized by the full storage method meets the entire cooling load during a predefined on-peak demand period with discharge from the thermal storage system; and a partial storage provides a portion of the on-peak cooling load, while the other cooling capacity is driven from operating the chilling equipment.

A more detailed hourly chilled water load schedule was computed based on the maximum hourly values for June 25th – 30th, 2014 measurements of net perch hourly sensible heat gain for each day and each replicate, following the examples provided in (ASHRAE, 2016). The accumulative sum of the hourly sensible system heat gain is the total daily cooling load expressed in units of kilowatt-hours (kWh). In an ideal situation, the daily 24 h cooling profile of the chiller must be met to satisfy the system's total daily energy demand on a peak-day, and so will be adequate for all other days as well. These values were tabulated for every hour, and the corresponding partial-storage TES sizing calculation for the experimental perches in this study was provided.

The value of the total thermal storage capacity and the temperature difference resultant from the chiller system can be used to calculate the required volume of the TES tank, using the following equation as provided by ASHRAE (2016):

$$V = \frac{X (3,600,000) J/kWh}{C_p \Delta t \times SG \left(998 \frac{kg}{m^3} \right) eff} \quad (3-21)$$

where V = TES tank volume (m³); X = amount of thermal capacity required, in kWh; C_p is the specific heat of water, a common value of C_p = 4184 J/(kgK) for water at 25°C is often used by engineers for thermal storage sizing purpose; Δt is the temperature difference, in K; SG is the specific gravity in $\frac{kg}{m^3}$; and eff is the storage efficiency, an efficiency value of 0.9 is typically assumed until further details of a specific design are known.

The volume of the thermal storage was estimated using the total sensible system cooling load on a peak-day and Equation 3-21. The results were compared with the thermal storage volume and the chiller capacity used in the experiment and to determine the sizing sufficiency of these two system components.

3.2.7 Implications to laying hens

The positive benefits to the laying hens in terms of physiology, foot health, and performance were acknowledged by the experimental cooled perch design (Hu et al., 2016; Hu et al., 2019a; Hu et al., 2019b; Hu et al., 2019c). This section provides an analysis of the hens' perching behavior for CP and AP perches, based on perching observations made during the

experiment. A side study was conducted separately to provide an updated value of chicken footpad contact area on the perch using thermal imaging technology, and a preliminary discussion regarding obtaining the thermal resistance of laying hens' footpad skin was provided.

3.2.7.1 Birds daily perching behavior

Perching behavior of the laying hens is an important factor indicating their acceptance and the preference toward the CP by the birds. It also represents a changing heat load to the CP as hens get onto or off the perch. Combined with the cage environmental profile, it is feasible to assess the potential cooling effect of the CP system by evaluating laying hens' perching behavior with cage air temperature changing over time of a day.

For this study, the birds' perching behavior is defined as when both of the bird's feet are on the perch (Hu et al., 2016). The proportion of hens perching was determined via live observations conducted on selected days. During observation, the same trained observer(s) walked through CP and AP cages and counted the number of hens with both feet on the perch. The live observation was conducted several times during several time periods on different days for good data quality, with a minimum of 15 min break between observations maintained. The number of hens perching was averaged for observation days and divided by the total birds housed per cage to represent bird's perch usage efficiency for each deck.

A two-sample student t-test was performed using PROC TTEST in SAS (version 9.4, SAS Institute, Inc., Cary, NC, USA) to determine significance in perch usage efficiency between

CP and AP units. The difference between variable means was considered significant at $P < 0.05$. Normality was checked by PROC UNIVARIATE and accepted for $P > 0.05$. The average perch usage efficiency of the two replicates was plotted for the AP and CP units for each deck.

To show the bird's perching behavior of the CP cages during a day, a closer look focused on a 24 h cyclic temperature regimen of hot days and cooler evenings simulated through use of room heaters. Ambient room temperature was increased using heaters from 6 am to 6 pm daily and then the heaters were turned off for the remaining hours of the day. For this analysis, the number of birds utilizing the perch in the top tier of CP-1 cages was plotted over time on July 14, 2014. Per the experimental protocol, room temperature was raised to heat stress status at 6 am and was always above 25°C, indicating that the chillers and perch water pumps were activated. Cage temperatures were averaged for every 30 mins and were included in the plot to show the effect of the ambient temperature on the perching behavior of the birds.

Thermal images of hens' feet on the perch loop were captured using an infrared thermal camera (Model T440, FLIR Systems, Inc., Wilsonville, OR, USA) to demonstrate hens' feet temperature during perching for different treatments and were demonstrated using FLIR Camera software (FLIR Tools, FLIR Systems, Inc., Wilsonville, OR, USA).

3.2.7.2 Estimating the hen footpad area

A side project was conducted separately in the Environmental Research Laboratory at the University of Illinois at Urbana-Champaign to estimate the contact area between the chicken's

footpad and the perch. The contact area was estimated from thermal images of perch surface immediately after removing a bird from the perch. At 27 wk of age, ten Hy-Line W36 White Leghorns, raised in a perching system resembling the cooled perch experiment cage setup were used.

Because of the lower thermal conductivity as compared to steel, a PVC pipe similar in size to the commercial perch (38 mm O.D.) was used to allow a more definite temperature contrast between chicken perched and unperched area on the perch surface for time to take a thermal image taking after taking the chicken off the perch. Ice with water was packed inside the PVC perch to ensure a low external surface temperature (approximately 16°C) when the surrounding air temperature was about 27°C. Two pieces of specialty paper with millimeter grid scales were fastened to the pipe surface along its length in the lateral direction and around the perimeter to provide a reference line. A thermal camera (FLIR Ex-Series E8 with 35 mm focal length, FLIR Systems Inc., Wilsonville, OR, USA) was used to obtain thermal images of perch surface immediately after a chicken had perched on it. Thermal Multi-Spectral Dynamic Imaging (MSX) feature and the tool packages provided in the FLIR Tools was used to choose surfaces of interest for analysis. The images were originally taken with the default settings of the camera (an emissivity of 0.98, a reflecting temperature of 20 °C, and an IR resolution of 320 x 240 pixels). All images were taken at a 10 cm distance from the pipe for uniformity of the pictures collected. The following criteria were used to standardize the image acquisition: a resolution of 72 dpi

(28.4 pixels/cm), a dimension of 320×240 pixels (width and height respectively), 24-bit depth, exposure time of 1/32 sec, and a maximum subject distance of 10 cm. Three color schemes were presented in the thermal images, reflecting the contact area, the perch surface, and the surrounding environment. To obtain an intact thermal image, three images were taken consecutively, and were layered to form one image to get a complete thermal print of the entire contact area (Figure 3-8). All images were stored in RGB color and JPG file format. Ten layered images were obtained for each hen that perched. Adobe Photoshop CC 2015 (Adobe Systems Incorporated, San Jose, CA, USA) was used to process the thermal images. The “Magic Wand Tool” in Adobe Photoshop CC 2015 was used to select a target area for analysis. The contact area was then simulated using the Computational Fluid Dynamics (CFD) tools, from which the contact area (A_c) was estimated using Equation 3-19. Three thermal images were taken for each bird, and the results were averaged over the total observations ($N=30$).

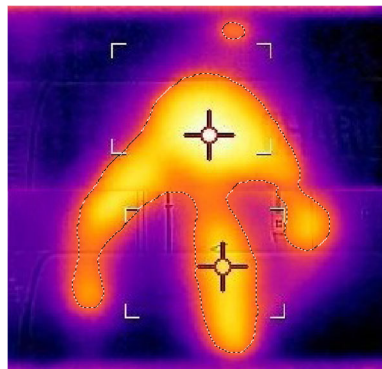


Figure 3-8. Example thermal image of the footpad of a laying hen perched on the PVC pipe. The shadow areas were created by placing a bird on the perch chilled by icy water. Image was taken immediately after the bird was removed from perch. Adobe Photoshop CC2015 was used to process the thermal images.

The entire perch surface area (A_p) in the image was calculated by multiplying the readings of the paper scales along the pipe length and the pipe perimeter (Equation 3-20). Pixels of the contact area (P_c) and the entire perch surface area (P_p) were provided from the software.

$$A_c = A_p \times \frac{P_c}{P_p} \quad (3-19)$$

$$A_p = L \frac{d}{P_d} \times W \frac{d}{2P_d} \quad (3-20)$$

where A_c is the contact area per foot of a laying hen perched on a cooled perch (cm^2); A_p is the entire perch surface area (cm^2); P_c is the pixels of the contact area; P_p is the pixels of the entire perch surface; L is the pixels along the length of the perch; d is the outside diameter of the perch ($=38 \text{ mm}$); P_d is the pixels of outside diameter in a thermal image ($=125$); and W is the pixels along the width of the perch.

A thermal image showing the contact area between the chicken footpad and the perch material picturing a bird's footprint right after she was taken off the perch, along with the simulation of the footprint using CFD tools were shown. The average pixels of the perch area, the average pixels of the footprints obtained, the range of the footpad area, and the average footpad contact area were calculated for the 10 laying hens ($N = 30$).

3.3 RESULTS AND DISCUSSION

3.3.1 Sensor calibration and data acquisition performance

An example of a complete calibration data set over the testing temperature range (10°C to 30°C) is shown in Figure 3-9. Accuracy of the pipe-plug sensors in this analysis, based on the

standard error (SE) of the predicted temperature of the sensors, ranged from 0.06°C to 0.31°C (1 sensor, for the middle tier supply temperature, was replaced; in this case only five data points were used for a calibration with resultant SE of 1.2°C, about 0.15% full-scale). According to the manufacturer declared accuracy ($\pm 0.1\%$) and the objectives of this study, the predicted error range of the pipe-plug sensors is considered to be acceptable after calibration. All other pipe-plug type thermistors used in this study (12 for the CP cages, and 6 for the AP cages) performed within an acceptable range of the standard error of the calibration model ($< 1.5^\circ\text{C}$) prior to installation. The performance of all environmental measurement sensors and the environmental control system was closely and regularly checked during the experiment. Replacement of any malfunctioning was done promptly if the corresponding measurements were showing abnormal behaviors. All replacement pipe-plug thermistors were calibrated according the calibration procedures.

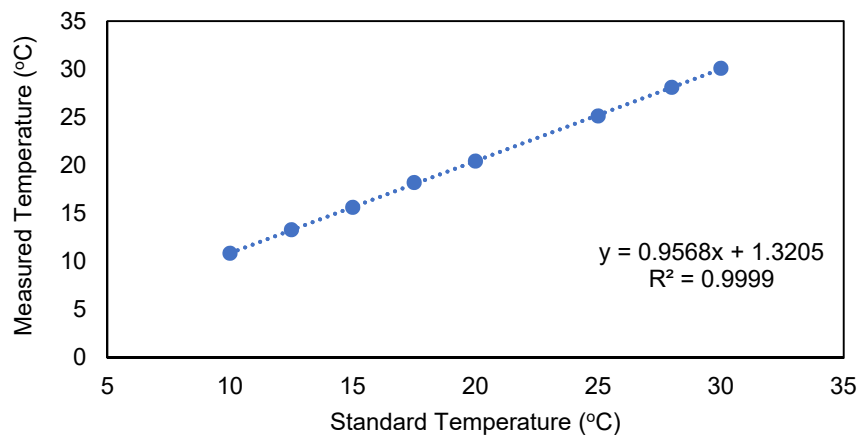


Figure 3-9. An example of one of nine calibration curves over testing temperature range from 10°C to 30°C against an NIST certified block temperature calibrator.

The data acquisition system performed well, logging air temperatures, RH and loop water temperatures continuously for the multi-year experiment. Once the wireless network was configured, it was found to be robust. The receiver for the network was placed inside the experimental room, and an extension USB cable was used to connect it to a desktop personal computer in the hallway of the facility. Without use of 120V power, nodes could become disconnected from the network, presumably because of so much metal present in the room that interfered with the radio signals. Thus, all wireless nodes were connected to 120V power, and had batteries in the event of a power outage. The controller and relay board were also connected to a battery backup system so that they would not lose their settings in event of a power outage.

3.3.2 Results of the water flowrate evaluation

The average water flowrate for each loop from repeated measurements on different days over two years of the chronic heat stress experiment are shown in Figure 3-10. The water flowrate significantly declined in 2016 compared to 2015. This decrease in water flowrate was observed for every loop in both CP-1 and CP-2. As listed in Table 3-2, the average water flowrate for each loop from the three days of measurements in 2015 was 4.85, 5.35, 5.34, 4.97, 5.34, and 6.03 kg/min for CP-1 top, CP-1 middle, CP-1 bottom, CP-2 top, CP-2 middle, and CP-2 bottom, respectively. These average values decreased to 3.87, 3.97, 3.89, 3.92, 4.05, and 4.12 kg/min correspondingly, which was a 20, 25, 27, 21, 24, 32% reduction in flowrate for CP-1 top, CP-1 middle, CP-1 bottom, CP-2 top, CP-2 middle, and CP-2 bottom, respectively.

Figure 3-10. Mean water flowrate for top, middle and bottom cooled perch loops in CP-1 and CP-2 measured on a total of seven days over two years during the chronic heat stress experiment. Multiple measurements were taken on seven day and the average (in kg/min) was taken to represent the water flowrate for each day. Yearly average of the measurements was shown for 2015 (N = 13) and 2016 (N = 12) for each loop. Error bars indicate the standard deviation of the mean.

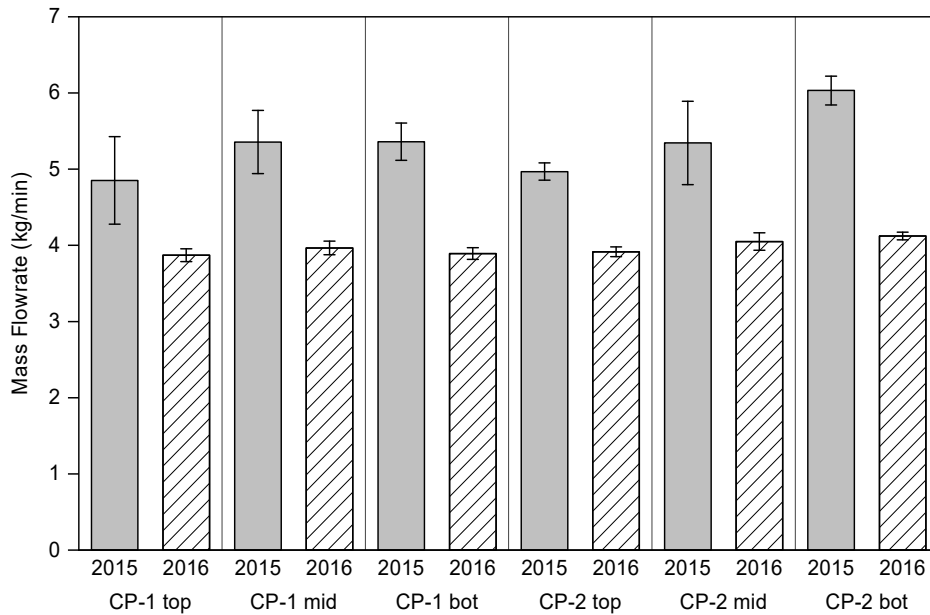


Table 3-2. Descriptive statistics including the yearly mean and the standard deviation of the mean (SD) of water flowrate measured in 2015 (N = 13) and 2016 (N = 12) in correspondence with Figure 3-10.

CP-1	2015		2016		CP-2	2015		2016	
	Mean (kg/min)	SD (kg/min)	Mean (kg/min)	SD (kg/min)		Mean (kg/min)	SD (kg/min)	Mean (kg/min)	SD (kg/min)
Top	4.85	0.574	3.87	0.084	Top	4.97	0.114	3.92	0.064
Middle	5.35	0.414	3.97	0.090	Middle	5.34	0.547	4.05	0.115
bottom	5.34	0.244	3.89	0.077	bottom	6.03	0.189	4.12	0.050
Overall	5.19	0.485	3.91	0.091	Overall	5.45	0.555	4.03	0.117

The measured water flowrate of the system design was compared to the value estimated using empirical equations (Equations 3-1 to 3-3) and provide an assessment of the uncertainty of the design, useful for larger-scale application in commercial egg laying farms. Table 3-3 lists key heat transfer properties of the CP system achieved by each iteration. The uncertainty of the design was about 77%.

Table 3-3. Results of thermodynamic properties of the CP system. Values list in the table are the corresponding means of the CP cages during a 24 h heat stress event.

Thermodynamic properties of cooled water estimated from equations					
Iteration	Reynolds number (<i>Re</i>)	Friction factor (<i>f</i>)	Pressure drop (kPa)	Flow rate (L/s)	Mass flow rate (kg/s)
1	14,738	0.0282	1.0	0.315	0.315
2	16,802	0.0273	1.3	0.359	0.359
3	16,507	0.0274	1.3	0.353	0.353
4	16,359	0.0275	1.2	0.350	0.350
Thermodynamic properties of cooled water estimated from measured flowrate					
				Averaged measured flowrate (kg/s)	0.08
				Reynolds number <i>Re</i>	3,776
				Uncertainty of estimation (%)	77.1

Four iterations were performed to numerically estimate the final pressure drop and the flowrate of the chilled water. According to the converged estimate, the Reynolds number was on the order of 10^4 , thus the estimated chiller water flow was in the turbulent flow regime. From the Moody diagram (ASHRAE, 2017a), the friction factor corresponding to the estimated Reynolds number range for smooth pipe was 0.0275. Subsequently, a 1.2 kPa theoretical final pressure drop of the CP system was computed. A 0.35 L s^{-1} volumetric flowrate of the cooled water was calculated using Equation (3-3) and the manufacturer pump curve, resulting in a 0.35 kg s^{-1} flow rate of the system. However, as indicated in Table 3-3, the mean measured water flowrate was only 0.08 kg s^{-1} , which yields a Reynolds number on the order of 10^3 (Equation 3-2). The discrepancy between the estimated and measured water flowrate generated an uncertainty as high as 77.1%. Based on the range of the Reynolds number calculated from measured water flowrate, the cooled water flow inside the loops was no longer in the turbulent flow regime, but in the transitional flow regime instead (Bergman et al., 2011). Our traditional understanding of heat transfer processes suggests that such a large discrepancy between calculated and measured water flowrate would likely lead to a corresponding large uncertainty in the heat transfer analysis.

3.3.3 Results of loop temperature rise and system net heat gain

Figure 3-11 demonstrates the loop temperature rise for the two representative heat stress periods. During these two periods, the room temperature setup followed the same heat stress regime, increasing to approximately 35°C from 0600 – 1800 h and stepping down to 26 – 28°C at 1800 until 0600 h the next day.

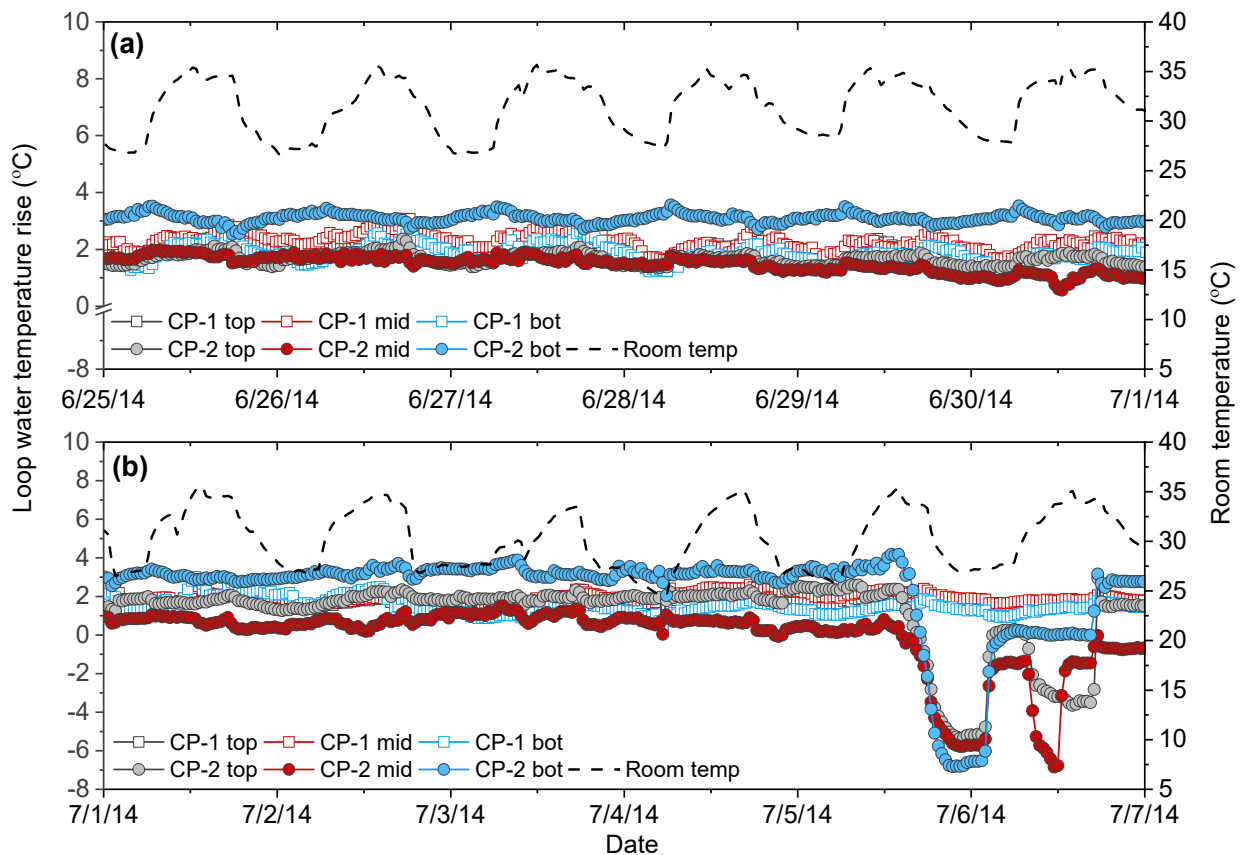


Figure 3-11. Loop temperature rise for both CP replicates. The temperature rise is calculated as return water temperature minus supply water temperature. Data were plotted for heat stress periods (a) June 25th to 30th, 2014 and (b) July 1st to 7th, 2014, with each symbol representing a temperature difference for a minute. The room air temperature was included for reference. During the plotted periods, the room temperature increased to approximately 35°C from 0600 – 1800 h and stepped down to 26 - 28°C from 1800 – 0600 h daily.

Table 3-4. Loop temperature rise mean and standard deviation (SD) for CP-1 and CP-2. The overall mean temperature rise and SD for each CP replicate are included.

CP-1	Loop temperature rise (°C)		CP-2	Loop temperature rise (°C)	
	Mean	SD*		Mean	SD*
Top	1.9	0.40	Top	1.7	0.27
Middle	2.1	0.41	Middle	1.2	0.48
Bottom	1.7	0.45	Bottom	3.1	0.24
<i>Overall</i>	1.9	0.19	<i>Overall</i>	2.0	0.99

* SD is the standard deviation of the mean (°C).

During system performance between June 25th to June 30th, 2014 (Figure 3-11a), the average (\pm standard deviation) water temperature rise between the return outlet and supply inlet for each loop was 1.9 ± 0.40 , 2.1 ± 0.41 , 1.7 ± 0.45 , 1.7 ± 0.27 , 1.2 ± 0.48 , and 3.1 ± 0.24 °C, for CP-1 top through CP-2 bottom. If the system performed as designed, with each circulating pump for each loop performing equally, there should be similar water temperature rise in each loop. However, this was not observed, as each loop had a different water temperature rise. The overall means of the loop temperature rise were similar between the two replicates, which were 1.9 and 2.0°C, for CP-1 and CP-2, respectively. However, substantial variation in measurements as indicated by their standard deviations, was observed (CP-1 = 0.19°C and CP-2 = 0.99°C). This indicates that although with the same system designs, experiment setup, and similar overall temperature differences were noted, the two replicates performed differently. The three loops in CP-1 were more repeatable and stable than those in CP-2.

After this relatively stable system performance period (June 25th to July 5th, Figure 3-11a), significant performance reductions were observed (Figure 3-11b), with a rapid disruption in the loop water temperature, as indicated by the supply water temperature being greater than the return water temperature in every loop of CP-2 after noon on July 5th, 2014. This trend of

negative temperature rise continued for approximately 24 h, after which CP-2 top and CP-2 bottom recovered to previous performance. The unequal performance of pumps for different loops was also supported by the results from water flowrate evaluation (Figure 3-10), from which the water flowrate was different between loops within and across the two CP replicates. Presumably, entrained air in the perches was at least partially responsible for the problem.

Hourly mean net loop heat gain and hourly mean room temperature during a stable system operation period from June 25 to June 30, 2014 are shown in Figure 3-12. During this period, room temperature ranged between 26.7 to 35.5°C, with an average of $31.5 \pm 2.85^\circ\text{C}$. Table 3-5 provides the results of the correlation analysis, including the Spearman rank correlation coefficients (r_s) and the *p-value* between the six net loop heat gains and the room temperature.

The net loop heat gain of CP-1 was reasonably similar for all three loops and paralleled indoor air temperature closely. The net heat gain of the CP-1 ranged from 690 to 850 W, with the bottom loop consistently having a lower net heat gain (690 ± 126.9 W), and the middle loop having the highest net heat gain (850 ± 118.7 W). No difference in net loop heat gain was observed for different levels within replication CP-1 ($P > 0.05$). For CP-2, large discrepancies were observed for the net loop heat gain of the top and middle levels versus that of the bottom ($P < 0.05$). The average net heat gain of CP-2 bottom loop (1298 ± 77.7 W) was significantly higher ($P < 0.05$) than that of the top (575 ± 73.9 W) or middle (551 ± 111.5 W) loops.

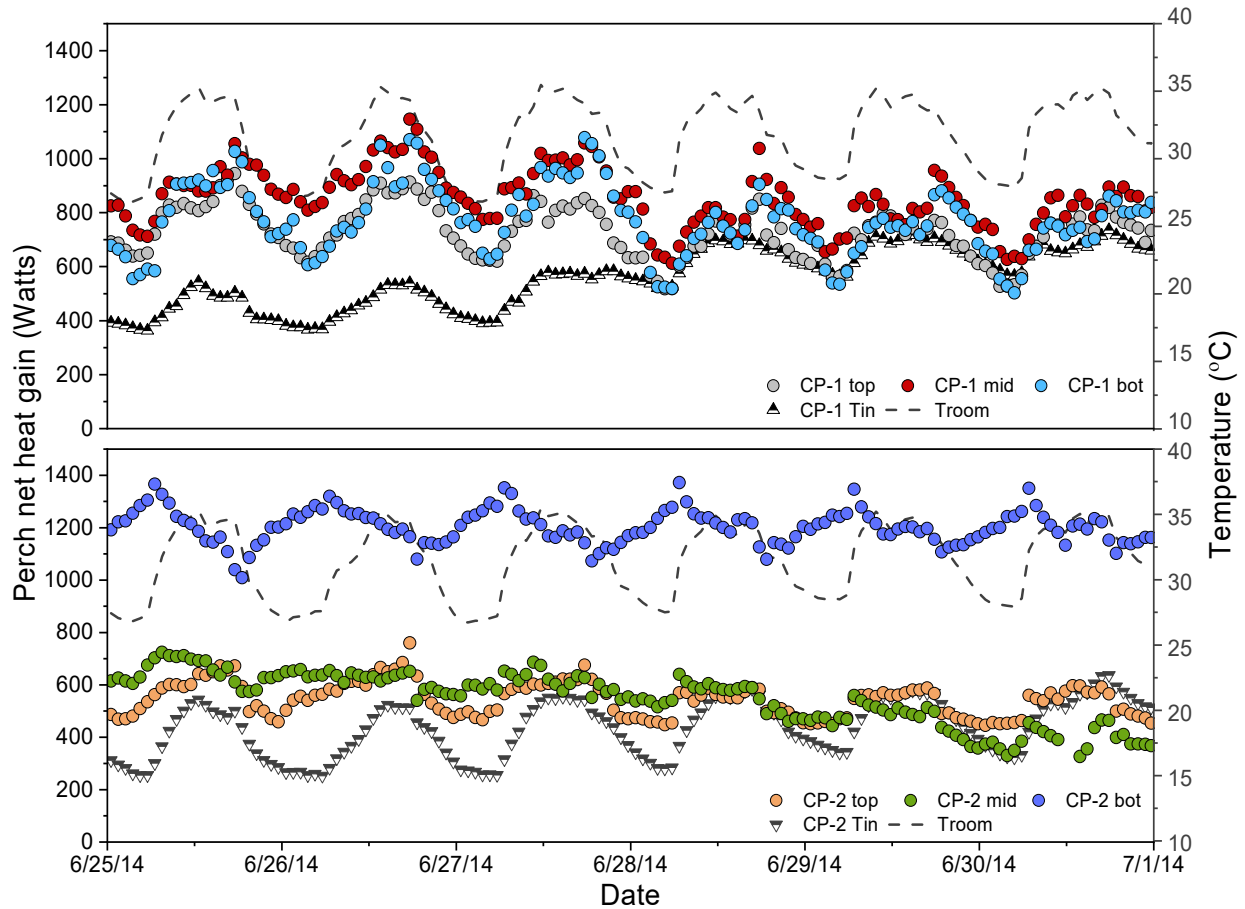


Figure 3-12. The hourly mean net loop heat gain during stable system operation (June 25 – 30, 2014, same Figure 3a). The heat gain was estimated from water flowrate measurements and loop temperature rise. Mean water inlet temperatures of the three loops in CP-1 and CP-2 were averaged hourly and plotted against time. The room air temperature was included. The room temperature increasing to approximately 35°C from 0600 – 1800 h and stepping down to 28°C from 1800 – 0600 h daily.

Table 3-5. The Spearman rank correlation coefficients (r_s) between the six perch loop net heat gain and the room temperature during stable system operation period from June 25 – 30, 2014 (N = 144).

Replicate	Perch level	r_s	$P - value$
CP-1	Top	0.73	< 0.0001
	Middle	0.43	< 0.0001
	Bottom	0.58	< 0.0001
CP-2	Top	0.75	< 0.0001
	Middle	0.04	0.6031
	bottom	-0.24	0.0042

There was a strong positive correlation between the room temperature and the net heat gain for all three loops in CP-1 ($p < 0.0001$). In other words, the net loop heat gain at different level in CP-1 increased with room temperature as would be expected. During heat stress events,

the net loop heat gain of CP-1 peaked around noon every day, when the room temperature also peaked, and declined to a minimum heat gain level after midnight, when the room temperature was at minimum. This is also valid for CP-2 top ($p < 0.0001$). However, there was lack of correlation between the net heat gain and the room temperature for the CP-2 middle ($p > 0.05$). Further, for the bottom loop in CP-2, a weak negative correlation was observed between the net heat gain and the room temperature ($p < 0.05$, $r_s = -0.24$), indicating the heat gain of this perch slightly decreased with increasing room temperature.

3.3.4 Results of heat transfer component analysis

The combination of the hourly average values of the environmental measurements selected for the heat transfer component analysis during a peak heat stress day is shown in Table 3-6. The results of heat transfer component analysis, containing heat transfer parameters, estimated values of convective heat transfer of the internal chilled water (Q_i), the convective heat transfer (Q_o) and the radiative heat transfer (Q_r) occurring in the CP system, and the equation numbers are provided in Table 3-7.

Table 3-6. A set of hourly averages of the environmental measures for the day June 27th, 2014 at noon time when a highest room temperature occurred. These environmental measurement values were used in the heat transfer component analysis.

Environmental Measures	Hourly value	CP-1	CP-2
Room ambient temperature, t_∞ (°C)	35.5	-	-
Loop water inlet temperature, $t_{w,in}$ (°C)	-	21.32	20.69
Loop water outlet temperatures, $t_{w,o}$ (°C)	-	23.74	22.87
Theoretical internal temperature, t_i (°C)	-	22.5	21.8

Estimated from the set of environmental measurements provided for a heat stress day (June 27th at noon, 2014) (Table 3-6), a Reynolds number of 3,747, in the magnitude of 10^3 was found. Because this value was greater than 2,300 but smaller than 10^4 , which is the boundary range between laminar and turbulent flow, the flow of the circulating cooled water in this study was characterized as transitional flow. Since this estimated Re number was closer to the laminar flow boundary value than that of the turbulent flow, a Nusselt *number* (Nu) of 3.66, the empirical value for fully developed laminar flow, was used for estimating the convective heat transfer coefficient, with assumptions that uniform flow and uniform surface temperature were met. The resultant convective coefficient of internal flow was $77.8 \text{ W/m}^2\text{K}$.

Two iterations were needed for estimating the convective and radiative heat gains. From the average loop water temperature measurements obtained from CP-1 and CP-2, a starting perch exterior surface temperature of 24°C was used in Equation (3-8) to get an estimate of the sum of h_o and h_r . Since the thermophysical properties of the saturated water and gaseous air needed for this analysis were acquired from textbook values, which were mostly derived from empirical experiments and approximation, corresponding thermophysical property values at the most proximate temperatures were used. Due to this limitation, only two iterations were needed to get a final converged value of t_{os} and h_{ot} , which was 23.8°C and $10.3 \text{ W/m}^2\text{K}$, respectively. Using the final converged values, a convective heat gain of the internal flow of 76.5 W , a free convective effect from the ambient air to the perch of 36 W , and a radiation gained from the

Table 3-7. Results of the heat transfer component analysis using a set of environmental measures for the day June 27th, 2014 at noon time when the highest room temperature occurred. Thermophysical properties of saturated water and gaseous air at desired temperatures were obtained from Bergman et al. (2011) and ASHRAE (2017c). The equations numbers included in the table are in reference to Sections 3.2.3.2 and 3.2.5.

Heat Transfer Parameter	Estimated value		Equation	Note
Mean theoretical internal temperature, t_i (°C)	22.0		(3-5)	All water properties were obtained at this mean temperature
<i>Reynolds number</i> (Re)	3,747		(3-2)	
<i>Nusselt number</i> (Nu) for internal flow	3.66			For developed laminar flow
Convective coefficient of internal flow, h_i ($\frac{W}{m^2K}$)	77.8		(3-7)	
Free Convection and Radiation Parameters				
	Iteration #1	Iteration #2	Equation	Note
Perch exterior surface temperature, t_{oS} (°C)	24.0	23.8	-	Started with an assumption $t_{oS} = 24$
Film temperature, t_f (°C)	29.75	29.65	$\frac{1}{2}(t_{oS} + t_{\infty})$	All air properties were obtained at film temperature, except for thermal expansion factor β , which was obtained at room temperature.
<i>Grashof Number</i> (Gr)	55,134	55,461	(3-9)	
<i>Raleigh Number</i> (Ra)	39,697	40,387	(3-9)	
<i>Nusselt number</i> (Nu, a) for free convection	6.16	6.18	(3-10)	
Free convection coefficient, h_o ($\frac{W}{m^2K}$)	4.74	4.75	(3-11)	
Radiation coefficient, h_r ($\frac{W}{m^2K}$)	5.56	5.55	(3-12)	
Estimated Heat Transfer Components				
	Estimated value		Equation	Note
Convective heat gain of internal flow, Q_i (W)	76.5		(3-13)	
Free convective heat gain from air, Q_o (W)	36.0		(3-14)	
Radiative heat gain from environment, Q_r (W)	42.1		(3-15)	
Forced Convection Parameter				
<i>Reynolds number</i> (Re_f) for forced convection	2,101		(3-16)	

ambient surrounding surfaces to the perch of 42.1 W were derived for the environmental measurements combination as provided in Table 3-6.

The possibility of a forced convection effect was ruled out using Equations (3-9) and (3-16), from which a magnitude of the relation between free convection and forced convection, expressed by the *Grashof number* and the *Reynolds number* (G_r/R_e^2) $\gg 1$ was found. Thus, the forced convection effect in this study was negligible (Bergman et al., 2011).

Results obtained from this analysis were useful for identifying the theoretical largest heat source for the cooled perch system. From Equation 3-8, the convective heat gain from the internal flow (cooled water) should equal the sum of radiation heat gain from the surrounding surfaces and the free convection heat gain from the external flow (ambient buoyancy air). This was proven by the values shown in Table 3-7. The analysis of system heat gain estimated using field measurements indicated that the convective heat transfer effect resultant from the ambient air was the largest contributor (Figure 3-12, Table 3-5). One possible reason for this is that large discrepancy and questionable accuracy exist between the estimation yield from field measurements and approximation obtained from empirical equations and proximal reference values. Furthermore, when quantifying the heat transfer components using empirical equations, many assumptions for ideal and uniform heat transfer environment were made, including assuming a fully developed laminar flow characteristic for the internal cooled water, a uniform temperature along the perch exterior surface, and a negligible forced convection effect. These

assumptions were necessary for solving problems that involving empirical equations, but also brought uncertainties of the accuracy to the yielding results.

3.3.5 Evaluation of System Performance

3.3.5.1 System heat gain, chiller capacity, and pump performance

The positive correlation noted between room temperature and perch loop net heat gain (Table 3-5) at all levels in CP-1, and the top loop in CP-2 indicates that natural convection from ambient air to the pipe outer surface was the major contributor to heat gain source over the other three heat transfer mechanisms (heat conduction transferred from the hens' footpads, and thermal radiation). However, the prediction generated from theoretical calculations (Table 3-7), suggested that the estimated convection heat gain of each CP replicate ($76.5 \text{ W/loop} \times 3 = 230 \text{ W}$) was about 1/10 of the system net heat gain calculated through measured water flowrate and loop temperature difference (2,334 W). One possible hypothesis for such discrepancy is that the nature of the loop flow was in the transition phase between laminar and turbulent, which made internal convective heat transfer difficult to predict. The characteristics of transitional flow are difficult to determine, as the nature of the flow is much more complicated than laminar or turbulent flow alone. Literature has demonstrated that natural convection can affect the heat transfer coefficient in the presence of weak forced convection, such as may have occurred. As the forced-convection effect increases, "mixed convection" (superimposed forced-on-free convection) gives way to pure forced convection. Bergman et al. (2011) pointed out the

complexity of situations where mix convections have to be both taken into consideration. Grigg et al. (1982) and Metais and Eckert (1964) found that the heat transfer coefficient for a mixed-convection flow regime is often larger than that calculated based on the natural or forced-convection calculation alone (ASHRAE, 2017a, 2017c), which supports our findings.

From Figure 3-12, the average water inlet temperature among the three loops within each replicate exhibited a steady daily increase, with CP-1 loop inlet temperatures rising more rapidly than CP-2. To further evaluate the system performance, individual loop inlet water temperatures for CP-1 top through CP-2 bottom during a 24 h interval for two representative days of stable operation (June 28th and July 4th, 2014) are shown in Figure 3-13. The majority of the loop inlet temperatures were significantly different from one and another ($p < 0.0001$), except for CP-1 top and middle on June 28th, 2014 ($p = 0.2049$).

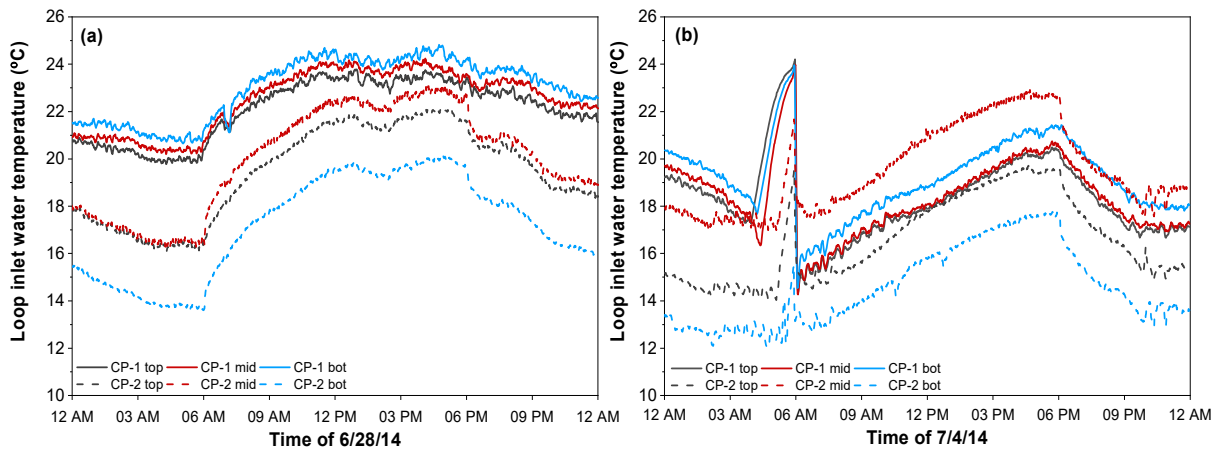


Figure 3-13. Inlet water temperatures for six loops (CP-1 top through CP-2 bottom) during a 24 h period of two representative days: **a)** June 28th, 2014 and **b)** July 4th, 2014. During the plotted periods, the room temperature increasing to approximately 35°C from 0600 – 1800 h and stepping down to 28°C from 1800 – 0600 (+1) h daily. Pump for each loop was activated when air temperature exceeded 25°C.

The difference in loop inlet water temperatures suggest that despite the use of the same model pump, water coolers and identical thermal storage manifolds, these components did not perform equally. The water pump to activate the flow on each deck was providing marginal performance, without providing enough flow to maintain the designed water flowrate as indicated by the pump curve from the manufacturer. As shown in Figures 3-11 and 3-12, the loop temperature rise and the net loop heat gain are different to one and another. If the water pump would perform and provide flow similarly, the inlet water temperatures should be similar for different loops, since the design provided for equal pressure drops in each loop. Given that each pump performed differently, we expected lower water flowrates should result in greater loop temperature rise, as the pumps were not providing enough flow to push the cooled water through the loop. Similarly, a higher water flowrate should result in smaller loop temperature rise. While the assumption was somewhat supported by the system performance observed for CP-1 regarding the relationship between the average measured water flowrate and the loop temperature rise, this was not consistent for CP-2. Specifically, as shown in Figure 3-11(a), CP-2 top had the second smallest water temperature rise, which suggested it should have a large water flowrate; however, from the measured flowrate, CP-2 top had the lowest water flowrate among all six loops. CP-2 bottom also presented similar contradictory behavior between temperature rise and the corresponding average water flowrate.

This behavior further indicates that the water coolers and thermal storage were incapable of extracting the total heat transferred to the cooled perch system. The water coolers were rated to provide 0.0134 kg/s (12.7 gal/h) flow rate of 10°C chilled water at 26.7°C (80°F) inlet water temperature and 32.2°C (90°F) room temperature, or a steady-state output of approximately 930 W (Equation 3-4). However, the 24 h average net heat gain calculated for each replicate was 2,241 and 2,426 W for CP-1 and CP-2, respectively, exceeding the maximum operational cooling capacity by 141 and 161%. This could explain the elevated water inlet temperatures, which were 21.1 and 18.6°C on average for CP-1 and CP-2, respectively. These values are significantly warmer than the cooled water temperature setpoint (approximately 10°C). The systems were only able to partially extract stored heat from the thermal storage manifolds, as noted in Figure 3-12. Proper thermal storage sizing is critical to limit loop inlet temperature rise during the daily heat stress period, while avoiding oversized chillers.

3.3.5.2 Design criteria for future application

The details of design criteria for each replicate cooled perch used in this study is listed in Table 3-8, from which useful information for other scales of application can be extrapolated. The average daily net perch heat gain was approximately 2,334 W, or about 128 W per meter perch length and 43.2 W per hen housed. These values are based on our system operating at a 12 h day/12-h night air temperature of 35/28°C and an average loop inlet water temperature of 20°C. Decreasing loop inlet temperature to 10°C with the same temperature schedule would increase

the average daily net perch heat gain by approximately 1.9 times. This increase arises from a greater average temperature difference between air and perch surface (21.5 K versus 11.5 K) average daily difference.

Table 3-8. Details of design criteria for each replicate cooled perch system in this study.

Design criteria	CP-1	CP-2	Average
Total average daily net heat gain (W)	2,241	2,426	2,334
Net heat gain per length (W/m)	122.5	132.5	127.5
Net heat gain per hen (W/hen)	41.5	44.9	43.2

Table 3-8 provides the maximum values of the hourly chilled water load for stable system operation period June 25th – 30th, 2014 measurements of net perch hourly sensible heat gain for each day and each replicate, and the corresponding partial-storage thermal energy storage (TES) sizing calculation for the experimental perches in this study. From the Q_{max} column, it indicates that using the same chiller design from this experiment and the same environmental condition settings, a total of 64.4 kWh peak-day load is required by the thermal energy storage. Chiller output of 2.7 kWh operating continuously would slightly exceed the peak-day load of 64.4 kWh and require a TES capacity and volume⁵ of 2.5 kWh and 0.26 m³, respectively (ASHRAE, 2016). These calculations suggest that the experimental perch, with approximately 900 W chiller output and 0.02 m³ water storage manifold (considered as a thermal energy storage) volume, was significantly undersized.

⁵ Equation 3-21 in Section 3. 2.7.2: TES volume is computed from Equation 4, Chapter 51 (ASHRAE, 2016) using 90% efficiency and a 9K temperature difference. Actual values depend on application and tank configuration.

Opportunities for energy savings and trade-offs between chiller capacity and TES volume could be further exploited with alternative system control settings. For example, for the daily full-storage load profile in Table 3-9 for this system, but with the water chiller shut down for 6 h during the afternoon peak electricity period could result in energy savings with larger capacity chiller (3.575 kWh). In this case, the TES volume must increase from 0.26 to 1.8 m³. In this example, the capital cost of added TES volume must be balanced against chiller power costs.

For future applications of a cooled perch system, the total thermal storage should be properly sized to meet both the total integrated load and the peak-hour load (ASHRAE, 2016). Either under-sizing or excessively oversizing the thermal storage should be avoided, as undersized thermal storage leads to limited capacity and a prolonged recovery time when exceeding its cooling capacity, while on the other hand, oversized thermal storage will compromise the energy savings and economic benefits, which should be the basic consideration for thermal storages (ASHRAE, 2016).

Table 3-9. Peak day full-storage thermal energy storage sizing calculation for a stratified chilled water (CHW) system.

Time	Cooled perch hourly sensible heat gain for each replicate (kW)												Qmax (kW)	Chiller Output (kW)	TES Charge (kWh)
	25-Jun		26-Jun		27-Jun		28-Jun		29-Jun		30-Jun				
	CP-1	CP-2	CP-1	CP-2	CP-1	CP-2	CP-1	CP-2	CP-1	CP-2	CP-1	CP-2			
12 AM	2.20	2.29	2.27	2.37	2.30	2.26	2.28	2.19	2.06	2.11	2.02	2.00	2.37	2.7	0.93
1:00	2.18	2.32	2.33	2.45	2.25	2.34	2.16	2.20	2.13	2.15	1.96	2.03	2.45	2.7	1.19
2:00	2.08	2.31	2.14	2.45	2.20	2.32	1.83	2.20	1.85	2.15	1.74	2.01	2.45	2.7	1.43
3:00	1.93	2.34	2.03	2.43	2.05	2.31	1.71	2.21	1.76	2.14	1.68	2.03	2.43	2.7	1.70
4:00	1.93	2.42	2.07	2.48	2.03	2.40	1.68	2.25	1.80	2.19	1.67	2.05	2.48	2.7	1.92
5:00	1.95	2.52	2.14	2.47	2.05	2.37	1.65	2.27	1.87	2.20	1.75	2.11	2.52	2.7	2.10
6:00	2.07	2.63	2.28	2.56	2.29	2.57	1.89	2.58	2.20	2.45	2.01	2.37	2.63	2.7	2.17
7:00	2.43	2.64	2.39	2.51	2.43	2.55	2.00	2.48	2.23	2.38	2.10	2.27	2.64	2.7	2.23
8:00	2.55	2.61	2.43	2.48	2.54	2.47	2.15	2.38	2.32	2.33	2.25	2.20	2.61	2.7	2.33
9:00	2.63	2.55	2.41	2.51	2.43	2.46	2.18	2.38	2.39	2.29	2.38	2.18	2.63	2.7	2.39
10:00	2.64	2.53	2.48	2.50	2.64	2.53	2.30	2.43	2.40	2.25	2.37	2.12	2.64	2.7	2.45
11:00	2.63	2.51	2.63	2.46	2.83	2.48	2.39	2.37	2.31	2.22	2.24	1.99	2.83	2.7	2.32
12 PM	2.61	2.52	2.83	2.51	2.69	2.39	2.29	2.34	2.30	2.27	2.32	2.05	2.83	2.7	2.19
1:00	2.60	2.48	3.02	2.50	2.77	2.38	2.22	2.31	2.21	2.27	2.40	2.14	3.02	2.7	1.87
2:00	2.69	2.45	2.88	2.47	2.77	2.39	2.10	2.36	2.33	2.27	2.25	2.12	2.88	2.7	1.69
3:00	2.76	2.47	2.79	2.48	2.72	2.40	2.27	2.40	2.24	2.24	2.22	2.24	2.79	2.7	1.60
4:00	2.77	2.43	2.83	2.52	2.78	2.44	2.56	2.40	2.31	2.30	2.43	2.28	2.83	2.7	1.46
5:00	3.03	2.32	3.13	2.58	2.99	2.44	2.79	2.26	2.59	2.22	2.58	2.17	3.13	2.7	1.03
6:00	2.87	2.18	3.05	2.25	2.93	2.25	2.49	2.07	2.58	2.04	2.47	2.00	3.05	2.7	0.68
7:00	2.66	2.16	2.83	2.29	2.82	2.29	2.31	2.16	2.46	2.04	2.46	2.06	2.83	2.7	0.55
8:00	2.58	2.23	2.80	2.26	2.66	2.26	2.45	2.14	2.35	2.02	2.41	2.00	2.80	2.7	0
9:00	2.46	2.28	2.64	2.22	2.41	2.20	2.33	2.08	2.30	1.99	2.41	2.00	2.64	2.7	0.06
10:00	2.32	2.30	2.47	2.20	2.33	2.16	2.17	2.11	2.18	1.98	2.30	2.01	2.47	2.7	0.29
11:00	2.30	2.30	2.39	2.20	2.31	2.19	2.12	2.13	2.04	1.97	2.39	1.98	2.39	2.7	0.60
	Total (kWh)												64.4	64.8	

3.3.6 Implications to laying hens

3.3.6.1 *Laying hen daily perching behavior*

The mean perch use efficiency of laying hens (represented in percentage) on each deck during days of heat stress is provided in Figure 3-14. The numbers of laying hens perching over a 24-hr period of the selected day (July 14, 2014) during the daily heat stress (6-11am, 2-4pm, 6-8pm and 11-12pm), along with cage air temperature measured at the center partition between the cages are shown 3-15. Hens housed in the CP units had an average of (61.3 ± 2.0) % perching rate, as compared to (14.8 ± 1.5) % for the AP units. Hens used the cooled perches with a much higher rate than the air perches ($p < 0.001$). Besides providing cooling effects to hens, the perch system also offered birds an opportunity to express their natural behavior, which was observed during the night cycle (1800 – 2400 h) in both AP and CP systems. Within a tier of two cages, the CP system was used by all hens at night, and by 3 to 13 hens during the day. As cage air temperature increased in the morning, the number of hens perched on the CP loop quickly increased to a peak number by 11 am. As the air temperature decreased in the afternoon, the number of birds perching also declined accordingly. Besides providing cooling effects to the birds, the perch system also offered birds an opportunity to express their natural behavior, which can be observed during the night cycle. After lights were turned off at 6 pm, all 18 hens perched through the night. The same trend was observed for other tiers analyzed. Although not shown, daytime use was higher in the CP cages than in the AP cages. Hens in the CP cages were also noted to have more body contact with the CP surface.

As shown in Figure 3-15, after lights were turned off at 6 pm, all 18 hens were observed to perch through the night. Behavioral analyses from the acute heat episode in the same study (Makagon et al., 2015; Hu et al., 2016) showed that hens in the CP cages utilized the perch at a higher frequency ($p < 0.001$) at all observation times as compared to the AP cages. At 21.4 wk of age, hens housed in the CP cages had an average of $71.6 (\pm 3.4)$ % perching rate, 17% higher than those in the AP cages $54.1 (\pm 3.4)$ %. During the acute heat stress events at hens' age of 27.6 wk, the perching rate in the CP cages was $64.2 (\pm 2.7)$ % significantly higher when compared to a $48.3 (\pm 2.7)$ % perch utilized by hens in the AP cages.

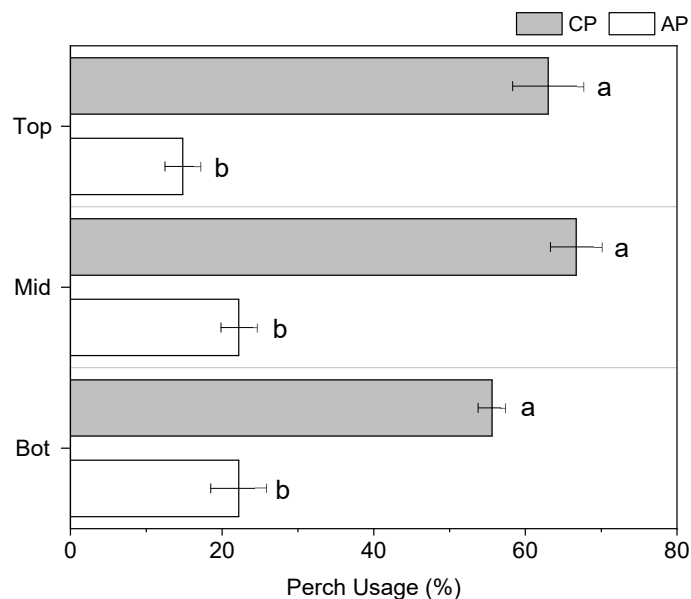


Figure 3-14. Average perch use efficiency of laying hens (represented in percentage) in CP and AP units on each deck during heat stress episodes on selected days. Error bars indicate standard error of the mean. Different letters indicate the mean of CP and AP treatment was different than the other using a paired t-test ($p < 0.05$).

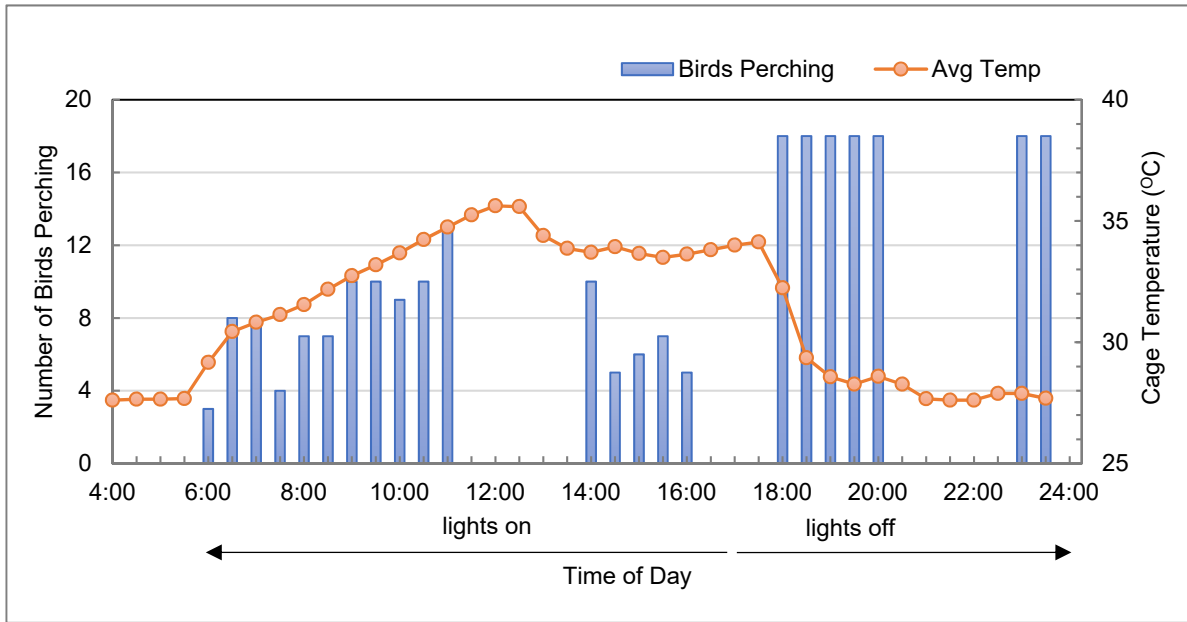


Figure 3-15. An example of the number of hens using the cooled perches over time for a selected day (July 14, 2014) during the heat stress event (0600 to 1600 h) along with average cage air temperatures at 30 min intervals. Note: hours without bars representing number of birds perching indicate that no sampling was taken, not that no birds were perching.

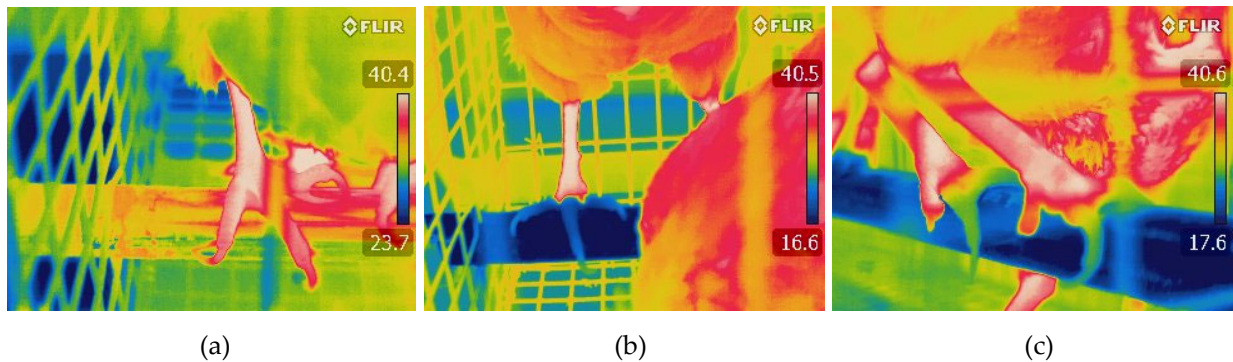


Figure 3-16. Sample infrared thermal images indicate (a) a side view of a hen perching on the air loop in air perch (AP) treatment; (b) a front view of a hen perching on the chilled water loop in cooled perch (CP) treatment; and (c) a side view of a hen perching on the chilled water loop in cooled perch (CP) treatment. In the thermal images, blue to green indicates cooler temperatures and yellow to red indicates warmer temperatures. (photos courtesy of Dr. Jiaying Hu, USDA-ARS).

Figure 3-16 demonstrates that hens perched on AP perches (a) had substantially warmer feet temperatures (approximately 37 – 38°C) than those on CP perches (approximately 17 – 20°C). Hens that perched on CP perches clearly had much cooler feet temperatures when

compared to their lower-portion body temperature. Chepete et al. (2011) identified the average core body temperature of the hen was about 41°C, which was shown as the maximum body temperature scale on Figure 3-16. Given this body temperature, a 17 – 20°C foot temperature is about 21 – 24°C temperature reduction from their body core, which suggest a great potential of relief of heat stress through conductive heat transfer from their feet.

3.3.6.2 Estimating the hen footpad area

Ten laying hens were used to measure the contact area between their footpad and the perch. Table 3-10 lists a summary of the result. Figure 3-17 provides a lateral view of the thermal image of a bird’s footpad right after she was taken off from the perch and the estimated contact area.

Table 3-10. Results of contact area between the chicken footpad and the perch.

Group analyzed (N)	Avg. perch pixels	Avg. total perch area (cm ²)	Avg. footprint pixels	Range of footpad area (cm ²)	Avg. footpad area (cm ²)
30	81551 ± 7312.1	118 ± 10.6	11724 ± 1496.6	11.9 – 21.8	17.01 ± 2.17

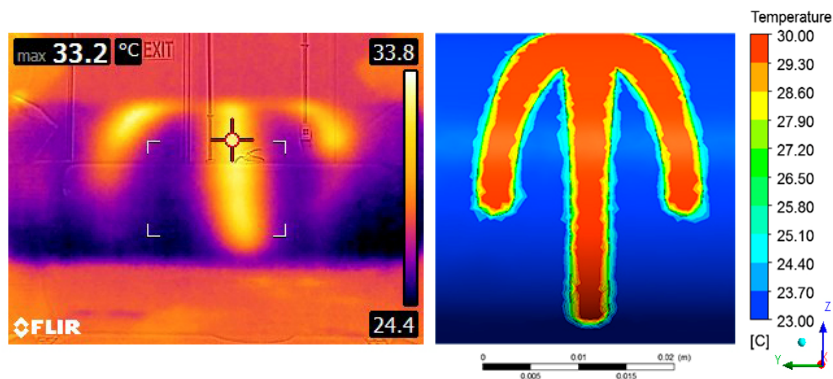


Figure 3-17. Contact area between the chicken footpad and the perch. (a) shows the thermal image of a bird’s footprint right after she was taken off the perch. (b) shows the simulation of the footprint using CFD tools.

An average of $17.0 \pm 2.17 \text{ cm}^2$ (14.4 % of the total perch area captured by the thermal camera) was estimated for the chicken's footpad area. Martland (1985) reported the plantar areas of bird's feet to be about 20.58 cm^2 . Results obtained from this study was slightly smaller than that reported by (Martland, 1985). Possible explanations for the difference include: advanced technologies, such as the use of thermal camera and modeling tools provides more accurate results; rather than the whole plantar areas of the chicken; different methods used between the studies regarding measuring the foot area; or, birds used in our study did not press their whole plantar and toe areas to the perch during perching, which consequently resulted in a smaller contact area.

3.3.6.3 Estimating thermal conductance of hen footpad area

The updated laying hen footpad area is useful for estimating thermal resistance of the foot skin of laying hens, if an approximate value of heat conduction contributed to the hens is provided. Albright (1990) provided an estimated values of 6.6 W/kg total heat production and 3.7 W/kg sensible heat production for leghorn laying hen with a typical body weight around 1.8 kg and kept under an air temperature of 28°C. Chepete et al. (2011) estimated the heat and moisture production of W-36 laying hens kept under 24 to 27°C temperatures and reported a daily time-weighted averaged (TWA) value of 6.1 to 7.2 W/kg total heat production for birds at age 28 – 33 wk. These values equivalent to an 8.9 – 10.4 W total heat production per bird.

For this analysis, the most recent sensible heat production data for W-36 hens, 3.8 W/kg, conducted by Chepete et al. (2011) was used. Given a 1.8 kg average body weight of laying hens at 30 wk of age, an average sensible heat production of 6.8 W was obtained. Hillman et al. (1982); Hillman and Scott (1989) claimed that a 25% of a bird's total sensible heat production (SHP) can be transferred from vasomotion through their feet, shank, and bottom leg area. If a 10% transfer rate to the perch is assumed, the conductive heat transfer of a hen through her footpad area can be estimated to be on the magnitude of 0.68 W.

With proper assumption of the temperature difference between the hen footpad area and the exterior perch surface, the thermal conductance (U_{hen}) and thermal resistance (R_{hen}) of the footpad can be derived using the following equation:

$$Q_{conduction} = U_{hen}A_{feet}\Delta t = \frac{1}{R_{hen}}A_{feet}\Delta t \quad (3-22)$$

where $Q_{conduction}$ is the estimated value of conductive heat contributed by the laying hens; U_{hen} is the acquired thermal conductance of chicken footpads ($\frac{W}{m^2K}$); R_{hen} is the acquired thermal resistance of chicken footpads ($\frac{m^2K}{W}$); A_{feet} is the total estimated value for chicken feet contact area (= 0.0034 m^2 , Table 3-10, assuming both feet were on the perch); and Δt is the temperature difference between chicken feet and the perch exterior surface temperature (K).

Using the estimated values previously discussed and a temperature gradient of 7 K from the hens' footpad to the perch exterior surface, the estimated thermal resistance of a laying hen's foot is 0.035 $\frac{m^2K}{W}$, resulting in a thermal conductance of 28.5 $\frac{W}{m^2K}$. However, cautions need to be

taken when utilizing these values, since many uncertain factors are associated with the estimation, which may lead to large error rate.

Several factors can introduce uncertainties to this analysis, including improved genetic, physiology performance and production of current strains of laying hens, different age of the laying hens between this study and those in Chepete et al. (2011) (the analysis in previous sections were carried over measurements made when the hens were 19 wk old in this study), different room temperature schedule (28 – 35.5°C for this study); and different assumptions of transfer rate and temperature gradient when obtaining the hen's conductive heat transfer values.

3.4 PERFORMANCE CHALLENGES AND RECOMMENDATION

Air lockage in the system was a persistent challenge throughout the study and impacted the ability to maintain desired system operation. Symptoms of air lockage included steadily increasing loop outlet temperatures combined with relatively elevated and stable loop inlet temperatures; visible air bubbles were occasionally seen being purged into the cooled water storage manifold. This may have been caused by the open top thermal storage manifold rather than a closed system. To prevent air lockage for potential future research or larger scale application, we recommend a closed system that does not have system flow change due to elevation change. The closed water system should have a properly sized expansion tank that is suitable to maintain a constant system pressure during operation, and an air/water separator. A water flowmeter on each loop would be useful for diagnosis and system performance validation.

Despite regular treatment with quaternary ammonia, biofilm buildup inside the system was observed throughout the study. Biofilm accumulated inside the cooled perch loops and on the inlet and outlet water temperature sensors (Figure 3-18). Similar accumulation was regularly seen for the water chiller filter, regardless of the replacement frequency of the filters (at least change once a month). The status of the water chiller filters, and the biofilm accumulation should be closely watched during the experiment, and the water filters should be replaced as frequent as possible. Such issues, such as biofilm accumulation or plugged filters may have reduced the response time of the water temperature sensors, and affected pump performance and pump lifespan. By using a closed system, the amount and frequency of biofilm buildup is expected to be at minimum.

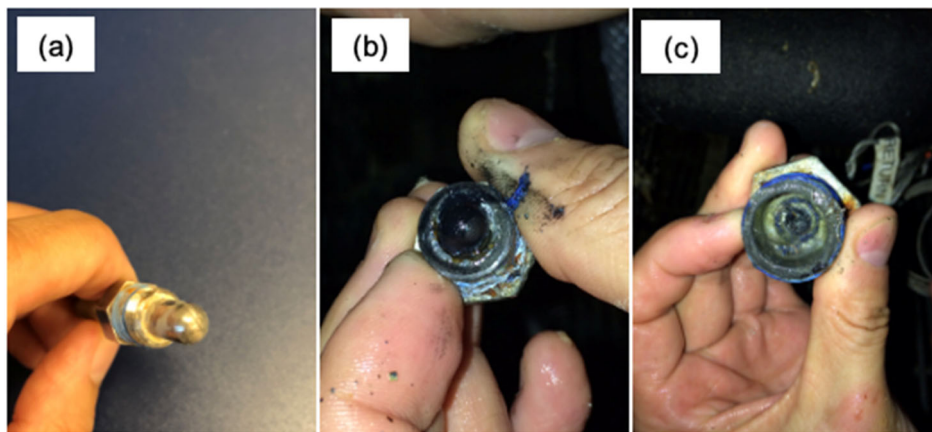


Figure 3-18. Sensor condition: (a) clean sensor prior installation; (b) sensor condition and (c) sensor housing condition after one year of installation.

3.5 SUMMARY AND CONCLUSIONS

The cooled perch system was designed and was used for an experiment assessing the effect of using the cooled perch as a cooling tool to relieve heat stress for laying hens. The data acquisition system performed well, logging air temperatures, RH and loop water temperatures continuously for the multi-year experiment. Once the wireless network was configured, it was found to be robust. The positive benefits to the laying hens in terms of physiology, foot health, and performance were realized by the experimental cooled perch design.

The performance of the cooled perch system was assessed for a stable system operation period (June 25th – 30th, 2014) by analyzing the water flowrate, characterizing the loop water temperature rise profile, and estimating the system net heat gain. The water flowrate measured in 2015 for each loop was 4.85, 5.35, 5.34, 4.97, 5.34, and 6.03 kg/min for CP-1 top, CP-1 middle, CP-1 bottom, CP-2 top, CP-2 middle, and CP-2 bottom, respectively. These values significantly reduced for 2016 measurements. When compared to water flowrate directly measured during experiment, a 77.1% difference rate was revealed for water flowrate estimated from empirical equations. The analysis of water flowrate indicate that the pumps were giving decreased performance gradually, and there was a discrepancy between the pump actual output than that was provided by the manufacturer.

Different loops and CP replicates did not have equal performance regarding loop water temperature rise and loop net heat gains. There was a strong correlation noted between room

temperature and perch net heat gain, indicating natural convection from ambient air to the pipe outer surface was the major contributor to heat gain source over other heat transfer mechanisms.

A heat transfer component analysis was performed using a set of environmental measurements to estimate the heat gain sources, including the convection of internal flow inside each perch loop, the free convection of ambient air to perch exterior, and radiation from surrounding surfaces to the perch exterior. A convective heat gain of the internal flow of 76.5 W, a free convective gain from the ambient air to the perch of 36 W, and a radiation gained from the ambient surrounding surfaces to the perch of 42.1 W were computed for representative conditions using empirical equations. Forced convection of ambient air in this environmental setting was negligible.

The design criteria useful for other scale applications of cooled perch were provided. An average daily heat gain of about 128 W/m perch length or 43.2 W/hen housed was estimated, based on 12-h day/12-h night air temperature of 35/28°C and an average loop inlet water temperature of 20°C. A peak-day system heat load of 64.4 kWh was estimated and required a thermal storage capacity of 2.5 kWh. A closed system should be considered for future cooled perch applications.

At 21.4 wk of age, hens housed in the CP cages had an average of 71.6 (± 3.4) % perching rate, 17% higher than those in the AP cages 54.1 (± 3.4) %. During the acute heat stress events at 27.6 wk old hens, the perching rate in the CP cages was (64.2 \pm 2.7) % significantly

higher when compared to a 48.3 (± 2.7) % perch utilized by hens in the AP cages. An average of 17.0 cm² was estimated for the hen's footpad area. With assumptions of the conductive heat transfer rate and temperature gradient, a 0.035 $\frac{m^2K}{W}$ thermal conductance, or a 28.5 $\frac{W}{m^2K}$ thermal resistance of both feet of a laying hen was found.

3.6 ACKNOWLEDGEMENTS

Funding for this work was supported by the USDA-NIFA Competitive Grants Program under the Award No. 2013-67021-21094. The authors would like to thank the staff and graduate students of the Department of Agricultural and Biological Engineering, University of Illinois Urbana-Champaign, the Livestock Behavior Research Unit, USDA-ARS, and the Department of Animal Sciences, Purdue University, as well as George W. Hester, Jr., for their efforts in conducting this study. Mention of commercial products in this article is solely for providing scientific information and does not imply recommendation.

CHAPTER 4 IMPROVEMENT TO THE INTELLIGENT PORTABLE MONITORING UNIT (IPMU) FOR AIR QUALITY MONITORING IN ALTERNATIVE POULTRY HOUSING SYSTEMS

4.1 INTRODUCTION

4.1.1 Ventilation and air quality in poultry houses

Ventilation is a crucial factor for optimum bird performance in poultry facilities, which is interlinked with the interior air quality of poultry houses. Proper ventilation promotes good air exchange, removes excessive heat, moisture, particulate matter, and common gases present in poultry housings such as carbon monoxide (CO), carbon dioxide (CO₂), and ammonia (NH₃) produced by poultry, bedding, and heating systems (Albright, 1990; ASHRAE, 2017d, 2019; Cândido et al., 2018; Corkery et al., 2013; Kocaman et al., 2006). Proper ventilation in livestock and poultry housing systems is important for optimum animal production, performance, disease control, and the well-being for both animals and human workers.

Figure 4-1 illustrates a logic diagram for the relationship between ambient temperature during all seasons and ventilation rate to achieve desired indoor air quality and animal comfort (ASHRAE, 2019). From Figure 4-1, achieving ideal ventilation rates (rates A, B, C and D) is critical for moisture removal, maintaining proper indoor air quality and interior temperature under a variety of ambient temperatures. During winter conditions, a minimum ventilation rate (curves A and B) is required to maintain an indoor relative humidity (RH) level at or below the

maximum desired RH, and an acceptable range of gas concentrations. It is acknowledged that the ventilation should function for moisture control rather than temperature control (curve C) as is desired during summer (ASHRAE, 2019). ASHRAE (2019) has established a general guideline for winter ventilation to be managed to maintain an indoor RH to be in the range of 70 – 80%. A minimum ventilation should always be provided to remove any excessive moisture buildup. During warmer weather conditions, a greater ventilation rate than the required by minimum moisture control and air quality control is needed to limit temperature rise in the building (curves C and D). During summer conditions, the ideal ventilation rate is chosen to provide sufficient air movements for the animals and to reduce the interior temperature rise to minimum practical extent. According to ASHRAE, the maximum practical ventilation rate for maintaining interior comfort conditions is often set at 60 air changes per hour (ASHRAE, 2019). An alternative design criterion is to size maximum ventilation rate to limit building temperature rise (Albright, 1990; MWPS, 1983).

Controlling the living space thermal environment, particularly the interior air temperature and air quality, e.g., ammonia (NH₃) and carbon dioxide (CO₂) levels, is crucial to poultry's health, welfare and productivity (Dawkins et al., 2004; Naseem and King, 2018; Webster and Czarick, 2000). Barn air temperature setpoints affect the ventilation management and ventilation rate, which consequently affects the air quality in poultry house. Particulate matter (PM) and gases are identified as the most common air contaminants in a livestock or poultry house

(ASHRAE, 2019). Compromised thermal conditions and air quality such as high indoor temperatures and RH, high levels of particulate matters (PM₁₀ or PM_{2.5}), and high concentrations of NH₃ and CO₂ may negatively affect poultry's health and performance.

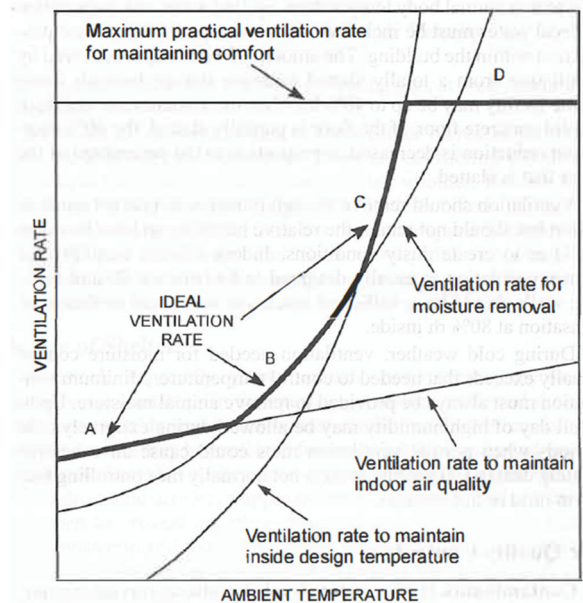


Figure 4-1. Logic for selecting appropriate ventilation rate in livestock buildings. (Source: 2019 ASHRAE Handbook – HVAC Applications (SI), pp.25.1. Originally adapted from (Christianson and Fehr., 1983))

Heat stress is one of the most common issues facing the global poultry industry and remains a challenge. Heat stress seriously compromises the welfare of laying hens in commercial egg production, negatively affects their performance, egg production and can cause death, leading to substantial economic losses. The negative impact of heat stress to the poultry industry was discussed in the previous Chapter, Section 3.1.

CO₂ is one of the most common gases produced in a poultry house. CO₂ in poultry houses is generated through several sources and can vary by many factors, including litter or manure handling conditions and heater use during winter (Calvet et al., 2011; Xin et al., 2009),

degradation of uric acid from poultry manure (Miles et al., 2006; Singh et al., 2009), number of birds, flock density, bird age, activity level, feed consumption, diet composition, and bird respiration (Calvet et al., 2011; Cândido et al., 2018; Pedersen et al., 2008). Interior CO₂ levels are important factors for ventilation management in poultry houses and are commonly used to design appropriate minimum winter ventilation rates for maintaining indoor air quality and controlling moisture (Albright, 1990; ASHRAE, 2019; Barber et al., 1993; Cândido et al., 2018; Donham et al., 1989; Liang et al., 2005; Ni et al., 2017; Xin et al., 2009). Donham et al. (1989) suggested an indoor CO₂ concentration below 2,770 mg/m³ (equivalent to 1,500 ppm) (ASHRAE, 2017d) to avoid respiratory disorder symptoms in workers in a controlled swine building. For other industries, a CO₂ concentration of 5,000 ppm is suggested as the 8-h time-weighted exposure threshold limit value (ACGIH, 1998). Barber et al. (1993) evaluated the CO₂ concentrations in 173 swine buildings and reported that the CO₂ concentrations were below 3,000 ppm for the majority of the swine buildings monitored when the ambient temperature was above 0°C, however, such low concentration was a challenge for outside temperatures below 0°C (ASHRAE, 2019). For cold climates, there was a very high penalty in heating cost if a less than 5,000 ppm CO₂ concentration is the maximum allowed value. For the turkey production industry, elevated levels of CO₂ were believed to act as a stressor and contribute to early poult mortality (Donaldson et al., 1995; Frame et al., 1999). In addition to early poult development, several researchers have associated increased CO₂ concentration to the cause of round hearts in poultry

(Olanrewaju et al., 2008; Owen et al., 1995; Wideman et al., 1999), although this hypothesis was not supported by the results reported by Cândido et al. (2018).

The magnitude of NH₃ concentration in poultry facilities varies by housing system (cage, on litter, alternative systems, or aviaries), bird density (in terms of either cage area or unit floor area), feed composition, farm management, and ventilation management (Alberdi et al., 2016; ASHRAE, 2017d, 2019; Cheng et al., 2011; Green et al., 2009; Hayes et al., 2013; Kilic and Yaslioglu, 2014; Naseem and King, 2018; Ni et al., 2017; Shepherd et al., 2015; Shepherd et al., 2017; Wheeler et al., 2006; Xin et al., 2011; Zhao et al., 2013b; Zhao et al., 2014; Zhao et al., 2015a; Zhao et al., 2015b; Zhao et al., 2016). High NH₃ concentrations in poultry houses can adversely affect the health and welfare of birds and workers (Xin et al., 2011; Zhao et al., 2013b) and may cause respiratory diseases (e.g., coughing, upper respiratory tract bleeding, excessive secretions, and lung bleeding or inflammation) (Kilic and Yaslioglu, 2014). The Occupational Safety and Health Administration (OSHA) sets 25 ppm of NH₃ as a permissible exposure limit (PEL) for eight-hour time weighted average (TWA) for human workers in different industries. Additional clarification was provided by OSHA, including excursions in the worker levels may exceed three times the PEL for no more than a total of 30 minutes during an eight-hour workday; and under no circumstances should exposure exceed five times the PEL, or 125 ppm, even when the eight-hour TWA is not exceeded. ASHRAE (2019) suggested that the NH₃ concentration should be maintained below 26 ppm, or ideally, and below 10 ppm for general HVAC

environments. Kristensen et al. (2000) subjected six groups of laying hens to three concentrations of NH_3 (0, 25, and 45 ppm) and evaluated their behavior in terms of their preference of NH_3 concentrations. A significant difference between the responses in 0 and 25 ppm was found, but not between 25 and 45 ppm, suggesting that ammonia may have negative effects to laying hens' behavior between 0 and 25 ppm (Kristensen et al., 2000). However, no literature or studies have suggested any NH_3 threshold concentrations above which symptoms of respiratory or physiological problems may occur for poultry.

The fundamentals of properly designed and managed controlled environment conventional caged laying facilities are reasonably well understood, but have challenges in maintaining comfortable conditions under extreme weather with current environmental control capabilities. In addition, alternative poultry housing systems, including vertical aviaries and various cage-free systems, also present their own unique challenges to both design and management for balancing comfortable environment and energy efficiency. Accurately and economically measuring ammonia concentration continuously in poultry facilities has been a challenge, specifically due to tough operating environment and lack of feasibility of most ammonia sensors currently available. Therefore, there is a critical need to better understand the housing environment in cage and cage-free hen houses for balancing comfortable environment and energy efficiency.

4.1.2 Measuring air quality in poultry houses

The air quality of poultry houses can be evaluated for interior air temperature, relative humidity (RH), particulate matter (PM), and concentrations of common gases present inside poultry housing, including NH₃ and CO₂. Air temperature is the most commonly used and an easily attained measure to assess interior thermal conditions. As a practical matter, temperature sensors, such as expansion types (i.e. thermometer), thermocouples, and electrical resistance types (i.e. thermistors, RTDs) are most commonly applied in air temperature measurements in agriculture and horticulture (Cox, 1997). As defined in ASHRAE (2019), relative humidity (RH) indicates the ratio of the partial pressure of water vapor in a space to the saturation partial pressure of water vapor. In short, it is a relative measure of the degree of moisture saturation of the air. RH is a useful parameter for effective and efficient management in the thermal environmental measurements relating to animal environmental management (Cox, 1997). Undesirable relative humidity can greatly impact thermal comfort, well-being, performance, disease, and mortality (Huynh et al., 2005; Lowen et al., 2007). Many types of sensors are widely applied to measure RH, including wet-bulb psychrometer, surface acoustic wave sensor, substrate or polymer-based sensor, lithium chloride-based sensors, thermal conductivity sensors, and infrared absorption hygrometer (Cox, 1997; Eigenberg et al., 2009).

Methods to measure CO₂ concentrations have been developed and used mostly in HVAC applications. The Infrared (IR) absorption principle is fundamental for two methods to measure

CO₂: 1) Non-Dispersive Infrared absorption sensor and 2) Photo-acoustic sensor (ASHRAE, 2017d, 2019). Measurements of NH₃ in rough environments such as swine or poultry houses remain a challenge. The majority of NH₃ sensors are designed for applications in residential buildings or factories for alarm purposes and are suitable for short-term exposure to relatively high NH₃ concentrations that are considered unsuitable for human workers. Many NH₃ sensors available in the market are not suitable for monitoring air quality inside livestock or poultry houses, where they are subjected to long-term exposure to a variety of NH₃ concentrations.

Several studies on thermal environment and air quality have been conducted for laying hen facilities, which were either survey-type investigations, or short duration studies (Dobeic and Pintarič, 2011; Green et al., 2009), with intermittent measurements (Shepherd et al., 2015; Wathes et al., 1997; Zhao et al., 2015a). Wathes et al. (1997) surveyed the concentrations and emission rates of aerial NH₃, nitrous oxide (N₂O), methane (CH₄), and CO₂ in typical UK broiler, cage and perchery (aviary) houses over a 24 h period during winter and summer and reported that the mean NH₃ concentrations ranged from 12.3 to 24.2 ppm. Kilic and Yaslioglu (2014) measured the NH₃ and CO₂ concentrations, air temperature RH in a three-tier laying hen house with 12,000 hens in Turkey. The average NH₃ concentration during the summer of 2013 was 8.1 ppm at exhaust fans and 5.4 ppm at inlet fans, while the average CO₂ concentration was 732 ppm at exhaust fans and 625 ppm at inlet fans throughout the summer. The temperature and RH sensors in the layer houses were installed in the middle of the aisle.

The overall minimum, average and maximum values for indoor air temperature and RH were obtained as 16.8, 24.7, and 34.7°C, and 33.6, 63.7, and 86.2%, respectively.

These survey-type and intermittent studies usually employed simple measurement techniques and periodic measurements, and thus depict a small part of the actual picture and cannot adequately cover diurnal or seasonal variations, or sufficiently represent the spatial variability of interior thermal environment encountered by the laying hens, which are critical characteristics for evaluating thermal comfort and air quality of animal housing (Ni et al., 2012). Ni et al. (2017) suggested that long-term (> 6 months) and continuous (or high frequency) monitoring were needed to reveal seasonal and diurnal variations and to obtain in-depth knowledge about thermal environment and air quality characteristics.

Xin et al. (2009) evaluated the ventilation rate in two broiler houses in Kentucky, USA and reported a difference in CO₂ concentration of 200 – 2,566 ppm was noted between house air inlet and exhaust, which equivalent to an interior CO₂ concentration of approximately 600 to 3,000 ppm (assuming a 400 ppm ambient CO₂ concentration was met). Their results agreed with an earlier study for manure belted layer houses in Iowa, USA (Li et al., 2005), for which an estimated range of 800 – 2,400 ppm CO₂ concentration at the ventilation fans was reported. Liang et al. (2005); Liang et al. (2006) estimated NH₃ emission rates for manure belted and high-rise layer houses. Their results showed that for manure belt houses recorded NH₃ concentrations at exhaust fans of up to 15 ppm for Pennsylvania buildings in winter, 2 to 4 ppm in summer; and

up to 8 ppm for Iowa buildings in winter, and 2-3 ppm in summer; for high-rise houses in Iowa with a manure-pit, a concentration range of 70 to 120 ppm during winter, and below 20 ppm during winter was noted at the manure-pit; those in Pennsylvania had NH₃ concentrations that ranged from 40-100 ppm for winter and 10-40 ppm for summer. Ni et al. (2012) studied the characteristics of air pollutant concentrations of NH₃, H₂S, CO₂, and particulate matter (PM₁₀) in two high-rise houses of A-frame cages with 180,000 hens and two ten-tier cages houses with manure-belt that housed 200,000 hens located in Indiana, USA over a 2-year period. Results showed that variations in pollutant concentrations were affected by outdoor temperature, ventilation, hen condition, and farm management practices. When compared to the manure-belt houses, gas concentrations in the high-rise houses were higher for NH₃, and lower for CO₂. However, the scope of this study was limited to report pollutant concentrations only at the ventilation outlets of the fans. (Zhao et al., 2015b) compared the indoor NH₃ and CO₂ concentrations, and thermal environment in three housing systems: a conventional caged facility (200,000 hen), an aviary (50,000 hen), and an enriched colony (50,000 hen). Results showed that the average indoor temperatures were 24.6, 25.2, and 26.7°C, the average relative humidity were 57%, 56%, and 54%, the daily mean indoor NH₃ concentrations were 4.0, 6.7 and 2.8 ppm, and the daily mean indoor CO₂ concentrations were 2083, 2475, and 2216 ppm for the conventional cage, aviary, and enriched colony house, respectively. In a recent study, Cândido et al. (2018) continuously subjected tom turkey poults to three elevated concentrations of CO₂ (2,000, 4,000, and 6,000 ppm) from day of hatch to 21 day of poult's age to examine the

effects of elevated CO₂ concentrations on turkey poult performance and behavior. Results of their study suggested that continuously exposing tom turkey poults to constant CO₂ concentrations of up to 6,000 ppm was not a strong contributing factor to reduced turkey poult performance during the first 3 weeks of brooding. Poults exposed to higher CO₂ concentrations had reduced cumulative body weight gain. An altered behavior pattern showing more movement was also observed for poults subjected to higher CO₂ concentrations. They did not report any direct evidence that CO₂ concentrations up to 6,000 ppm resulted in round heart issues for turkeys involved in the experiment. Table 4-1 provides a summary of these studies conducted on air quality in a variety of poultry housing systems.

A few other commissioning studies were conducted under the Air Compliance Agreement (ACA) between the U.S. EPA and certain sectors of the U.S. livestock and poultry industries (Hayes et al., 2013; Zhao et al., 2015a; Zhao et al., 2015b; Zhao et al., 2016). These studies researched the air quality parameters primarily in alternative laying hen housing systems, including enrichable caged house (EC) and vertical aviaries (AV), with comparison to that of conventional caged house (CC). Hayes et al. (2013) evaluated the gaseous concentrations and emissions of NH₃, CO₂, methane (CH₄), nitrous oxide (N₂O), and particulate matter PM₁₀ and PM_{2.5} for two side-by-side aviaries that each housed 50,000 birds over a 19-month consecutive monitoring period. The overall mean indoor gaseous concentrations for the two aviaries were found as 8.7 (± 8.4) ppm NH₃, 1,636 (± 1,022) ppm CO₂, 10.0 (± 6.8) ppm CH₄, 2.3 (± 1.6) mg

m^{-3} PM_{10} , and $0.25 (\pm 0.26) \text{ mg m}^{-3}$ $\text{PM}_{2.5}$. The authors concluded that the PM emissions were the major difference between aviaries and conventional manure-belt or high-rise systems. Slightly higher NH_3 emission rates were reported in aviaries when compared to a manure-belt cage house, but these values were lower than that reported for European laying hen houses. Prodanov et al. (2016) investigated ten laying hen houses equipped with battery cages and different manure handling systems for air temperature, RH, and concentrations of O_2 , H_2S , CO , NH_3 , and CO_2 . They noted daily ranges of interior air quality parameters of $15.3 - 25.6^\circ\text{C}$ temperature, $48 - 81\%$ RH, $0.39 - 8$ ppm NH_3 , and $696 - 1,466$ ppm CO_2 . They did not measure any particulate matter in their study.

It is noted that large variations exist among results from different studies, which are associated with differences in housing types, management practices, local climatic conditions, and to some extent, the associated measurement methods (Kaasik and Maasikmets, 2013). It was acknowledged that in previous studies, the sensors measuring the interior thermal environment (temperature, RH) or air quality (NH_3 , H_2S , CO_2 , PM_{10} , $\text{PM}_{2.5}$) in the manure-belt layer houses were generally installed in the middle of the aisle between cages (Dobeic and Pintarič, 2011; Green et al., 2009; Shepherd et al., 2015; Zhao et al., 2015a; Zhao et al., 2015b). In other words, these measurements are more appropriate to demonstrate the thermal environment representing the building environment, rather than that experienced by the laying hens.

A study was recently conducted in a commercial stacked cage laying hen house in the Midwest U.S. (425,000 laying hens) to continuously monitor the interior air temperature, NH₃ and CO₂ concentrations over a six-month period (Table 4-1, (Zheng et al., 2019) **). The interior thermal environment was assessed by comparing the air temperatures longitudinally, laterally, and vertically. Results from this study showed that the interior temperatures ranged from 22.1 to 28.1°C for cold climate, and 25.1 to 29.6°C for warm climate. During minimum ventilation mode, there was a spatial variation present in the barn, with barn center temperatures were consistently the highest in the longitudinal and lateral direction ($p < 0.001$), and the top floor warmer than that of the bottom floor ($p < 0.05$). During tunnel ventilation mode, the interior thermal environment was more uniform than during winter, resulting in a difference only in the longitudinal direction. The daily CO₂ and NH₃ concentrations ranged from 400 to 4,981 ppm, and 0 to 42.3 ppm inside the barn. Both CO₂ and NH₃ decreased linearly with increasing outside temperatures. The mean NH₃ and CO₂ concentrations varied with sampling locations and with the outside temperatures ($p < 0.001$). For CO₂, the minimum ventilation sidewall had lower values than those measured in the barn's center ($p < 0.05$) during cold weather, while the barn center and the manure room sidewall consistently measured the highest concentrations during warmer weather ($p < 0.05$). For NH₃, the tunnel ventilation inlet end of the building consistently had the lowest daily concentrations, and the cage aisle and manure drying tunnel sidewall measured the highest concentrations ($p < 0.001$). Higher NH₃ and CO₂ concentrations were recorded inside the cages when compared to the cage aisle ($p < 0.05$). The highest NH₃ concentration (42.3 ppm)

Table 4-1. A selection of studies conducted on air quality in a variety of poultry housing systems. The housing systems include conventional caged (CC), enrichable cage (EC) and aviaries (AV) for layer hen houses, and broiler houses. The air quality parameters evaluated in the listed studies include interior air temperature, RH, indoor aerial concentrations of ammonia (NH₃) and carbon dioxide (CO₂), and particulate matter (PM₁₀ and PM_{2.5}).

Authors	Hayes et al. (2013)	Zhao et al. (2013)	Zhao et al. (2015a)			Prodanov et al. (2016)
Bird and housing type	Layer AV	Layer AV	CC	Layer AV	EC	Layer CC
Interior temperature, °C	18 - 30	23.4 ± 0.3	24.6 ± 1.9	26.7 ± 1.1	25.2 ± 1.3	15.3 - 25.6
RH, %	70 - 80	64 ± 3	57 ± 9	54 ± 7	56 ± 9	48 - 81
NH ₃ , ppm	8.7 ± 8.4	5.2 ± 0.5	4.0 ± 2.4	6.7 ± 5.9	2.8 ± 1.7	0.39 - 8
CO ₂ , ppm	1,636 ± 1,022	1,520 ± 87	2,084 ± 1,034	2,475 ± 1,280	2,216 ± 1,112	696 - 1,466
PM ₁₀ , mg/m ³	2.3 ± 1.6	-	0.59 ± 0.16	3.95 ± 2.83	0.44 ± 0.18	-
PM _{2.5} , mg/m ³	0.25 ± 0.26	-	0.035 ± 0.013	0.410 ± 0.251	0.056 ± 0.021	-

Authors	Xin et al. (2009)	Li et al. (2005)	Liang et al. (2005)		Zheng et al. (2019**)
Bird and housing type	Broiler Built-up litter	Layer Manure-belted	Layer Manure-belted	Layer High-rise*	Layer EC
Interior temperature, °C	-	-	17 - 32	15.8 - 32	22.1 - 29.6
RH, %	-	-	-	-	-
NH ₃ , ppm	-	-	Up to 15 (winter) 2 - 4 (summer)	70 - 120 (winter) < 20 (summer)	0 - 42.3
CO ₂ , ppm	600 - 3,000	800 - 2,400	600 - 4,800	600 - 4,800	40 - 4,981
PM ₁₀ , mg/m ³	-	-	-	-	-
PM _{2.5} , mg/m ³	-	-	-	-	-

* NH₃ for the high-rise type layer houses were measured at the manure pit.

** Zheng, W., Y. Xiong, R. S. Gates, Y. Wang, and K. W. Koelkebeck. 2019. Air temperature, carbon dioxide and ammonia assessment inside a commercial cage layer barn with manure-drying tunnels. Submitted to *Poultry Science*.

was recorded above a minimum exhaust fan adjacent to the manure drying tunnel. The results indicated that high pressure (back pressure) between the production area and the manure drying tunnel allowed air leakage back into the barn through non-operating sidewall fan shutters. This back pressure resulted in locally high NH₃ concentrations near the sidewalls between the barn and the manure drying tunnel.

4.1.3 Overview of the intelligent Portable Monitoring Unit (iPMU)

The Portable Monitoring Unit (PMU) was designed and developed for measuring air temperature, NH₃ and CO₂ concentrations in livestock and poultry buildings (Gates et al., 2005) and had been widely used in air quality and emissions assessment in poultry houses (Gates et al., 2008; Liang et al., 2005; Wheeler et al., 2006; Zhao et al., 2015a). The use of the first-generation PMUs entailed a substantial degree of manual setup and data processing, making field deployment of multiple PMUs simultaneously a logistical challenge. To improve the functionality and data processing of the PMUs, the PMU design was upgraded to the Intelligent Portable Monitoring Unit (iPMU) as reported in Ji et al. (2016). The newer generation iPMUs are equipped with newly available ammonia and CO₂ sensors, capable of measuring the NH₃ and CO₂ concentrations and air temperature simultaneously, and providing real-time data processing and display, and wireless data transfer. The upgrade of iPMU has greatly improved the durability, accuracy and portability of the unit for field measurement in animal facilities. Figure 4-2 illustrates the iPMU, its key components, and interior tubing connections to measure air

quality in livestock and poultry houses (Ji et al., 2016). The iPMU ammonia sensor (EC-F9-NH₃, Honeywell Analytics, Olathe, KS, USA; ± 5% accuracy) and CO₂ sensor (GMT 220, Vaisala Inc., Louisville, CO, USA; ± (1.5% of range + 2% of reading)) for fast response and better accuracy in gas sampling. A total of six iPMU units were fabricated. In each iPMU, two solenoids were used, one for switching between barn air or ambient air during regular operation and the other to create a bypass to draw barn air into the sample lines without exposing the ammonia sensor to NH₃ prematurely (pre-sample circuit). Three flowmeters were used to adjust airflow to the NH₃ and CO₂ sensors, and provide a regulated bypass.

However, flaws in the air sampling programming existed and improvements were needed for improved sensor calibration and post-monitoring data processing. Two critical issues emerged since the deployment of the iPMU and are described as follows: 1) inappropriate selection of the calibration NH₃ gas. According to Honeywell Analytics, calibration-grade NH₃ gas with residual air is the only proper calibration gas for the NH₃ sensor (EC-F9- NH₃). This allows the NH₃ sensor access oxygen and maintains proper internal chemical functions, without being starved by other common residue gases (such as nitrogen) and thus lose its sensitivity. This is a very important detail but was not well explained in the product manual and was often neglected. Unfortunately, the NH₃ sensors in the units were previously calibrated with calibration-grade NH₃ balanced with nitrogen. This raised concerns regarding whether the

calibration process was adequately accurate, and if the calibration equations were correct for data processing or analysis. 2) *adequacy of the sampling duration*. Figure 4-2 identifies the duration

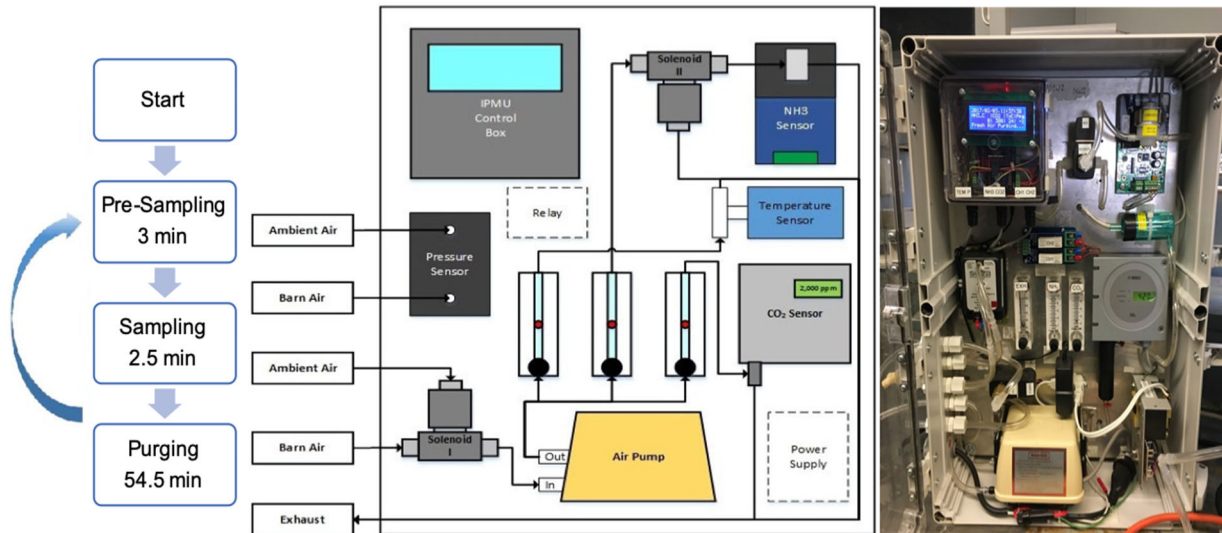


Figure 4-2. The upgraded intelligent Portable Monitoring Unit (iPMU) and its components to measure air quality in livestock and poultry houses. Left: Tubing connections used in the iPMU. Solenoid I for switching between barn air or ambient air during regular operation. Solenoid II was added to draw barn air into the sample lines without exposing the EC sensor to NH₃ prematurely (pre-sample circuit). The three flowmeters adjust flow to the NH₃ and CO₂ sensors, and provide a regulated bypass. Source: Ji et al. (2016). Right: one iPMU unit fabricated for use.

of each programmed process during air sampling, of which the Arduino microcontroller logs data for 2.5 min after a 3 min pre-sampling process. Figure 4-3 provides an example signal response during exposing the six iPMUs to calibration-grade NH₃ gas balanced with air (99.4 ppm ± 2%) in a laboratory environment. Using the “span signal formula” provided by the sensor manufacturer, applying gas at 99.4 ppm to the sensor should yield to a signal response of 199 mV. However, Figure 4-3 clearly shows that the six iPMUs did not respond equally during calibration, and not all units reached their peak signal response (199 mV) within 2.5 min. Of the six iPMUs, only three units reached the calculated signal response in 2.5 min. This suggests that

only 50% of the iPMUs previously deployed were capable of successfully capturing the correct signal responses within the programmed sampling duration. This brings uncertainty and lack of confidence in use of the iPMUs. Therefore, based on recent efforts to upgrade the iPMU, there were critical needs to validate and improve the calibration process of the ammonia sensor with proper calibration gas and more appropriate calibration equations, to adjust the coding to assure ample sampling duration to capture peak NH₃ signal response, and to develop user-friendly post-monitoring data processing and analysis procedures.

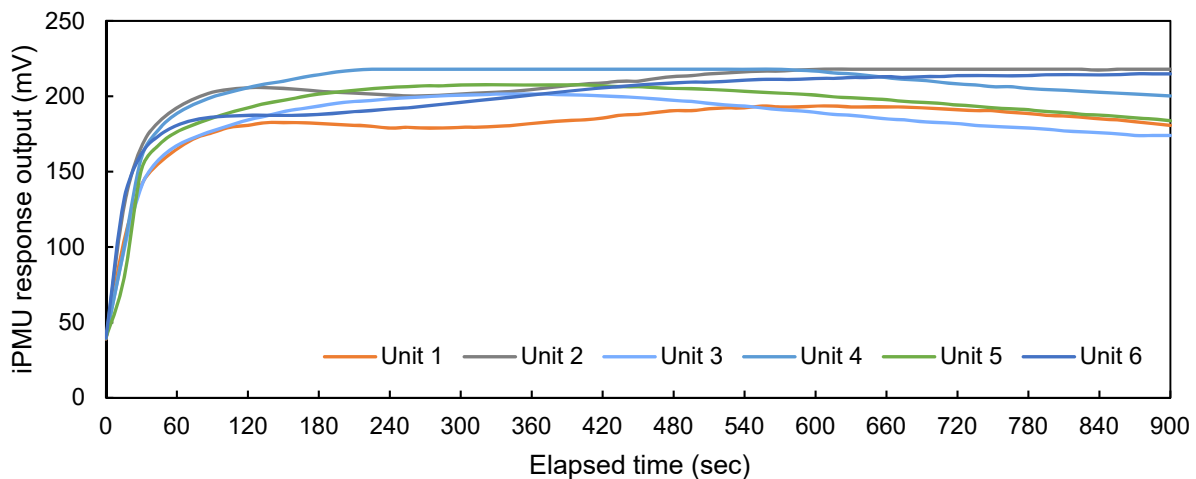


Figure 4-3. iPMU signal response to being exposed to calibration-grade NH₃ gas balanced with air (99.4 ppm \pm 2%) in a laboratory environment. Using the “span signal formula” provided by sensor manufacturer, gas concentration at 99.4 ppm corresponds to a signal response of 199 mV. Data was sampled every 15 sec.

4.1.4 Objectives

The U.S. egg industry has faced a growing pressure from consumers and retailers to transition egg production from conventional caged systems to alternative housing systems such as “caged-free” aviaries and enrichable caged systems. It was established in some studies

that alternative housing had more challenges to maintain desired indoor air quality parameters when compared to traditional housing types such as conventional cages or enriched colonies (Hayes et al., 2013; Shepherd et al., 2015; Shepherd et al., 2017; Zhao et al., 2015a; Zhao et al., 2015b; Zhao et al., 2016). Given the currently limited knowledge regarding maintaining desirable ranges of thermal comfort and gaseous concentrations in such housing types, it is important to evaluate the interior thermal environment and air quality parameters in order to provide more scientific information for alternative laying hen houses. Therefore, the specific objectives of this chapter were:

1. to improve the six iPMUs with proper NH_3 calibration procedure, develop appropriate calibration equations, improve coding programs to assure ample sampling duration, and develop user friendly post data processing and analysis procedures;
2. to use the iPMUs for air quality monitoring in different commercial laying hen systems, and provide simultaneous measurements of interior environmental parameters, including house temperature, ammonia (NH_3), and carbon dioxide (CO_2) concentrations during cold and warm weather conditions.

4.2 MATERIALS AND METHODS

Gas concentrations in this Chapter are expressed in parts per million (ppm) by volume, i.e. the volume of ammonia contained in a unit volume of air. Sometimes, a mass-based concentration is of interest. The conversion between a mass-based concentration ($mg\ m^{-3}$) of any gas and its equivalent volume-based concentration (ppm) at a given temperature and pressure can be obtained from the following equation: $C_{mass}(\frac{mg}{m^3}) = C_{volume} (ppm) \times \frac{M}{22.4} \times \frac{273.15}{(273.15 + T)} \times \frac{P}{1013}$, where M is the molecular weight of ammonia gas (g/mol), 22.4 (L) is the volume of 1 mol at 1 atmospheric pressure at 0°C, T is the corresponding thermodynamic temperature at which the gas concentration is measured, and P is the atmospheric pressure at the point of measurement (Pa).

4.2.1 Engineering improvement to the iPMU

4.2.1.1 Calibration improvement

Calibration-grade ammonia gases (101.3 and 53.55 ppm with $\pm 2\%$ error, balanced with air) were used for calibrating the NH₃ sensors. The calibration procedure and the NH₃ sensor signal response associated with the calibration gas concentration was calculated using the equation provided by the manufacturer (Technical Note - ECFX Calibration Procedure, revision 03, Honeywell, 2014⁶).

⁶ Accessible online at: https://www.honeywellanalytics.com/~media/honeywell-analytics/products/ec_fx_nh3/documents/english/ecfx-calibration-procedure-1998m0800-512final.pdf?la=en

$$Signal (mA) = \left[\left(\frac{ASGC}{SFSV} \right) \times 16 \right] + 4 \quad (4-1)$$

where ASGC = Available Span Gas Concentration. In our case, the ASGC = 101.3 ppm for the 101.3 ppm ammonia gas used during calibration. SFSV = Sensor Full Scale Concentration Value. In our case, the sensor's full span is labeled as 100/250 ppm. We expect the sensor to have fast static sensitivity (which means we expect the sensor to have fast response when exposed to gas), thus, the SFSV in our case is 100 ppm.

Therefore, the sensor response signal to 101.3 ppm calibration-grade NH₃ gas is calculated to be 20 mA, or 200 mV (using the relationship $V = I \times R$). The six NH₃ sensors in the iPMUs were subjected to multiple calibrations ($N \geq 2$) with the 101.3 ppm calibration gas until the signal response was tuned to approximately 200 mV for each sensor. Data collected from the calibration procedure was used to determine the most appropriate calibration equation to be applied to each sensor of each iPMU.

4.2.1.2 Selecting a calibration equation for NH₃ sensors

The data collected from the calibration of the ammonia sensor and the iPMU were tested and analyzed by the five mathematical methods described in the table below. These five mathematical methods were used to determine the static sensitivity of each individual sensor and were obtained from experiences gained during previous developments of the first generation of PMU and iPMU (Gates et al., 2005; Ji et al., 2016), and from observations raised during the current calibration processes. The static sensitivity, defined as the slope of the calibration curve,

is of the ratio of magnitude of an output signal or response to the magnitude of an input signal.

From an instrumentation and measurement perspective, the static sensitivity is expected to be as high as possible within the application realm. In this application, the static sensitivity (K) can be derived using Equation 4-2.

Table 4-2. Description of methods used to determine the static sensitivity of each sensor.

Method	Method of calculating V_i
1	Mean between voltage measured at 100 s and peak voltage
2	Mean between voltage measured at 150 s and peak voltage
3	Mean between voltage measured at 200 s and peak voltage
4	Peak value
5	Mean between 95% of the peak value and peak value

$$K_i = \frac{C_{NH_3}}{(V_i - V_0)} \quad (4-2)$$

where K_i = static sensitivity of each sensor (ppm/V), i = the i^{th} mathematic method to calculate the onset voltage of sensor response (V_i); C_{NH_3} = ammonia concentration measured (ppm); V_i = onset voltage of sensor response to each method (V); and V_0 = initial voltage of the sensor response (V).

All the data collected through the calibration process were individually tested for each of the five methods and then an analysis was performed to determine which method presented the best performance. For each mathematical method, the mean and the standard deviation of the corresponding static sensitivity K, the coefficient of variation, the initial and maximum sensor voltage response, and the calculated peak concentrations using the previous obtained static sensitivity were performed for all six units. Compared to other methods, the methods with a small coefficient of variation, and value not aggressively exceeding the sensor specified range of the calibration NH_3 gas, were considered. The calibration gas used for this test was NH_3 gas

rated at 101.3 ($\pm 2\%$) ppm, which yields a measurable gas concentration range of 99.3 to 103.3 ppm. The accuracy of the Honeywell EC-F9-NH₃ sensor was specified as $\pm 5\%$ for general calibration gases, resulting in a possible sensor response range of 94.3 to 108.5 ppm, corresponding to the measurable gas concentration listed above. Therefore, a better method should have a small coefficient of variation, and an estimated peak NH₃ concentration within the range of 94.3 – 108.5 ppm. Another important factor to consider is the feasibility of the mathematical methods during code development to the microcontroller. The methods were considered as options for selecting the onset voltage of sensor response (V_i) are discussed in the Results and Discussion section 4.3.1, and methods that were not selected were listed in Appendix 1 for reference purposes.

4.2.1.3 Data sampling and processing programs

Based on the average sensor response time among the six NH₃ sensors, the duration of each program was adjusted to guarantee sufficient sampling time to capture the peak gas concentrations during a measurement event, which was set to occur twice per hour. The adjusted duration of each process is described as follows: 1) pre-sampling: 45 sec; 2) sampling: 600 sec (10 min); and 3) fresh air purging: 1155 sec (19 min 15 sec). The air is being sampled and recorded every 10 sec during sampling, and every 5 min during fresh air purging. No data are logged during the pre-sampling process. Upon completion of these three components, the

program cycle continues with the pre-sampling (Figure 4-2), and the program cycle repeats until manual termination.

Given the relatively high data sampling rate (once each 10 sec), it brings challenge to data management, organization, and analysis. To save time and effort on organizing and processing the large set of data collected from long-term field studies, a MATLAB® program was developed for post-monitoring data processing of all variables, including sampling time, NH₃ and CO₂ concentrations, and temperatures. This program allows the user to select the appropriate equation for static sensitivity between Method 4 and Method 5 and provide the average values for the variables for every 30 min.

In order to assist any modification needed for future iPMUs applications, the upgraded Arduino code reflecting the calibration improvement are provided in Appendix 2, and the MATLAB® code for data processing is documented and provided in Appendix 3.

4.2.2 Air quality and thermal comfort assessment in commercial layer farm

4.2.2.1 Description of the poultry houses

The field study for iPMU application was conducted in a commercial egg production farm, located in the Midwest USA. The commercial farm had multiple laying hen house systems on the same site. Three laying hen houses were available for air quality monitoring and assessment, including two aviary houses with different layout and equipment and an enrichable cage house with manure belts and manure drying rooms.

The **enrichable caged barn (EC)** measured 25 × 168 m and had two floors (6 tiers on each floor, 12 tiers and 9 rows total). Two manure drying rooms with the same dimension (4.9 m wide × 85 m long) were constructed at both sides of the building. There were 14 ventilation fans (130 cm diameter) with shutters and cones (Officine Facco & C SpA, Via Venezia, Italy) on each sidewall. A total of 110 constant-speed fans (130 cm diameter, Officine Facco & C SpA, Via Venezia, Italy) were placed vertically in five rows at the building south end-wall and cooling pads were placed at the other end for hot weather operation. Building layout and fan placements for the EC barn are illustrated in Figure 4-4a. A portion of each sidewall was connected to an extended room that functioned as a manure-drying room (Figure 4-4b). The manure-drying room was designed to continuously dry feces produced in the barn by using the ventilation system and six exhaust fans and a curtain located on both exterior sidewalls of the manure drying tunnels. Barn air left the poultry house and entered the manure drying tunnel, circulating upwards through the feces on aerated manure belts to promote moisture removal, and eventually exited the building. A proper balance of static pressures between the hen occupied zone, the manure drying tunnels, and the outside air is critical for proper operation of this system. The two aviary houses measured 15 × 159 m but differed in interior cage layout and aviary equipment used. **Aviary 1 (AV1)** had 3 sets of aviary equipment (Bolegg Terrace, Vencomatic Group, The Netherlands), with each set forming its own lane (Figure 4-4b). **Aviary 2 (AV2)** had five sets of equally spaced aviary equipment (Natura 60, Big Dutchman Inc., Holland, MI, USA) inside (Figure 4-4c). A detailed schematic of the two types of aviary equipment were provided by the

manufacturer (Figure 4-6). Both AV1 and AV2 had ten 130 cm diameter variable speed fans with shutters and cones (Officine Facco & C SpA, Via Venezia, Italy) and two 60 cm diameter minimum ventilation fans (Aerotech Vortex, Munters Corp., Lansing, MI, USA) on each sidewall. At the time of this study, there were 46,400 LOHMANN BROWN hens (19 wk of age), 36,300 BOVANS BROWN hens (77 wk of age), and 497,000 LOHMANN LSL-LITE hens (25 wk of age) in AV1, AV2, and EC, respectively.

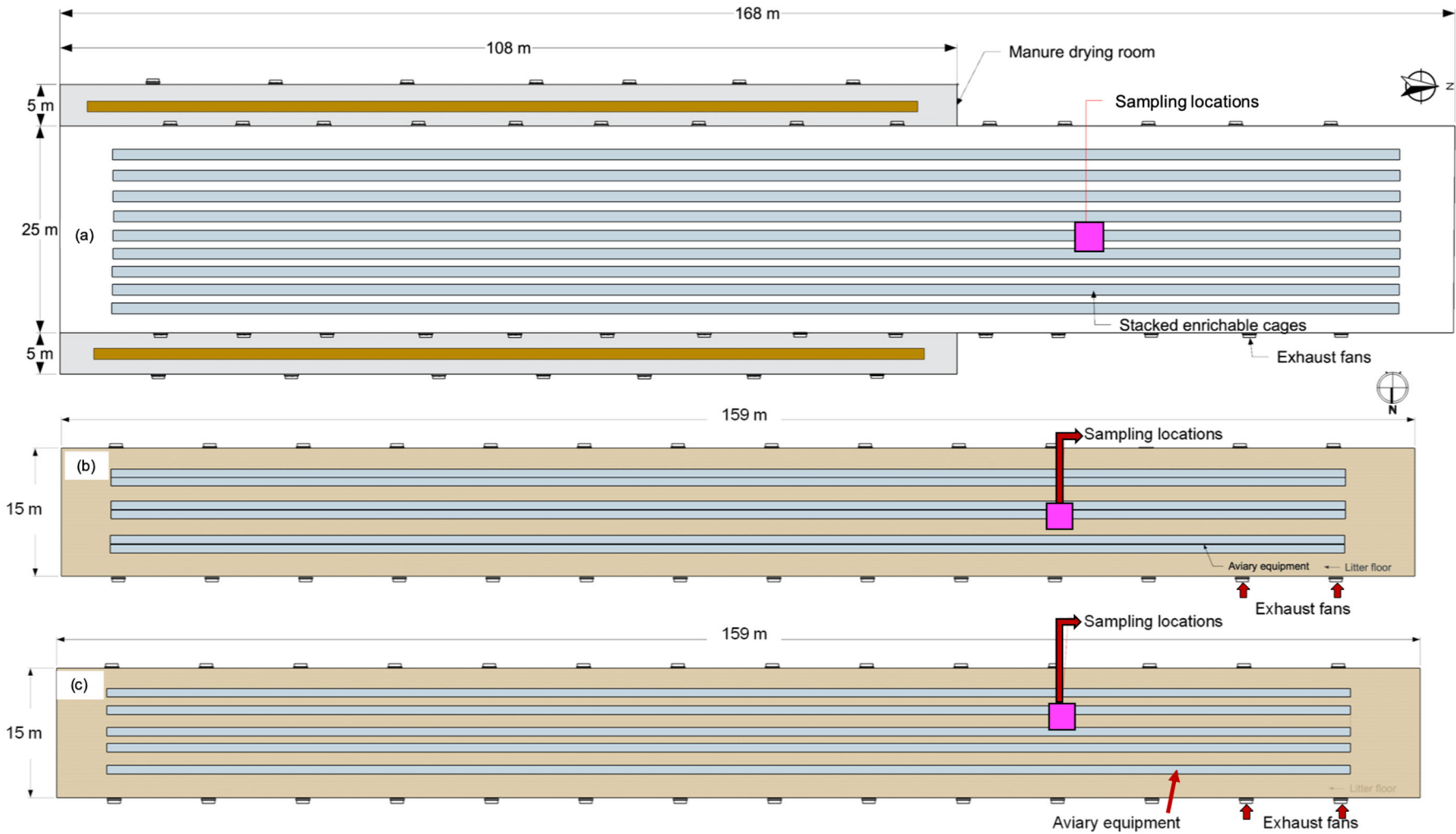


Figure 4-4. Top views showing the building layout, sensor locations, exhaust fan placements of the three laying hen houses. **(a)** Enrichable caged house (EC) with manure drying rooms on both sides. EC measured 25 x 168 m. **(b)** Aviary 1 (AV1) and **(c)** Aviary 2 (AV2). Both AV1 and AV2 measured 15 x 159 m, with two different types of aviary equipment and slightly different interior aviary layout.

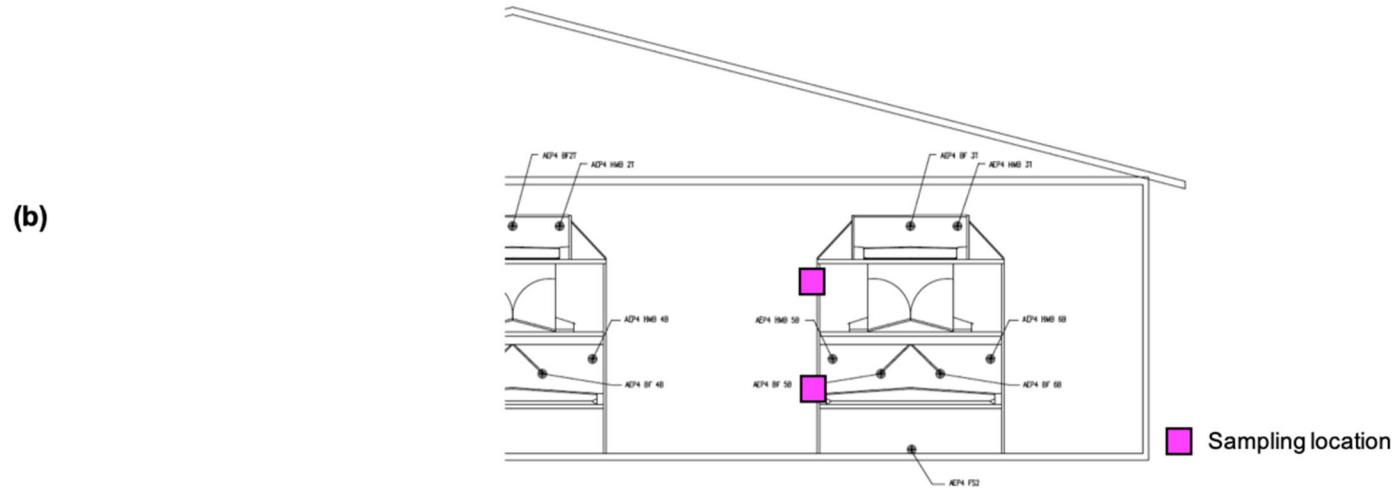
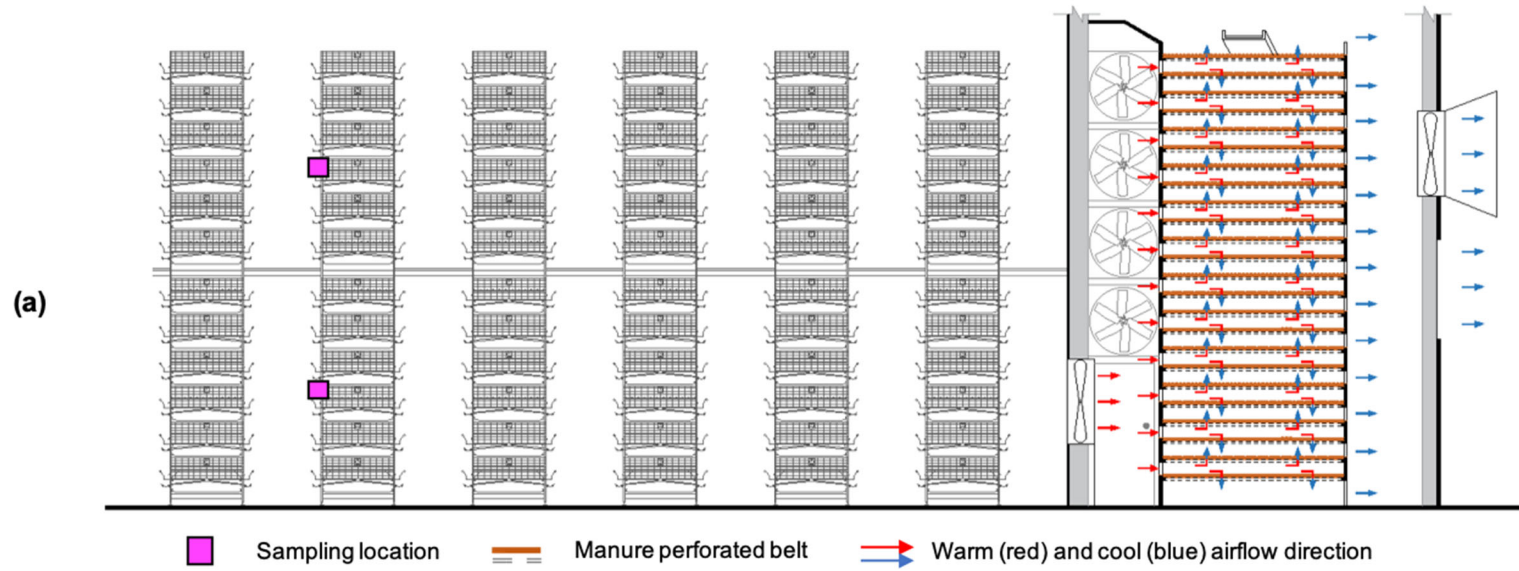
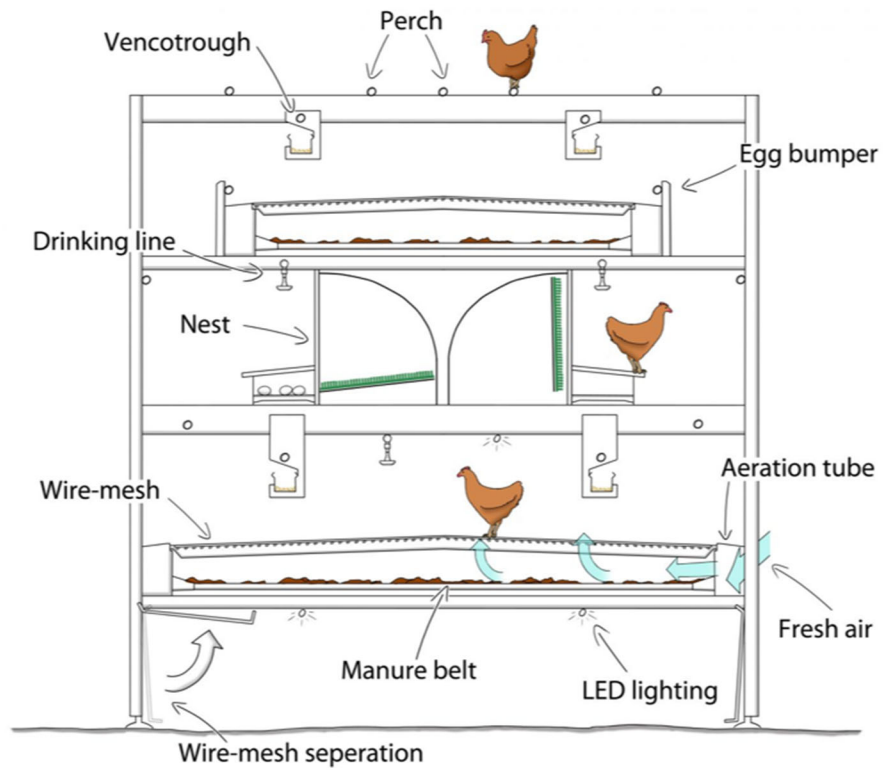
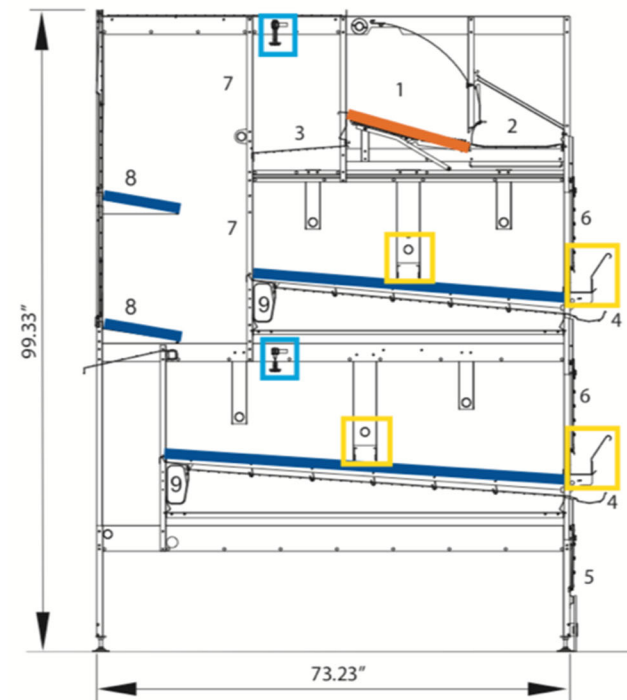


Figure 4-5. Building elevation views showing partial buildings and sampling locations in **(a)** Enrichable caged house (EC) and **(b)** Aviaries (AV1 and AV2).



(a)



(b)

Figure 4-6. Schematic showing aviary equipment in (a) Aviary 1 that utilized model Bolegg Terrace (Vencomatic Group, The Netherlands; source: <https://www.vencomaticgroup.com/en/products/layers/housing-solutions/bolegg-terrace>) and (b) Aviary 2 that utilized model Natura 60 (Big Dutchman Inc., Holland, MI, USA; source: https://www.bigdutchmanusa.com/wp-content/uploads/2016/08/Natura60_Eng.pdf).

4.2.2.2 Air quality measurements

Six iPMUs and six additional temperature/RH dataloggers (HOBO U23 Pro v2, Onset Computer Corp., Bourne, MA, USA) were used to continuously monitor air quality parameters including interior air temperatures, NH₃ and CO₂ concentrations in the three houses (EC, AV1, and AV2) from February 1st to July 05th, 2019. Two iPMUs and two HOBO temperature/RH dataloggers were placed into each house, located near the front of cages/structures for easier and safer access. Two 30.5 m long air sampling hoses were run from the iPMUs along the building centerline to measure the indoor gas concentrations at two elevations representing the **TOP** and **BOTTOM** levels of each house (approximately 1.5 and 2.5 m for AV1 and AV2; and 1.5 and 5.3 m for EC). The top and side views of the air sampling locations are shown in Figures 4-4 and 4-5. There was another sample line from outside of the barn for getting fresh air to purge the NH₃ sensor. The air inlets for the indoor sampling lines and the fresh air purging line were each protected with an air filter (47 mm filter membrane, 5-7 micron, Savillex LLC., Eden Prairie, MN, USA) housed in a protective assembly (47 mm single stage filter assembly, Savillex LLC., Eden Prairie, MN, USA) to avoid impurity plugging up such as dust and feather (Figure 4-7a). The temperature/humidity (RH) dataloggers were placed at the same locations where air was sampled to closely monitor the thermal environment experienced by the laying hens (Figure 4-7b). The temperature/RH information in each house was recorded at a 5-min sampling rate. The iPMUs were programmed with the adjusted procedure durations, which were set as 1) pre-

sampling: 45 sec; 2) sampling: 600 sec (10 min); and 3) fresh air purging: 1155 sec (19 min 15 sec). The house air was logged every 10 sec during the sampling procedure and every 5 min during fresh air purging, and the process was repeated continuously.

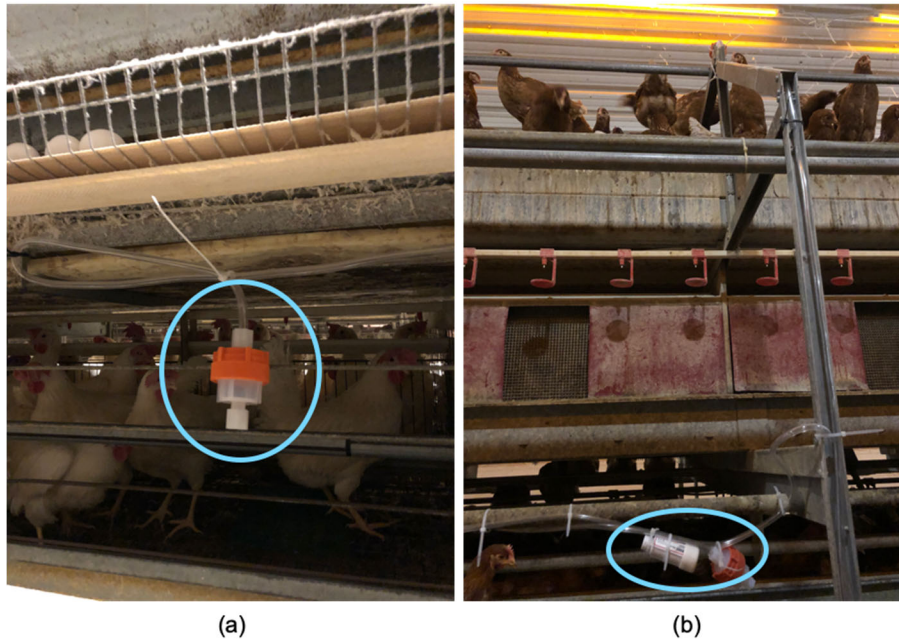


Figure 4-7. (a) Air sampling hose for NH_3 and CO_2 measurements. The air inlet was protected by an air filter membrane housed in a protective assembly. (b) additional temperature/RH sensors to record representative thermal environment experienced by the laying hens.

All sensors deployed in this study were checked and calibrated if needed prior to farm monitoring. The NH_3 and CO_2 sensors in the iPMUs were calibrated per manufacturer recommended procedure using calibration-grade reference gases prior to farm installation. The air temperature sensors were compared to a NIST certified Heating and Cooling Temperature Calibrator (CL134-1, OMEGA Engineering, Inc., Norwalk, CT, USA).

Air quality data were retrieved every 3 – 4 wks during the study. The performance of the iPMUs, temp/RH dataloggers, and sample tubes was checked during data downloading, and any

identified issues (i.e. kinks in air sampling hoses, dust accumulation in air filter assembly, battery replacement for Arduino microcontroller, etc.) were resolved on site. Unfortunately, we experienced a sample pump failure in the iPMU used to sample the upper gas concentrations in EC, resulting data loss of the gas concentrations of EC from February to May 2019. The problem was resolved, and the unit was brought back onsite in June 2019.

4.2.2.3 Data and statistical analysis

Mathematical Method 5 was selected in the GUI interface for raw data processing using the MATLAB® codes developed. The NH₃ and CO₂ concentrations, air temperatures and relative humidity (RH) data for every 30 mins were averaged and were used for the following analyses.

Daily outside temperature information, including the daily minimum, maximum, and time of observation bias temperatures during the monitoring of this study was retrieved from the National Centers for Environmental Information (National Oceanic and Atmospheric Administration, NOAA) database. The historical temperature data included in the NOAA database was recorded by a weather station within an 8-mile (12.8 km) distance from the poultry farm and was often used by the farm managers for farm-wide management decisions. The average daily outside temperatures (T_{OUT}) were derived from the minimum and the maximum temperatures provided by the NOAA database. The daily average T_{OUT} was categorized into five thermal

ranges, including < -5, -5 to 5, 5 to 15, 15 to 25, and > 25°C for evaluating the interior thermal comfort and air quality during different T_{OUT} ranges.

Indoor air temperature and RH measurements measured from the HOBO temperature/RH sensors were used to assess the thermal comfort in each house. When evaluating the thermal comfort for livestock animals or poultry, it is often inadequate to show temperature or RH characteristics alone since they cannot represent the sensible and latent thermal environment experienced by the animals. Therefore, a temperature and humidity index (**THI**) was computed using Equation (4-1) and the half-hour means of the temperature and RH measurements (Hahn et al., 2009; Xiong, 2013).

$$THI = 0.8T_{db} + RH(T_{db} - 14.4) + 46.4 \quad (4-1)$$

The THI values are often used to classify the occurrences of livestock weather and safety index conditions (Hahn et al., 2009; LCI, 1970). The Livestock Weather Safety Index conditions are associated with THI values and are categorized into four ranges: normal (THI ≤74), alert (75 ≤ THI ≤78), danger (79 ≤ THI ≤83), and emergency (THI ≥84) (Hahn et al., 2009; LCI, 1970). Although the THI and the Livestock Weather Safety Index were originally developed for beef cattle, using this referential information can provide useful and insightful information regarding assessing the thermal comfort level for poultry species.

The minimum, maximum, mean and the standard deviation (SD) of the indoor temperatures, THI, CO₂ and NH₃ concentrations for the two locations (top and bottom level) in the three hen houses were tabulated for the five outside temperature ranges. A box-whisker plot

was created for the half-hour means of the interior air temperature, CO₂ and NH₃ concentrations for different T_{OUT} ranges to depict the characteristics of their temporal and thermal profiles at the top and bottom level in each of the three-layer houses. The inter quartile range (IQR, 25 – 75% population of the measurements), the ±1.5 IQR, the median, and the mean are identified in the box-whisker plots.

The 30-min means of the air temperatures, NH₃ and CO₂ measurements for the first week of February 2019 (7 am Feb 2nd to 12 pm Feb 8th) during daily average T_{OUT} ranged between -3.9 to 6.1°C were used to closely evaluate the interior thermal environment and air quality at the two elevations of the three hen houses. Ventilation and farm management implications to the interior thermal environment and air quality were discussed.

4.3 RESULTS AND DISCUSSION

4.3.1 NH₃ sensor calibration equation

The summary results of key parameters for selecting the proper calibration equation using mathematical Methods 4 and 5 for selecting the peak sensor voltage response (V_i) are provided in Table 4-3. The key parameters included the averaged static sensitivity K obtained from multiple replications ($N \geq 2$), the standard deviation (ppm/V) and variation of coefficient (%) of the static sensitivity K, the initial voltage measured at 0 ppm NH₃ concentration, the maximum sensor signal recorded, and an estimated peak NH₃ concentration calculated using the average static sensitivity K. The results for Methods 1 through 3 are provided in Appendix 1 for reference.

Table 4-3. Summary results of key parameters for selecting the proper calibration equation using mathematic Methods 4 and 5 (as referenced in Table 4-2). The calibration grade NH₃ gas used for this test was rated at 101.3 (± 2%) ppm. The accuracy of the sensor was specified as 5% for general calibration gases.

Method 4 (Vi = peak voltage)						
	Unit 1	Unit 2	Unit 3	Unit 4	Unit 5	Unit 6
No. replication (N)	2	5	5	4	4	4
Average K (ppm/V)	29.354	26.979	30.125	26.541	27.922	30.019
Standard deviation of K (ppm/V)	0.646	2.67	3.395	1.424	1.064	2.506
Coefficient of Variation (%)	2.0	10.0	11.0	5.0	4.0	8.0
Vo (V)	0.846	0.86	0.873	0.873	0.873	0.87
Vmax (V)	4.365	4.795	4.486	4.795	4.593	4.808
Vmax - Vo (V)	3.519	3.935	3.613	3.922	3.72	3.94
Calculated peak concentration (ppm)	103.3	106.1	108.8	104.1	103.9	118.1
Method 5 (Vi = Mean between 95% peak voltage and peak voltage)						
	Unit 1	Unit 2	Unit 3	Unit 4	Unit 5	Unit 6
No. replication (N)	2	5	5	4	4	4
Average K (ppm/V)	30.177	27.035	29.811	26.185	27.595	27.058
Standard deviation of K (ppm/V)	0.859	1.869	1.532	0.291	0.593	1.063
Coefficient of Variation (%)	2.8	6.9	5.1	1.1	2.1	4.0
Vo (V)	0.846	0.86	0.873	0.873	0.873	0.87
Vmax (V)	4.365	4.795	4.486	4.795	4.593	4.808
Vmax - Vo (V)	3.519	3.935	3.613	3.922	3.72	3.94
Calculated peak concentration (ppm)	106.2	106.4	107.7	102.7	102.6	106.5

Among the five mathematical methods for selecting the peak sensor voltage response (V_i), Methods 4 and 5 resulted in the best results when compared to the other three methods. Method 5 (V_i = the mean between 95% of peak voltage and peak voltage) resulted in a minimum and maximum coefficient of variation of 1.1% and 5.1% for units 4 and 3, respectively, much smaller than that of the other methods (maximum of 6.5% for Method 1, 6.7% for Method 2, 9.8% for Method 3, and 11.0% for Method 4). Method 5 also resulted an estimated peak concentration using the average static sensitivity K that ranged from 102.6 to 107.7 ppm, within the 94.3 – 108.5 ppm possible sensor response range. On the other hand, Method 4 was the most convenient regarding facilitation in the program development, as only a peak voltage needed to be specified in the codes. Thus, both Methods 4 and 5 were included in the data collection and data processing code development using the Arduino (Appendix 2) and the MATLAB®

workspace (Appendix 3) using individual static sensitivity K for each unit, specifically, and the users are allowed to choose the appropriate method to process their data that fit in the specific application realm.

4.3.2 Air quality and thermal comfort in commercial layer farm

The thermal comfort and air quality parameters, including the indoor air temperature, RH, CO₂ and NH₃ concentrations were successfully and continuously monitored using the six iPMUs for the three laying hen houses (AV1, AV2, and EC) from February 1st to July 1st, 2019. The daily average data of the ambient condition was retrieved from the nearby weather station for testing period February 1st to July 1st, 2019. The ambient temperature ranged from -15.6 to 21.1, -13.1 to 26.7, and -10.6 to 32.2°C for daily minimum, mean, and maximum outside temperatures, respectively.

Table 4-4 provides descriptive statistics regarding the interior thermal comfort and air quality parameters, including the average values and standard deviation (SD) of interior temperature, THI, CO₂ and NH₃ concentrations for the top and bottom levels in the three layer houses. This summary information was tabulated by the five daily average T_{OUT} range categories, and the number of days encountered the T_{OUT} category was included.

Table 4-4. Descriptive statistic information for the average and standard deviation (SD) values for the indoor temperature, temperature and humidity index (THI), CO₂ and NH₃ concentrations measured at the top and bottom level in the three houses (AV1, AV2, and EC).

Daily mean T _{OUT} (°C)	No. Days	Housing Type and Level											
		Aviary 1 (AV1)				Aviary 2 (AV2)				Enrichable Cage (EC)			
		Top		Bottom		Top		Bottom		Top		Bottom	
		mean	SD	mean	SD	mean	SD	mean	SD	mean	SD	mean	SD
Air temperature (°C)													
< - 5	11	20.2	4.5	20.6	2.2	29.4	1.4	26.7	2.6	25.7	1.9	24.9	2.6
-5 to 5	42	22.1	2.4	22.2	2.5	29.1	1.7	26.7	2.2	25.0	1.8	24.1	2.3
5 to 15	48	27.8	3.7	27.7	2.7	27.1	4.5	26.1	4.3	27.6	1.7	27.8	1.3
15 - 25	47	30.2	1.7	29.4	1.6	28.6	2.3	26.4	3.9	28.5	1.5	29.7	1.7
> 25	3	31.1	0.7	30.5	1.1	30.2	1.6	NA		29.9	1.9	31.4	1.3
Temperature and Humidity Index, THI													
< - 5	11	67		67		79		76		72		72	
-5 to 5	42	69		70		79		76		71		71	
5 to 15	48	76		77		72		75		75		75	
15 - 25	47	80		79		77		75		77		79	
> 25	3	81		81		79		NA		79		81	
Carbon dioxide (CO₂) concentration (ppm)													
< - 5	11	3999	912.4	NA		4341	819.4	2296	1712.1	NA		2997	713.1
-5 to 5	42	2796	639.4	NA		3717	630.2	2575	1404.4	NA		2226	825.5
5 to 15	48	1992	496.1	1544	330.7	2453	919.0	2812	761.3	1943	443.4	1137	306.8
15 - 25	47	1139	505.2	1145	312.5	1408	589.3	1492	948.1	1476	351.9	1004	214.9
> 25	3	483	27.3	630	45.8	NA		770	174.3	NA		NA	
Ammonia (NH₃) concentration (ppm)													
< - 5	11	54.2	10.1	14.0	6.2	10.6	9.5	14.2	16.2	NA		47.3	10.6
-5 to 5	42	39.9	8.1	11.6	8.9	8.4	6.0	15.4	11.7	NA		35.1	10.8
5 to 15	48	28.1	5.0	2.0	1.6	2.5	1.7	10.7	5.4	1.6	1.4	21.0	3.8
15 - 25	47	19.1	5.0	1.9	0.8	2.7	1.5	4.2	4.0	NA		15.2	2.8
> 25	3	12.6	0.5	2.1	0.7	NA		1.5	0.9	NA		NA	

NA indicates the data for the listed area missing due to a variety of possible reasons including lost sensors from hen activity, power outages, and instrumentation malfunction.

4.3.2.1 Thermal environment

The 30-min indoor air temperature means computed from measurements at the top and bottom levels inside each layer barn during the entire course of the monitoring are shown in Figure 4-8. Aviary 2 bottom level experienced a temperature/RH sensor lost due to hen activity for T_{OUT} range $> 25^{\circ}\text{C}$ (No. Days = 3), thus data for this combination was not shown on the plot.

During monitoring from Feb 1st to July 1st, 2019, a large variation in the interior house temperatures were recorded for all the layer barns. The range in temperatures (minimum to maximum values) was 11.7 to 35.2, 9.6 to 35.0, and 14.2 to 39.5°C for Aviary 1, Aviary 2, and the EC barn, respectively, and the average for each house was 20.2 to 31.1, 27.1 to 30.2, and 24.1 to 31.4°C during different ambient temperatures. This is a surprising finding, given the use of modern environmental controllers, and well-designed ventilation systems.

On average, the interior temperatures in each house paralleled the trend of T_{OUT} , showing lower values for cold weather conditions, and warmer interior temperatures for hot weather conditions. Regardless of whether different target temperature setpoints were used during different time of the year owing to different bird age in each of the three houses, the interior temperature profile demonstrated an incredibly wide range of air temperature measured in each house.

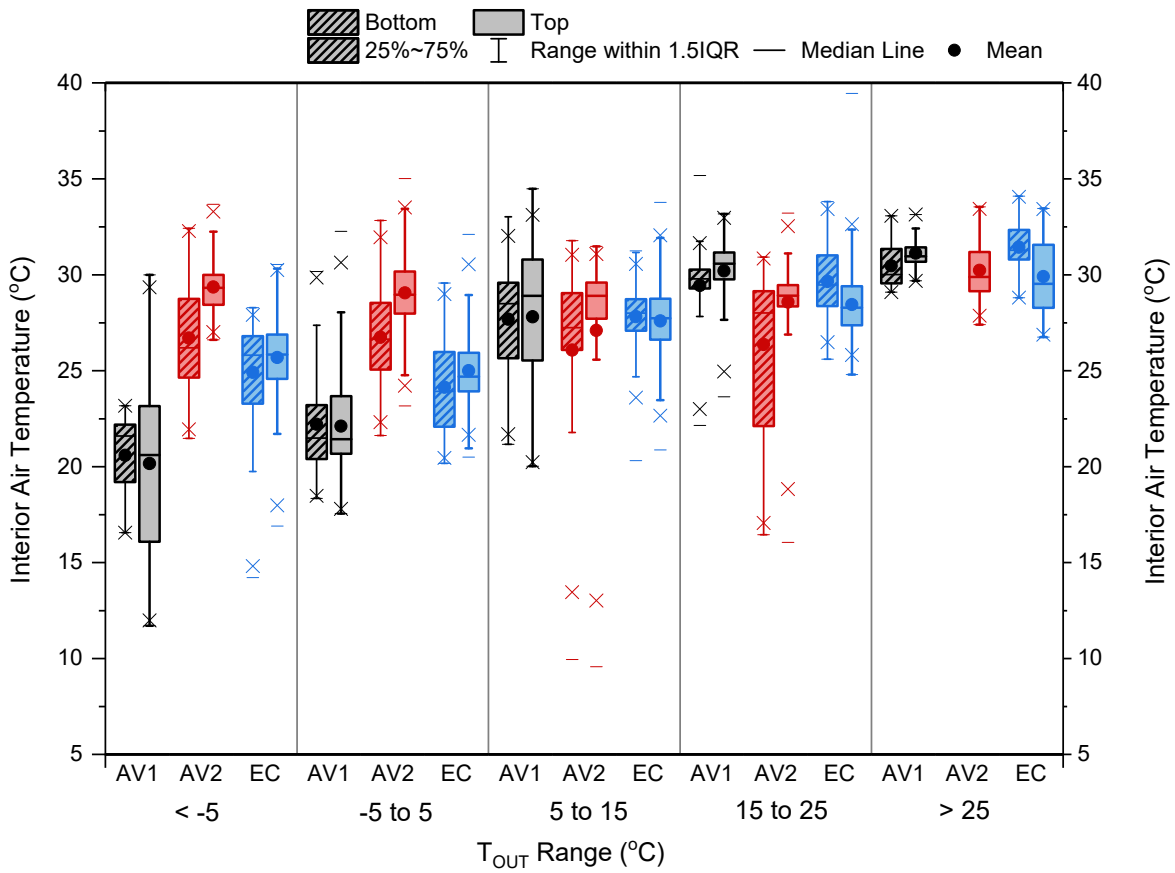


Figure 4-8. Distribution of the half-hour means of the indoor air temperatures measured at the top and bottom level in the Aviary 1 (AV1), Aviary 2 (AV2), and Enrichable cage (EC) houses under five different T_{OUT} thermal categories. The 25 – 75% population (Inter Quartile Range, IQR), the ± 1.5 IQR, the median, and the mean are identified in the box-whisker plots. A missing box for a level/house measurement (AV2 bottom, $T_{OUT} > 25^{\circ}\text{C}$) indicates the sensor/data was lost.

Some surprisingly extreme values were recorded in AV2 and EC, including a minimum temperature of 9.6°C that lasted for approximately 2.5 – 3 hours in AV2 for T_{OUT} range of 5 and 15°C; and a maximum temperature of 39.5°C was recorded in in EC during T_{OUT} category 15 to 25°C. Compared to AV1 and AV2, the EC had a smaller temperature distribution, showing that the temperature profile in EC was relatively more stable than the AV1 and AV2 during the entire course of the monitoring. For both AV1 and AV2, a wider range of temperature distribution was seen for $T_{OUT} < 15^{\circ}\text{C}$, indicating the hens in these two aviaries experienced colder interior temperatures (Figure 4-8) than those in the EC house. The range of temperature distribution significantly reduced for AV1 as T_{OUT} gradually went above 15°C, but maintained for AV2 until T_{OUT} was greater than 25°C.

There was some variation in temperature distribution between the top and the bottom levels for each of the three houses, indicating the thermal environment was not uniform in the vertical direction. For $T_{OUT} < 15^{\circ}\text{C}$, warmer temperatures were observed on the top level for all three houses, suggesting that there was insufficient fresh air circulation from inlets, and consequently thermal stratification. This same trend was continuously noted in AV1 and AV2 for $T_{OUT} > 15^{\circ}\text{C}$, but not in EC. In EC during warmer conditions, cooler air temperatures noted at the top level indicated more fresh air was introduced to the top floor and encouraged more air circulation than that of the bottom floor. However, warmer temperatures noted on the top level in AV1 and AV2 demonstrated that there was still insufficient air movement during warmer T_{OUT} ,

presumably during tunnel ventilation. The stagnant air in AV1 and AV2 during warmer weather indicates that there was not sufficient fresh air drawn into the barns, resulting in inefficient tunnel ventilation operation for these two aviary barns. When properly sized and operated, tunnel ventilation during the summer is designed to provide a high air velocity over the birds for effective convective cooling, although there will always be a longitudinal temperature gradient, coolest at tunnel ventilation inlet end and hottest at tunnel ventilation fan end. However, it is the thermal environment should be reasonably uniform vertically at any point along the length of the building, which was not observed in this study. In contrast to this study, uniform temperature distribution along the width and the height of a poultry barn with tunnel ventilation in the summer was observed in other studies (Webster and Czarick, 2000; Zheng et al., 2019). This uniform thermal environment is due to the air flow coming from the evaporative cooling pads (tunnel ventilation inlets), which are usually installed on the gable wall or/and both sidewalls in one end of the building, while fans are installed on the other end. Thus, continuous airflow from the evaporative cooling pads to the fans side was noted and provided air with uniform temperature along the width distribution of a poultry house (Hui et al., 2016), with a linear increase from bird heat production (Gates et al., 1992).

As for the THI profile during the monitoring period, similarly wide ranges as previously demonstrated for the air temperature were also observed for THI in the three poultry houses. Overall, the hens in all three houses during this study experienced THI conditions from normal to

emergency categories, as represented by the extreme THIs (Table 4-4). The overall range of the THI were 55 to 91, 52 to 90, and 58 to 96 for AV1, AV2, and EC, respectively. On average, dangerous THI conditions were observed for both cold and warm temperatures when T_{OUT} was below 5°C and above 15°C. No emergency Livestock Weather and Safety Index situations were noted for the average THIs, and the interior thermal environment of all three houses remained thermoneutral when T_{OUT} ranged between 5 and 15°C. No obvious difference between the housing types regarding the average THI conditions during summer was seen based on the data collected from this study, however, both AV1 and AV2 had higher THIs during winter conditions that surprisingly constituted an emergency condition, while alert THI conditions were observed in EC. When compared to the EC barn, the higher levels of THI in the aviaries were associated with high values of both the indoor air temperature and RH, indicating the hens in these two houses experienced more extreme thermal comfort conditions.

4.3.2.2 *CO₂ concentration evaluation*

The average values (\pm SD) of the indoor CO₂ concentrations for each housing type is shown in Table 4-4. Figure 4-9 provides a visualization of the overall distribution plotted using the 30-min averages of CO₂ concentrations measured at the top and bottom levels in AV1, AV2, and EC with regards to the five T_{OUT} ranges. CO₂ measurements for EC were not retrievable for T_{OUT} greater than 25°C (owing to a sensor failure), therefore, no representative data could be used for generating descriptive information for this combination.

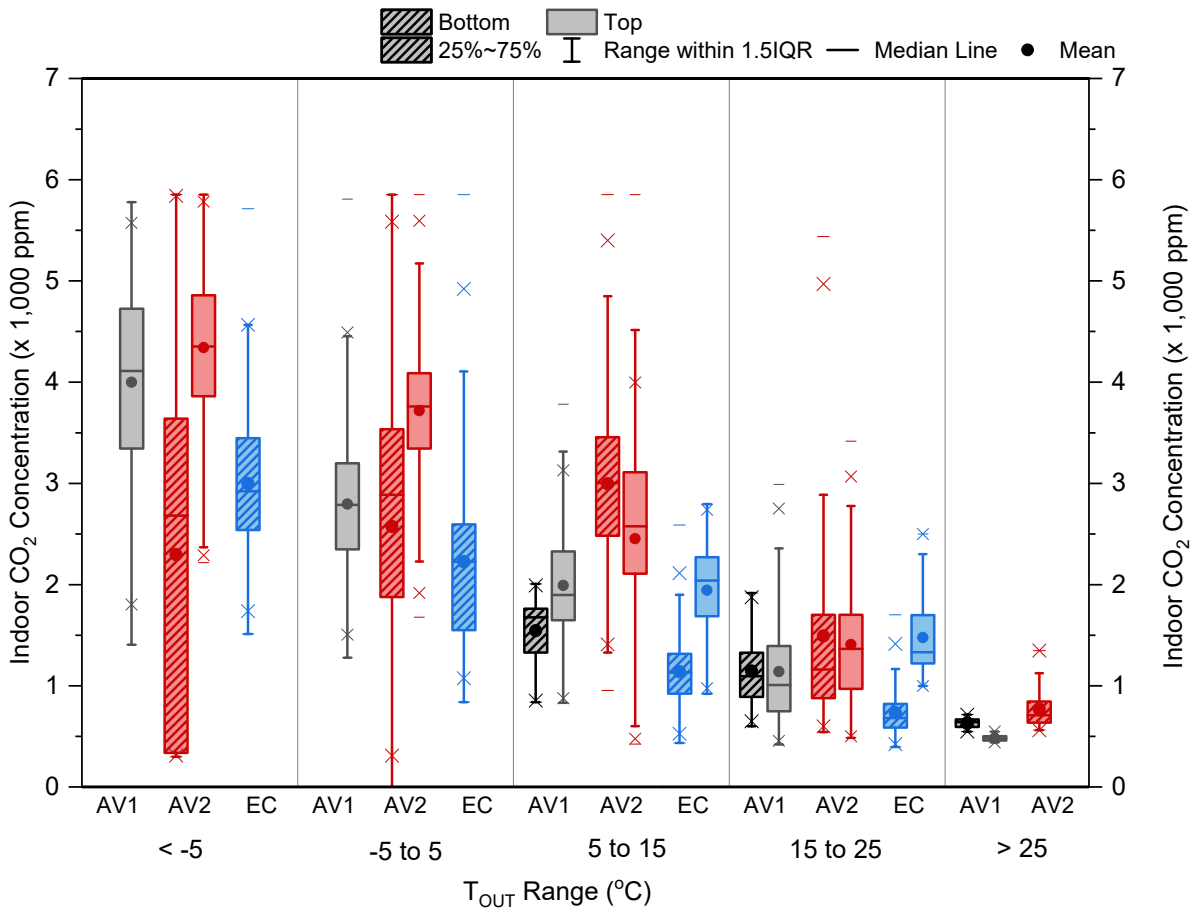


Figure 4-9. Distribution of the half-hour means of the indoor carbon dioxide (CO₂) concentrations measured at the top and bottom level in the Aviary 1 (AV1), Aviary 2 (AV2), and Enrichable cage (EC) houses, categorized by five different T_{OUT} thermal categories. The inter quartile range (IQR = 25 – 75% population), the \pm 1.5 IQR, the median, and the mean are identified in the box-whisker plots. A missing box for a level/house measurement indicates the data for this combination was lost.

Similar overall distribution patterns of CO₂ concentrations were observed for all three houses, although the aviaries tended to have higher mean concentrations than the EC barn for the three T_{OUT} categories below 15°C. The average CO₂ concentrations ranged from approximately 400 to 5800 ppm in each house. The mean CO₂ concentrations at all levels decreased with increasing T_{OUT} categories, presumably as ventilation rate increased; relatively high indoor CO₂ concentrations (uniform mean values about 5,800 ppm for AV1, AV2, and EC) were found in

cold weather due to the low ventilation rate to maintain room temperature, and low CO₂ concentrations at ambient levels (approximately 400 ppm) were observed during warm temperatures, with a strong linear decrease with ambient temperature. The results were similar to those from Ni et al. (2012), who reported high daily mean CO₂ concentrations between January and March (winter), and low values during July and August (summer). Zheng et al. (2009) studied the air quality characteristics at four sampling points in a commercial caged layer facility using the iPMUs, and reported means of 2,924, 3,352, 3,214 and 3,046 ppm for different sampling points measured during winter conditions, and low levels (<1,000 ppm) of CO₂ were observed when the ambient temperature exceeded 25°C and the barn was in tunnel ventilation mode. Ni et al. (2012) and Zhao et al. (2013) also observed low CO₂ levels with increased air temperature, as barn ventilation rates increased to limit interior temperature rise during summer conditions.

When comparing the different housing types regarding their interior CO₂ concentrations, different patterns were observed for $T_{OUT} < 5^{\circ}C$ and $T_{OUT} > 5^{\circ}C$. When the daily average T_{OUT} was below 5°C during wintertime, AV2 bottom and EC bottom consistently had lower concentrations than the AV1, suggesting more fresh air was available in these locations. When T_{OUT} reached above 5°C, EC had lower CO₂ levels while AV1 and AV2 were not different. For the entire course of monitoring, 75% of the CO₂ measurements were lower than 5,000 ppm for all three poultry houses.

4.3.2.3 NH_3 concentration evaluation

Mean (\pm SD) concentrations derived from the 30-min average of NH_3 concentrations for the bottom and top levels in AV1, AV2, and EC under different ambient thermal categories are provided in Table 4-4. The temporal and thermal profile of the NH_3 measurements with its relationship with ambient temperatures are shown in Figure 4-10. As explained in the previous section, NH_3 measurements for EC top during all temperatures, and for both levels in EC were not retrievable for T_{OUT} greater than 25°C , therefore, no representative data could be used for generating descriptive information for these combinations.

Figure 4-10 shows that the NH_3 in the layer hen houses exhibited a wide range of mean concentrations over the course of this monitoring. The NH_3 concentrations recorded within the barn ranged from 2 to 54.2, 1.5 to 14.2, and 1.6 to 47.3 ppm on average, for AV1, AV2, and EC, respectively, with extreme values above 80 ppm observed in all three barns during colder outside temperatures. The patterns of the seasonal distribution and variation of NH_3 concentrations shown in Figures 4-10 resemble those of the CO_2 concentrations (Figure 4-9), where lower mean NH_3 concentrations always corresponded to higher T_{OUT} , and higher NH_3 concentrations with lower T_{OUT} . Minimum barn ventilation rates (ideally, $0.6 \text{ m}^3 \text{ h}^{-1}$ per bird) are used to conserve energy while maintaining adequate indoor air quality (Zheng et al., 2019), however they may have been too low for some of the period studied. For $T_{\text{OUT}} < 5^\circ\text{C}$, 75% of the NH_3 concentrations measurements was below 60, 22, and 52 ppm for AV1, AV2, and EC,

respectively; for $T_{OUT} > 5^{\circ}\text{C}$, the magnitude of the NH_3 concentrations was substantially reduced, of which 75% measurements stayed below 35, 18, and 20 ppm for AV1, AV2, and EC, respectively.

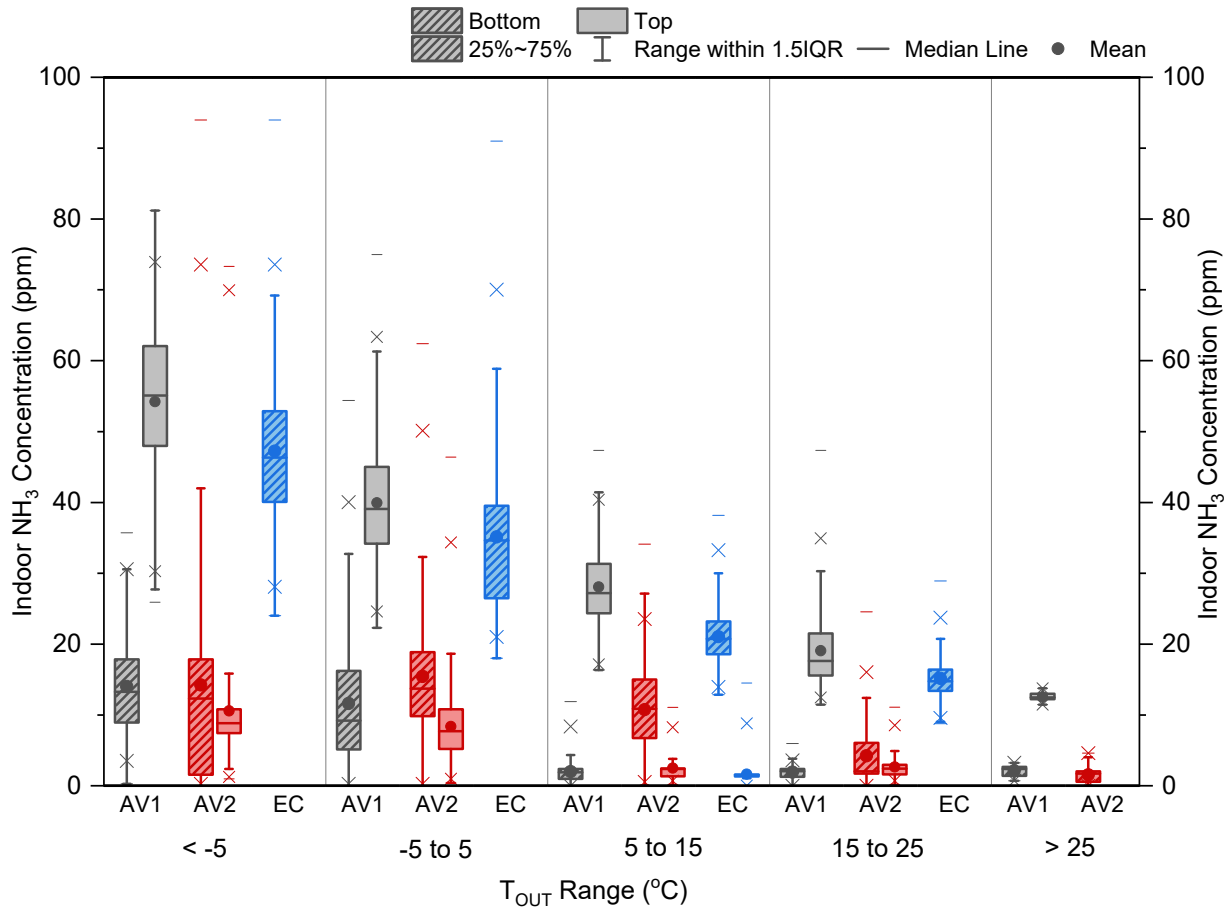


Figure 4-10. Distribution of the half-hour means of the indoor ammonia (NH_3) concentrations measured at the top and bottom level in the Aviary 1 (AV1), Aviary 2 (AV2), and Enrichable cage (EC) houses under five different T_{OUT} thermal categories. The inter quartile range (IQR = 25 – 75% population), the ± 1.5 IQR, the median, and the mean are identified in the box-whisker plots. A missing box for a level/house measurement indicates the data for this combination was lost.

Results show that a significant variation for NH₃ concentrations measured between the top and bottom levels for houses that had data available for both levels. The mean NH₃ concentration difference between the top and bottom level in each house ranged from 10.5 to 40.2 ppm, and 1.5 to 8.2 ppm during the entire course of monitoring for AV1 and AV2, respectively, but was not retrievable for EC due to instrumentation failure for EC top measurements. This pattern indicates that there was a vertical NH₃ concentration stratification, while greater stratification was observed during colder weather conditions, and was reduced when T_{OUT} gradually increased, although it was never eliminated.

A few studies previously conducted and assessed NH₃ concentrations inside layer facilities, with different layer farms showing unique characterization of their interior NH₃ conditions. Wathes et al. (1997) monitored a NH₃ concentration range of 12 – 24 ppm in a layer barn, Cheng et al. (2011) measured NH₃ concentrations in layer houses with cage systems, of which the NH₃ concentration ranged from 0.5 to 12.5 ppm. In a recent study conducted using iPMUs, Zheng et al. (2019) reported a daily mean NH₃ concentrations ranged from 0 – 28.1 ppm on average with extreme values approximately 40 ppm observed for a large-scale commercial stacked-cage layer facility with 500,000 laying hens. NH₃ concentrations were positively correlated to the moisture contents (Ni et al. 2017), and higher in-house NH₃ concentrations in winter were caused by lower ventilation rates and wetter litter conditions due to insufficient drying.

4.3.2.4 Ventilation implications

Results demonstrated in the previous sections indicate that the thermal environment and the gas concentrations were not uniformly distributed in the houses. Evidence for this includes inconsistent air temperature distribution, the CO₂ and NH₃ profiles were observed for different housing types. For example, with regards to temperature distribution, for AV1, warmer conditions were recorded at the bottom level, and colder temperatures were observed at the top level for T_{OUT} < 5°C, but a completely opposite trend was noted for the top and bottom levels when T_{OUT} was greater than 5°C. In contrast, for EC, the top level had warmer temperatures than the bottom level during winter conditions, but lower temperatures during summer T_{OUT} temperatures. For the CO₂ and NH₃ characteristics in poultry houses, since the molecular weight of the CO₂ (44 g/mol) is heavier than air (29 g/mol), and that of the NH₃ (17 g/mol) is lower than air, the bottom level should observe higher levels of CO₂ and lower levels of NH₃, and the top level should have higher NH₃ but lower CO₂. However, this theoretical trend in gas concentration profile was not always seen in the three barns which suggests incomplete or poor mixing between fresh air and room air.

Ventilation design and management can potentially explain the inconsistency presented for air temperature, CO₂ and NH₃ characteristics. As reported by layer production producers, although multiple ventilation stages are made available for the producers, the ventilation of the laying hen houses can be categorized into two main modes: 1) minimum winter ventilation:

during cold conditions, fresh air entered the barn through evenly distributed ceiling air inlets, and barn air is exhausted through the fans placed along both sidewalls ; and 2) tunnel ventilation: during hotter conditions, fresh air entered the barn through the evaporative cooling pads placed at the building north end wall and barn air exhausted through tunnel fans at the south end wall and both sidewalls. As T_{OUT} gradually increased during the year, stages of fans were sequentially activated as interior temperature rose above desired room temperature. Under minimum winter ventilation setting, fresh air was drawn into the barn through ceiling inlets and distributed to the barn interior. The stagnant air then exited through continuously running minimum ventilation fans located on both side walls and continued into the manure drying rooms or outside. Warmer temperatures observed on the top floor indicated that there was insufficient fresh air circulation at higher elevations in the barn as compared to the bottom floor. Under tunnel ventilation mode, as more fans are operating, more fresh air is drawn into the barn than during the winter conditions and this should encourage more rigorous air circulation of the barn interior, and thus create a more uniform thermal environment and air quality. The results from this study, including high RH recorded for winter, high air temperatures observed for both winter and summer, and the nonuniform thermal comfort and air quality, did not support the fundamental theories of proper ventilation design or operation, further indicates that the ventilation management inside the three houses was insufficient to promote removal of excessive heat during summer or excessive moisture during winter.

4.3.2.5 Farm management implications

Substantially higher values of interior air temperatures and NH₃ concentrations were realized for the poultry houses monitored in this study when compared to the values reported in other studies (Table 4-1). The CO₂ concentrations found during this study were slightly higher than previous studies but were considered to be within acceptable ranges. In addition to ventilation management strategies, farm management practices play an equally important role in terms of controlling and maintaining proper interior housing environment and hen welfare. Comparing to other ambient temperature conditions, maintaining acceptable air quality and thermal comfort during winter can be a challenge for most producers.

To closely evaluate the interior thermal environment and air quality at the two elevations of the three hen houses, the 30-min means of the air temperatures, NH₃ and CO₂ concentrations were plotted for the first week of February 2019 (7 am Feb 2nd to 12 pm Feb 8th), when the daily average T_{OUT} ranged between -3.9 to 6.1°C. The farm management practices were assessed by comparing the barn setpoints during the monitored period and industrial recommended values available for NH₃ and CO₂. An occurrence plot was created for air temperature, NH₃ and CO₂ measurements to represent the relative frequency of the certain levels of the parameters encountered between noon Feb 2nd and noon Feb 8th. The barn air temperatures were compared to target temperature setpoints, 22.2, 27.8, and 25.5°C for AV1, AV2, and EC, respectively. The NH₃ measurements were compared to 25 ppm, the Occupational Safety and Health

Administration (OSHA) set permissible exposure limit (PEL) for NH₃ eight-hour time weighted average (TWA) for human workers in different industries. The CO₂ measurements were compared to 5,000 ppm, the 8-h time-weighted exposure threshold limit value for other industries (ACGIH, 1998).

Results for early February 2019 showed that, among 125 h of consecutive monitoring, mean values for indoor temperature, NH₃, and CO₂ concentrations were 22.6, 26.9, and 25.4°C, 31, 20, and 36 ppm (NH₃), and 2375, 2823, and 2376 ppm (CO₂), for AV1, AV2, and EC, respectively. The average daily outside temperature ranged from -3.9 to 6.1°C. Substantial temperature stratification (3 to 6°C) was observed in the two aviaries, but not the EC barn. The proportion of hours below the temperature setpoint in each house was 45.6, 62.4, and 53.7% for AV1, AV2, and EC, respectively (Figure 4-12). For NH₃, the occurrence of hours exceeding the 25 ppm OSHA 8 h time-weighted average was 71.8, 23.9, and 98.3% in AV1, AV2, and EC, respectively (Figure 4-14). The 25-ppm value is proposed for humans but is often used for management guidelines within poultry houses.

Shown in Figure 4-11, during the first few days of data (7 am Feb 2 – 12 pm Feb 7), when it was very cold and when the pullets had just been placed, we observed very high ammonia in AV2 especially at the bottom sample location. A few hours later, the ammonia level in AV2 dropped down nicely but the other two houses remained about the same. During this time and before, it had been quite cold and we observed some fan shutters frozen up, ice forming

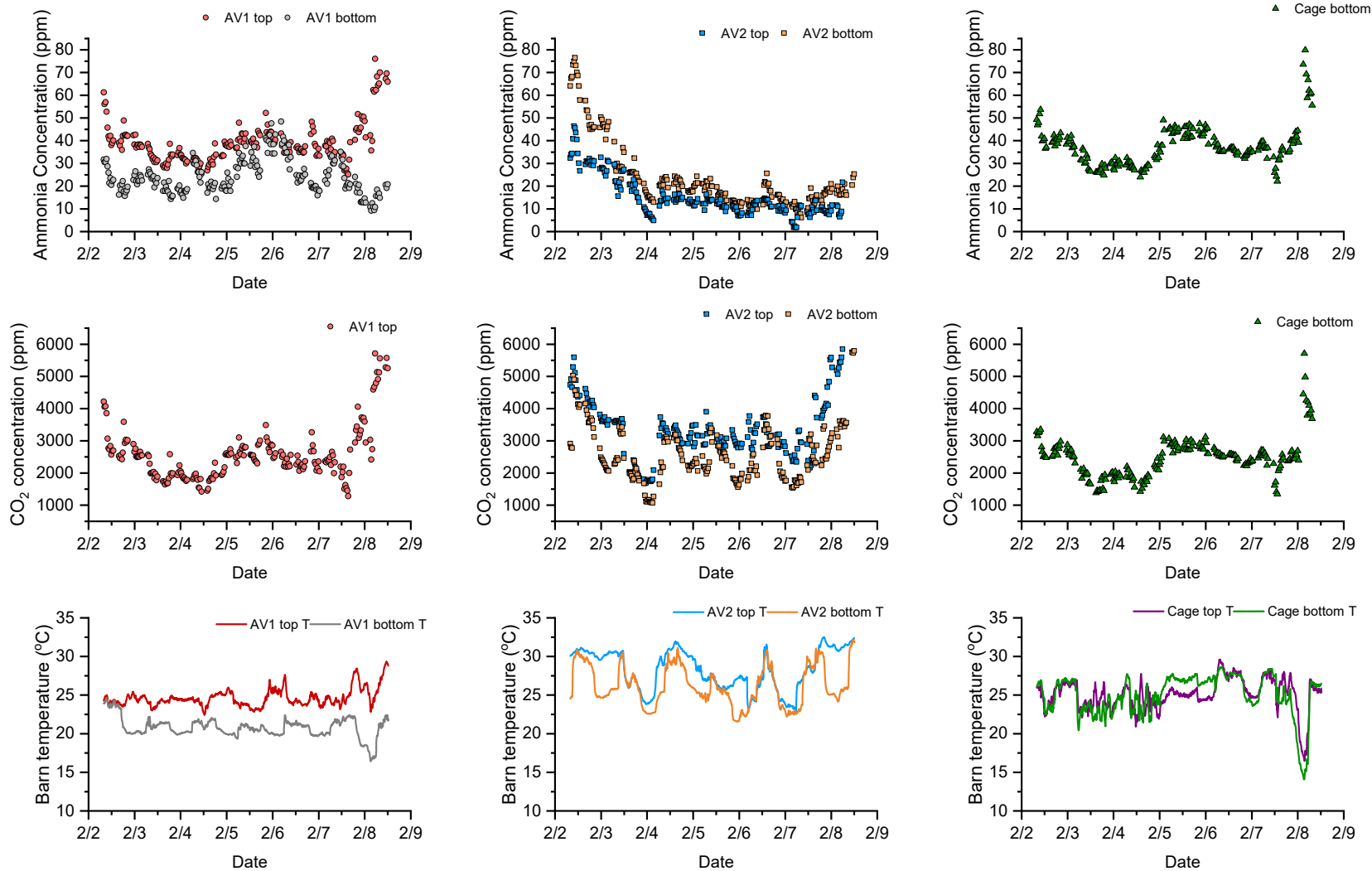


Figure 4-11. Means of the air temperatures, NH₃ and CO₂ concentrations for top and bottom levels in AV1, AV2, and EC during the first week of February 2019 (7 am Feb 2nd to 12 pm Feb 8th). The daily average T_{OUT} during this period ranged between -3.9 to 6.1°C.

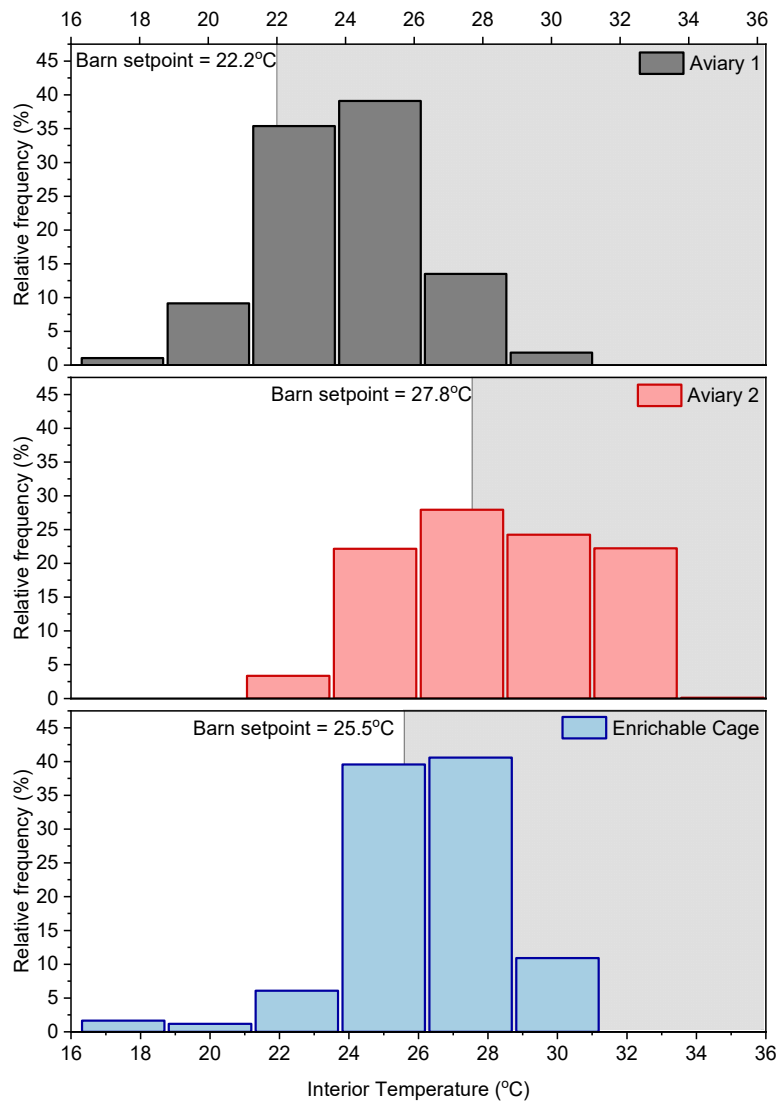


Figure 4-12. Occurrence (%) of the interior air temperature measurements for 16 – 34°C for hen houses AV1, AV2, and EC from noon Feb 2nd to noon Feb 8th. The target barn air temperature setpoints were 22.2, 27.8, and 25.5°C for AV1, AV2, and EC, respectively.

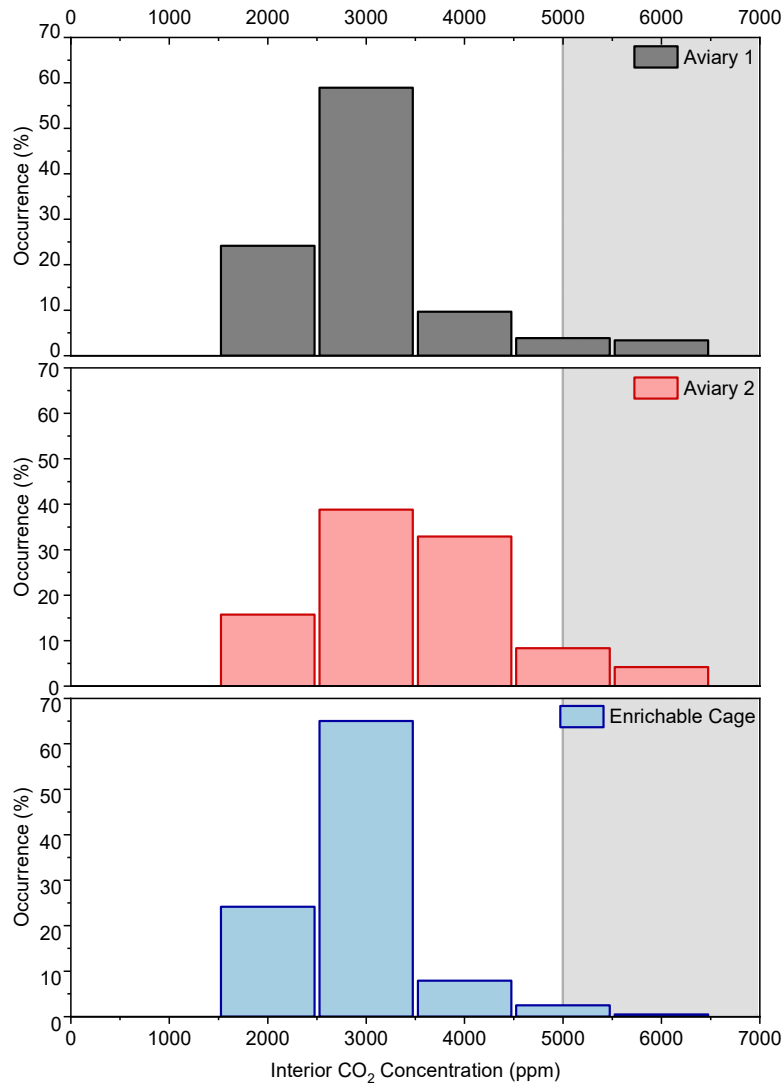


Figure 4-13. Occurrence (%) of the interior CO₂ measurements for range between 1,000 – 6,500 ppm for hen houses AV1, AV2, and EC from noon Feb 2nd to noon Feb 8th. The CO₂ measurements were compared to 5,000 ppm, the 8-h time-weighted exposure threshold limit value for other industries (ACGIH, 1998).

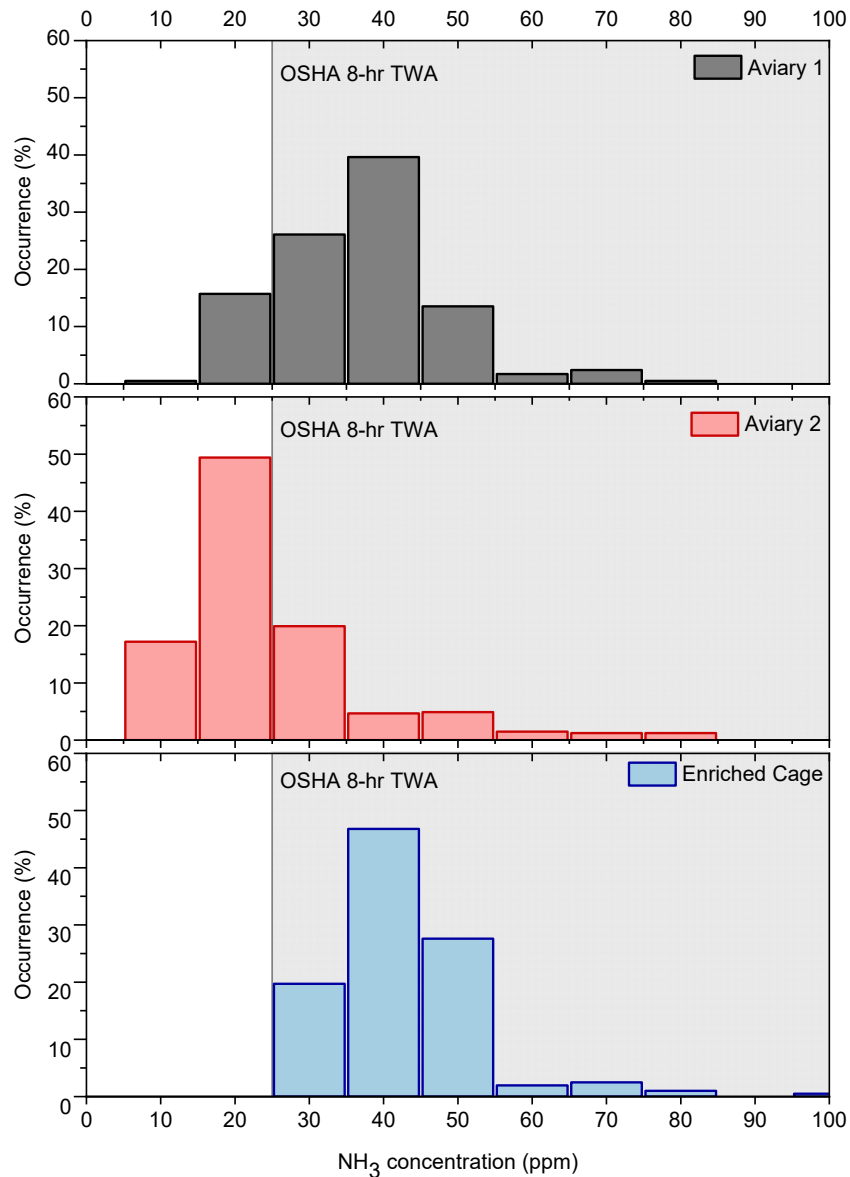


Figure 4-14. Occurrence (%) of the interior NH₃ measurements for range between 5 to 94 ppm for hen houses AV1, AV2, and EC from noon Feb 2nd to noon Feb 8th. The NH₃ measurements were compared to 25 ppm, the Occupational Safety and Health Administration (OSHA) set permissible exposure limit (PEL) for NH₃ eight-hour time weighted average (TWA) for human workers in different industries.

in various points where cold outside air was leaking into the structures, and pools of water forming on the floor at points along the perimeter. Maintaining good fresh air mixing in these more extreme conditions is tough, and the measurements of temperature for both aviaries show stratification, with higher locations warmer than lower which suggests the fresh air is coming in but not getting well-mixed – probably because air is leaking in from places other than from the ceiling inlets and thus not getting a chance to mix with inside air, and instead coming in other places without much velocity and stagnating near the floor. Zheng et al. (2019) evaluated the hypothesis that air was leaking into the structures, and found the highest mean NH_3 concentration of 42.3 ppm during the entire course of the monitoring recorded above the minimum exhaust fan adjacent to the manure drying tunnel for $T_{\text{OUT}} < 0^\circ\text{C}$. They concluded that the relatively high NH_3 concentrations (about half of the NH_3 level observed during this study) were caused by high pressure (back pressure) between the production area and the manure drying tunnel that allowed air leakage back into the barn through non-operating sidewall fan shutters. In cold weather, dilution from the minimum ventilation rate deployed in the three different houses was not sufficient to remove ammonia leaking back into the barn from the manure drying room.

Ammonia concentrations measured in this study were lower in both aviaries at the bottom location, and along with the observed temperature stratification, support the idea that minimum ventilation was not operating to promote good air mixing. During the first week of February 2019, the EC barn had more uniform temperature, suggesting the minimum ventilation was

operating better for that house. Average CO₂ levels in all houses remained under 3,000 ppm, suggesting sufficient ventilation rates being used during this cold weather condition.

In summary, both winter minimum ventilation and summer tunnel ventilation were inadequate for the farm monitored, and further improvement to the ventilation management strategies would be helpful. Issues regarding farm management practices also emerged during the 6-month continuous monitoring, as extreme values of the thermal comfort and air quality parameters were observed in all three houses.

4.4 SUMMARY AND CONCLUSIONS

Calibration of the ammonia sensors were successfully reperformed for all six iPMUs. The calibration data of the ammonia sensor and the iPMU were tested and analyzed by mathematical methods for determination of the static sensitivity and calibration equations. A MATLAB® program was developed for data processing for all variables, including sampling time, NH₃ and CO₂ concentrations, and temperatures. This program allows the user to select desired equation for static sensitivity and provide the average values for the variables for every 30 min.

The thermal comfort and air quality parameters, including the indoor air temperature, RH, CO₂ and NH₃ concentrations were successfully and continuously monitored using the six iPMUs for three different laying hen houses, including two aviaries (AV1 and AV2) and an enrichable cage house (EC) from February 1st to July 1st, 2019. The average daily ambient temperature ranged from -13.1 to 26.7°C.

The overall averaged interior air temperatures were 11.7 to 35.2°C, and 9.6 to 35.0°C (AV1 top and bottom, respectively); 14.2 to 39.5°C, and 20.2 to 31.1°C (AV2 top and bottom, respectively); and 27.1 to 30.2, 24.1 to 31.4°C (EC top and bottom, respectively). An extreme low temperature of 9.6°C that lasted for approximately 2.5 – 3 hours was observed in AV2 when T_{OUT} ranged between 5 and 15°C. A maximum temperature of 39.5°C was recorded in the EC barn during T_{OUT} category 15 to 25°C. There was a variation in temperature distribution between the top and the bottom levels for all three houses, indicating the thermal environment was not uniform in the vertical direction. Overall, the hens in all three houses experienced THI conditions from normal to emergency categories, as represented by the minimum and maximum THIs.

The average CO₂ concentrations ranged from approximately 400 to 5800 ppm for the three hen houses. For the entire course of monitoring, 75% of the CO₂ measurements were lower than 5,000 ppm for all three poultry houses. The NH₃ concentrations recorded within the barn ranged from 2 to 54.2, 1.5 to 14.2, and 1.6 to 47.3 ppm on average, for AV1, AV2, and EC, respectively, with extreme values above 80 ppm observed during colder outside temperatures. During monitoring, 75% of the NH₃ concentrations were below 60 ppm for all three houses. A variation was notable for NH₃ concentrations measured between the top and bottom levels for houses that had data available for both levels. The mean NH₃ concentrations difference between the top and bottom level in AV1 and AV2 ranged from 10.5 to 40.2 ppm, and 1.5 to 8.2 ppm.

The thermal environment and the gas concentrations in these facilities during the study were not uniformly distributed in the houses. Both winter minimum ventilation and summer tunnel ventilation were not sufficient during some monitoring periods, and further improvement to the ventilation management strategies would be helpful. Management practices to monitor the interior thermal environment, investigate the air inlets performance (number of inlets and air velocity), adjust operational static pressure (which drives the air inlets), or which fans to operate during coldest conditions, should be considered by the producer.

4.5 ACKNOWLEDGEMENTS

This work was funded in part by USDA-NIFA Program (Award No. 5020-32000-011-16) and multistate Project NE1442: Poultry Production Systems and Well-being: Sustainability for Tomorrow. The author thanks Dr. Rich S. Gates from Department of Agricultural and Biological Engineering, Dr. K. W. Koelkebeck from Department of Animal Sciences at University of Illinois at Urbana-Champaign for their guidance and assistance during the field measurement of this study. The author also thanks undergraduate students Lucas Vicente Pizeta Bragagnolo and Vitor Nejar Badu Mahfud de Oliveira from University of São Paulo at Pirassununga, and Nico Vassilakis from University of Illinois at Urbana-Champaign for their efforts in assisting in this study. Special thanks are extended to the commercial egg producer company and personnel that provided me access to their facility. Mention of commercial products in this article is solely for providing scientific information and does not imply recommendation.

CHAPTER 5 SUMMARY

Three research projects were designed and conducted, namely: prediction of neonatal piglets body temperature from surface temperature measurements, design and performance evaluation of an experimented water cooled thermal perch to reduce heat stress in laying hens, and improvement to the Intelligent Portable Monitoring Unit (iPMU) for air quality monitoring in alternative poultry housing systems. The contents of each project were included and formulated in a chapter of this dissertation. The highlighted summaries for these three projects are provided in the following paragraphs.

Rectal temperatures of the piglets dropped immediately after birth, with a mean drop of 4.4°C recorded in the first 15 min. Piglets experienced the lowest rectal temperature at 30 min after birth, reaching a mean low temperature of 33.6°C, approximately 5°C below birth temperature. Linear regression models were developed and assessed, with the refined linear regression model providing a more reliable prediction of piglet RT. The refined regression model can be used to provide a direct prediction of RT from the piglet ear surface temperature, with an uncertainty of about 1°C, and thus can be used as a convenient prediction tool for rapid estimation of piglet RT under typical farrowing conditions.

The cooled perch system was designed and used in an experiment assessing its suitability as a cooling tool to relieve heat stress for laying hens. The performance of the cooled perch system was assessed for a stable system operation period (June 25th – 30th, 2014) by analyzing

the water flowrate, characterizing the loop water temperature rise profile, and using this information to establish estimates of the system net heat gain. It was noted that the loop circulation pumps gave decreased performance over time, and there was a discrepancy between the pumps' actual output and that provided by the manufacturer. Different loops and CP replicates did not have equal performance regarding loop water temperature rise and loop net heat gains. There was a strong correlation noted between room temperature and perch net heat gain, indicating natural convection from ambient air to the pipe outer surface was the major contributor to heat gain source over other heat transfer mechanisms including bird heat conduction. Design criteria useful for other scale applications of cooled perch were provided. An average daily heat gain of about 128 W/m perch length or 43.2 W/hen housed was estimated, based on 12-h day/12-h night air temperature of 35/28°C and an average loop inlet water temperature of 20°C. A peak-day system heat load of 64.4 kWh was estimated and required a thermal storage capacity of 2.5 kWh. Information regarding hens' perching behavior, footpad area estimation, and thermal conductance or resistance of the footpad were provided.

A standard operation procedure for calibration of the ammonia sensors was developed and used for all six iPMUs. Thermal comfort and air quality parameters, including the indoor air temperature, RH, CO₂ and NH₃ concentrations were successfully and continuously monitored using the six iPMUs for three different laying hen houses, including two aviaries and an enrichable cage house from February 1st to July 1st, 2019. The thermal environment and the gas

concentrations during the study were not uniformly distributed spatially in the houses. There was a variation in temperature distribution between the top and the bottom levels for all three houses. Hens in all three houses experienced THI conditions from normal to emergency (hot and cold) categories. The average CO₂ and NH₃ concentrations for the three hen houses ranged from approximately 400 to 5800 ppm and 0 to 94 ppm, respectively. For the entire course of monitoring, 75% of the measurements in the three houses were lower than 5,000 ppm for CO₂ and below 60 ppm for NH₃ concentrations. Both winter minimum ventilation and summer tunnel ventilation were not sufficient during some monitoring periods, and further improvement to the ventilation management strategies would be helpful. Management practices to monitor the interior thermal environment, investigate the air inlets performance (number of inlets and air velocity), adjust operational static pressure (which drives the air inlets), or which fans to operate during coldest conditions, should be considered by the producer.

REFERENCES

- ACGIH. (1998). Industrial ventilation: A manual of recommended practice. In *American Conference of Government Industrial Hygienists*. Cincinnati, OH, USA.
- AetnaPlastics. (2015). Thermoplastic Piping Technical Manual – Chemtrol (C-CHTM-0909). Retrieved from www.aetnaplastics.com
- Alberdi, O., H. Arriaga, S. Calvet, F. Estellés, and P. Merino. (2016). Ammonia and greenhouse gas emissions from an enriched cage laying hen facility. *Biosystems Engineering*, 144, 1-12.
- Albright, L. D. (1990). *Environment control for animals and plants* (1st ed.). St. Joseph, MI: The American Society of Agricultural Engineers (ASAE).
- Alonso-Spilsbury, M., R. Ramirez-Necoechea, M. González-Lozano, D. Mota-Rojas, and M. Trujillo-Ortega. (2007). Piglet survival in early lactation: a review. *Journal of Animal and Veterinary Advances*, 6(1), 76-86.
- ASHRAE. (2016). Thermal storage. In *ASHRAE Handbook - HVAC Systems and Equipment* (SI ed., pp. 51.7-51.9). Atlanta, GA: ASHRAE.
- ASHRAE. (2017a). Chapter 3: Fluid flow. In *ASHRAE Handbook-Fundamentals* (SI ed.). Atlanta, GA: ASHRAE.
- ASHRAE. (2017b). Chapter 33: Physical properties of materials. In *ASHRAE Handbook-Fundamentals* (SI ed., pp. 33.1 - 33.4). Atlanta, GA: ASHRAE.
- ASHRAE. (2017c). Chapter 4: Heat transfer. In *ASHRAE Handbook-Fundamentals* (SI ed.). Atlanta, GA: ASHRAE.
- ASHRAE. (2017d). Chapter 11: Air contaminants. In *ASHRAE Handbook-Fundamentals* (SI ed.). Atlanta, GA: ASHRAE.
- ASHRAE. (2019). Chapter 25: Environmental control for animals and plants. In *ASHRAE Handbook – HVAC Applications* (SI ed., pp. 25.1-25.5). Atlanta, GA: ASHRAE.
- Barber, E. M., J. A. Dosman, C. S. Rhodes, G. I. Christison, and T. S. Hurst. (1993). *Carbon dioxide as an indicator of air quality in swine buildings*. Paper presented at the Third International Livestock Environment Symposium (ILES III), St. Joseph, MI.
- Baxter, E. M., and S. A. Edwards. (2018). Piglet mortality and morbidity: Inevitable or unacceptable? In *Advances in Pig Welfare* (pp. 73-100): Elsevier.
- Bell, C., and A. C. Rome. (1984). Pharmacological investigations of the vasodilator nerves supplying the duck's foot. *British Journal of Pharmacology*, 82(4), 801.
- Bell, D. D., W. D. Weaver, and M. O. North. (2002). *Commercial chicken meat and egg production* (5th ed.). New York, NY: Springer Science & Business Media.
- Bergman, T. L., F. P. Incropera, D. P. DeWitt, and A. S. Lavine. (2011). *Fundamentals of heat and mass transfer* (7th ed.). Hoboken, NJ: John Wiley & Sons.

- Bottcher, R., J. Brake, G. Baughman, and J. Magura. (1995). Vertically directed mixing fans for cooling floor-raised poultry. *Applied Engineering in Agriculture*, 11(4), 591-599.
- Bottcher, R. W., G. R. Baughman, R. S. Gates, and M. B. Timmons. (1991). Characterizing efficiency of misting systems for poultry. *Transactions of the ASAE*, 34(2), 586-590.
- Brown-Brandl, T. M., T. Yanagi, H. Xin, R. S. Gates, R. A. Bucklin, and G. S. Ross. (2003). A new telemetry system for measuring core body temperature in livestock and poultry. *Applied Engineering in Agriculture*, 19(5), 583-589.
- Busija, D. W., and C. W. Leffler. (1987). Hypothermia reduces cerebral metabolic rate and cerebral blood flow in newborn pigs. *American Journal of Physiology-Heart and Circulatory Physiology*, 253(4), H869-H873.
- Caldara, F. R., L. S. dos Santos, S. T. Machado, M. Moi, I. de Alencar Nääs, L. Foppa, R. G. Garcia, and R. d. K. S. dos Santos. (2014). Piglets' surface temperature change at different weights at birth. *Asian-Australasian Journal of Animal Sciences*, 27(3), 431.
- Calvet, S., F. Estelles, M. Cambra-Lopez, A. G. Torres, and H. F. Van den Weghe. (2011). The influence of broiler activity, growth rate, and litter on carbon dioxide balances for the determination of ventilation flow rates in broiler production. *Poultry Science*, 90(11), 2449-2458. doi:10.3382/ps.2011-01580
- Cândido, M. G. L., Y. Xiong, R. S. Gates, I. F. F. Tinoco, and K. W. Koelkebeck. (2018). Effects of carbon dioxide on turkey poult performance and behavior. *Poultry Science*, 97(8), 2768-2774. doi:10.3382/ps/pey128
- Carroll, J. A., R. L. Matteri, C. J. Dyer, L. A. Beausang, and M. E. Zannelli. (2001). Impact of environmental temperature on response of neonatal pigs to an endotoxin challenge. *American Journal of Veterinary Research*, 62(4), 561-566.
- Cheng, H. W., P. Y. Hester, R. S. Gates, M. M. Makagon, W. Wigle, and N. J. O. Widmar. (2013). Thermal perches as cooling devices for reducing heat stress in caged laying hens. In: West Lafayette, IN: USDA NIFA AFRI Competitive Grant Program.
- Cheng, W.-H., M.-S. Chou, and S.-C. Tung. (2011). Gaseous ammonia emission from poultry facilities in Taiwan. *Environmental Engineering Science*, 28(4), 283-289.
- Chepete, H. J., and H. Xin. (2000). Cooling laying hens by intermittent partial surface sprinkling. *Transactions of the ASAE*, 43(4), 965.
- Chepete, H. J., H. Xin, L. Mendes, and H. Li. (2011). Heat and moisture production of W-36 laying hens at 24 C to 27 C temperature conditions. *Transactions of the ASABE*, 54(4), 1491-1493.
- Christianson, L. L., and R. L. Fehr. (1983). Ventilation – energy and economics. In *Ventilation of Agricultural Structures* (pp. 335 - 349). St. Joseph, MI: ASABE.
- Cieslak, D. G., V. D. Leibbrandt, and N. J. Benevenga. (1983). Effect of a high fat supplement in late gestation and lactation on piglet survival and performance. *Journal of Animal Science*, 57(4), 954-959.

- Cooper, N. C., M. Ellis, Y. Xiong, and R. Gates. (2018). Effect of piglet birth weight on post-natal changes in body temperature. *Journal of Animal Science*, 96, 2-3 (abstr.).
- Corkery, G. P., S. Ward, and P. Hemmingway. (2013). *The effect of air quality parameters on poultry broiler performance*. Paper presented at the 2013 ASABE Annual International Meeting, Kansas City, MO.
- Cox, S. W. R. (1997). *Measurement and control in agriculture*. Oxford, United Kingdom: Oxford: Blackwell Science.
- Curtis, S. E. (1970). Environmental—thermoregulatory interactions and neonatal piglet survival. *Journal of Animal Science*, 31(3), 576-587.
- Curtis, S. E., and J. C. Rogler. (1970). Thermoregulatory ontogeny in piglets: sympathetic and adipokinetic responses to cold. *American Journal of Physiology-Legacy Content*, 218(1), 149-152.
- Dawkins, M. S., C. A. Donnelly, and T. A. Jones. (2004). Chicken welfare is influenced more by housing conditions than by stocking density. *Nature*, 427(6972), 342.
- Dickson, J. A., A. Mackenzie, and K. Mcleod. (1979). Temperature gradients in pigs during whole body hyperthermia at 42 degrees C. *Journal of Applied Physiology*, 47(4), 712-717.
- Dobeic, M., and Š. Pintarič. (2011). Laying hen and pig livestock contribution to aerial pollution in Slovenia. *Acta Veterinaria (Beograd)*, 61(2/3), 283-293.
- Donaldson, W., V. Christensen, J. Garlich, J. McMurtry, and N. Olson. (1995). Exposure to excessive carbon dioxide: A risk factor for early poult mortality. *Journal of Applied Poultry Research*, 4(3), 249-253.
- Donham, K., P. Haglind, Y. Peterson, R. Rylander, and L. Belin. (1989). Environmental and health studies of farm workers in Swedish swine confinement buildings. *British Journal of Industrial Medicine*, 46(1), 31-37. doi:10.1136/oem.46.1.31
- Douglas, S. L., S. A. Edwards, and I. Kyriazakis. (2014). Management strategies to improve the performance of low birth weight pigs to weaning and their long-term consequences. *Journal of Animal Science*, 92(5), 2280-2288. doi:10.2527/jas.2013-7388
- Dyck, G. W., and E. E. Swierstra. (1987). Causes of piglet death from birth to weaning. *Canadian Journal of Animal Science*, 67(2), 543-547. doi:10.4141/cjas87-053
- Ebeid, T., T. Suzuki, and T. Sugiyama. (2012). High ambient temperature influences eggshell quality and calbindin-D28k localization of eggshell gland and all intestinal segments of laying hens. *Poultry Science*, 91(9), 2282-2287.
- Edwards, S. A., and E. M. Baxter. (2015). Piglet mortality: causes and prevention. *Gestating and Lactating Sow*, 253-278. doi:10.3920/978-90-8686-803-2_11
- Eigenberg, R. A., R. A. Bucklin, and T. M. Brown-Brandl. (2009). Instrumentation for research and management in animal agriculture. In J. A. DeShazer (Ed.), *ASABE Monograph No. 25: Livestock energetics and thermal environment management* (1st ed., pp. 113 - 126). St. Joseph, MI: ASABE.

- Ellis, M., N. C. Cooper, K. VandePol, R. S. Gates, and Y. Xiong. (2017), December. Measuring postnatal changes in piglet body temperature. *National Hog Farmer*. Retrieved from <http://www.nationalhogfarmer.com/animal-health/measuring-post-natal-changes-piglet-body-temperature>
- EngineeringToolBox. (2001). Emissivity coefficients materials Retrieved from https://www.engineeringtoolbox.com/emissivity-coefficients-d_447.html
- English, P. R., and V. Morrison. (1984). Causes and prevention of piglet mortality. *Pig News Info*, 5(4), 369-376.
- English, P. R. (1993). Factors affecting neonatal piglet losses and management practices to minimize such losses. *Veterinary Annual*, 33, 107-119.
- Felver-Gant, J., L. Mack, R. Dennis, S. Eicher, and H. Cheng. (2012). Genetic variations alter physiological responses following heat stress in 2 strains of laying hens. *Poultry Science*, 91(7), 1542-1551.
- Frame, D. D., R. E. Buckner, and G. L. Anderson. (1999). *Causes and control of spontaneous cardiomyopathy or round heart disease in Utah turkeys. Fact sheet*. Retrieved from Utah State University Cooperative Extension
- Gardner, I. A., D. W. Hird, and C. E. Franti. (1989). Neonatal survival in swine - Effects of low birth weight and clinical disease. *American Journal of Veterinary Research*, 50(5), 792-797.
- Gates, R. S., and M. Timmons. (1988). Stochastic and deterministic analysis of evaporative cooling benefits for laying hens. *Transactions of the ASAE*, 31(3), 904-0909.
- Gates, R. S., M. Timmons, and R. Bottcher. (1991a). Numerical optimization of evaporative misting systems. *Transactions of the ASAE*, 34(1), 275-0280.
- Gates, R. S., J. Usry, J. Nienaber, L. Turner, and T. Bridges. (1991b). An optimal misting method for cooling livestock housing. *Transactions of the ASAE*, 34(5), 2199-2206.
- Gates, R. S., D. G. Overhults, R. W. Bottcher, and S. H. Zhang. (1992). Field calibration of a transient model for broiler misting. *Transactions of the ASAE*, 35(5), 1623-1631.
- Gates, R. S., H. Xin, K. Casey, Y. Liang, and E. Wheeler. (2005). Method for measuring ammonia emissions from poultry houses. *Journal of Applied Poultry Research*, 14(3), 622-634.
- Gates, R. S., K. Casey, E. Wheeler, H. Xin, and A. Pescatore. (2008). US broiler housing ammonia emissions inventory. *Atmospheric Environment*, 42(14), 3342-3350.
- Green, A. R., S. G. Gates, and L. M. Lawrence. (2005). Measurement of horse core body temperature. *Journal of Thermal Biology*, 30(5), 370-377.
doi:10.1016/j.jtherbio.2005.03.003
- Green, A. R., I. Wesley, D. W. Trampel, and H. Xin. (2009). Air quality and bird health status in three types of commercial egg layer houses. *Journal of Applied Poultry Research*, 18(3), 605-621.

- Grigull, U., I. Straub, E. Hahne, and K. Stephan. (1982). *Heat transfer*. Paper presented at the Seventh International Heat Transfer Conference, Munich.
- Hahn, G. L., J. B. Gaughan, T. L. Mader, and R. A. Eigenberg. (2009). Thermal indices and their applications for livestock environments. In J. A. DeShazer (Ed.), *ASABE Monograph No. 25: Livestock Energetics and Thermal Environment Management* (1st ed., pp. 113-126). St. Joseph, MI: ASABE.
- Hayes, M., H. Xin, H. Li, T. Shepherd, Y. Zhao, and J. Stinn. (2013). Ammonia, greenhouse gas, and particulate matter emissions of aviary layer houses in the Midwestern US. *Transactions of the ASABE*, 56(5), 1921-1932.
- Herpin, P., M. Damon, and J. Le Dividich. (2002). Development of thermoregulation and neonatal survival in pigs. *Livestock Production Science*, 78(1), 25-45.
doi:10.1016/S0301-6226(02)00183-5
- Hester, P., S. Enneking, K. Jefferson-Moore, M. Einstein, H. W. Cheng, and D. Rubin. (2013). The effect of perches in cages during pullet rearing and egg laying on hen performance, foot health, and plumage. *Poultry Science*, 92(2), 310-320.
- Hester, P., M. Makagon, R. Gates, J. Hu, S. Enneking, and H. Cheng. (2014). The musculoskeletal health of caged White Leghorn hens with access to thermally cooled perches. *Poultry Science*, 93(E-Suppl. 1), 93.
- Hillman, P. E., N. Scott, and A. Van Tienhoven. (1982). Vasomotion in chicken foot: dual innervation of arteriovenous anastomoses. *American Journal of Physiology-Regulatory, Integrative and Comparative Physiology*, 242(5), R582-R590.
- Hillman, P. E., and N. Scott. (1989). Energy budget of the chicken foot. *Journal of Thermal Biology*, 14(4), 205-217.
- Hoffmann, G., M. Schmidt, C. Ammon, S. Rose-Meierhofer, O. Burfeind, W. Heuwieser, and W. Berg. (2013). Monitoring the body temperature of cows and calves using video recordings from an infrared thermography camera. *Veterinary Research Communications*, 37(2), 91-99. doi:10.1007/s11259-012-9549-3
- Hu, J. Y., P. Y. Hester, M. M. Makagon, G. Vezzoli, R. S. Gates, Y. J. Xiong, and H. W. Cheng. (2016). Cooled perch effects on performance and well-being traits in caged White Leghorn hens. *Poultry Science*, 95(12), 2737-2746. doi:10.3382/ps/pew248
- Hu, J. Y., P. Y. Hester, M. M. Makagon, Y. Xiong, R. S. Gates, and H. W. Cheng. (2019a). Effect of cooled perches on performance, plumage condition, and foot health of caged White Leghorn hens exposed to cyclic heat. *Poultry Science*, 98(7), 2705-2718.
doi:10.3382/ps/pez039
- Hu, J. Y., P. Y. Hester, M. M. Makagon, Y. Xiong, R. S. Gates, and H. W. Cheng. (2019b). Effect of cooled perches on physiological parameters of caged White Leghorn hens exposed to cyclic heat. *Poultry Science*, 98(6), 2317-2325. doi:10.3382/ps/pez012
- Hu, J. Y., P. Y. Hester, Y. Xiong, R. S. Gates, M. M. Makagon, and H. W. Cheng. (2019c). Effect of cooled perches on the efficacy of an induced molt in White Leghorn laying hens

- previously exposed to heat stress. *Poultry Science*, 98(10), 4290-4300.
doi:10.3382/ps/pez317
- Hui, X., Q. Zhu, J.-Q. Ni, B. Li, Z. Shi, and S. Zhao. (2016). Effect of cooling pad installation on indoor airflow distribution in a tunnel-ventilated laying hen house. *International Journal of Agricultural and Biological Engineering*, 9(4), 169-177.
- Huynh, T., A. Aarnink, W. Gerrits, M. Heetkamp, T. Canh, H. Spoolder, B. Kemp, and M. Verstegen. (2005). Thermal behaviour of growing pigs in response to high temperature and humidity. *Applied Animal Behaviour Science*, 91(1-2), 1-16.
- Ikeguchi, A., and H. Xin. (2001). Field evaluation of a sprinkling system for cooling commercial laying hens in iowa. *Applied Engineering in Agriculture*, 17(2), 217.
- Ji, B., W. Zheng, R. S. Gates, and A. Green. (2016). Design and performance evaluation of the upgraded portable monitoring unit for air quality in animal housing. *Computers and Electronics in Agriculture*, 124, 132-140.
- Kaasik, A., and M. Maasikmets. (2013). Concentrations of airborne particulate matter, ammonia and carbon dioxide in large scale uninsulated loose housing cowsheds in Estonia. *Biosystems Engineering*, 114(3), 223-231.
- Karlekar, B. V., and R. M. Desmond. (1977). Fluid flow background for convective heat transfer. In *Engineering heat transfer* (1st ed., pp. 283-294). St. Paul, MN: West Publishing Company.
- Kelley, K. W. (1985). Immunological consequences of changing environmental stimuli. In *Animal stress* (pp. 193-223). New York, NY: Springer.
- Kilic, I., and E. Yaslioglu. (2014). Ammonia and carbon dioxide concentrations in a layer house. *Asian Australasian Journal of Animal Science*, 27(8), 1211-1218.
doi:10.5713/ajas.2014.14099
- Kocaman, B., N. Esenbuga, A. Yildiz, E. Laçın, and M. Macit. (2006). Effect of environmental conditions in poultry houses on the performance of laying hens. *International Journal of Poultry Science*, 5(1), 26-30.
- Koelkebeck, K. W., S. DePersio, K. Lima, P. Harrison, C. Utterback, P. Utterback, R. N. Dilger, R. S. Gates, A. Green, and J. Campbell. (2014). Evaluation of feeding spray-dried bovine plasma protein on production performance of laying hens exposed to high ambient temperatures. *Journal of Applied Poultry Research*, 23(3), 393-402.
- Kristensen, H. H., L. R. Burgess, T. G. Demmers, and C. M. Wathes. (2000). The preferences of laying hens for different concentrations of atmospheric ammonia. *Applied Animal Behavior Science*, 68(4), 307-318. doi:10.1016/s0168-1591(00)00110-6
- Lara, L. J., and M. H. Rostagno. (2013). Impact of heat stress on poultry production. *Animals*, 3(2), 356-369. doi:10.3390/ani3020356
- Lay, D. C., R. L. Matteri, J. A. Carroll, T. J. Fangman, and T. J. Safranski. (2002). Preweaning survival in swine. *Journal of Animal Science*, 80(E-suppl_1), E74-E86.

- Lay, D. C., R. M. Fulton, P. Y. Hester, D. M. Karcher, J. B. Kjaer, J. A. Mench, B. A. Mullens, R. C. Newberry, C. J. Nicol, and N. P. O'sullivan. (2011). Hen welfare in different housing systems. *Poultry Science*, 90(1), 278-294.
- LCI. (1970). *Patterns of transit losses*. Omaha, NE: Livestock Conservation, Inc.
- Le Dividich, J., and J. Noblet. (1981). Colostrum intake and thermoregulation in the neonatal pig in relation to environmental temperature. *Neonatology*, 40(3-4), 167-174.
- Li, H., H. Xin, Y. Liang, R. S. Gates, E. F. Wheeler, and A. J. Heber. (2005). Comparison of direct vs. indirect ventilation rate determinations in layer barns using manure belts. *Transactions of the ASAE*, 48(1), 367-372.
- Liang, Y., H. Xin, E. Wheeler, R. Gates, H. Li, J. Zajackowski, P. Topper, K. D. Casey, B. Behrends, and D. J. Burnham. (2005). Ammonia emissions from US laying hen houses in Iowa and Pennsylvania. *Transactions of the ASAE*, 48(5), 1927-1941.
- Liang, Y., H. Xin, H. Li, R. S. Gates, E. F. Wheeler, and K. D. Casey. (2006). Effects of measurement intervals on estimation of ammonia emissions from layer houses. *Transactions of the ASABE*, 49(1), 183-186.
- Liang, Y., G. T. Tabler, T. A. Costello, I. L. Berry, S. E. Watkins, and Y. V. Thaxton. (2014). Cooling broiler chickens by surface wetting: Indoor thermal environment, water usage, and bird performance. *Applied Engineering in Agriculture*, 30(2), 249-258.
- Lowen, A. C., S. Mubareka, J. Steel, and P. Palese. (2007). Influenza virus transmission is dependent on relative humidity and temperature. *PLoS Pathogens*, 3(10), e151.
- Mack, L., J. Felver-Gant, R. Dennis, and H. Cheng. (2013). Genetic variations alter production and behavioral responses following heat stress in 2 strains of laying hens. *Poultry Science*, 92(2), 285-294.
- Makagon, M., V. Cussen, R. Gates, P. Hester, and H. Cheng. (2015). Effects of cooled perch access during chronic heat stress on the behavior of White Leghorn hens. *Poultry Science*, 94, 79 (abstr.).
- Malmkvist, J., L. J. Pedersen, B. M. Damgaard, K. Thodberg, E. Jorgensen, and R. Labouriau. (2006). Does floor heating around parturition affect the vitality of piglets born to loose housed sows? *Applied Animal Behaviour Science*, 99(1-2), 88-105. doi:10.1016/j.applanim.2005.10.007
- Marchant, J. N., A. R. Rudd, M. T. Mendl, D. M. Broom, M. J. Meredith, S. Corning, and P. H. Simmins. (2000). Timing and causes of piglet mortality in alternative and conventional farrowing systems. *Veterinary Record*, 147(8), 209-214. doi:DOI 10.1136/vr.147.8.209
- Martineau, L., and J. Larochelle. (1988). The cooling power of pigeon legs. *Journal of Experimental Biology*, 136(1), 193-208.
- Martland, M. F. (1985). Ulcerative dermatitis dm broiler chickens: The effects of wet litter. *Avian Pathology*, 14(3), 353-364. doi:10.1080/03079458508436237
- Metais, B., and E. R. G. Eckert. (1964). Forced, mixed and free convection regimes. *ASME Journal of Heat Transfer* 86(C2)(5), 295.

- Midtgård, U. (1981). The rete tibiotarsale and arteriovenous association in the hind limb of birds: A comparative morphological study on counter-current heat exchange systems. *Acta Zoologica*, 62(2), 67-87.
- Mignon-Grasteau, S., U. Moreri, A. Narcy, X. Rousseau, T. Rodenburg, M. Tixier-Boichard, and T. Zerjal. (2015). Robustness to chronic heat stress in laying hens: a meta-analysis. *Poultry Science*, 94(4), 586-600.
- Miles, D., P. Owens, and D. Rowe. (2006). Spatial variability of litter gaseous flux within a commercial broiler house: Ammonia, nitrous oxide, carbon dioxide, and methane. *Poultry Science*, 85(2), 167-172.
- Monteith, J. (1981). Evaporation and surface temperature. *Quarterly Journal of the Royal Meteorological Society*, 107(451), 1-27.
- Monteith, J., and M. Unsworth. (2013). Heater transfer. In *Principles of environmental physics: plants, animals, and the atmosphere* (4th ed., pp. 151-178). The Netherlands: Academic Press: Elsevier Ltd.
- Morrison, V., P. English, and G. Lodge. (1983). *The effect of alternative creep heating arrangements at 2 house temperatures on piglet lying behavior and mortality in the neonatal-period*. Paper presented at the Animal Production.
- Muiruri, H. K. (1989). *Conductive cooling and the metabolism of chicken hens in hot environment*. (Ph.D.). University of Illinois Urbana-Champaign, Urbana, IL.
- Muiruri, H. K., and P. C. Harrison. (1991). Effect of roost temperature on performance of chickens in hot ambient environments. *Poultry Science*, 70(11), 2253-2258. doi:10.3382/ps.0702253
- Mutaf, S., N. Ş. Kahraman, and M. Firat. (2008). Surface wetting and its effect on body and surface temperatures of domestic laying hens at different thermal conditions. *Poultry Science*, 87(12), 2441-2450.
- Mutaf, S., N. Seber Kahraman, and M. Firat. (2009). Intermittent partial surface wetting and its effect on body-surface temperatures and egg production of white and brown domestic laying hens in Antalya (Turkey). *British Poultry Science*, 50(1), 33-38.
- MWPS. (1983). *Structures and environment handbook, MWPS-1* (11th ed. Vol. 1). Ames, IA: Midwest Plan Service.
- NAHMS. (1995). *National animal health monitoring system: swine' 95 Part I: reference of 1995 swine management practices*. (32739). Retrieved from https://www.aphis.usda.gov/aphis/ourfocus/animalhealth/monitoring-and-surveillance/nahms/nahms_swine_studies
- Naseem, S., and A. J. King. (2018). Ammonia production in poultry houses can affect health of humans, birds, and the environment—techniques for its reduction during poultry production. *Environmental Science and Pollution Research*, 25(16), 15269-15293.
- Ni, J.-Q., L. Chai, L. Chen, B. W. Bogan, K. Wang, E. L. Cortus, A. J. Heber, T.-T. Lim, and C. A. Diehl. (2012). Characteristics of ammonia, hydrogen sulfide, carbon dioxide, and

- particulate matter concentrations in high-rise and manure-belt layer hen houses. *Atmospheric Environment*, 57, 165-174.
- Ni, J.-Q., S. Liu, C. A. Diehl, T.-T. Lim, B. W. Bogan, L. Chen, L. Chai, K. Wang, and A. J. Heber. (2017). Emission factors and characteristics of ammonia, hydrogen sulfide, carbon dioxide, and particulate matter at two high-rise layer hen houses. *Atmospheric Environment*, 154, 260-273.
- Olanrewaju, H., W. Dozier, J. Purswell, S. Branton, D. Miles, B. Lott, A. Pescatore, and J. Thaxton. (2008). Growth performance and physiological variables for broiler chickens subjected to short-term elevated carbon dioxide concentrations. *International Journal of Poultry Science*, 7(8), 738-742.
- Owen, R. L., R. Wideman Jr, G. Barbato, B. Cowen, B. Ford, and A. Hattel. (1995). Morphometric and histologic changes in the pulmonary system of broilers raised at simulated high altitude. *Avian Pathology*, 24(2), 293-302.
- Pattison, R., P. English, O. MacPherson, J. Roden, and M. Birnie. (1990). Hypothermia and its attempted control in newborn piglets. *Proceedings of the British Society of Animal Production (1972)*, 1990, 81-81.
- Pedersen, L. J., M. L. V. Larsen, and J. Malmkvist. (2016). The ability of different thermal aids to reduce hypothermia in neonatal piglets. *Journal of Animal Science*, 94(5), 2151-2159.
- Pedersen, S., V. Blanes-Vidal, H. Jørgensen, A. Chwalibog, A. Haeussermann, M. Heetkamp, and A. Aarnink. (2008). Carbon dioxide production in animal houses: A literature review. *Agricultural Engineering International: CIGR Journal*, 10(BC 08 008).
- Porter, W. P., and D. M. Gates. (1969). Thermodynamic equilibria of animals with environment. *Ecological Monographs*, 39(3), 227-&. doi:Doi 10.2307/1948545
- Prodanov, M., M. Radeski, and V. Ilieski. (2016). Air quality measurements in laying hens housing. *Macedonian Veterinary Review*, 39(1), 91-95. doi:10.1515/macvetrev-2016-0071
- Reilly, W., K. W. Koelkebeck, and P. Harrison. (1991). Performance evaluation of heat-stressed commercial broilers provided water-cooled floor perches. *Poultry Science*, 70(8), 1699-1703.
- Rudd, A. R., and J. N. Marchant. (1995). Aspects of farrowing and lactating sow behaviour. *Pig Journal*, 34, 21-30.
- Shepherd, T. A., Y. Zhao, H. Li, J. P. Stinn, M. D. Hayes, and H. Xin. (2015). Environmental assessment of three egg production systems—Part II. Ammonia, greenhouse gas, and particulate matter emissions. *Poultry Science*, 94(3), 534-543.
- Shepherd, T. A., H. Xin, J. P. Stinn, M. D. Hayes, Y. Zhao, and H. Li. (2017). Ammonia and carbon dioxide emissions of three laying-hen housing systems as affected by manure accumulation time. *Transactions of the ASABE*, 60(1), 229-236.

- Shinder, D., M. Rusal, J. Tanny, S. Druyan, and S. Yahav. (2007). Thermoregulatory responses of chicks (*Gallus domesticus*) to low ambient temperatures at an early age. *Poultry Science*, 86(10), 2200-2209.
- Singh, A., K. Casey, W. King, A. Pescatore, R. S. Gates, and M. Ford. (2009). Efficacy of urease inhibitor to reduce ammonia emission from poultry houses. *Journal of Applied Poultry Research*, 18(1), 34-42.
- Smith, R., J.-L. Rault, R. Gates, and D. Lay. (2018). A two-step process of nitrous oxide before carbon dioxide for humanely euthanizing piglets: on-farm trials. *Animals*, 8(4), 52.
- St-Pierre, N., B. Cobanov, and G. Schnitkey. (2003). Economic losses from heat stress by U.S. livestock industries. *Journal of Dairy Science*, 86, E52-E77.
- Steen, I., and J. B. Steen. (1965). The importance of the legs in the thermoregulation of birds. *Acta Physiol Scand*, 63, 285-291. doi:10.1111/j.1748-1716.1965.tb04054.x
- Tactacan, G. B., W. Guenter, N. J. Lewis, J. C. Rodriguez-Lecompte, and J. D. House. (2009). Performance and welfare of laying hens in conventional and enriched cages. *Poultry Science*, 88(4), 698-707. doi:10.3382/ps.2008-00369
- Timmons, M., and R. S. Gates. (1988). Predictive model of laying hen performance to air temperature and evaporative cooling. *Transactions of the ASAE*, 31(5), 1503-1502.
- USDA. (2015). Farrowing productivity and preweaning death loss. In *Swine 2012 Part I: Baseline reference of swine health and management in the United States* (pp. 45 - 49). Fort Collins, CO: USDA-APHIS-VS, Center for Epidemiology and Animal Health.
- Wathes, C., M. Holden, R. Sneath, R. White, and V. Phillips. (1997). Concentrations and emission rates of aerial ammonia, nitrous oxide, methane, carbon dioxide, dust and endotoxin in UK broiler and layer houses. *British Poultry Science*, 38(1), 14-28.
- Webster, A. B., and M. Czarick. (2000). Temperatures and performance in a tunnel-ventilated, high-rise layer house. *Journal of Applied Poultry Research*, 9(1), 118-129.
- Westin, R., J. Hultgren, and B. Algers. (2015). Strategic use of straw increases nest building in loose housed farrowing sows. *Applied Animal Behaviour Science*, 166, 63-70.
- Wheeler, E. F., K. D. Casey, R. S. Gates, H. Xin, J. L. Zajackowski, P. A. Topper, Y. Liang, and A. J. Pescatore. (2006). Ammonia emissions from twelve US broiler chicken houses. *Transactions of the ASAE*, 49(5), 1495.
- Wideman, R. F., P. Maynard, and W. G. Bottje. (1999). Venous blood pressure in broilers during acute inhalation of five percent carbon dioxide or unilateral pulmonary artery occlusion. *Poultry Science*, 78(10), 1443-1451.
- Wolfenson, D., D. Bachrach, M. Maman, Y. Graber, and I. Rozenboim. (2001). Evaporative cooling of ventral regions of the skin in heat-stressed laying hens. *Poultry Science*, 80(7), 958-964. doi:10.1093/ps/80.7.958
- Xin, H., H. Zhou, and D. S. Bundy. (1997). Comparison of energy use and piglet performance between conventional and energy-efficient heat lamps. *Applied Engineering in Agriculture*, 13(1), 95-99.

- Xin, H., R. S. Gates, M. C. Puma, and D. U. Ahn. (2002). Drinking water temperature effects on laying hens subjected to warm cyclic environments. *Poultry Science*, 81(5), 608-617. doi:10.1093/ps/81.5.608
- Xin, H., H. Li, R. T. Burns, R. S. Gates, D. G. Overhults, and J. W. Earnest. (2009). Use of CO₂ concentration difference or CO₂ balance to assess ventilation rate of broiler houses. *Transactions of the ASABE*, 52(4), 1353-1361.
- Xin, H., R. S. Gates, A. R. Green, F. M. Mitloehner, P. Moore, and C. M. Wathes. (2011). Environmental impacts and sustainability of egg production systems. *Poultry Science*, 90(1), 263-277.
- Xiong, Y. (2013). *Evaluation of trailer thermal environment during commercial swine transport*. (M.S.). University of Illinois at Urbana-Champaign Urbana, IL.
- Xiong, Y., R. S. Gates, J. Y. Hu, K. S. O. Rocha, M. M. Makagon, P. Y. Hester, and H. W. Cheng. (2015). *Performance assessment of cooled perch system for heat stress trials in egg laying production: Year 1 (Paper 15 - 2183667)*. Paper presented at the 2015 ASABE Annual International Meeting, New Orleans, LA
- Xiong, Y., R. S. Gates, N. C. Cooper, and M. Ellis. (2018). *Neonatal piglet core body temperature model from surface temperature and environment measurements*. Paper presented at the 10th International Livestock Environment Symposium (ILES X), Omaha, NE.
- Yanagi, T., H. Xin, and R. S. Gates. (2002). Optimization of partial surface wetting to cool caged laying hens. *Transactions of the ASAE*, 45(4), 1091.
- Zhang, Q., and H. Xin. (2000). Static and dynamic temperature distribution of heat mats for swine farrowing creep heating. *Applied Engineering in Agriculture*, 16(5), 563-569.
- Zhao, J. P., H. C. Jiao, Y. B. Jiang, Z. G. Song, X. J. Wang, and H. Lin. (2012). Cool perch availability improves the performance and welfare status of broiler chickens in hot weather. *Poultry Science*, 91(8), 1775-1784. doi:10.3382/ps.2011-02058
- Zhao, J. P., H. C. Jiao, Y. B. Jiang, Z. G. Song, X. J. Wang, and H. Lin. (2013a). Cool perches improve the growth performance and welfare status of broiler chickens reared at different stocking densities and high temperatures. *Poultry Science*, 92(8), 1962-1971.
- Zhao, Y., H. Xin, T. Shepherd, M. Hayes, J. Stinn, and H. Li. (2013b). Thermal environment, ammonia concentrations, and ammonia emissions of aviary houses with white laying hens. *Transactions of the ASABE*, 56(3), 1145-1156.
- Zhao, Y., T. A. Shepherd, H. Xin, and H. Li. (2014). *Concentrations of ammonia, greenhouse gases and particulate matters in conventional cage, aviary, and enriched colony laying-hen houses*. Paper presented at the 2014 ASABE Annual International Meeting Montreal, Quebec, Canada.
- Zhao, Y., T. A. Shepherd, H. Li, and H. Xin. (2015a). Environmental assessment of three egg production systems—Part I: Monitoring system and indoor air quality. *Poultry Science*, 94(3), 518-533.

- Zhao, Y., T. A. Shepherd, J. Swanson, J. Mench, D. Karcher, and H. Xin. (2015b). Comparative evaluation of three egg production systems: Housing characteristics and management practices. *Poultry Science*, 94(3), 475-484.
- Zhao, Y., D. Zhao, H. Ma, K. Liu, A. Atilgan, and H. Xin. (2016). Environmental assessment of three egg production systems—Part III: Airborne bacteria concentrations and emissions. *Poultry Science*, 95(7), 1473-1481.
- Zheng, W., Y. Xiong, R. S. Gates, Y. Wang, and K. K. Koelkebeck. (2019). Air temperature, carbon dioxide and ammonia assessment inside a commercial cage layer barn with manure-drying tunnels. *Poultry Science*, under review.
- Zhou, H., and H. Xin. (1999). Responses of piglets to variable vs. constant output heat lamp with clear vs. red color. *Applied Engineering in Agriculture*, 15(4), 327-330.
- Zolnier, S., R. S. Gates, R. G. Anderson, S. E. Nokes, and G. A. Duncan. (2001). Non-water-stressed baseline as a tool for dynamic control of a misting system for propagation of poinsettias. *Transactions of the ASAE*, 44(1), 137-147.
- Zolnier, S., R. S. Gates, R. L. Geneve, and J. W. Buxton. (2003). Evapotranspiration-based misting control for poinsettia propagation. *Transactions of the ASAE*, 46(1), 135-145.
- Zulkifli, I., A. Al-Aqil, A. R. Omar, A. Q. Sazili, and M. A. Rajion. (2009). Crating and heat stress influence blood parameters and heat shock protein 70 expression in broiler chickens showing short or long tonic immobility reactions. *Poultry Science*, 88(3), 471-476. doi:10.3382/ps.2008-00287

APPENDIX A SELECTING CALIBRATION EQUATION FOR NH₃

SENSORS – RESULTS FOR METHODS NOT SELECTED

The summary results of key parameters for selecting the proper calibration equation using mathematic methods 1 to 3 (as referenced in Table 4-2) for calculating the onset of stable voltage (V_i) are provided below. The key parameters listed below are the averaged static sensitivity K obtained from multiple replications ($N \geq 2$), the standard deviation (ppm/V) and coefficient of variation (%) of the static sensitivity K, the initial voltage measured at 0 ppm NH₃ concentration, the maximum voltage of sensor signal recorded, and the estimated peak NH₃ concentration using the average static sensitivity K. These methods were not adopted for use in data processing due to either high coefficient of variation or high calculated peak concentrations when compared to the other methods. The results for Methods 4 and 5 are provided in Section 4.3.1.

Table A-1. Summary results of key parameters for selecting the proper calibration equation using mathematic Methods 1 to 3 (as referenced in Table 4-2). The calibration grade NH₃ gas used for this test was rated at 101.3 ($\pm 2\%$) ppm.

Method 1 (Mean between voltage measured at 100 s and peak voltage)						
	Unit 1	Unit 2	Unit 3	Unit 4	Unit 5	Unit 6
No. replications (N)	2	5	5	4	4	4
Average K (ppm/V)	31.0	27.3	30.6	26.5	27.8	27.5
Standard deviation of K (ppm/V)	0.79	1.74	2.00	0.62	0.67	0.69
Coefficient of Variation (%)	2.6	6.4	6.5	2.3	2.4	3.0
Vo (volt)	0.846	0.86	0.873	0.873	0.873	0.87
Vmax (volt)	4.365	4.795	4.486	4.795	4.593	4.808
Vmax - Vo (volt)	3.519	3.935	3.613	3.922	3.72	3.94
calculated peak concentration (ppm)	109.0	107.5	110.5	104.2	103.5	108.2

Table A-1 (continued).

Method 2 (Mean between voltage measured at 150 s and peak voltage)						
	Unit 1	Unit 2	Unit 3	Unit 4	Unit 5	Unit 6
No. replications (N)	2	5	5	4	4	4
Average K (ppm/V)	30.9	27.0	30.2	26.3	27.6	27.3
Standard deviation of K (ppm/V)	0.75	0.95	2.01	0.29	0.69	0.49
Coefficient of Variation (%)	2.4	3.5	6.7	1.1	2.5	2.0
Vo (volt)	0.846	0.86	0.873	0.873	0.873	0.87
Vmax (volt)	4.365	4.795	4.486	4.795	4.593	4.808
Vmax - Vo (volt)	3.519	3.935	3.613	3.922	3.72	3.94
calculated peak concentration (ppm)	109.0	106.0	109.0	103.0	102.0	107.4
Method 3 (Mean between voltage measured at 200 s and peak voltage)						
	Unit 1	Unit 2	Unit 3	Unit 4	Unit 5	Unit 6
No. replications (N)	2	5	5	4	4	4
Average K (ppm/V)	31.0	26.5	29.8	25.9	26.0	26.9
Standard deviation of K (ppm/V)	0.63	0.48	1.97	0.23	2.56	0.81
Coefficient of Variation (%)	2.0	1.8	6.6	0.9	9.8	3.0
Vo (volt)	0.846	0.86	0.873	0.873	0.873	0.87
Vmax (volt)	4.365	4.795	4.486	4.795	4.593	4.808
Vmax - Vo (volt)	3.519	3.935	3.613	3.922	3.72	3.94
calculated peak concentration (ppm)	109.1	104.2	107.9	101.9	96.8	106.0

APPENDIX B UPDATED CORE ARDUINO CODE

The Arduino microcontroller AT MEGA-2560 was used to control all functions of the iPMUs as well as data acquisition. The MEGA-2560 microcontroller function on demand of a 5V power input and has 54 input and output (I/O) pins. The MEGA-2560 has both digital and analog inputs, which allows the microcontroller to robustly handle different types of signal sensing.

The programs used to control the iPMU systems were composed based on reading analog inputs from desired measurement variables (NH₃, CO₂, temperature, and building static pressure). The codes were developed by Ji et al. (2016) and consisted of main program file (`iPMU_MasterCode_date modified`) and accessory function files, including `Buttons`, `Datalog`, `Dataread`, `LCDscreen`, `Real_Time_Data_Process`, `Timechange`, `Timeinformation`, `Timeset` and `Wireless`.

Important information for properly understanding and making modification to the Arduino codes is discussed below. An important note to bear in mind is that due to inconsistencies of internal package updates from Arduino environment, this set of Arduino codes works specifically with Arduino version 1.5.5.

B.1 Setting the sampling parameters

The main program file begins with defining all variables in the iPMU application such as timer and sampling control parameters, controlling logging rates and switching between relays. The pins used in the existing Arduino MEGA-2560 microcontroller were pin 9 for relay 1, pin 8 for replay 2, pins 5 and 6 controlled the LED lights indicating fresh air purging and sampling procedures.

```

//////////////////////////////////TIMER and Sampling Control Parameters//////////////////////////////////
int system_time = 0; //system time parameter.
int Timespan = 0;
int WaitforMIX = 45; //original value was 120, then 12, now 45 seconds
int Barn_time = 645; // Dont forget to add WaitforMIX time in Barn_time, they start together in
the main loop
int Purge_time = 1155;
//****
int PURE_STAT = 0;
int PURE_SAMPLE = 50;
int PURE_PURGE = 22;
//****
const int Relay1 = 9; //Define the pin for Relays
const int Relay2 = 8;
const int PurgeLED = 5;
const int SampLED = 6; //LED signal for purge and sampling.
//////////////////////////////////TIMER and Sampling Control Parameters//////////////////////////////////

```

The time control variables defined in the program were `WaitforMIX` for pre-sampling, `Barn_time` for sampling, and `Purge_time` for fresh-air purging procedures. Desired durations in seconds can be modified accordingly. Note that the duration defined in `WaitforMIX` in line 92, has to be added in `Barn_time`, since they start together in the main loop of the code. For example, if the desired duration for sampling is 600 sec, and 45 sec for pre-sampling, `WaitforMIX` needs to be 45, and `Barn_time` 645.

B.2 Changing datalogging rates

This section explains the data logging variables and how to adjust data logging frequency to desired values. The variable `Datalog_Barn` is the data logging rate at which the measurements are saved to the SD card. The `Datalog_Fresh` is the datalogging frequency for the fresh air purging procedure. For example, the codes listed below indicate that the air is sampled every 10 sec during sampling, and every 60 sec during fresh air purging procedure. Data is not logged during pre-sampling.

```

//////////////////////////////////Datalogging Rates//////////////////////////////////
int Datalog_time = 600; //Data log interval during fresh air purging. Unit is second
int Datalog_Barn = 10; // Data log interval during SAMPLING; was 10, now it is 5. Unit is second
int Datalog_Stable = 1;
int Datalog_Fresh = 60;
int StableReading_NUM = 20;
int Relay_I = 0;
int Relay_II = 0;
//////////////////////////////////Datalogging Rates//////////////////////////////////

```

B.3 Matching date and time with a computer

The date and time programmed to the Arduino control board are often reset to factory default and needed modification due to reasons such as changing battery for the LCD screen, experienced power outage, or the time changed to Saving Times. If the date and time are incorrectly shown on the LCD screen, a function file called `SetTime` needs to be properly uploaded to the Arduino board. This code is native from Arduino Time library, and could be found in Arduino community website. When uploading a program file to Arduino, make sure the board (MEGA-2560) and port (the active serial port recognized uniquely by individual computer) are selected correctly. After `SetTime` is uploaded, execute the following steps in the order below: (1) open the `Serial Monitor` from the top right of the Arduino IDLE, (2) select bound rate 9600, which is the frequency of data that is been received by your computer, (3) wait until the current date and time are printing on the screen, (4) close the `Serial Monitor` and upload your master code for iPMU (`iPMU_MasterCode_date modified`). The `SetTime` function is available at

```
https://github.com/thijse/Arduino-Code-and-Libraries/blob/master/Libraries/RTCDCF77/examples/SetTime/SetTime.ino
```

B.4 Printing NH₃ concentrations in real time

The programming codes previously developed for the iPMUs were not capable of printing the NH₃ concentrations on the LCD screen in real time. This issue was solved in the updated set of Arduino codes. Key functions, variables, and methods to adjust the real time data printing parameters and to apply the calibration equations are developed in the `Real_Time_Data_Process` function file and are explained below.

In the `Real_Time_Data_Process` function file, an `if` loop command was written to calculate the difference of the current and the previous voltages being read. This command uses an approximation equation to convert analog values from voltage output read by the NH₃ sensor to

concentration (ppm). If the difference is greater than 0.022 V, it is considered the NH₃ concentration is still changing thus not a stable reading. Other control parameters considered in this if command include `Barn_time` and `Sensortesting`. If either parameter is greater than 0 (was set to 60 in the previous set of codes), it means that the iPMU is in process of fresh air purging and the sensor is still working. If all the parameters listed above turn out to be `TRUE`, we can proceed to calculate the NH₃ concentrations and print them on the LCD screen in real time.

```

////////////////////////////////////Printing NH3 concentration //////////////////////////////////////
void Processing(int i)
{
Wireless();
if (i == 1)//Processing in Sample time
{NH3_voltage_cur = NH3_voltage;
  if (NH3_voltage_cur-NH3_voltage_pre<0.022&&WaitforMIX>2&&system_time<
Barn_time&&Sensortesting>=0)//If the difference of two voltage readings is less than 0.022v is
will be regard as a stable reading.
  {delay (9000);
    NH3_sample_SUM = NH3_voltage_cur;
    NH3_sample_NUM = NH3_sample_NUM + 1;
    NH3_PPM = (NH3_sample_SUM-0.86) * 27.500; //it was about 4.3V at full span, and 0.86V
offset, or Cspan/dV=50ppm/3.4V=15 ppm/V
    if (NH3_PPM <0)
    {NH3_PPM=0;
    }
  }
}
////////////////////////////////////Printing NH3 concentration //////////////////////////////////////

```

Starting line 9 is the process to calculate the real time NH₃ concentrations. This equation uses the current NH₃ voltage read by the sensor, subtracting it by an offset value of 0.86V (is the sensor voltage output corresponding to a NH₃ concentration at 0 ppm), then multiply the value by unit specific static sensitivity K (for example, K for iPMU 5 is 27.5 ppm/V).

APPENDIX C MATLAB CODE FOR DATA PROCESSING

A set of MATLAB® codes was developed to process the intensive amount of environmental data collected. The MATLAB® codes were capable of providing an hourly average data for the NH₃, CO₂ concentrations and temperatures collected by the iPMUs during the sampling procedure, selecting desired mathematic method (Method 4 or Method 5) to calculate the onset sensor response voltage, and plotting the providing plots for the processed hourly average values. The specific static sensitivity K (ppm/V) and the onset voltage V_0 for each iPMU are included in the Matlab codes. Important information for properly understanding and making modification to the MATLAB® codes is provided below.

C.1 The Graphical User Interface (GUI)

A graphical user interface (GUI) [MATLAB file name: iPMU2.m] was developed for interactive usage of the code described above and to facilitate operation experience for users that are not familiarize with MATLAB. In the GUI interface, the user needs to select the excel file, the iPMU unit number, and select the desired method for static sensitivity K (Figure A2-1). If the excel file is imported properly, the Matlab code will process the data in background, and multiple plots will be showing when the data is finished processed. The user can choose to save the processed results in the original excel file by the “Write” button from the GUI interface. If every step is processed correctly by the codes, two notification are shown to indicate the “Plots” and the “Write” steps are DONE.

Important step: The excel file requires the following change before running the GUI interface: the date column in the excel file must be changed to general format for the GUI interface to properly read the date entries. Otherwise an error reading the excel file will show.

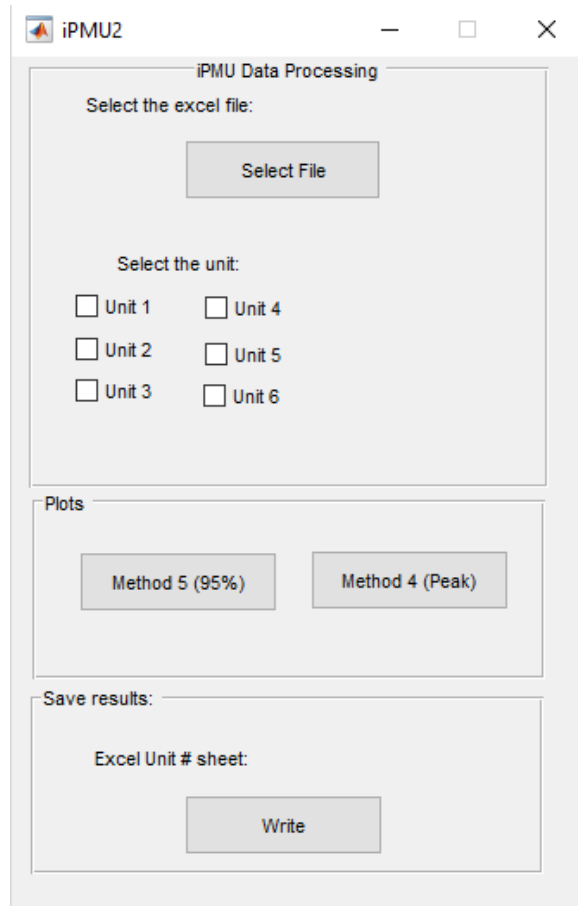


Figure C-1. The Graphical User Interface (GUI) for processing the data collected by the iPMUs.

C.2 Explanation of key components of the code

The code listed below explains the process for importing formatted data from excel. In the code, the correct range of the data are also specified. The main loop of the code collects those data from excel variable and save them in matrices.

```

////////////////////////////////////Importing Excel File and Select static sensitivity K //////////////////////////////////////
FileName='DATALOG_unit5_Barn_fds.xlsx';
excel=xlsread(FileName,'B2:I99999');
%select the exact name of the EXCEL file and the range between time and concentration
from SD card
%K=[29.570,26.453,28.741,26.597,27.746,30.019]%K Static Sensitivity for each Unit. 1st
value -> unit1. 2nd->Unit2
K=[29.570,26.453,28.741,26.597,27.746,30.019];%K for method 5(Static Sensitivity for
each unit for 95% method)
Voltagezero=[0.86,0.869,0.865,0.877,0.868,0.85];
Kmethod5=K(5);%Statistic Sesitivity (K) from unit 5
V0=Voltagezero(5); %Change here to select the v0 of unit#

for a=1:size(excel,1)

```

```

if (excel(a,3)==1) & (excel(a,4))==1 %when both relays are on (1 and 1)
    if flag==0
        j=j+1;
        i=2;
        V(1,j)=excel(a,2); %set time at 1st row
        V(2,j)=excel(a,5); %set voltage
        Date(1,j)=excel(a,1);%set date ate Date array
        flag=1;
    else
        i=i+1;
        V(i,j)=excel(a,5);
        Temp(i,j)=excel(a,8);
        Co2(i,j)=excel(a,7);
        flag=1;
    end
else
    flag=0;
end
end
%%%%%%%%%%%%%%%%%%%%%%%%%%%%%%%%%%%%%%%%%%%%%%%%%%%%%%%%%%%%%%%%%%%%%%%%%Converting Time to HH:MM format %%%%%%%%%%%%%%%%%%%%%%%%%%%%%%%%%%%%%%%%%%%%%%%%%%%%%%%%%%%%%%%%%%%%%%%%%%
%setting time conversion, collect from 1st row of V and saving in another array
T=V(1,:);
Tconverted=datestr(T, 'HH:MM');
%%%%%%%%%%%%%%%%%%%%%%%%%%%%%%%%%%%%%%%%%%%%%%%%%%%%%%%%%%%%%%%%%%%%%%%%%Selecting the desired method for K %%%%%%%%%%%%%%%%%%%%%%%%%%%%%%%%%%%%%%%%%%%%%%%%%%%%%%%%%%%%%%%%%%%%%%%%%%
%Concentration methods, find PEAK value
for h=1:size(V,2)
    VPEAK(h)=max(V(:,h)); %max of each column of V (voltage of each sampling)
    [value2,index2]=max(V(:,h));%save value and index at valueandindex array
    valueandindex(3,h)=value2;
    valueandindex(4,h)=index2;
    %method 4 (find 95% of peak)
    for k=1:size(V,1)
        m4=0.95*(VPEAK);
        menor(k,h)=abs(m4(h)-V(k,h));%lowest value is the closets to 0.95
        [value,index]=min(menor(:,h));%save value and index at valueandindex array
        valueandindex(1,h)=value;
        valueandindex(2,h)=index;
    end
%%%%%%%%%%%%%%%%%%%%%%%%%%%%%%%%%%%%%%%%%%%%%%%%%%%%%%%%%%%%%%%%%%%%%%%%%Plotting processed data%%%%%%%%%%%%%%%%%%%%%%%%%%%%%%%%%%%%%%%%%%%%%%%%%%%%%%%%%%%%%%%%%%%%%%%%%
for tam=51:50:size(V,2) %This loop splits the NH3,Temp and Co2 arrays to plot 50 in 50
in each figure
    b=1;
    for cc=tam2:1:tam
        T1(b)=T(cc);
        Tconverted1=datestr(T1, 'HH:MM');
        C1(b)=C(cc);
        averageCo22(b)=averageCo2(cc);
        averageTT(b)=averageT(cc);
        b=b+1;
    end
    %Plots parameters....
    figure(a);
    neworder=Tconverted1;
    subplot(3,1,1)
    plot(C1, 'Marker','o','MarkerSize',4, 'MarkerFaceColor', 'b',
'MarkerEdgeColor', 'b');

```

```

        set(gca,'XTick',1:size(C1,2),'XtickLabel',neworder(:,1),'YLim',[0
50],'XLim',[1 size(C1,2)]);
        set(gca,'fontsize',6)
        title('NH3 (PPM)');

        subplot(3,1,2) %CO2
        plot(averageCo2, 'Marker','o','MarkerSize',4, 'MarkerFaceColor', 'm',
'MarkerEdgeColor', 'm');
        set(gca,'XTick',1:size(C1,2),'XtickLabel',neworder(:,1),'YLim',[0
4000],'XLim',[1 size(C1,2)]);
        set(gca,'fontsize',6)
        title('CO2 (PPM)');

////////////////////////////////////Save Processed Data to the Original Excel File //////////////////////////////////////
% Date,Time, NH3 concentration, Co2 and Temperature, respectively, in excel
% columns of A,B,C,D and E
xlswrite(fileName,Date,'Unit#','A');
xlswrite(fileName,T,'Unit#','B');
xlswrite(fileName,C,'Unit#','C');
xlswrite(fileName,averageCo2,'Unit#','D')
xlswrite(fileName,averageT,'Unit#','E')
disp("Write DONE ----- OK")

```

C.3 Complete set of code for data processing

The complete set of the MATLAB codes for data processing is provided in the following pages. Main files include:

- 1) Posprocess_iPMU_method5.m;
- 2) iPMU2.m; and
- 3) mat2str.m.

[File name: Posprocess_iPMU_method5.m]

```
%By Vitor Nejar Badu M de Oliveira
%This script calculate the NH3 concentration using
Method 5, which is
%calculated the mean between the values of 95% of Peak
and the Peak
%This script also plots the results and save them in the
excel file
% 1 - First of all, the user have to change the DATE
format in Excel file
%Change the MM/DD/YY to number (general) format, and
save it.
% 2 - Select the exactly Excel file name at FileName
variable
% 3 - Select the range, using the same excel syntax (B2
to I99999) to select
% the Date column until Temperature column
% 4 - Change the V0 and K values for the specific UNIT #
number
% 5- RUN the code
```

```
FileName='DATALOG_unit5_Barn_fds.xlsx';
excel=xlsread(FileName,'B2:I99999');
%select the exactly name from EXCEL file and the range
between time and concentration from SD card
%K=[29.570,26.453,28.741,26.597,27.746,30.019]%K Static
Sensitivity for each Unit. 1st value -> unit1.
2nd->Uni2 ...
K=[29.570,26.453,28.741,26.597,27.746,30.019]; %K for
method 5(Static Sensitivity for each unit for 95%
method)
Voltagezero=[0.86,0.869,0.865,0.877,0.868,0.85];
Kmethod5=K(5);%Statistic Sesityivity (K) from unit 5
V0=Voltagezero(5); %Change here to select the v0 of
unit#
```

```
V(1:507,1:103)=0;%pre allocating V to recieve time and
voltage values
Temp(1:507,1:103)=0;%pre allocating T
Co2(1:507,1:1)=0;
Date(1:1,1:103)=0;
j=0;
i=0;
flag=0;
for a=1:size(excel,1)
```

```
    if (excel(a,3)==1) & (excel(a,4))==1 %when both
relays are on (1 and 1)
        if flag==0
            j=j+1;
            i=2;
            V(1,j)=excel(a,2); %set time at 1st row
            V(2,j)=excel(a,5); %set voltage
            Date(1,j)=excel(a,1);%set date ate Date
        array
            flag=1;
        else
            i=i+1;
            V(i,j)=excel(a,5);
            Temp(i,j)=excel(a,8);
            Co2(i,j)=excel(a,7);
            flag=1;
        end
    else
        flag=0;
    end
end

%setting time conversion, collect from 1st row of V and
saving in another array
T=V(1,:);
Tconverted=datestr(T,'HH:MM');

%Concentration methdos, find PEAK value
for h=1:size(V,2)
    VPEAK(h)=max(V(:,h)); %max of each column of V
(voltage of each sampling)
    [value2,index2]=max(V(:,h));%save value and index at
valueandindex array
    valueandindex(3,h)=value2;
    valueandindex(4,h)=index2;

    %method 4 (find 95% of peak)
    for k=1:size(V,1)
        m4=0.95*(VPEAK);
        menor(k,h)=abs(m4(h)-V(k,h));%lowest value is
the closets to 0.95
        [value,index]=min(menor(:,h));%save value and
index at valueandindex array
        valueandindex(1,h)=value;
        valueandindex(2,h)=index;
```

```

end
AVM(h)=valueandindex(2,h); %index to calculate
average (AVM=index of 95%)
AVMA(h)=valueandindex(4,h);%(AVMA=Index of Max
(peak))
end

x=1;
w=1;
z=1;
for ww=1:size(V,2)
    if (AVMA(ww)>AVM(ww))%sometimes, the index of peak
is before index of 95%
        step=1;
    else
        step=-1;%to run the for loop backward and find
the 95%
    end
    z=AVM(w);
    while z~=0
        vectoraverage(x,w)=V(z,w);%allocate numbers
between AVM and AVMA to calculate mean
        x=x+1;
        if z==AVMA(w)%check if the column between 95%
and peak has been ended
            w=w+1;
            z=0;
            x=1;
        else
            z=z+step;
        end
    end
end
end
%Calculate the average of 95% and PEAK
average=sum(vectoraverage,1)./sum(vectoraverage~=0,1);
C=(average-V0)*Kmethod5; %Concentration of NH3 equation,
using the average between .95 and peak
averageT=sum(Temp,1)./sum(Temp~=0,1); %Average of Temp
of each sampling
averageCo2=sum(Co2,1)./sum(Co2~=0,1); %Average of Co2 of
each sampling

%plottig time X concentration
left=mod(size(V,2),50)
tam2=1;
a=1;

```

```

for tam=51:50:size(V,2) %This loop splits the NH3,Temp
and Co2 arrays to plot 50 in 50 in each figure
    b=1;
    for cc=tam2:1:tam
        T1(b)=T(cc);
        Tconverted1=datestr(T1,'HH:MM');
        C1(b)=C(cc);
        averageCo22(b)=averageCo2(cc);
        averageTT(b)=averageT(cc);
        b=b+1;
    end

    %Plots parameters...
    figure(a);
    neworder={Tconverted1};
    subplot(3,1,1)
    plot(C1, 'Marker','o','MarkerSize',4,
'MarkerFaceColor','b','MarkerEdgeColor','b');

set(gca,'XTick',1:size(C1,2),'XtickLabel',neworder(:,1),
'YLim',[0 50],'XLim',[1 size(C1,2)]);
set(gca,'fontsize',6)
title('NH3 (PPM)');

    subplot(3,1,2) %CO2
    plot(averageCo22, 'Marker','o','MarkerSize',4,
'MarkerFaceColor','m','MarkerEdgeColor','m');

set(gca,'XTick',1:size(C1,2),'XtickLabel',neworder(:,1),
'YLim',[0 4000],'XLim',[1 size(C1,2)]);
set(gca,'fontsize',6)
title('CO2 (PPM)');

    subplot(3,1,3)%Temperature
    plot(averageTT, 'Marker','o','MarkerSize',4,
'MarkerFaceColor','g','MarkerEdgeColor','g');

set(gca,'XTick',1:size(C1,2),'XtickLabel',neworder(:,1),
'YLim',[0 40],'XLim',[1 size(C1,2)]);
set(gca,'fontsize',6)
title('Temperature (C)');

    a=a+1;
    tam2=tam;
end

```

```

b=1;
for ccc=tam:1:(left+tam-1) %If there is any data
left,this loop plot what is left of the preveously loop
in a new figure
    C2(b)=C(ccc);
    T2(b)=T(ccc);
    averageCo222(b)=averageCo2(ccc);
    averageTTT(b)=averageT(ccc);
    Tconverted2=datestr(T2,'HH:MM');
    b=b+1;
end

figure(a);
    neworder={Tconverted1,Tconverted2}; %saving time in
a cell to plot as a string
    subplot(3,1,1)
    plot(C2, 'Marker','o','MarkerSize',4,
'MarkerFaceColor','b','MarkerEdgeColor','b');

set(gca,'XTick',1:size(C2,2),'XtickLabel',neworder(:,2),
'YLim',[0 50],'XLim',[1 size(C2,2)]);

    subplot(3,1,2) %C02
    plot(averageCo222, 'Marker','o','MarkerSize',4,
'MarkerFaceColor','m','MarkerEdgeColor','m');

set(gca,'XTick',1:size(C1,2),'XtickLabel',neworder(:,2),
'YLim',[0 4000],'XLim',[1 size(C2,2)])
    set(gca,'fontsize',6)
    title('CO2 (PPM)');

    subplot(3,1,3) % Temperature
    plot(averageTTT, 'Marker','o','MarkerSize',4,
'MarkerFaceColor','g','MarkerEdgeColor','g');

set(gca,'XTick',1:size(C1,2),'XtickLabel',neworder(:,2),
'YLim',[0 40],'XLim',[1 size(C2,2)])
    set(gca,'fontsize',6)
    title('Temperature (C)');

%plotting Date in X axes
Date(Date==0) = []; %remove extra zeros from array
for d=2:1:size(Date,2)-1 %this loop finds the changing
of date and save the dates at differentdate array
    if (Date(d+1))>(Date(d))
        differentdate(d)=Date(d);

```

```

    else
        %differentdate=0;
    end
end

differentdate(differentdate==0) = []; %remove the extra
zeros
%differentdate=datestr(differentdate,'mm/dd/yy'); %chang
e to format mm/dd/yy

for b=1:size(T,2) %this loop check the begginin of each
day to plot date in X axes
    if (T(b)<0.02)%the begginin of each day is when the
T(b) is <0.02
        index3(b)=b; %Saving the index of the begginin
of each day, to plot
        index3(index3==0) = [];
    end
end

tamanho=size(index3,2);
index3(tamanho+1)=b;%saving the last day index
sizedifferentdate=size(differentdate,2);
differentdate(sizedifferentdate+1)=differentdate(sizedif
ferentdate)+1;
differentdate=datestr(differentdate,'mm/dd/yy'); %change
to format mm/dd/yy

%plots parameters
a=a+1;
sizeC=size(C,2);
neworder={Tconverted,C,differentdate};
figure(a)%whole graph
suptitle('Plot by day');
subplot(3,1,1);
plot(C, 'Marker','o','MarkerSize',4, 'MarkerFaceColor',
'b', 'MarkerEdgeColor','b');
set(gca,'XTick',index3,'XtickLabel',neworder(:,3),'YLim'
,[0 50],'XLim',[1 sizeC])
set(gca,'fontsize',7)
title('NH3 (PPM)');

subplot(3,1,2) %C02
plot(averageCo2, 'Marker','o','MarkerSize',4,
'MarkerFaceColor','m','MarkerEdgeColor','m');
set(gca,'XTick',index3,'XtickLabel',neworder(:,3),'YLim'
,[0 4000],'XLim',[1 sizeC])

```

```

set(gca,'fontsize',7)
title('CO2 (PPM)');

subplot(3,1,3)%Temperature
plot(averageT, 'Marker','o','MarkerSize',4,
'MarkerFaceColor','g','MarkerEdgeColor','g');
set(gca,'XTick',index3,'XtickLabel',neworder(:,3),'YLim',
,[0 40],'XLim',[1 sizeC])
set(gca,'fontsize',7)
title('Temperature (C)');
disp("Plots DONE-----
----- OK")

% Date,Time, NH3 concentration, Co2 and Temperature,
respectively, in excel
% columns of A,B,C,D and E
xlswrite(FileName,Date,'Unit#','A');
xlswrite(FileName,T,'Unit#','B');
xlswrite(FileName,C,'Unit#','C');
xlswrite(FileName,averageCo2,'Unit#','D')
xlswrite(FileName,averageT,'Unit#','E')
disp("Write DONE -----
----- OK")

```

[File name: iPMU2.m]

```

%By Vitor Nejar Badu M de Oliveira - Spring 2018 - IPMU
POSPROCESSING
%This program is an application in GUI, responsible to
POS PROCESS data
%from IPMU Units. Here the user have to keep the iPMU.m
and iPMU.fig files in the
%same folder. Than, open the iPMU.m and click RUN.
% 1 - First of all, the user have to change the DATE
format in Excel file
%Change the MM/DD/YY to number (general) format, and
save it.
% 2 - The user selects the EXCEL file in the GUI
application
% 3 - Select the unit# number
% 4 - Select the method
% 5 - Save the results at same EXCEL file, in unit#
sheet

function varargout = iPMU2(varargin)
% IPMU2 MATLAB code for iPMU2.fig

```

```

%IPMU2, by itself, creates a new IPMU2 or raises the
existing
%singleton*.
%
%H = IPMU2 returns the handle to a new IPMU2 or the
handle to
%the existing singleton*.
%
%IPMU2('CALLBACK',hObject,eventData,handles,...) calls
the local
%function named CALLBACK in IPMU2.M with the given input
arguments.
%
%IPMU2('Property','Value',...) creates a new IPMU2 or
raises the
%existing singleton*. Starting from the left, property
value pairs are
%applied to the GUI before iPMU2_OpeningFcn gets called.
An
%unrecognized property name or invalid value makes
property application
%stop. All inputs are passed to iPMU2_OpeningFcn via
varargin.
%
%*See GUI Options on GUIDE's Tools menu. Choose "GUI
allows only one
%instance to run (singleton)".
%
% See also: GUIDE, GUIDATA, GUIHANDLES

% Edit the above text to modify the response to help
iPMU2

% Last Modified by GUIDE v2.5 06-Jun-2018 14:24:15

% Begin initialization code - DO NOT EDIT
gui_Singleton = 1;
gui_State = struct('gui_Name',       mfilename, ...
                  'gui_Singleton',   gui_Singleton, ...
                  'gui_OpeningFcn',  @iPMU2_OpeningFcn, ...
                  'gui_OutputFcn',   @iPMU2_OutputFcn, ...
                  'gui_LayoutFcn',   [] , ...
                  'gui_Callback',    []);
if nargin && ischar(varargin{1})

```

```

    gui_State.gui_Callback = str2func(varargin{1});
end

if nargin
    [varargout{1:nargout}] = gui_mainfcn(gui_State,
varargin{:});
else
    gui_mainfcn(gui_State, varargin{:});
end
% End initialization code - DO NOT EDIT

% --- Executes just before iPMU2 is made visible.
function iPMU2_OpeningFcn(hObject, eventdata, handles,
varargin)
% This function has no output args, see OutputFcn.
% hObject    handle to figure
% eventdata  reserved - to be defined in a future
version of MATLAB
% handles    structure with handles and user data (see
GUIDATA)
% varargin   command line arguments to iPMU2 (see
VARARGIN)

% Choose default command line output for iPMU2
handles.output = hObject;

% Update handles structure
guidata(hObject, handles);

% UIWAIT makes iPMU2 wait for user response (see
UIRESUME)
% uiwait(handles.figure1);

% --- Outputs from this function are returned to the
command line.
function varargout = iPMU2_OutputFcn(hObject, eventdata,
handles)
% varargout  cell array for returning output args (see
VARARGOUT);
% hObject    handle to figure
% eventdata  reserved - to be defined in a future
version of MATLAB
% handles    structure with handles and user data (see
GUIDATA)

% Get default command line output from handles structure

```

```

varargout{1} = handles.output;

% --- Button to import EXCEL to matlab.....
function pushbutton1_Callback(hObject, eventdata,
handles)
% Here is the button resposable to import the excel file
to GUI
%there is also a setting to K and V0 arrayys....

global FileName K4 K5 Voltagezero
K4=[28.898,25.829,28.037,25.829,27.228,27.058]; % K for
method 4(Static Sensitivity for each unit for PEAK
method)
K5=[29.570,26.453,28.741,26.597,27.746,30.019]; %K for
method 5(Static Sensitivity for each unit for 95%
method)
Voltagezero=[0.86,0.869,0.865,0.877,0.868,0.85]; % V0
for each unit

FileName = uigetfile('*.xls;*.xlsx;', 'Select
file'); %importing the file

% --- Here is the Button to calculate the Concentration
trought METHOD 5
% (Mean between 95% and peak)
function pushbutton2_Callback(hObject, eventdata,
handles)
global FileName Kmethod5 V0 DateGlobal T C averageCo2
averageT
excel=xlsread(FileName,'B2:I99999'); %read date from
excel
%select the exacly name from EXCEL file and the range
between time and concentration from SD card
%K5=[29.570,26.453,28.741,26.597,27.746,30.019]%K Static
Sensitivity for each Unit. 1st value -> unit1.
2nd->Unit2 ...

V(1:500,1:100)=0;%pre allocating V to recieve time and
voltage values
Temp(1:500,1:100)=0;%pre allocating Temp to recieve
Temperature values
Co2(1:500,1:100)=0; %pre allocating Co2 to recieve Co2
values
Date(1:1,1:100)=0; %Pre allocating Date

%Here starts the first loop to collects data from excel

```



```

j=0;
i=0;
flag=0;
for a=1:size(excel,1)
    if (excel(a,3)==1) & (excel(a,4))==1 %when both
relays are on (1 and 1)
        if flag==0
            j=j+1;
            i=2;
            V(1,j)=excel(a,2); %set time at 1st row
            V(2,j)=excel(a,5); %set voltage
            Date(1,j)=excel(a,1);%set date ate Date
array
                flag=1;
            else
                i=i+1;
                V(i,j)=excel(a,5);
                Temp(i,j)=excel(a,8);
                Co2(i,j)=excel(a,7);
                flag=1;
            end
        else
            flag=0;
        end
    end
end

%setting time conversion, colect from 1st row of V and
saving in another array
T=V(1,:);
Tconverted=datestr(T, 'HH:MM');

%Concentration methdos, find PEAK value
for h=1:size(V,2)
    VPEAK(h)=max(V(:,h)); %max of each column of V
(voltage of each sampling)
    [value2,index2]=max(V(:,h));%save value and index at
valueandindex array
    valueandindex(3,h)=value2;
    valueandindex(4,h)=index2;

    %method 4 (find 95% of peak)
    for k=1:size(V,1)
        m4=0.95*(VPEAK);
        menor(k,h)=abs(m4(h)-V(k,h));%lowest value is
the closets to 0.95

```

```

        [value,index]=min(menor(:,h));%save value and
index at valueandindex array
        valueandindex(1,h)=value;
        valueandindex(2,h)=index;

    end
    AVM(h)=valueandindex(2,h); %index to calculate
average (AVM=index of 95%)
    AVMA(h)=valueandindex(4,h);%(AVMA=Index of Max
(peak))
end

x=1;
w=1;
z=1;
for ww=1:size(V,2)
    if (AVMA(ww)>AVM(ww))%sometimes, the index of peak
is before index of 95%
        step=1;
    else
        step=-1;%to run the for loop backward and find
the 95%
    end
    z=AVM(w);
    while z~=0
        vectoraverage(x,w)=V(z,w);%allocate numbers
between AVM and AVMA to calculate mean
        x=x+1;

        if z==AVMA(w)%check if the column betwenn 95%
and peak has been ended
            w=w+1;
            z=0;
            x=1;
        else
            z=z+step;
        end
    end
end

%Calculate the average of 95% and PEAK
average=sum(vectoraverage,1)./sum(vectoraverage~=0,1);
C=(average-V0)*Kmethod5; %Concentration of NH3 equation,
using the average between .95 and peak

```

```

averageT=sum(Temp,1)./sum(Temp~=0,1); %Average of Temp
of each sampling
averageCo2=sum(Co2,1)./sum(Co2~=0,1); %Average of Co2 of
each sampling

%plottig time X concentration
left=mod(size(V,2),50)
tam2=1;
a=1;
for tam=51:50:size(V,2) %This loop splits the NH3,Temp
and Co2 arrays to plot 50 in 50 in each figure
    b=1;
    for cc=tam2:1:tam
        T1(b)=T(cc);
        Tconverted1=datestr(T1,'HH:MM');
        C1(b)=C(cc);
        averageCo22(b)=averageCo2(cc);
        averageTT(b)=averageT(cc);
        b=b+1;
    end

    %Plots parameters...
    figure(a);
    neworder={Tconverted1};
    subplot(3,1,1)
    plot(C1, 'Marker','o','MarkerSize',4,
'MarkerFaceColor','b','MarkerEdgeColor','b');

set(gca,'XTick',1:size(C1,2),'XtickLabel',neworder(:,1),
'YLim',[0 50],'XLim',[1 size(C1,2)]);
set(gca,'fontsize',6)
title('NH3 (PPM)');

    subplot(3,1,2) %CO2
    plot(averageCo22, 'Marker','o','MarkerSize',4,
'MarkerFaceColor','m','MarkerEdgeColor','m');

set(gca,'XTick',1:size(C1,2),'XtickLabel',neworder(:,1),
'YLim',[0 4000],'XLim',[1 size(C1,2)])
set(gca,'fontsize',6)
title('CO2 (PPM)');

    subplot(3,1,3)%Temperature
    plot(averageTT, 'Marker','o','MarkerSize',4,
'MarkerFaceColor','g','MarkerEdgeColor','g');

```

```

set(gca,'XTick',1:size(C1,2),'XtickLabel',neworder(:,1),
'YLim',[0 40],'XLim',[1 size(C1,2)])
set(gca,'fontsize',6)
title('Temperature (C)');

    a=a+1;
    tam2=tam;

end

b=1;
for ccc=tam:1:(left+tam-1) %If there is any data
left,this loop plot what is left of the preveously loop
in a new figure
    C2(b)=C(ccc);
    T2(b)=T(ccc);
    averageCo222(b)=averageCo2(ccc);
    averageTTT(b)=averageT(ccc);
    Tconverted2=datestr(T2,'HH:MM');
    b=b+1;
end

figure(a);
    neworder={Tconverted1,Tconverted2}; %saving time in
a cell to plot as a string
    subplot(3,1,1)
    plot(C2, 'Marker','o','MarkerSize',4,
'MarkerFaceColor','b','MarkerEdgeColor','b');

set(gca,'XTick',1:size(C2,2),'XtickLabel',neworder(:,2),
'YLim',[0 50],'XLim',[1 size(C2,2)]);

    subplot(3,1,2) %CO2
    plot(averageCo222, 'Marker','o','MarkerSize',4,
'MarkerFaceColor','m','MarkerEdgeColor','m');

set(gca,'XTick',1:size(C1,2),'XtickLabel',neworder(:,2),
'YLim',[0 4000],'XLim',[1 size(C2,2)])
set(gca,'fontsize',6)
title('CO2 (PPM)');

    subplot(3,1,3) % Temperature
    plot(averageTTT, 'Marker','o','MarkerSize',4,
'MarkerFaceColor','g','MarkerEdgeColor','g');

```

```

set(gca,'XTick',1:size(C1,2),'XtickLabel',neworder(:,2),
'YLim',[0 40],'XLim',[1 size(C2,2)])
set(gca,'fontsize',6)
title('Temperature (C)');

%plotting Date in X axes
Date(Date==0) = []; %remove extra zeros from array
for d=2:1:size(Date,2)-1 %this loop finds the changing
of date and save the dates at differentdate array
    if (Date(d+1))>(Date(d))
        differentdate(d)=Date(d);
    else
        %differentdate=0;
    end
end

differentdate(differentdate==0) = []; %remove the extra
zeros
%differentdate=datestr(differentdate,'mm/dd/yy'); %chang
e to format mm/dd/yy

for b=1:size(T,2) %this loop check the begginin of each
day to plot date in X axes
    if (T(b)<0.02)%the begginin of each day is when the
T(b) is <0.02
        index3(b)=b; %Saving the index of the begginin
of each day, to plot
        index3(index3==0) = [];
    end
end
tamanho=size(index3,2);
index3(tamanho+1)=b;%saving the last day index
sizedifferentdate=size(differentdate,2);
differentdate(sizedifferentdate+1)=differentdate(sizedif
ferentdate)+1;
differentdate=datestr(differentdate,'mm/dd/yy'); %change
to format mm/dd/yy

%plots parameters
a=a+1;
sizeC=size(C,2);
neworder={Tconverted,C,differentdate};
figure(a)%whole graph
title('Plot by day');
subplot(3,1,1);

plot(C, 'Marker','o','MarkerSize',4, 'MarkerFaceColor',
'b', 'MarkerEdgeColor', 'b');
set(gca,'XTick',index3,'XtickLabel',neworder(:,3),'YLim'
,[0 50],'XLim',[1 sizeC])
set(gca,'fontsize',7)
title('NH3 (PPM)');

subplot(3,1,2) %CO2
plot(averageCo2, 'Marker','o','MarkerSize',4,
'MarkerFaceColor','m','MarkerEdgeColor','m');
set(gca,'XTick',index3,'XtickLabel',neworder(:,3),'YLim'
,[0 4000],'XLim',[1 sizeC])
set(gca,'fontsize',7)
title('CO2 (PPM)');

subplot(3,1,3)%Temperature
plot(averageT, 'Marker','o','MarkerSize',4,
'MarkerFaceColor','g','MarkerEdgeColor','g');
set(gca,'XTick',index3,'XtickLabel',neworder(:,3),'YLim'
,[0 40],'XLim',[1 sizeC])
set(gca,'fontsize',7)
title('Temperature (C)');
disp("Plots DONE-----")
----- OK")
DateGlobal=Date;

% --- Executes on button press in checkbox1.
function checkbox1_Callback(hObject, eventdata, handles)
%This checkbox selects the unit# and also selects its K
and V0

% Hint: get(hObject,'Value') returns toggle state of
checkbox1
global Kmethod5 Kmethod4 K5 K4 Voltagezero V0 Sheet
if get(hObject,'Value')==1
    Kmethod5=K5(1);
    Kmethod4=K4(1);
    V0=Voltagezero(1);
    Sheet="Unit1"
end

% --- Executes on button press in checkbox2.
function checkbox2_Callback(hObject, eventdata, handles)
%This checkbox selects the unit# and also selects its K
and V0)

```

```

global Kmethod5 Kmethod4 K5 K4 Voltagezero V0 Sheet
if get(hObject,'Value')==1
    Kmethod5=K5(2);
    Kmethod4=K4(2);
    V0=Voltagezero(2);
    Sheet="Unit2"
end

% --- Executes on button press in checkbox3.
function checkbox3_Callback(hObject, eventdata, handles)
%This checkbox selects the unit# and also selects its K
and V0

global Kmethod5 Kmethod4 K5 K4 Voltagezero V0 Sheet
if get(hObject,'Value')==1
    Kmethod5=K5(3);
    Kmethod4=K4(3);
    V0=Voltagezero(3);
    Sheet="Unit3"
end

% --- Executes on button press in checkbox4.
function checkbox4_Callback(hObject, eventdata, handles)
%This checkbox selects the unit# and also selects its K
and V0
global Kmethod5 Kmethod4 K5 K4 Voltagezero V0 Sheet
if get(hObject,'Value')==1
    Kmethod5=K5(4);
    Kmethod4=K4(4);
    V0=Voltagezero(4);
    Sheet="Unit4"
end

% --- Executes on button press in checkbox5.
function checkbox5_Callback(hObject, eventdata, handles)
%This checkbox selects the unit# and also selects its K
and V0
global Kmethod5 Kmethod4 K5 K4 Voltagezero V0 Sheet
if get(hObject,'Value')==1
    Kmethod5=K5(5);
    Kmethod4=K4(5);
    V0=Voltagezero(5);
    Sheet="Unit5"
end

```

```

% --- Executes on button press in checkbox6.
function checkbox6_Callback(hObject, eventdata, handles)
%This checkbox selects the unit# and also selects its K
and V0
global Kmethod5 Kmethod4 K5 K4 Voltagezero V0 Sheet
if get(hObject,'Value')==1
    Kmethod5=K5(6);
    Kmethod4=K4(6);
    V0=Voltagezero(6);
    Sheet="Unit6"
end

% --- HEre is the Method 4, which calculate the NH3
concentration using only
% PEAK
function pushbutton5_Callback(hObject, eventdata,
handles)
global FileName Kmethod4 V0 DateGlobal T C averageCo2
averageT
excel=xlsread(FileName,'B2:I99999'); %read date from
excel
%select the exacly name from EXCEL file and the range
between time and concentration from SD card
%K4=[28.898,25.829,28.037,25.829,27.228,27.058];%K
Static Sensitivity for each Unit. 1st value -> unit1.
2nd->Uni2 ...

V(1:500,1:100)=0;%pre allocating V to recieve time and
voltage values
Temp(1:500,1:100)=0;%pre allocating Temp to recieve
Temperature values
Co2(1:500,1:100)=0; %pre allocating Co2 to recieve Co2
values
Date(1:1,1:100)=0; %Pre allocating Date

%Here starts the first loop to collects data from excel
j=0;
i=0;
flag=0;
for a=1:size(excel,1)
    if (excel(a,3)==1) & (excel(a,4))==1 %Collect the
data when relays are 1 and 1
        if flag==0
            j=j+1;
            i=2;
            V(1,j)=excel(a,2);%set time at 1st row

```

```

        V(2,j)=excel(a,5);%set voltage
        Date(1,j)=excel(a,1);%set date ate Date
array
    flag=1;
    else
        i=i+1;
        V(i,j)=excel(a,5);
        Temp(i,j)=excel(a,8);
        Co2(i,j)=excel(a,7);
        flag=1;
    end
    else
        flag=0;
    end
end
%setting time conversion, colect from 1st row of V and
saving in another array
T=V(1,:);
Tconverted=datestr(T,'HH:MM');

for h=1:size(V,2)
    VPEAK(h)=max(V(:,h)); %find the Peak value from each
sampling of V
end

C=(VPEAK-V0)*Kmethod4;%Concentration equation for NH3
averageT=sum(Temp,1)./sum(Temp~=0,1); %Average of Temp
of each sampling
averageCo2=sum(Co2,1)./sum(Co2~=0,1); %Average of Co2 of
each sampling

%%plot string time X concentration
left=mod(size(V,2),50)
tam2=1;
a=1;
for tam=51:50:size(V,2) %This loop splits the NH3,Temp
and Co2 arrays to plot 50 in 50 in each figure, to fit
in those figures
    b=1;
    for cc=tam2:1:tam
        T1(b)=T(cc);
        Tconverted1=datestr(T1,'HH:MM');
        C1(b)=C(cc);
        averageCo22(b)=averageCo2(cc);
        averageTT(b)=averageT(cc);
        b=b+1;
    end
end

```

```

end
    figure(a);
    neworder={Tconverted1};
    subplot(3,1,1)
    plot(C1, 'Marker','o','MarkerSize',4,
'MarkerFaceColor','b','MarkerEdgeColor','b');

set(gca,'XTick',1:size(C1,2),'XtickLabel',neworder(:,1),
'YLim',[0 50],'XLim',[1 size(C1,2)]);
set(gca,'fontsize',6)
title('NH3 (PPM)');

    subplot(3,1,2) %CO2
    plot(averageCo22, 'Marker','o','MarkerSize',4,
'MarkerFaceColor','m','MarkerEdgeColor','m');

set(gca,'XTick',1:size(C1,2),'XtickLabel',neworder(:,1),
'YLim',[0 4000],'XLim',[1 size(C1,2)]);
set(gca,'fontsize',6)
title('CO2 (PPM)');

    subplot(3,1,3)%Temperature
    plot(averageTT, 'Marker','o','MarkerSize',4,
'MarkerFaceColor','g','MarkerEdgeColor','g');

set(gca,'XTick',1:size(C1,2),'XtickLabel',neworder(:,1),
'YLim',[0 40],'XLim',[1 size(C1,2)]);
set(gca,'fontsize',6)
title('Temperature (C)');

    a=a+1;
    tam2=tam;
end
b=1;
for ccc=tam:1:(left+tam-1)%If there is any data
left,this loop plot what is left of the preveously loop
in a new figure
    C2(b)=C(ccc);
    T2(b)=T(ccc);
    averageCo222(b)=averageCo2(ccc);
    averageTTT(b)=averageT(ccc);
    Tconverted2=datestr(T2,'HH:MM');
    b=b+1;
end
figure(a);

```

```

neworder={Tconverted1,Tconverted2};
subplot(3,1,1)
plot(C2, 'Marker','o','MarkerSize',4,
'MarkerFaceColor','b','MarkerEdgeColor','b');
set(gca,'XTick',1:size(C2,2),'XtickLabel',neworder(:,2),
'YLim',[0 50],'XLim',[1 size(C2,2)]);
subplot(3,1,2) %C02
plot(averageCo222, 'Marker','o','MarkerSize',4,
'MarkerFaceColor','m','MarkerEdgeColor','m');
set(gca,'XTick',1:size(C1,2),'XtickLabel',neworder(:,2),
'YLim',[0 4000],'XLim',[1 size(C2,2)])
set(gca,'fontsize',6)
title('CO2 (PPM)');
subplot(3,1,3)
plot(averageTTT, 'Marker','o','MarkerSize',4,
'MarkerFaceColor','g','MarkerEdgeColor','g');
set(gca,'XTick',1:size(C1,2),'XtickLabel',neworder(:,2),
'YLim',[0 40],'XLim',[1 size(C2,2)])
set(gca,'fontsize',6)
title('Temperature (C)');
%-----
%plotting Date in X axes
Date(Date==0) = []; %remove extra zeros from array
for d=2:1:size(Date,2)-1 %this loop finds the changing
of date and save the dates at differentdate array
    if (Date(d+1))>(Date(d))
        differentdate(d)=Date(d);
    else
        %differentdate=0;
    end
end
differentdate(differentdate==0) = []; %remove the extra
zeros
%differentdate=datestr(differentdate,'mm/dd/yy'); %chang
e to format mm/dd/yy

for b=1:size(T,2) %this loop check the begginin of each
day to plot date in X axes
    if (T(b)<0.02)%the begginin of each day is when the
T(b) is <0.02
        index3(b)=b; %Saving the index of the begginin
of each day, to plot
        index3(index3==0) = [];

```

```

        end
    end
    tamanho=size(index3,2);
    index3(tamanho+1)=b;%saving the last day index
    sizedifferentdate=size(differentdate,2);
    differentdate(sizedifferentdate+1)=differentdate(sizedif
ferentdate)+1;
    differentdate=datestr(differentdate,'mm/dd/yy'); %change
to format mm/dd/yy

a=a+1;
sizeC=size(C,2);
neworder={Tconverted,C,differentdate};
figure(a)%whole graph
title('Plot by day');
subplot(3,1,1);
plot(C, 'Marker','o','MarkerSize',4, 'MarkerFaceColor',
'b','MarkerEdgeColor','b');
set(gca,'XTick',index3,'XtickLabel',neworder(:,3),'YLim'
,[0 50],'XLim',[1 sizeC])
set(gca,'fontsize',7)
title('NH3 (PPM)');

subplot(3,1,2) %C02
plot(averageCo2, 'Marker','o','MarkerSize',4,
'MarkerFaceColor','m','MarkerEdgeColor','m');
set(gca,'XTick',index3,'XtickLabel',neworder(:,3),'YLim'
,[0 4000],'XLim',[1 sizeC])
set(gca,'fontsize',7)
title('CO2 (PPM)');

subplot(3,1,3)%Temperature
plot(averageT, 'Marker','o','MarkerSize',4,
'MarkerFaceColor','g','MarkerEdgeColor','g');
set(gca,'XTick',index3,'XtickLabel',neworder(:,3),'YLim'
,[0 40],'XLim',[1 sizeC])
set(gca,'fontsize',7)
title('Temperature (C)');
disp("Plots DONE-----
----- OK")
DateGlobal=Date;

% --- THis button is responsible to write the result in
the excel file,
% creating a new sheet with the name and number of unit#

```

```

% Date,Time, NH3 concentration, Co2 and Temperature,
respectively, in excel
% columns of A,B,C,D and E
function pushbutton8_Callback(hObject, eventdata,
handles)
global FileName DateGlobal T C averageCo2 averageT Sheet
%Date=Date-693960;
xlswrite(FileName,DateGlobal',Sheet,'A');
xlswrite(FileName,T',Sheet,'B');
xlswrite(FileName,C',Sheet,'C');
xlswrite(FileName,averageCo2',Sheet,'D')
xlswrite(FileName,averageT',Sheet,'E')
disp("Write DONE -----
----- OK")

```

[File name: mat2str.m]

```

function string = mat2str(matrix, varargin)
%MAT2STR Represent matrix as character vector in MATLAB
syntax
% STR = MAT2STR(MAT) represents the matrix MAT as a
character
% vector so that EVAL(STR) produces the original
matrix (to
% within 15 digits of precision). Conversions of non-
scalar matrices
% contain brackets [].
% STR = MAT2STR(MAT,N) uses N digits of precision.
% STR = MAT2STR(MAT, 'class') creates a character
vector with the name of
% the class of MAT included. This option ensures that
the result of evaluating
% STR will also contain the class information.
% STR = MAT2STR(MAT, N, 'class') uses N digits of
precision and includes
% the class information.
% Example
% mat2str(magic(3)) produces the character vector
'[8 1 6; 3 5 7; 4 9 2]'.
% a = int8(magic(3))
% mat2str(a,'class') produces the character vector
% 'int8([8 1 6; 3 5 7; 4 9 2])'.
% See also NUM2STR, INT2STR, SPRINTF, CLASS, EVAL.
% Copyright 1984-2017 The MathWorks, Inc.
if nargin > 1
[varargin{:}] = convertStringsToChars(varargin{:});
end

```

```

narginchk(1,3);
numoptions = length(varargin);
useclass = false;
usedigits = false;
for i = 1:numoptions
if ischar(varargin{i})
switch lower(varargin{i})
case 'class'
useclass = true;
otherwise
error(message('MATLAB:mat2str:InvalidOptionString',
varargin{ i }));
end
elseif isnumeric(varargin{i})
usedigits = true;
n = varargin{i};
else
error(message('MATLAB:mat2str:InvalidOptionType'));
end
if ~ismatrix(matrix)
error(message('MATLAB:mat2str:TwoDInput'));
end
enumerationFlag = isenumeration(matrix);
if ~(isnumeric(matrix) || ischar(matrix) ||
islogical(matrix) || enumerationFlag)
error(message('MATLAB:mat2str:NumericInput'));
end
if enumerationFlag
useclass = false;
end
[rows, cols] = size(matrix);
if usedigits == false
n = 15;
form = '%.15g';
else
form = sprintf('%.%dg',n);
end
if issparse(matrix)
[i,j,s] = find(matrix);
string = ['sparse(' mat2str(i) ', ' mat2str(j), ',
'];
if useclass
string = [string mat2str(s, n, 'class')];

```

```

else
    string = [string mat2str(s, n)];
end
string = [string ' ' mat2str(rows) ' ' , '
mat2str(cols) ' '];
return;
end

if useclass
    string = [class(matrix), '('];
else
    if ischar(matrix) && ~isempty(matrix)
        strings = cell(rows,1);
        for row=1:rows
            strings{row} = matrix(row,:);
        end
        needsConcatenation = rows > 1;

        dangerousPattern = '[\0\n-\r]';
        hasDangerousChars = regexp(strings,
dangerousPattern, 'once');

        needsConcatenation = needsConcatenation |
~isempty([hasDangerousChars{:}]);

        strings = strep(strings, ' ', ' ');
        strings = regexprep(strings, dangerousPattern,
''' char(sprintf('%d', $0)) ' ');

        if needsConcatenation
            string = '[';
        else
            string = '';
        end

        string = [string ' ' strings{1} ' '];

        for row = 2:rows
            string = [string ' ' strings{row}
' ']; %#ok
        end

        if needsConcatenation
            string = [string ' '];
        end
end

```

```

return;
end
string = '';
end

if isempty(matrix)
    if enumerationFlag
        string = [string class(matrix) '.empty('
int2str(rows) ' ' int2str(cols) ' '];
    elseif (rows==0) && (cols==0)
        if ischar(matrix)
            string = [string ' '];
        else
            string = [string '[]'];
        end
    else
        string = [string 'zeros(' int2str(rows) ' ' , '
int2str(cols) ' '];
    end
    if useclass
        string = [string, ' '];
    end
    return;
end

if isfloat(matrix) && ~enumerationFlag
    matrix = 0+matrix; % Remove negative zero
end

pos = length(string)+1;
% now guess how big string will need to be
% n+7 covers (space) or +-i at the start of the string,
the decimal point
% and E+-00. The +10 covers class string and
parentheses.
if enumerationFlag
    spaceRequired = (2*length(class(matrix)) *
numel(matrix)) + 10;
elseif ~isreal(matrix)
    spaceRequired = (2*(n+7)) * numel(matrix) + 10;
    realFlag = false;
else
    spaceRequired = ((n+7) * numel(matrix)) + 10;
    realFlag = true;
end
string(1,spaceRequired) = char(0);

```



```

if rows*cols ~= 1
    string(pos) = '[';
    pos = pos + 1;
end

for i = 1:rows
    for j = 1:cols
        if(matrix(i,j) == Inf)
            string(pos:pos+2) = 'Inf';
            pos = pos + 3;
        elseif (matrix(i,j) == -Inf)
            string(pos:pos+3) = '-Inf';
            pos = pos + 4;
        elseif islogical(matrix(i,j))
            if matrix(i,j) == true
                string(pos:pos+3) = 'true';
                pos = pos + 4;
            else
                string(pos:pos+4) = 'false';
                pos = pos + 5;
            end
        else
            if enumerationFlag
                tempStr = [class(matrix) '.'
char(matrix(i,j))];
            elseif realFlag || isreal(matrix(i,j))
                tempStr = sprintf(form,matrix(i,j));
            else
                realStr =
sprintf(form,real(matrix(i,j)));
                imagVal = imag(matrix(i,j));
                if imagVal < 0
                    sign = '-';
                    imagVal = abs(imagVal);
                else
                    sign = '+';
                end
                imagPart = sprintf(form,imagVal);
                if isfinite(imagVal)
                    imagStr = [sign, imagPart, 'i'];
                else
                    imagStr = [sign, 'li*', imagPart];
                end
                tempStr = [realStr, imagStr];
            end
        end

        len = length(tempStr);
        string(pos:pos+len-1) = tempStr;
        pos = pos+len;
    end
    string(pos) = ' ';
    pos = pos + 1;
end
string(pos-1) = ';';
end
% clean up the end of the string
if rows * cols ~= 1
    string(pos-1) = ']';
else
    % remove trailing space from scalars
    pos = pos - 1;
end
if useclass
    string(pos) = ')';
    pos = pos+1;
end
string = string(1:pos-1);
% end mat2str
end
function b = isenumeration(m)
    b = ~isempty(enumeration(class(m)));
end

```